HPLC-BASED ACTIVITY PROFILING FOR HERG CHANNEL INHIBITORS FROM *GALENIA AFRICANA* AND *GNIDIA POLYCEPHALA*, AND COUNTER-CURRENT CHROMATOGRAPHIC ISOLATION OF ANTIMICROBIALS FROM *COLOPHOSPERMUM MOPANE*

KUN DU

HPLC-BASED ACTIVITY PROFILING FOR HERG CHANNEL INHIBITORS FROM *GALENIA AFRICANA* AND *GNIDIA POLYCEPHALA*, AND COUNTER-CURRENT CHROMATOGRAPHIC ISOLATION OF ANTIMICROBIALS FROM *COLOPHOSPERMUM MOPANE*

Thesis submitted in fulfillment of the requirements for the degree

PHILOSOPHIAE DOCTOR

in the

Department of Chemistry

Faculty of Natural and Agricultural Sciences

at the

University of the Free State

by

Kun Du

Supervisors

Professor Jan Van der Westhuizen

(University of the Free State, South Africa)

Professor Matthias Hamburger

(University of Basel, Switzerland)

January 2015

Bloemfontein

DECLARATION

I, Kun Du, hereby declare that this thesis is submitted by me for the degree of Philosophiae Doctor in Chemistry, at the University of the Free State. To the best of my knowledge, this is my own original work with the exception of such references used. This thesis has not been previously published or submitted to any university for a degree. I further cede copyright of the thesis in favor of the University of the Free State.

This thesis is dedicated to my MSc/PhD supervisor the Late Professor Andrew Marston (November 16, 1953 - March 26, 2013).

Kun Du

January 2015

ACKNOWLEDGMENTS

At the end of this road, I would like to express my sincere gratitude and appreciation to the following people for their contribution towards this study:

- My late MSc/PhD supervisor Prof. Andrew Marston for believing in me, for introducing me into phytochemistry, and for his supervision, support, encouragement, persistent, guidance and friendship. I miss the years that we worked together on the same bench often until the late night. You were a true inspiration. You may be gone but you will never be forgotten. I keep you in my heart forever.
- Prof. Jan van der Westhuizen and Prof. Matthias Hamburger for their supervision, assistance, guidance, patience, invaluable advice, and correcting and giving suggestions to this thesis.
- Dr. Maria De Mieri for her guidance, assistance, patience, and contribution to the projects of this thesis.
- I would particularly like to thank Prof. M. Hamburger for kindly accommodating me in his group at the University of Basel (Switzerland) and introducing me the state-of-the-art techniques and research strategies, and Dr. M. De Mieri from the same group for her kind help and support all the time in the laboratory.
- Prof. Sandy van Vuuren for running the antimicrobial assay, Prof. Steffen Hering and co-workers (Priyanka, Khanya and Elmarie) for running the hERG assay, Dr. Markus Neuburger for X-ray crystallography and Dr. Pieter Zietsman for collection and identification of the plant materials.
- My group colleagues in University of the Free State and University of Basel for the help and the good times we shared and most of all the friendly environment conductive for this study.
- The South African National Research Foundation (NRF), and European Union Framework 7 (NO. PIRSES-GA-2011-295174) are gratefully thanked for financial support.
- Finally, this work would not have been possible without the support of my family. They have always been the source of my motivation for work and study.

Mr. Kun Du

Bloemfontein

January 2015

LIST OF ABBREVIATIONS

AC	Absolute configuration
APCI	Atmospheric pressure chemical ionization
API	Atmospheric pressure ionization
CAM	Complementary and alternative medicine
CCC	counter-current chromatography
CD	Circular dichroism
CDA	Chiral derivatizing agent
COSY	Correlation spectroscopy
DAD	Diode array detector
DMSO	Dimethyl sulfoxide
ECD	Electronic circular dichroism
ECG	Electrocardiogram
ELSD	Evaporative light scattering detection
ESI	Electrospray ionization
FDA	Food and Drug Administration
$GABA_A$ receptor	Gamma aminobutyric acid type A receptor
HDES	Hydrodynamic equilibrium system
hERG	Human ether-a-go-go related gene
HM	Herbal medicine
HMBC	Heteronuclear multiple bond correlation
HPLC	High performance liquid chromatography
HSCCC	High-speed counter-current chromatography
HSES	Hydrostatic equilibrium system
HSQC	Heteronuclear single quantum correlation
HTS	High-throughput screening
IC_{50}	Half inhibitory concentration
LQT	A long time interval from the point Q to point T in an electrocardiogram
MDR	Multidrug resistant
MIC	Minimal Inhibitory Concentration

MPA	α-methoxyphenylacetic acid
MS	Mass spectrometry
NMR	Nuclear magnetic resonance spectroscopy
NOESY	Nuclear Overhauser enhancement spectroscopy
NP	Natural product
OR	Optical rotation
ORD	Optical rotatory dispersion
OTC	Over the counter
PDA	Photo-diode array
QT	The time from the point Q to point T in an electrocardiogram
ROESY	Rotating frame Overhauser effect spectroscopy
TCM	Traditional Chinese Medicine
TD DFT	Time-dependent density function theory
TdP arrhythmia	Torsadesde pointes arrhythmia
TEVC	Two-microelectrode voltage clamp
TLC	Thin-layer chromatography
TM	Traditional medicine
TOCSY	Total correlation spectroscopy
TOF	Time-of-flight
UV	Ultraviolet
VCD	Vibrational circular dichroism
Vis	Visable
WHO	World Health Organization
XRD	X-ray diffraction

KEYWORDS

Natural products, drug discovery, hERG channel inhibitors, antimicrobials, HPLC-based activity profiling, high-speed counter-current chromatography, medicinal plants, *Galenia africana* (Aizoaceae), *Gnidia polycephala* (Thymelaeaceae), *Colophospermum mopane* (Fabaceae).

ABSTRACT

The human ether-a-go-go-related gene (hERG) channel plays a critical role in cardiac action potential repolarization. Blocking of the channel by drugs may lead to a fatal type of arrhythmia, named “torsades de pointes” (TdP). The hERG channel is thus considered as a primary antitarget in safety pharmacology. Several drugs have been withdrawn from the market or received severe restrictions on use for this reason, and numerous compounds have been blocked from progressing further into phases of clinical development because of hERG channel inhibition. In contrast to the routine screening in industry for potential hERG liabilities of drug leads, comparably little is known about hERG inhibitors in medicinal plants (*viz*. phytomedicine). These are widely used as complementary medicines and continue to increase in popularity. There is an urgent need to critically assess the potential risks of these botanical products.

A library of 700 extracts from different parts of 142 South African medicinal plants has been screened by our research group for the potential of hERG channel inhibition with a *Xenopus laevis* oocytes based bioassay. The DCM extracts from stems and leaves of *Galenia africana* (Aizoaceae) and from roots of *Gnidia polycephala* (Thymelaeaceae) showed the strongest inhibition [50.3 ±5.4% (n = 3) and 58.8 ±13.4% (n = 3) respectively at a concentration of 100 μg/mL]. The molecules responsible for the blocking activity were investigated with the HPLC-based activity profiling approach. Compounds in the active time window were isolated for further pharmacological testing. We also isolated structurally related compounds in the inactive fractions in view of deriving some structure-activity related information. Structures were elucidated by a combination of advanced off-line analytical methods including MS and highly sensitive microprobe NMR. The absolute configurations were determined by single-crystal X-ray diffraction with Cu Kα radiation or by comparison of their experimental and calculated ECD spectra.

HPLC-based activity profiling of *Galenia africana* enabled the identification of nine flavonoids in the active time windows. However, the hERG-channel inhibition of isolated compounds was less pronounced than that of extract and active microfractions (hERG inhibition between 10.1 ±5% and 14.1 ± 1.6% at 100 μM). The two major constituents, 7,8-methylenedioxyflavone and 7,8-dimethoxyflavone were quantified (4.3% and 9.4%, respectively) in the extract. Further hERG inhibition tests for 7,8-methylenedioxyflavone and 7,8-dimethoxyflavone at 300 μM showed a

concentration-dependent inhibitory activity (33.2 ± 12.4% and 30.0 ± 7.4%, respectively). In a detailed phytochemical profiling of the active extract, a total of 20 phenolic compounds, including six new ones were isolated and characterized.

HPLC-based activity profiling of *Gnidia polycephala* enabled the identification of three daphnane-type diterpenoid orthoesters (DDOs) as the hERG channel inhibitors with inhibition of 55.4 ± 7.0% (n = 4); 42.5 ± 16.0% (n = 3) and 51.3 ± 9.4% (n = 4) respectively at 100 μM. DDOs have demonstrated remarkable bioactivities. This is the first report of DDOs as hERG channel inhibitors and they represent a new scaffold for hERG channel inhibition. In a detailed phytochemical profiling of the active extract, a total of sixteen compounds, including two new DDOs, two new guaiane sesquiterpenoids, polycephalone A and B with an unprecedented carbon skeleton and ten known compounds were isolated and characterized.

New antimicrobials need to be discovered and developed urgently due to the constant evolution of resistant microorganism phenotypes, the emergence of new diseases, and toxicity associated with current drugs. A preliminary screen of the lipophilic extracts (DCM) of seeds, leaves and hulls of *Colophospermum mopane* (Fabaceae) had shown positive antimicrobial activities. Our antimicrobial bioassay requires relatively a larger quantity of sample (2 to 5 mg for pure compounds), thus an efficient preparative isolation of the secondary metabolites in the mixture was needed. High-speed counter-current chromatography (HSCCC) an all-liquid technique with an unique separation mechanism was employed. Three new and two known labdane diterpenoids, one new isolabdane, three new and two known clerodane diterpenoids, were isolated from the seeds, husks and leaves of *Colophospermum mopane*. The structures of the isolates were elucidated with spectroscopic (1D and 2D NMR) and spectrometric methods (MS). The absolute configurations of compounds with a crystalline form were determined by single-crystal X-ray diffraction with Cu Kα radiation. The absolute configuration of a labdane diterpenoid and an isolabdane diterpenoid without a crystalline form was established by modified the Mosher's method, and corroborated by comparison of experimental and calculated ECD spectra of their 3-*p*-bromobenzoate derivatives. The compounds were evaluated for antimicrobial activities. A clerodane diterpenoid was the most active with MIC values as low as 51.3 μM, 51.3 μM and 102.9 μM against *Escherichia coli*, *Staphylococcus aureus* and *Enterococcus faecalis*, respectively.

TABLE OF CONTENTS

1. INTRODUCTION

1.1. Natural products in drug discovery

For thousands of years plants were virtually the sole therapeutic agents available to humans [1]. The human tradition of sourcing treatment from plants was presumably initially instinctive [2] but it has developed into the practice of traditional herbal medicine on which the majority of the world population [3] still relies to alleviate and treat diseases. An interesting study on the feeding patterns of African primates indicates the use of non-nutritional plants with medicinal properties for diseases such as intestinal parasites [4, 5], suggesting the origins of herbal medicine may have their roots within the animal kingdom [6].

The earliest records in traditional medicine dates from around 2600 BCE and written records on the uses of approximately 1000 plant-derived substances were found in Mesopotamia [7]. The oils of *Cedrus* species (cedar), *Cupressus sempervirens* (cypress), *Glycyrrhiza glabra* (licorice), *Commiphora* species (myrrh) and *Papaver somniferum* (poppy juice) in these records are still used today to treat ailments ranging from coughs and colds to parasitic infections and inflammation [7]. In Egyptian medicine the best known record is the "Ebers Papyrus" that dates from 1500 BCE and documents over 700 drugs mostly of plant origin [7, 8]. Chinese Medicine has been extensively documented over the centuries. The first record (Wu Shi Er Bing Fang, containing 52 prescriptions) dates from ca. 1100 BCE and the later works include the Shennong Herbal (ca. 100 BCE; 365 drugs) and the Tang Herbal (659 CE; 850 drugs) [7, 8]. The traditional medicine of Indian ayurvedic system had been documented before 1000 BCE (Charaka; Sushruta and Samhitas with 341 and 516 drugs respectively) [7, 8]. The Greeks and Romans contributed significantly to the rational use of medicinal plants in the ancient western world, with Dioscorides (100 CE) accurately recording the collection, storage, and uses of medicinal herbs. Galen (130–200 CE.) is known for complex prescriptions and formulae for drugs [6, 7, 8]. The Arabs preserved much of the Greco-Roman expertise in the Dark and Middle Ages, and expanded it to include the use of their own resources together with Chinese and Indian Herbs [6, 7, 8].

The bioactive ingredients in medicinal plants have been fascinating human for centuries. Paracelsus (1493–1541) firstly proposed the idea of active principles contained in a medicinal plant (the so-called *Arcanum*, which he considered as an immaterial principle), and the concept of dose dependency of drug action and toxicity (*sola dosis facit venenum*) [6]. In 1805, a German pharmacist Friedrich Sertürner isolated analgesic morphine, the first pure pharmacologically active natural product, from opium latex (*Papaver somniferum*, Papaveraceae) [6]. Subsequently, a number of substances have been discovered, the classical examples including the antimalarial agent quinine from the bark of *Cinchona officinalis* (Rubiaceae), the well-known antitussive codeine from *Papaver somniferum* (Papaveraceae), atropine from *Atropa belladonna* and other Solanaceae species, and the cardiac glycoside digoxin from *Digitalis* spp. (Scrophulariaceae) [1]. These discoveries initiated an era where drugs from plants could be purified, studied and administered in precise dosages that did not vary with the source or age of the material [9].

At the end of the 19th Century, the rapidly growing in the understanding of organic synthesis and chemical structures led to synthesis of derivatives of natural products [6]. Salicin was discovered from willow tree extracts and chemically modified to aspirin in 1899 [10]. The discovery of penicillin in 1928 and its subsequent development as an anti-infective agent marked a new era in which bacteria and fungi were the new sources for bioactive compounds [10]. Today, with marine and other living organisms as additional sources, natural products and related structures are essential in the discovery of new pharmaceuticals. Indeed, a large portion of today's major drugs have their origins in nature. In a review published in 2012 by Newman *et al.*, it is noted that more than 40% of today's prescription drugs, and even more of anticancer agents, can trace their origins to a natural product [11].

Natural products and their derivatives have been successfully developed for clinical use to treat human diseases in almost all therapeutic areas [11, 12] (Figure 1 and Figure 2). By 1990, about 80% of drugs were either natural products or their derivatives. Antibiotics (e.g., penicillin, tetracycline, erythromycin), antiparasitics (e.g., avermectin), antimalarials (e.g., quinine, artemisinin), lipid control agents (e.g., lovastatin and analogs), immunosuppressants for organ transplants (e.g., cyclosporine, rapamycins) and anticancer drugs (e.g., taxol, doxorubicin) revolutionized medicine [9]. Remarkable examples includes Paclitaxel (Taxol®) (Figure 2), a unique tubulin interacting

anticancer agent with novel mechanism of action [13, 14], which was isolated from the stem bark of the Pacific yew *Taxus brevifolia* (Taxaceae) in the late 1960s and approved by the FDA in 1992. Artemisinin (Figure 1), a sesquiterpene lactone containing an endoperoxide group, was isolated in 1972 from qinghao (*Artemisia annua*, Asteraceae) in China, representing a completely new chemical class of antimalarial compounds [1]. Galanthamine (Figure 2), first isolated in the 1950s from *Galanthus nivalis* (Amaryllidaceae), now is one of the few therapeutics used in the management of Alzeimer's disease, by a mechanism involving maintenance of acetylcholine levels in the brain [1].

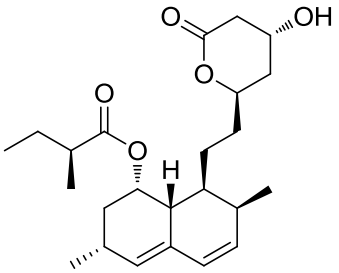

Lovastatin
Target: HMG Co-A reductase
Cholesterol-lowering agent

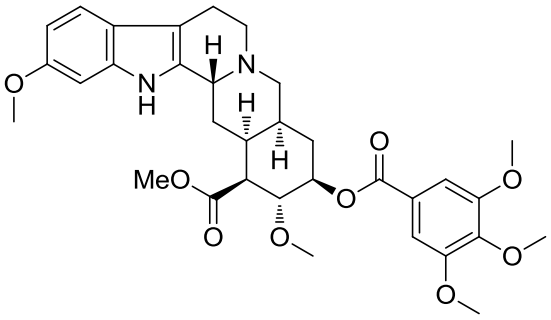

Reserpine
Target: neurotransmitter vesicles
Antihypertensive/sedative

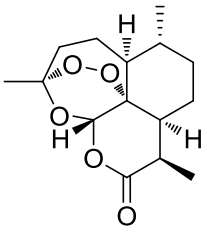

Artemisinin
Antimalarial

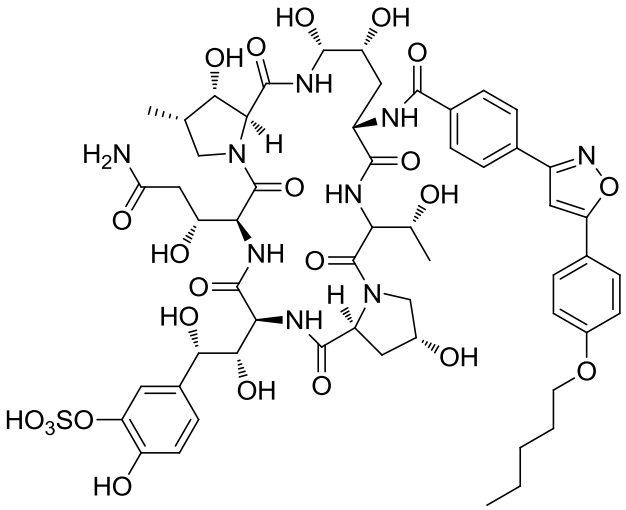

Micafungin
Target: β (1. 3) Glucan synthase
Antifungal

Figure 1. Examples of natural-product drugs [15].

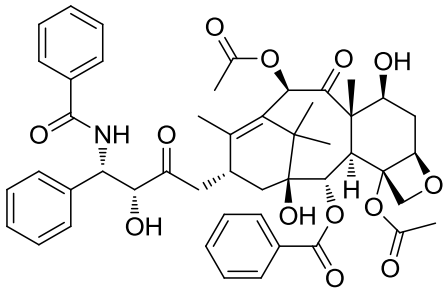

(a) **Paclitaxel**

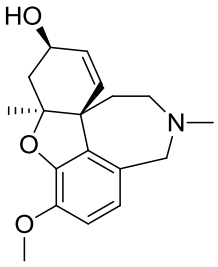

(b) **Galanthamine**

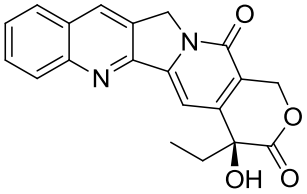

(c) **Camptothecin**

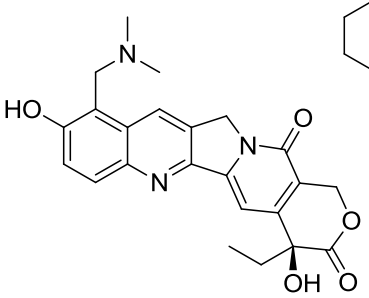

(d) **Topotecan**

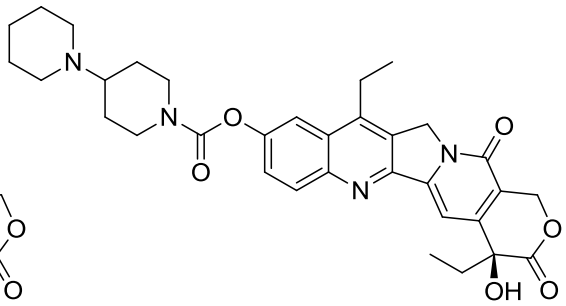

(e) **Irinotecan**

Figure 2. Paclitaxel (Taxol®), camptothecin and its derivatives, and galanthamine.

The extent of preference and effectiveness of natural products in the treatment and prevention of disease can be estimated indirectly by the number or economic value of prescriptions. Natural products or related substances accounted for 40%, 24%, and 26%, respectively, of the top 35 worldwide ethical drug sales in 2000, 2001, and 2002 [16, 17]. The plant-derived anticancer drug paclitaxel (ranked at 25 in 2000) had sales of $1.6 billion in 2000 [18]. The sales of the two categories of plant-derived anticancer drugs, the taxanes (paclitaxel and docetaxel) (Figure 2) and the camptothecin derivatives (irinotecan and topotecan) (Figure 2), were responsible for approximately one third of the total anticancer drug sales worldwide, or close to $3 billion in 2002 [16-18].

Only a small percentage of the ca. 400,000 plant species on the earth has been phytochemically investigated and the fraction screened for biological or pharmacological activities is even smaller [1]. A plant extract may contain hundreds of different secondary metabolites and usually only a narrow spectrum of its constituents is revealed by a phytochemical investigation. The plant

kingdom thus still remains an enormous reservoir of pharmacologically valuable molecules to be explored [1]. Furthermore, bacteria, fungi, marine organisms and other living creatures such as insects, remain virtually unexplored as potential natural sources for drug discovery.

1.2. Structural features and biosynthesis of natural products

Natural products can be viewed as privileged structures selected by evolutionary pressures to interact specifically with a wide variety of proteins and other biological targets, for purposes such as defense, communication, and protection against predation. A well-defined three-dimensional structure is designed in a biological system and its functional groups are fine tuned into a precise spatial orientation. As a consequence, the structures of natural products have general distinctions from synthetic drugs. Typically, natural products have more stereogenic centres and more structural complexity. They incorporate more oxygen atoms but less nitrogen, sulfur, and halogen atoms, and many have larger molecular masses (>500 Daltons) and higher polarities (greater water solubility) [19]. In addition, natural products have a lower ratio of aromatic ring atoms to total atoms and a higher number of hydrogen-bond donors and acceptors [15]. Natural products have more diversity in ring systems. About 40% of the chemical scaffolds found in natural products are absent in non-natural product derived drugs [20, 21].

Biosynthesis operates under different principles than laboratory synthesis (Table 1), although both aim to produce bioactive molecules. In nature, few building blocks are utilized, whereas tens of thousands of commercially available starting materials are used in synthetic chemistry. As a consequence, synthesis achieves numbers by repeating an established sequence of reactions over and over again with different starting materials. In contrast, nature diversifies by partitioning its limited number of starting materials into a multitude of pathways to build libraries of privileged structures [22]. Further differences are in synthetic transformations. Nature is oxophilic and the enzymes selectively activate the C-H site to introduce oxygen in the presence of numerous functional groups at different oxidation levels. Organic synthesis concentrates on nitrogen and often includes ancillary atoms such as sulfur and halogens that are relatively rare in nature [22]. Finally, the chiral enzymes of biosynthesis usually yield enantiomerically pure products; whilist synthesis generally yields racemic mixtures [22].

Table 1. Some fundamental differences between biosynthesis and synthesis [22]

	Biosynthesis	Synthesis
Building blocks	Few	Many
Strategy	Branching of intermediate	Alteration of building block
Scaffold diversity	High	Low
Functional group tolerance	High	Low
Novel motifs	Common	Rare
C-H activation	Common, site-specific	Rare
Stereocontrol	Easy, enantioselective	Difficult, case-by-case basis

1.3. Challenges facing drug discovery from natural sources

With the success in development of new drugs and the identification of novel scaffolds from natural sources, it might be expected that the identification of new metabolites from natural resources would be the core of pharmaceutical discovery efforts. However, many pharmaceutical companies have eliminated their natural product research in the past decade [9, 23]. The main reasons are probably the difficulties in dealing with natural sources and the technical limitations in discovering new bioactive compounds in complex extracts.

Pharmaceutical companies favor high-throughput screening (HTS) of massive libraries of pure synthetic compounds. The hit rate has been low, but hits are usually easy to synthesize and modify with simple chemistry. Libraries of pure compounds of known amounts are easy to screen and allow the examination of a large number of molecules in a short time [9]. In contrast, natural extracts are often complex, and often pose several difficulties in a HTS program [9, 23]. Minor bioactive products, often present in a mixture with structurally related molecules, may remain undetected. Identification of the active constituents may need extensive research. The key compound may decompose during isolation. Synergistic action of two compounds may cause bioactivity to diminish or disappear upon separation. The probability to identify a known compound that may not be patentable may be high. False positives may result from the compounds displaying non-specific activities such as tannins which form complexes with a wide range of proteins in most assays. Detergent-like compounds such as saponins may produce

misleading results in cell-based assays because they are toxic and can rapidly lyse assay cells before the target of interest can be interrogated. Strong metal chelators may react with nickel beads used as linkers. UV quenchers such as phaeophorbide A (the chlorophyll breakdown product) and auto fluorescent compounds such as coumarins may interfere with light-based assay read-outs [23]. In addition, the reliable access and supply of higher plants and marine organisms may be inhibited by the intellectual property concerns of local governments and the Rio Convention on Biodiversity [9]. The composition of extracts may vary with different seasons and environments. This may cause problems in detection of the active compounds in medicinal plants and the repetition of results in the subsequent assays and purification. Loss of source is also possible since the current extinction rates for natural species are high. It has been suggested that 15,000 out of 50,000 to 70,000 medicinal plant species are threatened with extinction [9].

Despite the complexity in dealing with natural sources, the historic hit rate for HTS of natural products is much higher than that of synthetic compound libraries. For example, about 7000 known polyketides have yielded more than 20 commercial drugs with a “hit rate” of 0.3%. This is much better than the <0.001% hit rate for HTS of synthetic compound libraries [9].

1.4. Classical approach in natural product based drug discovery and its disadvantages

The classical approach of natural product based drug discovery is bioactivity-guided isolation. A bioactive extract is fractionated and purified under the guidence of a specific bioassay to generate a single biologically active compound (Figure 3). This is a costly and time-consuming process. All fractions of each chromatographic step need to be tested with a bioassay, and identification of the pure compounds is usually conducted at the end of the process. Often already known compounds are re-isolated and identified.

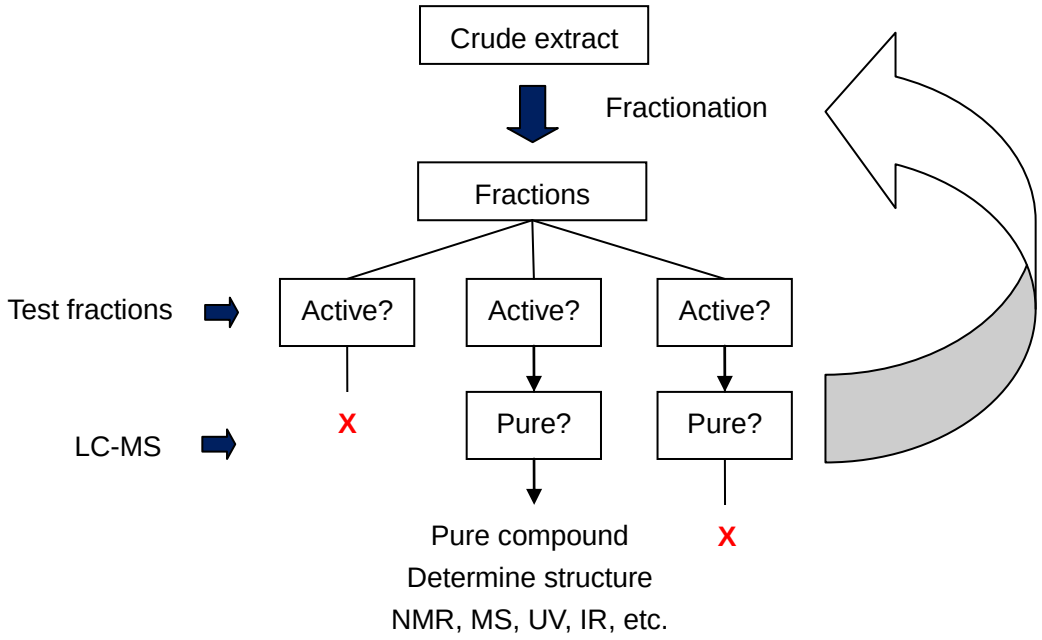

Figure 3. The general paradigm for bioassay-guided purification, the classical approach of natural product drug discovery.

1.5. Developments of analytical techniques in natural products research

Innovations in analytical technology have often played an important role in the progress of natural product chemistry. A recent development in the characterization of metabolites in complex natural extracts relies on hyphenated techniques that should provide good sensitivity, selectivity and structural information on the molecules of interest [1].

A pivotal development in modern LC-MS was the introduction of 'soft ionization' methods, i.e. electrospray ionization (ESI) and atmospheric pressure ionization (API). ESI facilitates the transfer of analyte molecules from uncharged liquid phase species to gas phase ions, hence making the hyphenation of mass spectrometers to liquid chromatography systems technically feasible [25]. Two API techniques, atmospheric pressure chemical ionization (APCI) and the more recent atmospheric pressure photo ionization (APPI) extend the range of the analytes to non-polar molecules difficult to ionize by ESI [15, 24-25]. The correlation of both molecular mass and UV absorption data with known compounds by database searching is normally sufficient to classify sets of compounds. [15] However, mass spectrometry data alone, even if tandem mass spectrometers are employed to analyze fragmentation patterns and high-resolution MS provide the accurate mass, can hardly

provide more than the molecular formula without databases, unless the elucidation process is restricted to structures with a common scaffold such as peptides or flavonoids [25].

A diode array detector (DAD) with online recording of UV/VIS spectra allows acquisition of a broad range of wavelengths that can be used in parallel with the MS detector. Since light absorption in the UV/VIS range requires chromophores, this technique is limited to analytes bearing conjugated double bond systems [25]. In addition, UV/VIS detection limits the use of HPLC mobile phases and mobile phase additives to ones that do not absorb light in the detection wavelengths ranges [25]. Non or weakly UV active compounds such as saponins and sugars have to be derivatized with chromophore-bearing ligands or have to be detected by alternative techniques, such as an evaporative light scattering detector (ELSD). The technique is unselective and has non linear concentration-signal relationships [25].

Structure elucidation of organic molecules has been revolutionized by the advent of high-resolution NMR technologies with multidimensional pulse methods and sensitivity improvements [15]. New multidimensional pulse experiments including the scalar (through bond) ^{1}H-^{1}H and ^{1}H-(^{13}C, ^{15}N, ^{31}P) correlations and the ^{1}H-^{1}H dipolar (through space) connectivity data essentially map out the structure of the compound [15]. Sensitivity improved by superconducting magnets, cryogenic electronics and micro-probe technologies have dramatically lowered the amount of sample required for structural analysis to less than one milligram [15, 26].

Multidimensional pulse experiments are based on the application of pulse sequences. Precisely timed radio-frequency and magnetic-field gradient pulses (usually on the microsecond and millisecond timescale) are designed to excite the atomic nuclei and produce diagnostic resonances that are used to establish the connectivity of the ^{1}H, ^{13}C, ^{15}N and ^{31}P nuclei in a molecule [15]. Hundreds of these pulse sequences with special application have been developed, however, only a few of them are commonly used in natural product structure determination. ^{1}H-NMR, ^{13}C-NMR, COSY (^{1}H-^{1}H, ^{3}J correlation), HSQC (^{1}H-^{13}C, ^{1}J correlation) and HMBC (^{1}H-^{13}C, ^{2}J or ^{3}J correlations) are the standard experiments for elucidating the structure of a small molecule. In case of complex overlapping of resonances occurring in ^{1}H NMR spectra, for example, from glycosides, further experiments such as (^{1}H, ^{1}H)-TOCSY can be used. NOESY and ROESY experiments

display through space correlations that are used to determine relative stereochemistry [15].

These techniques have facilitated dereplication, the process of identifying molecules for which the structure is already known. It is critical to the drug discovery work productivity that known molecules can be triaged from further study quickly and efficiently in order to save time and resources [24].

1.6. HPLC-based activity profiling as a new approach in natural product based drug discovery

The complexity of the bioactive extract made it unfavorable for HTS. Moreover, bioactivity-guided fractionation can't keep pace with the fast assay turnaround and the tight deadlines required by HTS-based programs [23]. The solution to this obstacle would be automated separation of all constituents in the extract into individual components, coupled with full spectroscopic/spectrometric identification prior to HTS [9]. The impressive improvement in HPLC column performance (highly separation efficiency and high resolution stationary phase materials with 2 mm particle sizes) [25], and the availability of HPLC-coupled spectroscopy/spectrometry techniques allow aquisition a wealth of structural information on compounds contained in an extract or fraction in a short time. This information can nowadays be obtained with minute amounts of material. Full structural characterization of compounds eluted in microgram quantities from a HPLC column has become a reality with the microprobe and cryoprobe NMR technologies, and highly sensitive high-resolution MS detection online [23, 25].

Further combination of HPLC-coupled spectroscopy/spectrometry with bioassays allowed the correlation of bioactivity data with structural information of discrete HPLC peaks, and hence tracking bioactive compounds in an extract. Three different approaches have been developed [23]: on-flow post-column bioassays, at-line settings, and off-line activity profiling. The on-flow method was described by Irth as 'high resolution screening', which has stated the essential of the strategy. However, among the three approaches, the off-line HPLC-based activity profiling (Figure 4) is the most versatile and probably has the highest potential for broad implementation in drug discovery programs [23].

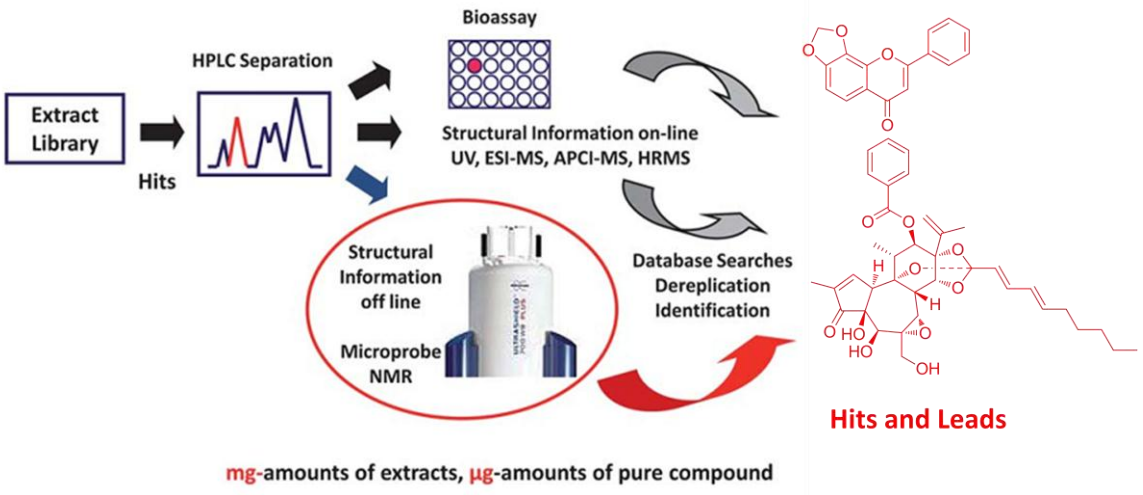

Figure 4. A schematic view of HPLC-based activity profiling of a bioactive extract [23].

In off-line HPLC-based activity profiling [23, 27], extracts (mg amounts) are separated by analytical or semipreparative HPLC. UV spectra and MS data are recorded online and time-based fractions are collected in parallel via a T-split of the column effluent. Fractions are dried, re-dissolved in a small amount of a suitable solvent, usually DMSO, and assayed for bioactivity. The chromatogram and the activity profile of each fraction are matched manually to identify active peaks. NMR data are typically recorded off-line for the active fractions or peaks using microprobe NMR technology. Furthermore, a straightforward peak-based preparative isolation of the interesting compounds can be conducted without a bioassay for each chromatography step.

The group of Prof. Hamburger and coworkers at the University of Basel, Switzerland, have established a dedicated technology platform for the dereplication and HPLC-based activity profiling of extracts (Figure 4). The platform combines on-line HPLC-UV-MS data with off-line microprobe NMR analysis and micro-fractionations in vials. Various bioassays have been successfully coupled to this platform, including whole organism assays (tropical parasitic diseases), cell based functional assays (e.g. $GABA_A$ receptor modulation), and mechanism-based screens (e.g. DYRK1A kinase) [23]. This has led to the discovery of a number of novel bioactive compounds [28-52]. Recent examples including pterocarpans from *Adenocarpus cincinnatus* [49], a labdane diterpene zerumin A from *Curcuma kwangsiensis* [50], a dihydrostilbene from *Pholidota chinensis* as $GABA_A$ receptor modulators [51], cynaropicrin from *Centaurea salmantica* as the first plant natural product with *in vivo* activity against *Trypanosoma brucei* [37],

protostane triterpenoids from *Alisma plantago-aquatica* [39], ordonopicrin from *Arctium nemorosum* [40], isoflavan quinones from *Abrus precatorius* [45], phenathrenones from *Drypetes gerrardii* as antiplasmodial constituents [52], daphnetoxin and related daphane diterpenes from *Daphne gnidium* as the antiviral constituents in a screening for anti-HIV inhibitors [47], and the hERG channel inhibitors from a traditional Chinese medicine (TCM) herbal drug Coptidis rhizoma (*Coptis chinensis*) as an antitarget in screening [48].

In this thesis, the same HPLC-based activity profiling platform was employed for a project to identify hERG channel blockers (in a functional assay based on *Xenopus oocytes*) in herbal extracts. The choice of HPLC column diameter to be used depends on the degree of miniaturization and sensitivity of the bioassay [53]. An analytical HPLC column (3 mm i. d.; 300 µg of extract; 30 µL of DMSO) can be used for most cellular and biochemical assays. For the more complex pharmacological *Xenopus oocytes* assays, the separation has to be performed on a semi-preparative scale (10 mm i. d.; 5 mg of extract; 100 µL of DMSO) [53].

HPLC-based activity profiling is not only restricted to the mere identification of bioactive peaks, but also provides additional useful information [53]. Screens often deliver a large number of hits (active extracts) that exceeds the capacities for targeted preparative purification of compounds of interest. Activity profiles greatly facilitate the selection of bioactive extracts with discrete chromatographic peaks correlating to distinct activity. Low priorities are assigned to the ones whose activity is lost after fractionation or is dispersed over a broad time window. Activity profiling is also efficient for the dereplication of active extracts. Activities due to unwanted interferences, for example tannins, can be characterized in the profile by a wide activity window correlating with broad humps and unresolved peaks in the HPLC chromatogram. In conjunction with on-line spectroscopy and off-line NMR microprobe technology, activity profiles may contain additional structural information for the discrete chromatographic peaks in both active and inactive windows. Preliminary structure-activity data can thus be obtained for structurally related molecules.

However, as for every strategy, there are intrinsic limitations for HPLC-based activity profiling [53]. This approach is limited to bioassays with relative high sensitivity, because few milligrams

of an active extract are often the optimal quantity for generating a highly resolved activity profile in HPLC. Detection of minor bioactive products may need a less complex fraction obtained by the classical bioactivity-guided approach prior to the activity profiling.

1.7. Determination of the absolute configuration of natural products

Isomers are compounds that contain the same atoms bonded together in differing ways. Two isomers with different connectivity of the atoms are constitutional isomers, and isomers with the same connectivity are stereoisomers. Enantiomers with opposite absolute configurations are mirror images of each other that are non-superposable (not identical) and need chiral chromatography to separate. Diastereoisomers are stereoisomers that are not mirror images. Two diastereoisomers have different relative configurations and are different compounds. Thus they can be separated and distinguished by common nonchiral techniques.

An absolute configuration (AC) in stereochemistry is the spatial arrangement of the atoms of a chiral molecular entity (or group). Enzymes are chiral, and their interactions with ligands are stereoselective. Thus, chirality of biomolecules is very important for the expression of their bioactivity, and determination of the absolute configuration of a bioactive natural product is important.

When reference standards are available, determination of the AC of an unknown sample of enantiomers is straightforward. For example, glucose moiety is a common moiety in natural product (e.g. saponin and flavonol glucosides). The glucose can be cleaved off by hydrolysis and derivatized with a chiral reagent. The same chiral reagent is reacted with the reference standards (D-glucose and L-glucose) to convert them into two diastereoisomers. The AC of the glucose can then be determined by comparing the retention time of its derivative with that of the two diasteroisomers in a HPLC or GC analysis. However, reference standards are generally unavailable for most of natural products, particularly, new products. Their AC determination is thus challenging. The techniques commonly used are described below.

Total synthesis has a long-history and is a classical approach to determine the AC. However, it is

challenging and time consuming. It is still considered to be the most reliable means for AC determination. In current natural product research, single-crystal X-ray diffraction (XRD) [54], nuclear magnetic resonance (NMR) with chiral shift reagents [55, 56] and chiroptical methods [57-58] are the most important and popular tools for determining the AC of novel natural products.

XRD of single crystals has been developed as a preferable and reliable technique by chemists to establish the AC of natural products, for it can "see" the arrangement of atoms in a single crystal [54]. Anomalous scattering effect introduced by Bijvoet in 1951 could be used to distinguish two enantiomers and determine the AC directly [59]. However, only heavy atoms (e.g. S, P, halogen, etc.) exhibit observable scattering, while most natural products consists of C, H, O and N exhibiting weak scattering. The magnitude of the anomalous scattering increases with the atomic number and the radiation wavelength. Thus, the scattering of a natural product containing only C, H, O and N is weak with the Mo Kα radiation but should be observable with the Cu Kα radiation [60, 61]. A large number of experiments on the basis of Cu Kα radiation have been applied to determine the AC of natural products in a crystalline form [62-64]. However, this approach is limited to a molecule that can form a crystal directly or co-crystallize with a suitable chiral reagent.

An NMR-based method for AC determination was established by Mosher in 1973 [65], and it has been developed and modified by many other researchers [55, 56]. This method transforms one chiral molecule into two diastereoisomers that have different chemical shifts by reacting it with a pair of enantiomeric chiral derivatizing agents (CDAs) respectively [61]. Differences in chemical shifts between the two diastereoisomers are represented by $\Delta\delta$, and the sign of this parameter (+ or -) provides information about the absolute configuration (Figure 5a) [56]. The CDAs are essentials to this method, and generally have following characteristics: (1) a polar or bulky group to maintain a particular conformation, (2) a functional group (e.g. carboxylic acid) for forming a covalent bond with the substrate, and (3) a group (e.g. an aromatic moiety) producing a strong and space-oriented anisotropic effect that selectively affects different regions of the substrate [56, 61]. MTPA (α-methoxy-α-trifluoromethylphenylacetic acid) (Mosher's reagent) and its acid chloride (MTPA-Cl) are the most popular CDAs. Other CDAs includes α-methoxyphenylacetic acid

(MPA). Monofunctional molecules with one alcohol, amine or carboxylic acid are commonly analyzed by using this method. In contrast, polyfunctional compounds may involve a more complex situation due to the overlap of anisotropic effects produced by two or more aromatic groups in CDAs [56, 61]. However, polyfunctional groups far apart from each other in a molecule can be considered as monofunctional [56]. The disadvantage of this approach is that a relatively large quantity of sample is required for derivatization with the two CDA enantiomers. Single derivatization methods have been developed for this reason (Figure 5b), in which a single derivative was prepared from the substrate with one enantiomer of the CDA. This method involves comparing the NMR spectrum of the derivative with that recorded at a lower temperature, or with the spectrum of the same derivative after forming a complex with a metal salt (e.g. barium) [55, 66-67]. The key to the methods lies in the modulation of the conformational equilibrium and the changes that are reflected in the NMR spectra [55].

Another approach to determine AC by NMR involves adding of chiral solvating agents (CSAs), ion-pairing agents, or metal complexes to the substrate, and comparing the differences in chemical shifts of two enantiomers [55, 61]. The sample is analyzed by NMR in a chiral environment but since there is no covalent bond between the substrate and the added chiral agent the chiral environment produces only small differences in chemical shifts for the two enantiomers that is the main limitation for this method. As a result, no clear-cut correlations between the AC and the NMR spectra can be established, and the two enantiomers must be available for their comparison. For these reasons, the application of this method is practically restricted to the determination of enantiomeric purity [55].

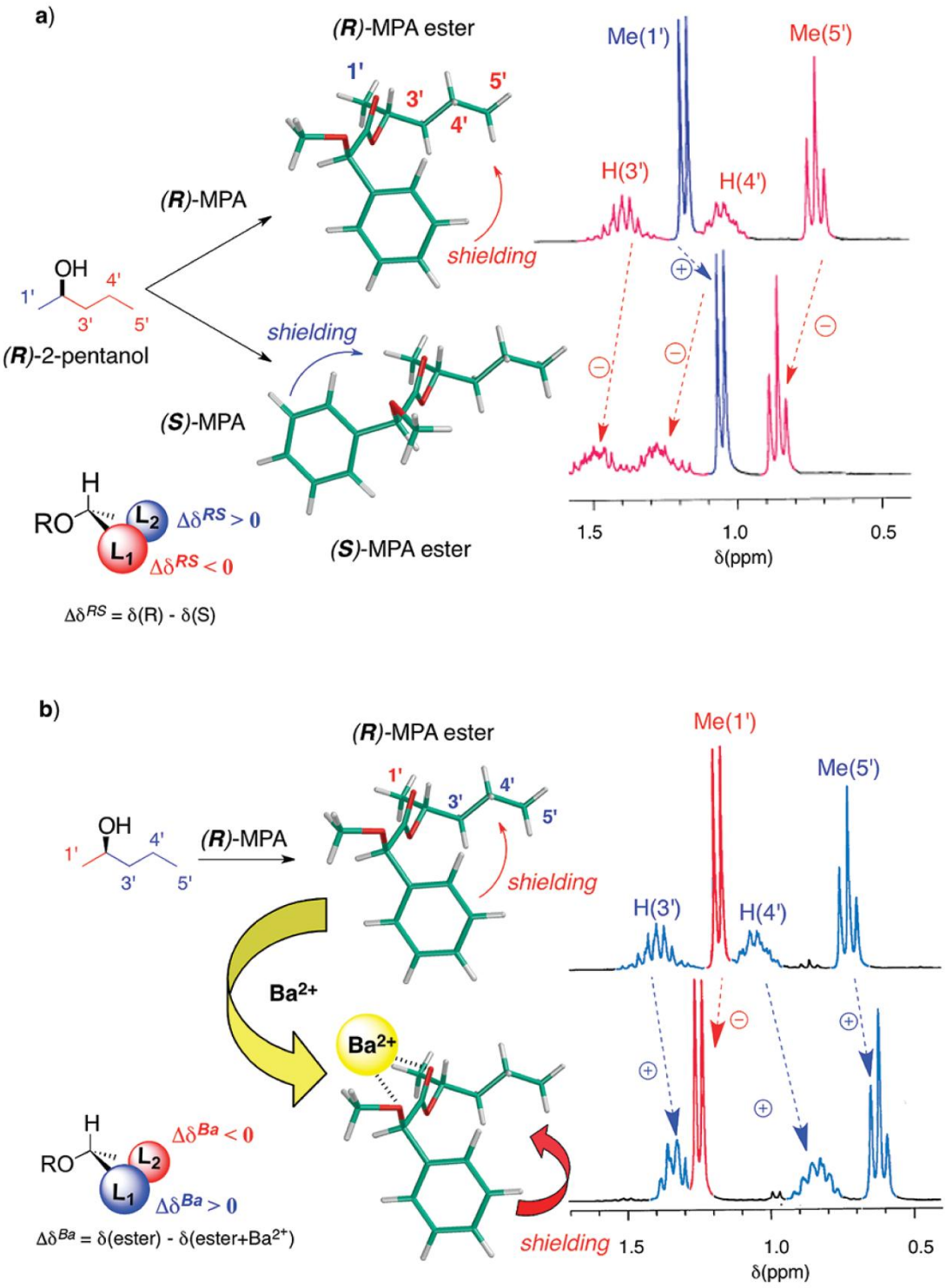

Figure 5. Assignment of the absolute configuration of a secondary alcohol using MPA by double (a) and single derivatization (b) [55].

Chiroptical-based methods involving the interactions of chiral molecules with left- and right-circularly polarized light. Optical rotation (OR) and optical rotatory dispersion (ORD) are based on the difference in velocity of circularly polarized lights through the medium (Δn), while electronic circular dichroism (ECD), vibrational circular dichroism (VCD) and Raman optical activity (ROA) depends on the difference in absorbance (ΔA or Δε). ECD concerns the absorption of UV-Vis light (electronic transition) and VCD and ROA involve the absorption at mid-IR region (vibrational transition and Raman scattering, respectively) [61]. CD is much more popular than OR (ORD) since its spectra is easier to interpret [61]. The early application of CD relied on empirical rules, such as the octant rule. Since electronic and vibrational transitions are involved in ECD and VCD respectively, the spectra can be theoretically predicted by quantum chemical calculations. With revolutionary advancements in the area of quantum chemical calculations and the availability of the super computers over the past decade, the calculation of electronic circular dichroism (ECD) spectra has become routine. [68]. The principle is based on the comparison of the time-dependent density functional theory (TD DFT) calculated CD spectrum of the most stable configuration with the experimental ECD spectra: the more closely they match, the more reliable conclusion for the AC assignment can be drawn. The most popular software for DFT calculation is Gaussian with the best performing functional and basis set B3LYP/6-31G* with a good balance between accuracy and calculation time cost [61, 68]. CD spectra are generally recorded in solution for natural products, so the conformational analysis is the most important and inevitable step in the whole process. Different conformers with the same absolute configuration may vary in their ECD band, so it is significant that all predominant conformations are identified. However, conformational analysis for those molecules with high conformational flexibility may become a very time-consuming or even impossible process due to the large number of calculations required (Figure 6) [61]. The measurement of ECD needs only μg amount of sample. This approach is limited to molecules with UV/VIS active chromophores in sufficient vicinity to the stereogenic center of interest.

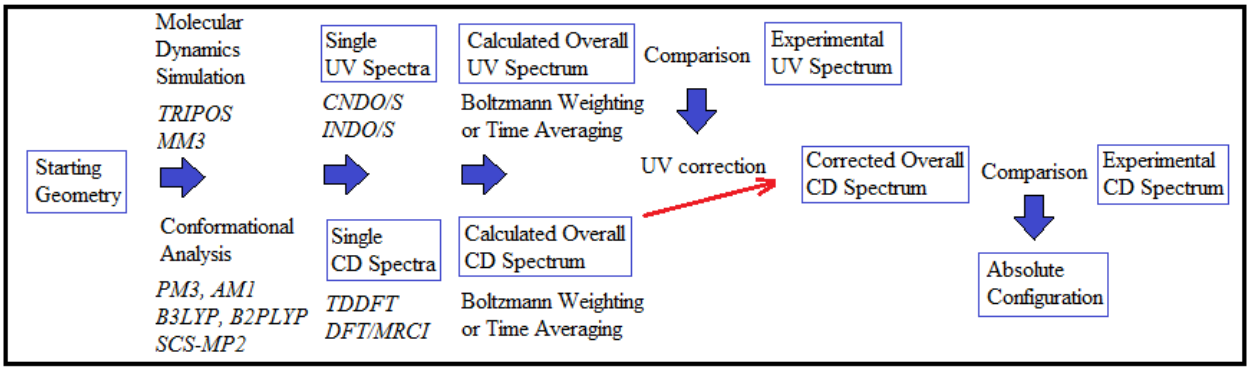

Figure 6. The principle approaches for the assignment of absolute stereostructures of chiral compounds by quantum chemical CD calculations in combination with CD measurements; the conformation-dependent chiroptical behavior is interpreted by conformational analysis or by MD simulations [69].

1.8. Preparative isolation of natural products and counter-current chromatography (CCC)

The rapid development of spectroscopic techniques, including 2D NMR methods, automated instrumentation and routine availability of X-ray crystallography, has greatly simplified the structure elucidation of natural products. However, the efficient preparative (large scale) isolation and purification of bioactive components from an exceptionally complex matrix still remain a challenge [70]. Larger quantities of purified natural products are required for biological testing (for example, ca. 2 to 5 mg of pure compound was required for the antimicrobial assay in this thesis), pharmaceuticals, standards, and starting materials for synthetic work [71].

The main purification techniques used in recent years are adhesion based (silica normal and reverse phases), size exclusion based (Sephadex LH-20) and liquid-liquid partition based (CCC) chromatography [70]. Isolation of natural products generally requires separation techniques with different mechanisms. Although liquid-solid based chromatography is widely employed, the more recently developed liquid-liquid partition based high-speed counter-current chromatography (HSCCC) is a useful complementary or alternative technique. Fractions obtained with HSCCC are often different from those obtained with liquid-solid based chromatography and can thus be efficiently simplified with silica-based phases or Sephadex (e.g. LH-20). An efficient fractionation is the prerequisite for a bio-guided isolation, which plays an important role in the discovery of minor bioactive natural products when a sensitive bioassay is not available. Furthermore, HSCCC is easy to scale up that often allows preparative isolation of larger amounts

of targeted compounds.

CCC is an all-liquid method and no solid phases are involved. The separation mechanism is based on the partition of a sample between two immiscible solvents. The relative proportion of the molecule dissolving into each of the two phases is described by the respective partition coefficients [72]. There are two basic types of CCC, the hydrostatic equilibrium system (HSES) and the hydrodynamic equilibrium system (HDES) (Figure 7).

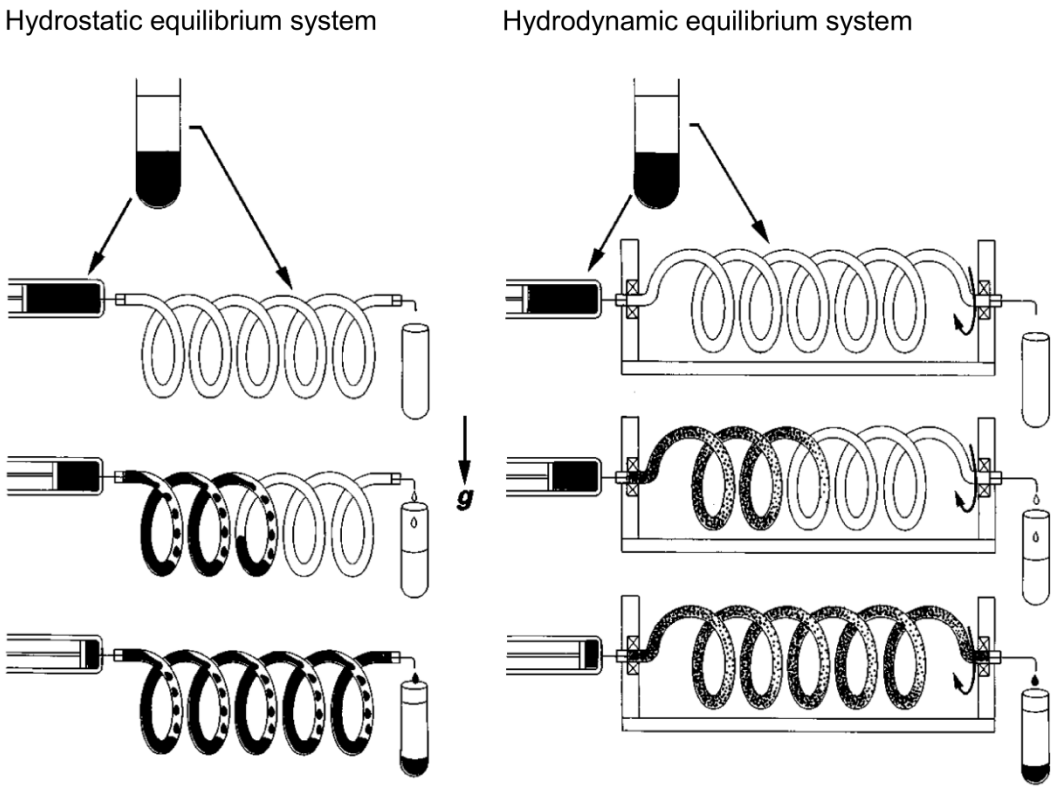

Figure 7. Basic counter-current chromatography system [71].

In the HSES system (Figure 7) [71-73], the coil is firstly filled with the stationary phase of a biphasic solvent system, and the other mobile phase is pumped through the coil without rotation at a suitable speed until no further displacement of stationary phase occurs. The apparatus contains approximately 50% of each phases and steady pump-in of mobile phase results in elution of mobile phase alone. However, this system uses only 50% of the efficient column space for actual mixing of the two phases. A more effective approach is to rotate the coil while eluting the mobile phase. A HDES (Figure 7) is rapidly established between the two phases and almost 100% of the column space is used for the actual mixing. Thus the interfacial area of the two phases is

dramatically increased. A centrifugal force is required for the rotating coil to prevent excessive loss of stationary phase due to displacement by the mobile phase. Samples can be dissolved in the mobile phase, stationary phase or a mixture of both for injection depending on the solubility. Different constituents in a natural extract or a fraction are partitioned between the two phases and are separated according to their partition coefficient. Solute retention depends only on the partition coefficient as there is no solid support.

The most widely-used machine of HDES is the high-speed counter-current chromatograph (Figure 8) [71-73]. Typical features of this rotating coil instrument are illustrated in Figure 9. A PTFE or Tefzel tube (1.6 mm or 2.6 mm i.d.) is wrapped as a coil around a spool to form a bobbin [72]. During the rotation, the coil describes a planetary motion about a central axis [71]. The holder revolves around the central axis of the centrifuge and simultaneously rotates about its own axis at the same angular velocity [71]. The planetary motion creates a heterogeneous force field which causes vigorous agitation of the two solvent phases and a repetitive mixing and settling process for solute partitioning. This may occur at over 13 times per second if the rotation speed is operated at 1500 rpm [73]. This rapid exchange permits the efficient separations with small volumes of solvent. The motion and distribution of the two phases are illustrated in Figure 10. The area in the spiral column is divided into two zones: the mixing zone occupying about one quarter of the area near the center of revolution and the settling zone in the rest of the area [73]. Thus HSCCC radically improved the resolution, separation time and sample loading capacity of CCC [70]. Multi-gram quantities of samples can be efficiently separated in several hours, and it has been used as a complementary technique to the preparative HPLC.

Figure 8. Instrumentation of high-speed counter-current chromatography.

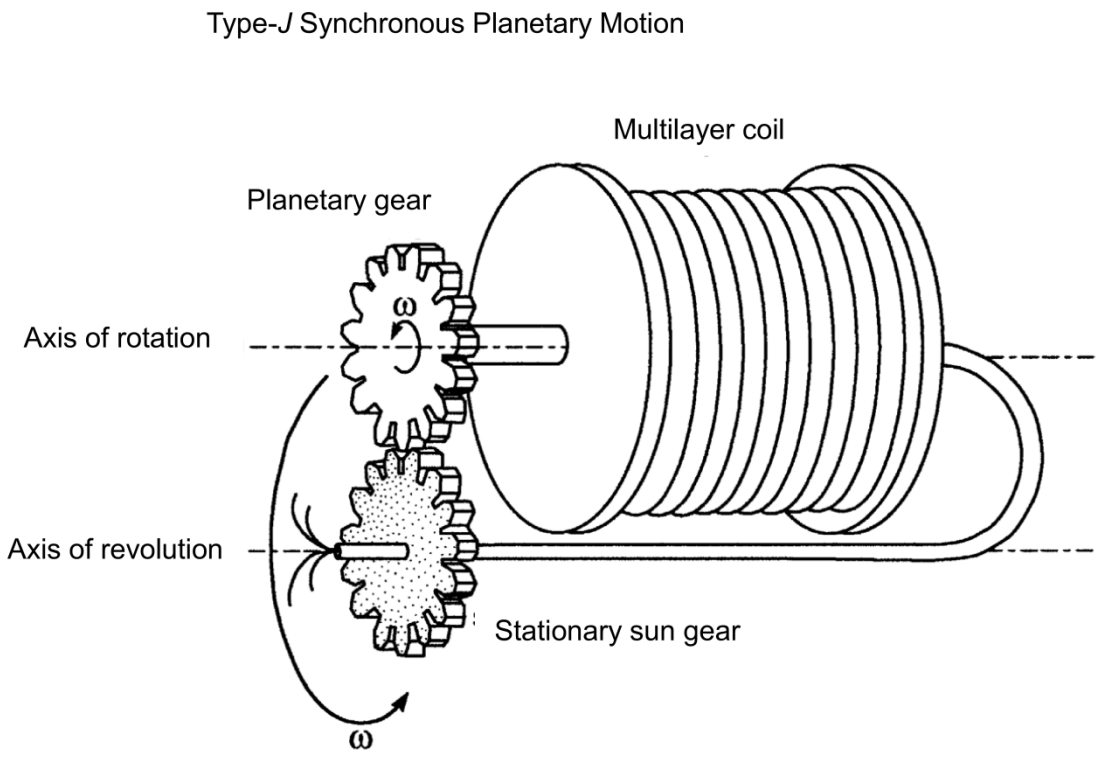

Figure 9. Type-*J* planetary motion of a multilayer coil separation column. The column holder rotates about its own axis and revolves around the centrifuge axis at the same angular velocity (ω) in the same direction. This planetary motion prevents twisting the bundle of flow tubes allowing continuous elution through a rotating column without risk of leakage and contamination [73].

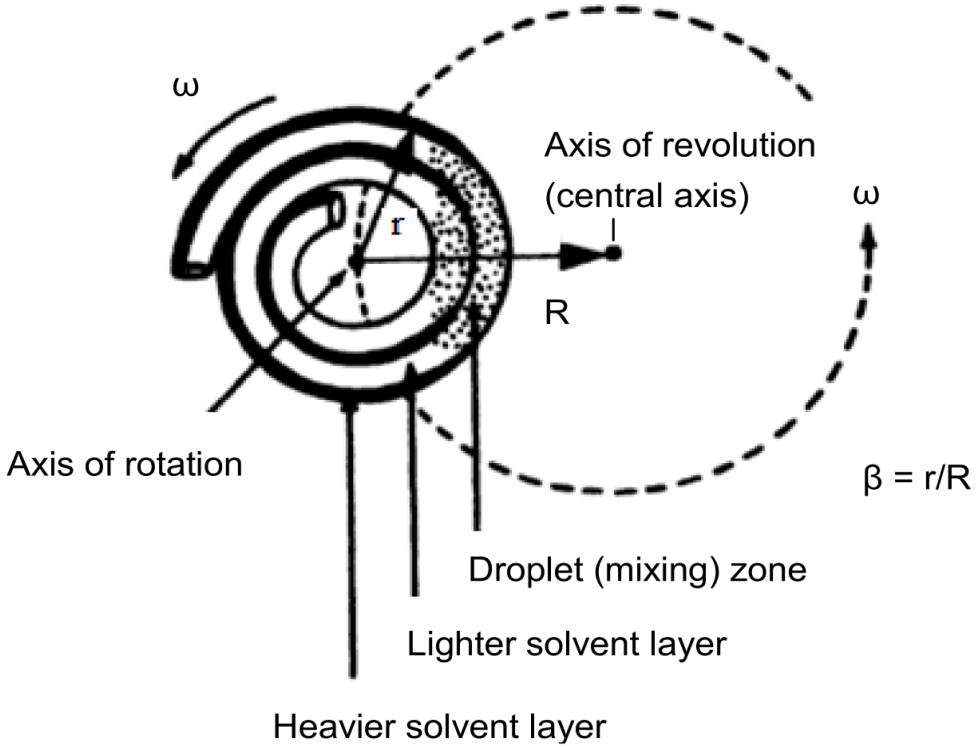

Figure 10. Planetary motion of a rotating coil (bobbin) around a central axis in HSCCC [71].

The essence of a successful CCC separation is the correct choice of the solvent system [73]. The two-phase solvent systems can be chosen theoretically from an enormous number of possible combinations of solvents, enabling separation of compounds with a wide range of polarities. The selected solvents should satisfy the following requirements [73]: (1) The settling time of the solvent system should be shorter than 30 s for satisfactory retention of the stationary phase. (2) The partition coefficient (K) of the target compounds should lie in the range of $0.5 < K < 2.0$ for an efficient separation. The separation factor between any two components ($\alpha = K_2/K_1$, $K_2 > K_1$) should be greater than 1.5. Smaller K value results in a loss of peak resolution, and larger value produces excessive band broadening. (3) To avoid wastage of solvent, it is advantageous if the chosen solvent system provides roughly equal volumes of upper and lower phases [72]. Various methods for selection of appropriate biphasic solvent systems have been reported in the literature, such as the GUESS approach [70-73].

HSCCC benefits from a number of advantages when compared to the liquid-solid separation methods [72]. No irreversible adsorption is found in this all-liquid method. The injected sample can be totally recovered if the constituents are not separated. The peak tailing common in

liquid-solid chromatography is minimized. Denature or decomposition of the sample can usually be avoided. The organic solvents used are common and relative small quantities are required, and no expensive columns are required. HSCCC is flexible, including the fact that flow-rates can be varied during a chromatographic run, solvent gradients are possible, upper and lower phases can be interchanged as mobile phases during a separation, instruments can be stopped during chromatography and re-started hours later without affecting separation efficiency [70, 72].

1.9. Searching hERG channel inhibitors from medicinal plants

hERG (human Ether-a-go-go Related Gene) codes the inner pore-forming portion of a critical membrane bound potassium (K^+) channel in heart muscle tissue [74]. This protein product forms a tetramer and each monomer has six transmembrane regions [74]. It is controlled by membrane potential and manages the K^+ ion flowing out of the cell. The rapidly activating delayed rectifier K^+ current (I_{Kr}) is created when the K^+ ions are moving across the cell membrane [74].

The potassium channel plays a part role of the ion channels in creating the cardiac action potential at the cellular level (Figure 11a) [74]. The process of the cardiac action potential consists of three stages. It is initiated with the opening of sodium (Na^+) channels with Na^+ ions flowing quickly into the cell. Rapid depolarization of the membrane potential from ca. -90 mV (the resting state) to ca. +20 mV (voltage inside the cell compared to outside) is created. This depolarization is maintained with the opening of calcium (Ca^{2+}) ion channels that allow the Ca^{2+} ions flow into the cell. Subsequent opening of the potassium ion channels with K^+ ions moving out of the cells lead to the repolarization to the initial resting state -90 mV [74]. The hERG channel is the most important potassium ion channel for repolarization [74].

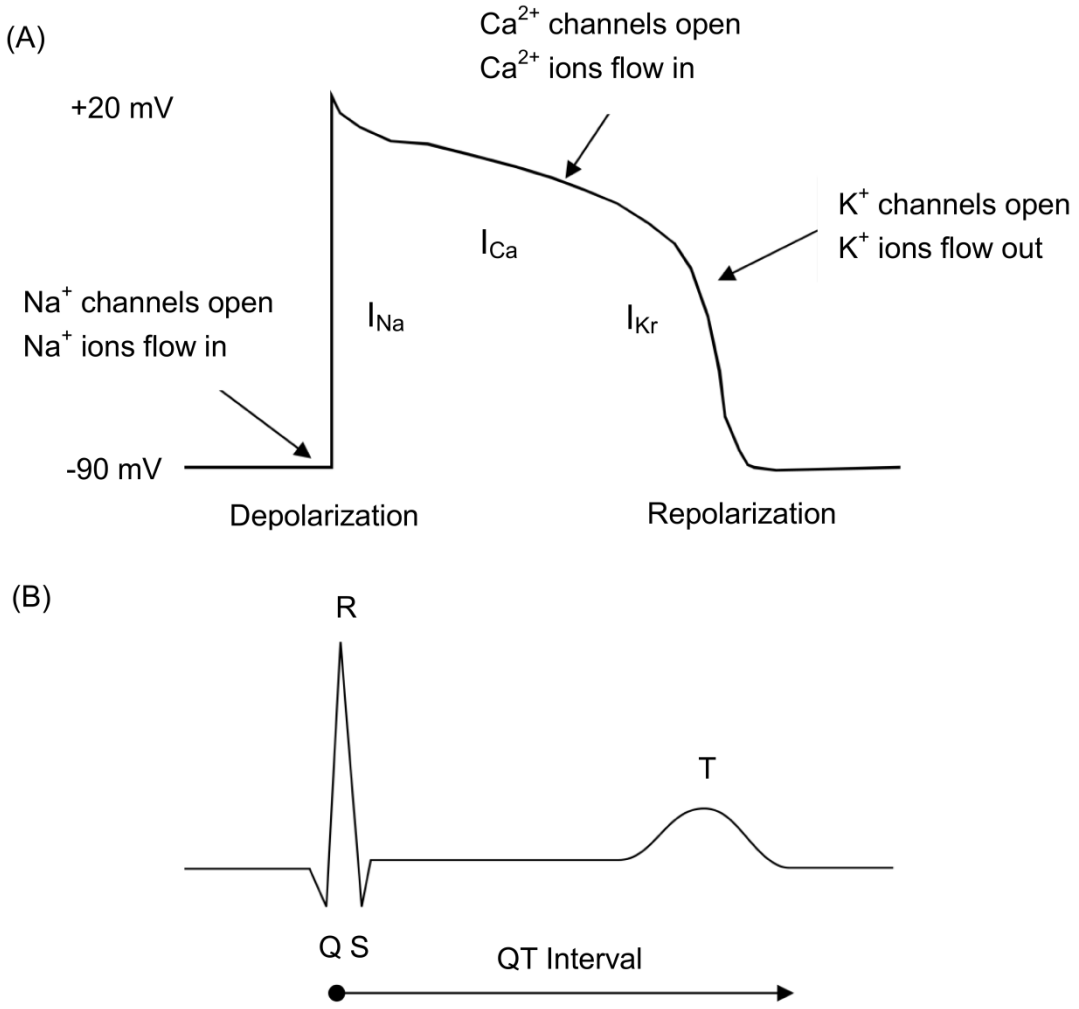

Figure 11. Cardiac action potential at the cellular level (A) and ECG on the surface of the heart (B) [74].

This action potential accounts for the overall electrical activity of the heart and is measured by an electrocardiogram (ECG) on the surface of the heart tissue (Figure 11b). The time from the point Q to point T in an ECG is called the QT interval (from depolarization to repolarization). The change in the action potential (e.g. the delay in repolarization) will be reflected on the QT interval in an ECG [74].

If the hERG K^+ channel is blocked by binding of a compound, the flow of the K^+ ions out of the cell is obstructed. This leads to the slower outflow of the K^+ ions that lengthens the time required for repolarization (Figure 13). Consequently, the T event in the ECG is delayed leading to a long QT (LQT) interval [74]. LQT may trigger a life-threatening torsadesde pointes (TdP) arrhythmia. TdP arrhythmia leads to ventricular fibrillation that can cause sudden death. Many physiological

and genetic factors also increase the chances of LQT, these including low serum K^+ levels, slow heart rate, other cardiac conditions, gender etc [74]. Some patients may have LQT without progressing to TdP, or with only slight lengthening of the QT interval. In addition, mutations in hERG leading to partial or complete loss of the channel function may further lead to LQT, TdP, and ventricular fibrillation [74].

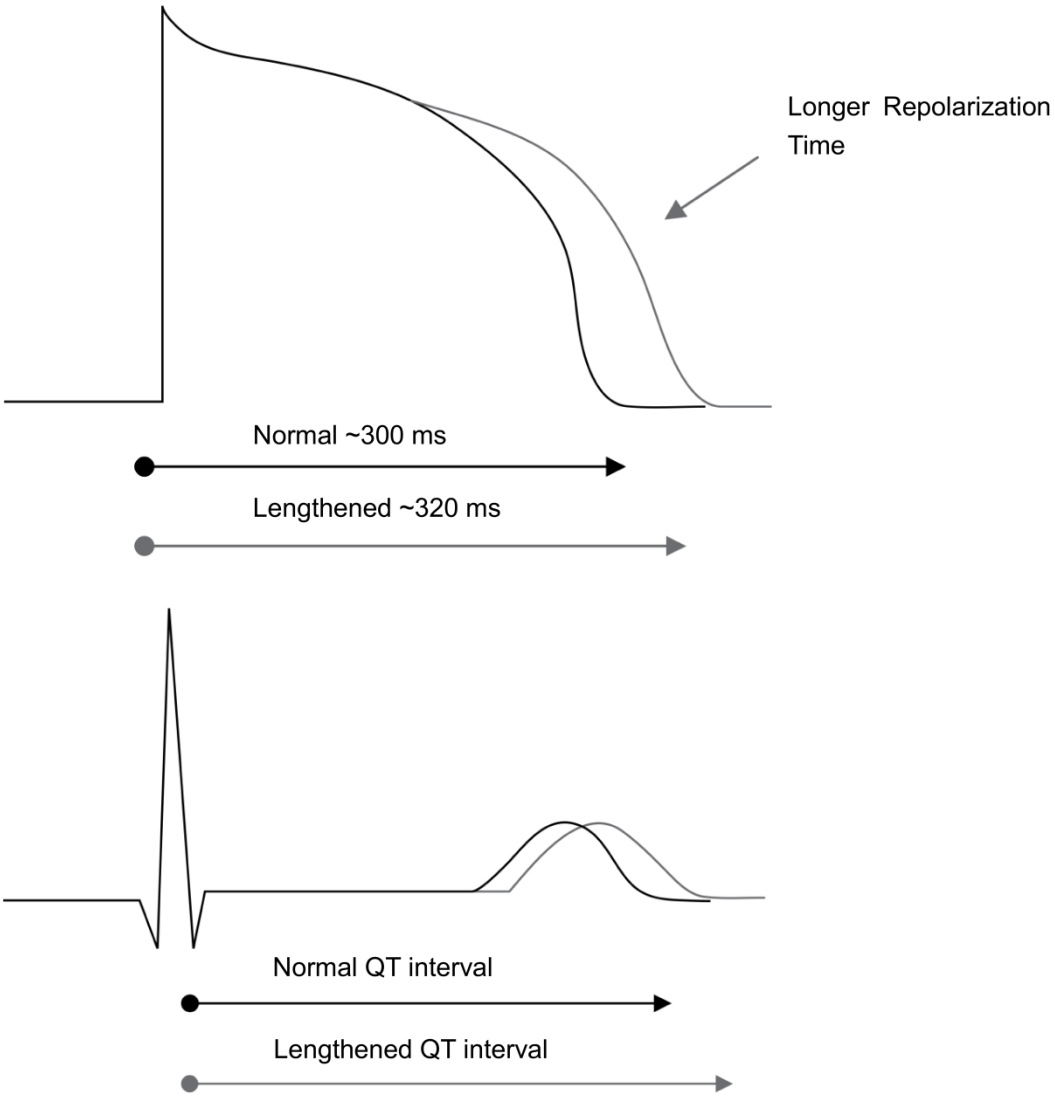

Figure 12. hERG potassium channel blocking lengthens the time until repolarization, resulting in LQT [74].

Blocking of the hERG channel can lead to cardiac arrhythmia, which may proceed to fatal cardiac arrest in a small portion of the patient population [74, 75]. In the past, such arrhythmia was observed only after the drug was approved by the Food and Drug Administration (FDA) and had been used by a large population of patients [74]. Since the mechanism of this arrhythmia was

elucidated, new drug applications can be reviewed for this side effect before approval [74]. In recent years, hERG blocking has become one of the leading causes for withdrawing drugs from the market by the FDA, or restricting their use [75]. Examples of these drugs are shown in Figure 13. Pharmaceutical companies now study this potential problem during the discovery phase [76], and screening for possible hERG liabitities is nowadays part of the early pharmacological/toxicological profiling of drug leads [76], and various in vitro and in vivo models have been established for the purpose [77].

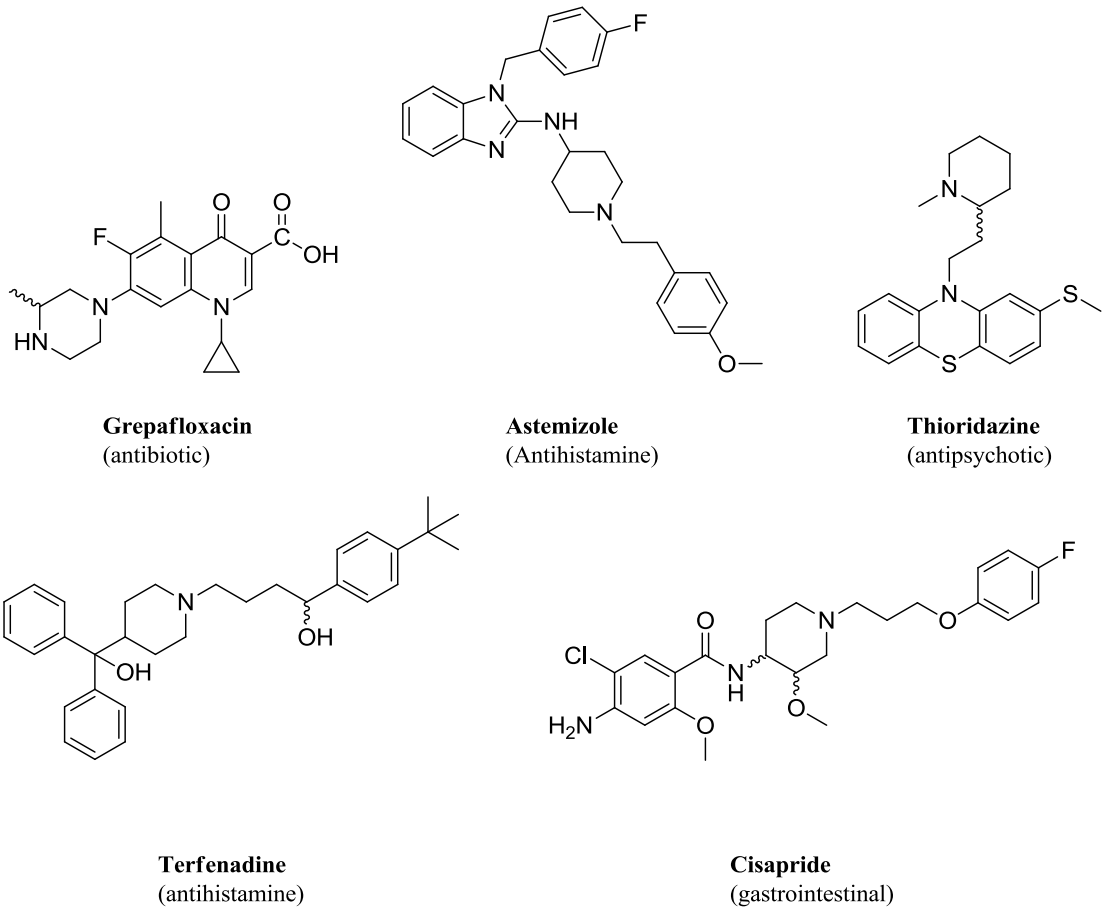

Figure 13. Commercial drugs that were withdrawn or had major labeling restrictions due to hERG blocking [74].

Comparably little is known about hERG channel inhibition by natural products. One case in point is naringenin in grapefruit juice (Figure 14). The compound occurs at high concentrations and the intake of 1L of juice has been shown to lead to QT prolongation in healthy voluteers [78-80]. Hamburger *et al.* recently screened widely used food and medicinal plants [48, 81-82], and identified the major alkaloid dihydroberberine (Figure 14) in the traditional Chinese herbal drug

Huanglian (rhizome of *Coptis chinensis* Franch., Ranunculaceae), as a compound with mild hERG inhibitory properties in the *Xenopus* oocyte assay [48]. It is noteworthy to mention that I_{Kr} blockade and proarrhythmic potential are concentration-dependent. Thus, the concomitant use of pharmaceuticals known to prolong the QT interval together with hERG channel blocking botanicals could increase the cardiotoxic risk [82]. As botanicals (comprising dietary supplements, spices, herbal medicinal products) continue to increase in popularity there is an urgent need for studies aimed to assess the potential cardiotoxic risks of these products.

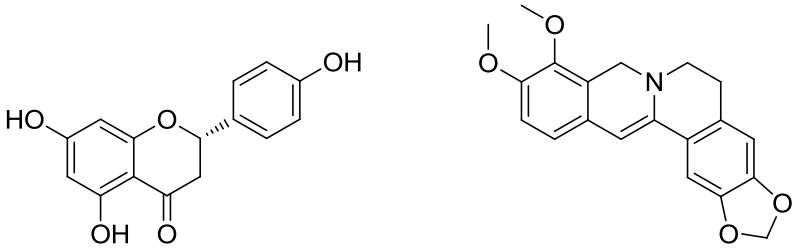

naringenin
(grapefruit juice)

dihydroberberine
(TCM drug Huanglian)

Figure 14. Naringenin from grapefruit juice and dihydroberberine from the traditional Chinese herbal drug Huanglian, as examples of hERG channel blockers found from widely used food and medicinal plants.

1.10. *Xenopus* oocyte assay

Traditional methods for screening of compound for ion channel inhibition/activation include binding assays, fluorescence-based assays and flux assays. These methods allow high-throughput but sacrifice high data quality, because they provide indirect measurements of ion channel function by monitoring changes in membrane potential or the intracellular concentration of Ca^{2+} [83]. This indirect measurement can be easily influenced by the change of the uncontrolled membrane potential and artifacts. More recent electrophysiological techniques can record the charge transfer (i.e. electrical current) during ion flux across the cell membrane upon the activation of the ion channels as a direct and quantitative measurement of the ion channel function. This provides high-resolution information about ion channel functions on a sub-millisecond timescale. The membrane potential is controlled (i.e., clamped) and the current required in order to maintain the desired membrane potential is measured [83]. However, these electrophysiological techniques also suffer from being labor-intensive and time-consuming. For instance, automated

patch-clamp instruments generally require that the target of interest is either transiently or stably expressed in a mammalian cell line. The maintenance of this cell line can be expensive. The more flexible automated two-electrode voltage-clamp (TEVC) instruments that use *Xenopus* oocytes for heterologous expression of the target of interest have circumvented some of the disadvantages [83].

Xenopus oocytes (Figure 15) are the immature egg cells of the South African clawed frog *Xenopus laevis*. They have a striking appearance with two colors, the light colored vegetal pole and the dark animal pole, where the nucleus is found [83]. *Xenopus* oocytes are easy to handle, are robust with a large diameter (1-1.2 mm) and can be readily obtained in large numbers. These properties of *Xenopus* oocytes permit the impalement of pipettes for RNA injection and repeated insertion of two fine microelectrodes used in TEVC recordings for characterizing electrogenic membrane proteins [83].

Figure 15 [83] shows the workflow from a female *Xenopus laevis* to data analysis. The oocytes are removed from the female *Xenopus laevis* by surgical excision, and defolliculated by collagenase treatment. cRNA (transcripted from cDNA) is injected into the oocytes and the molecular channel (e.g. hERG, $GABA_A$) of interest is expressed at high levels. The expressing oocytes are used for TEVC recordings to measure modulations of channel and the data are analyzed.

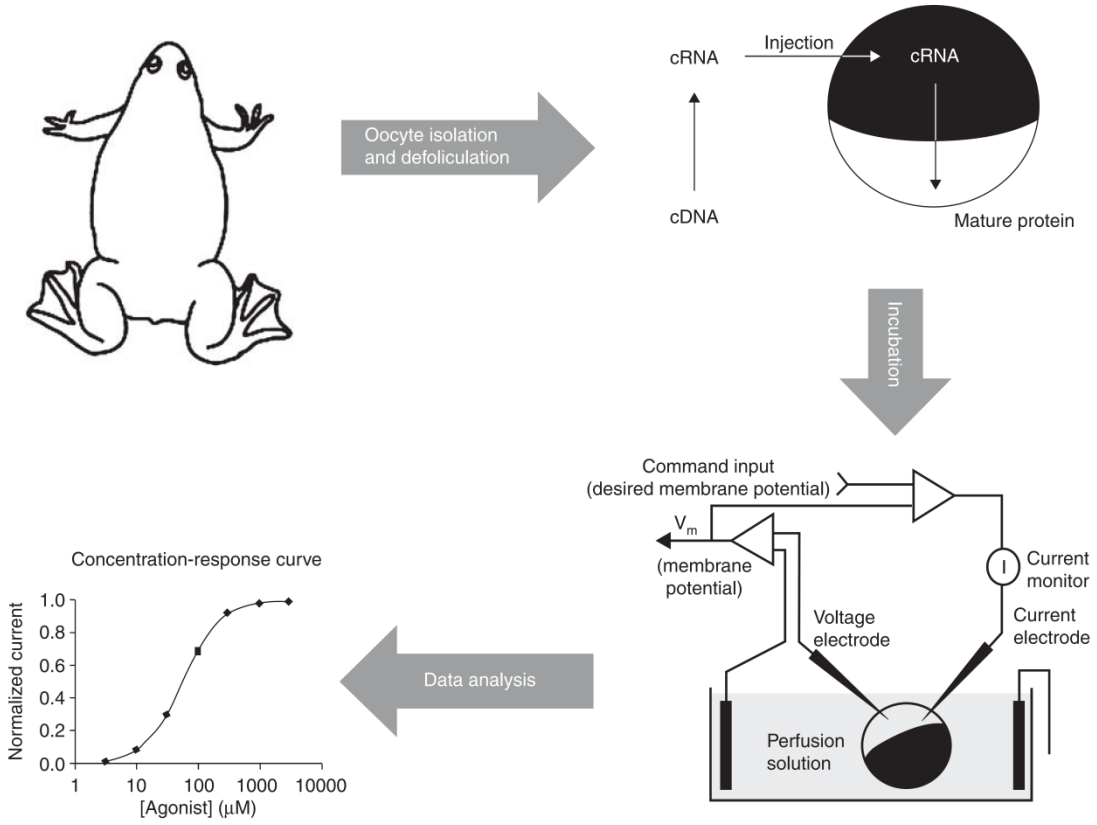

Figure 15. Schematic representation of the workflow from a female *Xenopus laevis* to data analysis [83].

In TEVC recording, the membrane potential of the oocyte is clamped at a preset value (i.e. voltage-clamped). Two electrodes impale the oocytes, one intracellular microelectrode measures the membrane potential (voltage electrode) and the other intracellular one controls the current (current electrode). The current electrode uses a feedback circuit to pass sufficient current to the oocyte for maintaining the voltage clamp. The current in current electrode measures the current flowing through the ion channels [83]. When molecular target of interest is activated and the ion channels are open/closed, the flux of ions across the cell membrane changes. The current electrode needs to pass more (or less) current in order to maintain the preset membrane potential. In this way, the amount of current flowing through the ion channels (ion channel activity) can be measured directly by the current electrode. The system used in this study in Professor Hering's laboratory in University of Vienna is shown in Figure 16 [84].

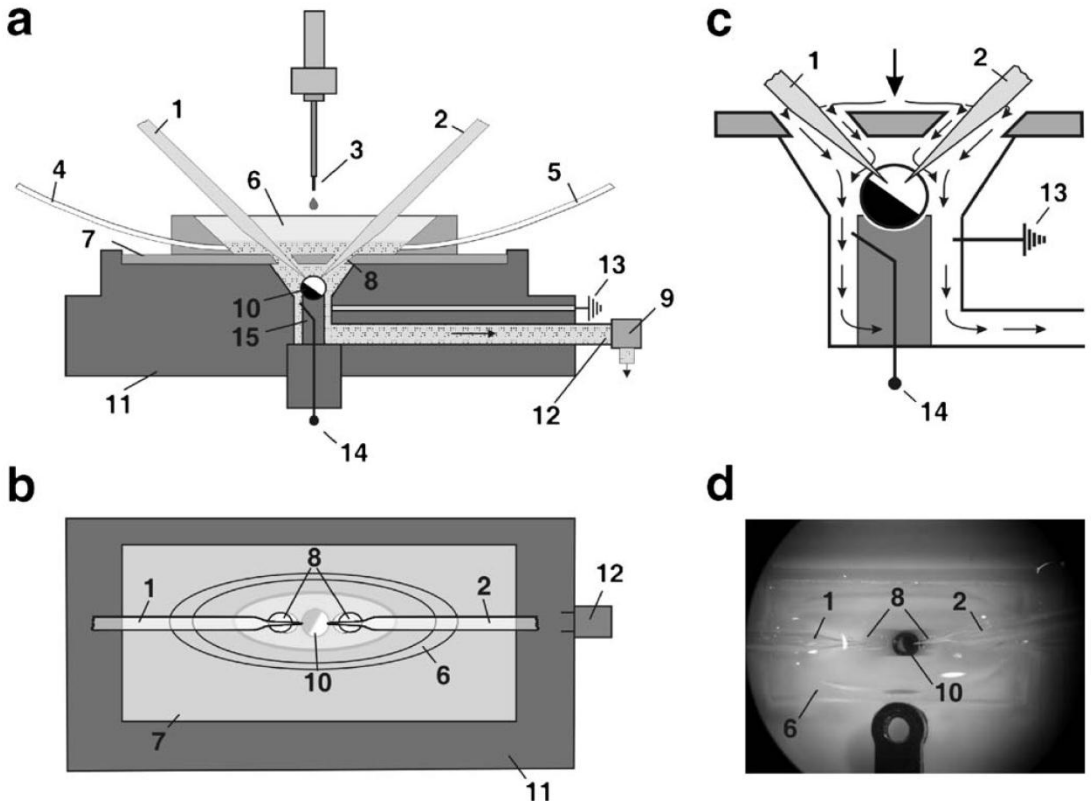

Figure 16. Cross-section view (a) and top view (b) of the oocyte perfusion chamber. Two microelectrodes (1 and 2) are inserted via the sloping access inlets (8) through a glass cover plate (7) into the small (~15 µl) oocyte chamber. Drug is applied by the tip of the liquid handling arm (3) of a TECAN Miniprep 60 to a funnel reservoir made of quartz (6) surrounding the microelectrode access holes. Perfusion of the oocyte (10) that is placed on a cylindrical holding device (15) is enabled by means of the syringe pump (9) of the Miniprep 60 connected to the chamber body (11) via the outlet (12). Residual solution is removed from the funnel before drug application via the funnel outlets (4 and 5). In addition to the ground reference electrode (13), the cylindrical holder for the oocyte contains a reference electrode (14) that serves as an extracellular reference for the potential electrode. Salt bridges can be inserted into the side outlet for the ground electrode (13). (c) Schematic drawing of the solution flow inside the perfusion chamber and in the annular gap around the cylinder with oocyte. (d) Photo of the oocyte perfusion chamber. An oocyte (10) is placed on a cylinder and impaled with two microelectrodes (1, 2) surrounded by the funnel (6) [84].

Xenopus oocyte TEVC recordings generate high-quality and reproducible data. This allows the excellent determination of concentration-response relationships (i.e. IC_{50} or EC_{50}). The current measured and ion channel function have a tight linear relationship. This permits the precise assessment of the relative efficacy of a compound (e.g. partial agonist vs full agonist). These advantages make *Xenopus* oocyte TEVC recordings a good option for in-depth analysis of the activity of a ligand on a certain target, or multiple targets [83]. In addition, the *Xenopus* oocyte expression system has high flexibility with respect to expression of the membrane protein of interest (for example, in this study we screened plant extracts for hERG channel modulation), and

relatively high expression levels can be achieved. This advantage allows rapid assessment of the activity of a specific compound or a smaller compound library on many different membrane proteins. The major disadvantage of this system is the lower throughput.

1.11. Discovery of antimicrobials from medicinal plants

Bacterial infections are an increasing problem due to the emergence and propagation of microbial drug resistance and the slow development of new antimicrobials [85]. The general misuse of antibiotics is a major factor in the emergence and dissemination of resistance [85]. In the past thirty years only two new classes of antibiotics (oxazolidinones and the cyclic lipopeptides) have entered the market for Gram-positive bacterial infections (Figure 17a), and no new anti-Gram-negative drugs have been developed [85]. Only six new antibiotics have been approved from 2003 to 2012 (Figure17b) [85].

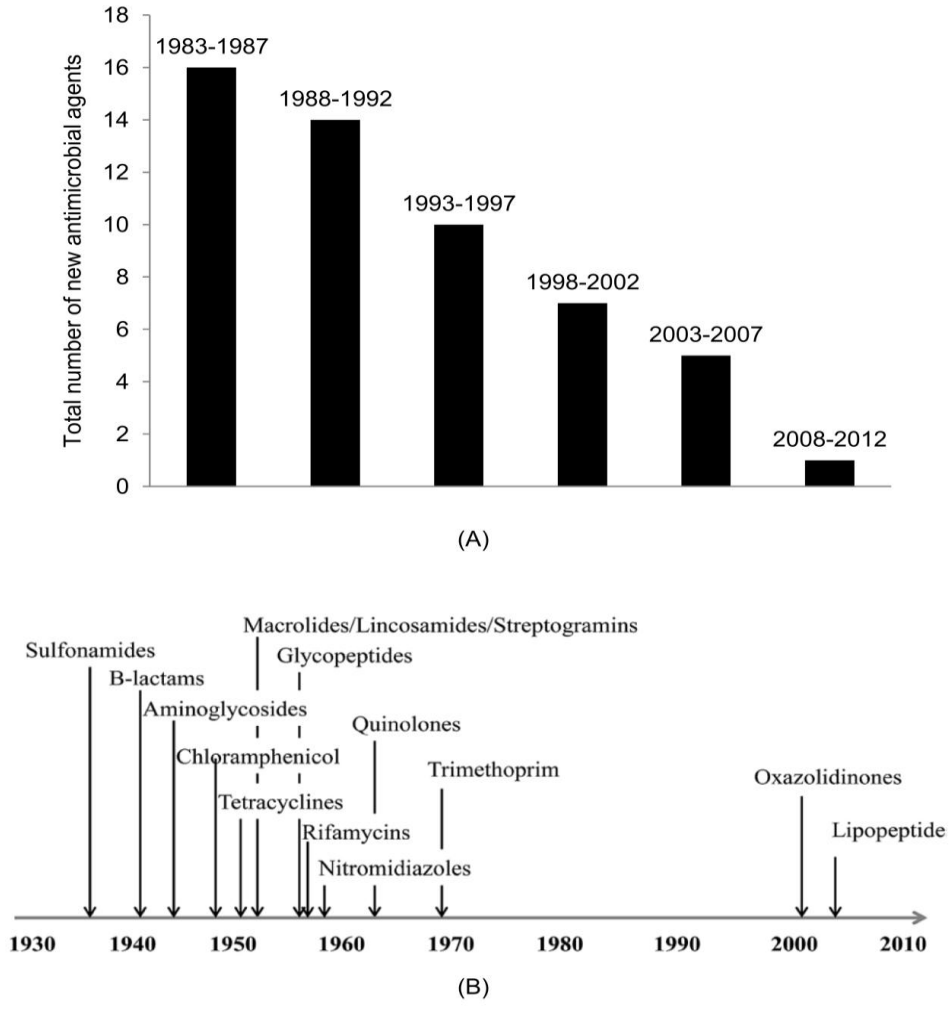

Figure 17. (A) Antibiotic approvals from 1983 to present; (B) History of antibacterial drug introductions and approval [85].

Approximately 50% of hospital-acquired infections worldwide are caused by multidrug resistant (MDR) microorganisms [85]. MDR bacteria may persist for prolonged periods and cause epidemics [85]. Among the most problematic MDR bacteria [85] are vancomycin-resistant enterococci (VRE), methicillin-resistant *Staphylococcus aureus* (MRSA), vancomycin-resistant MRSA and bacteria producing extended-spectrumb-lactamases (ESbL), such as *Pseudomonas aeruginosa*, *Helicobacter pylori*, *Acinetobacter baumannii*, *Escherichia coli* and *Klebsiella pneumoniae*. Other important MDR pathogens include *Mycobacterium tuberculosis*, *Legionella pneumophila*, penicillin-resistant *Streptococcus pneumonia*, and *Shigella* and *Salmonella* species [85]. New antimicrobials thus need to be discovered and developed urgently [86-89].

Natural products (NPs), mainly those from microorganisms, have provided the pharmaceutical industry with many important leads in the search for new antimicrobials [89, 90]. The production of effective antimicrobial compounds in an organism can give it an evolutionary advantage over the others. It is therefore not surprising that many different NPs have evolved to interact with specific antibiotic protein targets [91]. The majority of current antimicrobial drugs in clinical use are NPs or their derivatives [11, 91]. Plants may also be an effective source of antimicrobial leads. Phytochemicals may act with different mechanisms from that of conventional antibiotics, and could be valuable pharmaceuticals in the treatment of resistant bacteria [89]. The rich diversity of the phytochemicals is probably due to the evolutionary selection for improved defence mechanisms against different kinds of microorganisms, insects, nematodes and even other plants [89, 92-93]. The plant ‘‘immune systems’’ effectively prevent infections from most phytopathogens [89].

1.12. Problem statement

The use of traditional medicine (TM) still remains widespread in developing countries. For example, 80% of the population in Africa uses TM to meet their health care needs, and 40% of all health care delivered in China is from TM [94]. The use of complementary and alternative medicine (CAM) is also increasing rapidly in developed countries. The majority of the population in first world has used CAM at least once (48% in Australia, 70% in Canada, 42% in USA, 38% in Belgium and 75% in France, 2002-2005) [94]. Herbal medicine (HM) is one of the most widely

used therapies/therapeutic techniques in TM or CAM, and it has been recognized as an essential component of primary healthcare by the WHO [94]. In Germany, the overall population using HM increased from 52% in 1970 to 70% in 2010, and HM accounts for approximately 20% (about one billion euro) of the total expenditure for over the counter (OTC) drugs in 2011 [95]. The broad use of HM may due to some of its advantages. Medicinal plants are generally accessible and affordable in developing countries. In many developed countries, patients usually concern the adverse effects of synthetic drugs and question the approaches of allopathic medicine. HM is believed that may provide alternative treatments and gentler effects with the same efficacy as the synthetic drugs.

Herbal extracts are complex mixtures of organic chemicals. Their constituents are usually unknown. This has challenged the management and administrative regulations of these popular botanical products. Safety is the key issue in HM and also the core issue in pharmacology. Uncertainty of this issue often limits the regulation, standardization and modernization of the HM.

Drug-induced inhibition of the hERG channel is nowadays considered a major safety liability in preclinical drug development and clinical practice. Inhibition of the hERG channel may lead to QT prolongation which can lead to sudden death. Many drugs have been withdrawn from the market or received severe restrictions on use because of their hERG-related cardiotoxicity [75]. HM is widely accepted and assumed as natural and safe. However, little is known about hERG channel inhibitors in herbal medicine. Naringenin occurs at high concentrations in grapefruit juice, and intake of 1L of juice has been shown to lead to QT prolongation in healthy volunteers [78-80]. Another study identified the alkaloid dihydroberberine in the traditional Chinese herbal drug Huanglian (rhizome of *Coptis chinensis* Franch., Ranunculaceae) as a compound with mild hERG-inhibitory properties in the *Xenopus* oocyte assay [48]. Therefore, there is an urgent need for the extensive safety assessment of hERG channel inhibitors in HM.

This study forms part of a European Framework 7 project named “hERG related risk assessment of botanicals” to assess the potential cardiotoxic risks of commonly used plant derived products. We collected different parts of 142 medicinal plants from Southern Africa, where many people are still using a wide variety of plants in their primary health care [96] and screened the extracts for

hERG channel inhibition. We identified two plants (stems and leaves of *Galenia africana* and roots of *Gnidia polycephala*) with potent hERG channel inhibitions. The pure single chemical entities responsible for the hERG channel inhibition in the two extracts need to be identified, isolated and characterized for re-testing to confirm their inhibition activities.

New antimicrobials need to be discovered and developed urgently due to the constant evolution of resistant microorganism phenotypes, the emergence of new diseases, and toxicity associated with current antimicrobials [89]. A preliminary screen the DCM extracts of the seeds, hulls and leaves of *Colophospermum mopane* (Fabaceae) showed positive antimicrobial activities. We thus decided to identify the pure single chemical entities in these extracts responsible for the antimicrobial activity. Because our bioassays for each microorganism strain required 2 to 5 mg of pure compounds, an efficient semi-preparative isolation was required.

Despite the fact that TLC analysis of the DCM extracts of *C. mopane* (seeds, hulls and leaves) reveals an abundance of secondary metabolites, only six compounds have been isolated in the literature from the lipophilic extracts [97-99]. Aldehydes from the roots, corresponding to the alcohols of Mopaneols A and B were reported as an inseparable mixture on silica gel [97]. Some of these compounds are characterized by the presence of a carboxylic acid moiety that explains their tailing nature on silica-based chromatographic material that interferes with isolation of pure compounds. Therefore, we decided to explore the potential of HSCCC, an all-liquid technique, to isolate additional pure compounds in larger quantities from *C. mopane* to determine their antimicrobial activities. HSCCC has the particular advantage that it can be scaled up to obtain large quantities of pure materials.

References

1. *Hostettmann K, Gupta MP, Marston A, Queiroz EF.* Handbook of strategies for the isolation of bioactive Natural products. SECAB & CYTED, Colombia, **2008**.
2. *Stojanoski N.* Development of health culture in Veles and its region from the past to the end of the 20th century. Veles: society of science and art **1999**; 13-34.
3. *Salim AA, Chin YW, Kinghorn AD.* Drug discovery from plants. Bioactive molecules and medicinal plants. Springer-Verlag Berlin, Heidelberg, **2008**.
4. *Huffman MA.* Current evidence for self-medication in primates: A multidisciplinary perspective. Yearbook Phys Anthropol **1997**; 40: 171-200.
5. *Krief S, Huffman MA, Sevenet T, Hladik CM, Grellier P, Loiseau PM, Wrangham RW.* Bioactive properties of plants ingested by chimpanzees (*Pan troglodytes schweinfurthii*) in the Kibale National Park, Uganda. Am J Primat **2006**; 68: 51-71.
6. *Potterat O, Hamburger M.* Drug discovery and development with plant-derived compounds. Prog Drug Res **2008**; 65: 45, 7-118.
7. *Cragg GM, Newman DJ.* Natural products: a continuing source of novel drug leads. Biochim Biophys Acta **2013**; 1830: 3670-3695.
8. *Butler MS, Newman DJ.* Mother Nature's gifts to diseases of man: the impact of natural products on anti-infective, anticholestemics and anticancer drug discovery. Prog Drug Res **2008**; 65: 45, 7-118.
9. *Li JWH, Vederas JC.* Drug discovery and natural products: end of an era or endless frontier? Science **2009**; 325 (5937): 161-165.
10. *Nicolauo KC, Montagnon T.* Molecules that changed the world. Wiley, **2008**.
11. *Newman DJ, Cragg GM.* Natural products as sources of new drugs over the 30 years from 1981 to 2010. J Nat Prod **2012**; *75* (3): 311-335.
12. *Baker DD, Chu M, Oza U, Rajgarhia V.* The value of natural products to future pharmaceutical discovery. Nat Prod Rep **2007**; 24: 1225-1244.
13. *Vyas DM, Kadow JF.* Paclitaxel: a unique tubulin interacting anticancer agent. Prog Med Chem **1995**; 32: 289-337.
14. *Oberlies NH, Kroll DJ.* Camptothecin and taxol: historic achievements in natural products research. J Nat Prod **2004**; 67 (2):129-35.
15. *Koehn FE, Carter GT.* The evolving role of natural products in drug discovery. Nat Rev Drug Discov

2005; 4(3): 206-20.

16. *Chin YW, Balunas MJ, Chai HB, Kinghorn AD.* Drug discovery from natural sources The AAPS Journal **2006**; 8 (2): Article 28.
17. *Butler MS.* The role of natural product chemistry in drug discovery. J Nat Prod **2004**; 67: 2141-2153.
18. *Thayer A.* Bristol-Myers to settle suits. Chem Eng News **2003**; 81: 6.
19. *Clardy J, Walsh C.* Lessons from natural molecules. Nature **2004**; 432: 829-837.
20. *Lahlou M.* The success of natural products in drug discovery. Pharmacology and Pharmacy **2013**; 4: 17-31.
21. *Müller-Kuhrt L.* Putting nature back into drug discovery. Nat Biotechnol **2003**; 21: 602.
22. *Ganesan A.* The impact of natural products upon modern drug discovery. Curr Opin Chem Bio **2008**; 12: 306-317.
23. *Potterat O, Hamburger M.* Concepts and technologies for tracking bioactive compounds in natural product extracts: generation of libraries, and hyphenation of analytical processes with bioassays. Nat Prod Rep **2013**; 30: 546-564.
24. *Bouslimani A, Sanchez LM, Garg N, Dorrestein PC.* Mass spectrometry of natural products: current,emerging and future technologies. Nat Prod Rep **2014**; 31: 718-729.
25. *Seger C, Sturm S, Stuppner H.* Mass spectrometry and NMR spectroscopy: modern high-end detectors for high resolution separation techniques-state of the art in natural product HPLC-MS, HPLC-NMR, and CE-MS hyphenations. Nat Prod Rep **2013**; 30: 970-987.
26. *Molinski TF.* NMR of natural products at the ‘nanomole-scale. Nat Prod Rep **2010**; 27: 321-329.
27. *Potterat O, Hamburger M.* Natural products in drug discovery concepts and approaches for tracking bioactivity. Curr Org Chem **2006**; 10(8): 899-920.
28. *Zaugg J, Baburin I, Sommer B, Kim HJ, Hering S, Hamburger M.* HPLC-based activity profiling-Discovery of piperine as a positive $GABA_A$ receptor modulator targeting a benzodiazepine-independent binding site. J Nat Prod **2010**; 73: 185-191.
29. *Kim HJ, Baburin I, Zaugg J, Ebrahimi SN, Hering S, Hamburger M.* HPLC-based activity profiling-discovery of sanggenons as $GABA_A$ receptor modulators in the traditional Chinese drug Sang Bai Pi (*Morus alba* root bark). Planta Med **2012**; 78: 440-447.
30. *Rueda DC, Zaugg J, Quitschau M, Reich E, Hering S, Hamburger M.* Discovery of $GABA_A$ receptor modulator aristolactone in a commercial sample of the Chinese herbal drug “Chaihu” (*Bupleurum chinense* roots) unravels adulteration by nephrotoxic *Aristolochia manshuriensis* roots. Planta Med

2012; 78: 207-210.

31. *Zaugg J, Ebrahimi SN, Smiesko M, Baburin I, Hering S, Hamburger M.* Identification of $GABA_A$ receptor modulators in *Kadsura longipedunculata* and assignment of absolute configurations by quantum-chemical ECD calculations. Phytochemistry **2011**; 72: 2385-2395.
32. *Zaugg J, Khom S, Eigenmann D, Baburin I, Hamburger M, Hering S.* Identification and characterization of $GABA_A$ receptor modulatory diterpenes from *Biota orientalis* that decrease locomotor activity in mice. J Nat Prod **2011**; 74: 1764-1772.
33. *Li Y, Plitzko I, Zaugg J, Hering S, Hamburger M.* HPLC-based activity profiling for $GABA_A$ receptor modulators – a new dihydroisocoumarin from *Haloxylon scoparium*. J Nat Prod **2010**; 73: 768-770.
34. *Zaugg J, Eickmeier E, Rueda DC, Hering S, Hamburger M.* HPLC-based activity profiling of *Angelica pubescens* roots for new positive $GABA_A$ receptor modulators. Fitoterapia **2011**; 82: 434-440.
35. *Zaugg J, Eickmeier E, Ebrahimi SN, Baburin I, Hering S, Hamburger M.* Positive $GABA_A$ receptor modulators from *Acorus calamus* L., and structural analysis of (+) dioxosarcoguaiacol by 1D and 2D NMR and molecular modeling. J Nat Prod **2011**; 74: 1437-1443.
36. *Yang X, Baburin I, Plitzko I, Hering S, Hamburger M.* HPLC-based activity profiling for $GABA_A$ receptor modulators from the traditional Chinese herbal drug *Kushen* (*Sophora flavescens* root). Mol Diversity **2011**; 15: 361-372.
37. *Zimmermann S, Kaiser M, Brun R, Hamburger M, Adams M.* Cynaropicrin: the first plant natural product with *in vivo* activity against *Trypanosoma brucei*. Planta Med **2012**; 78: 553-556.
38. *Julianti T, Hata Y, Zimmermann S, Kaiser M, Hamburger M, Adams M.* Antitrypanosomal sesquiterpene lactones from *Saussurea costus*. Fitoterapia **2011**; 82: 955-959.
39. *Adams M, Gschwind S, Zimmermann S, Kaiser M, Hamburger M.* Renaissance remedies: Antiplasmodial protostane triterpenoids from *Alisma plantago-aquatica* L. (Alismataceae). J Ethnopharmacol **2011**; 135: 43-47.
40. *Zimmermann S, Thomi S, Kaiser M, Hamburger M, Adams M.* Screening and HPLC-based activity profiling for new antiprotozoal leads from European plants. Sci Pharm **2012**; 80: 205-213.
41. *Adams M, Christen M, Plitzko I, Zimmermann S, Brun R, Kaiser M, Hamburger M.* Antiplasmodial lanostane triterpenoids from *Ganoderma lucidum* mushroom. J Nat Prod **2010**; 73: 897-900.
42. *Adams M, Plitzko I, Kaiser M, Brun R, Hamburger M.* Anti-plasmodial flavonoid from *Pistacia atlantica*. Phytochem Lett **2009**; 2: 159-162.
43. *Slusarczyk S, Zimmermann S, Kaiser M, Matkowski A, Hamburger M, Adams M.* Antiplasmodial and

Antitrypanosomal Activity of Tanshinone-Type Diterpenoids from *Salvia miltiorrhiza*. Planta Med **2011**; 77: 1594-1596.

44. *Hata Y, Zimmermann S, Quitschau M, Kaiser M, Brun R, Hamburger M, Adams M.* Antiplasmodial and antitrypanosomal activity of pyrethrins and pyrethroids. J Agric Food Chem **2011**; 59: 9172-9176.
45. *Hata Y, Raith M, Ebrahimi SN, Zimmermann S, Mokoka T, Naidoo D, Maharaj V, Kaiser M, Brun R, Hamburger M.* Antiprotozoal isoflavan quinones from *Abrus precatorius ssp. Africanus*. Planta Med **2013**; 79: 492-498.
46. *Grabher P, Durieu E, Kouloura E, Halabalaki M, Skaltsounis LA, Meijer L, Hamburger M, Potterat O.* Library-based discovery of DYRK1A/CLK1 inhibitors from natural product extracts. Planta Med **2012**; 78: 951-956.
47. *Vidal V, Potterat O, Louvel S, Hamy F, Mojarrab M, Sanglier JF, Klimkait T, Hamburger M.* Library-based discovery and characterization of daphnane diterpenes as potent and selective HIV inhibitor in *Daphne gnidium*. J Nat Prod **2012**; 75: 414-419.
48. *Schramm A, Baburin I, Herring S, Hamburger M.* hERG channel inhibitors in extracts of Coptidis Rhizoma. Planta Med **2011**; 77: 692-697.
49. *Rueda DC, De Mieri M, Hering S, Hamburger M.* HPLC-based activity profiling for GABAA receptor modulators in *Adenocarpus cincinnatus*. J Nat Prod **2014**; 77(3): 640-9.
50. *Schramm A, Ebrahimi SN, Raith M, Zaugg J, Rueda DC, Hering S, Hamburger M.* Phytochemical profiling of *Curcuma kwangsiensis* rhizome extract, and identification of labdane diterpenoids as positive $GABA_A$ receptor modulators. Phytochemistry **2013**; 96: 318-329.
51. *Rueda DC, Schöffmann A, De Mieri M, Raith M, Jähne E, Hering S, Hamburger M.* Identification of dihydrostilbenes in *Pholidota chinensis* as a new scaffold for GABAA receptor modulators. Bioorg Med Chem **2014**; 22: 1276-1284.
52. *Hata Y, De Mieri M, Ebrahimi SN, Mokoka T, Fouche G, Kaiser M, Brun R, Potterat O, Hamburger M.* Identification of two new phenathrenones and a saponin as antiprotozoal constituents of *Drypetes gerrardii*. Phytochem Lett **2014**; 10: cxxxiii-cxl.
53. *Potterat O, Hamburger M.* Combined use of extract libraries and HPLC-based activity profiling for lead discovery: potential, challenges, and practical considerations. Planta Med **2014**; 80: 1171-1181.
54. *Flack HD, Bernardinelli G.* The use of X-ray crystallography to determine absolute configuration. Chirality **2008**; 20(5): 681-690.
55. *Seco JM, Quiñoá E, Riguera R.* Assignment of the absolute configuration of polyfunctional

compounds by NMR using chiral derivatizing agents. Chem Rev **2012**; 112: 4603-4641.

56. *Seco JM, Quinoa E, Riguera R.* The assignment of absolute configuration by NMR. Chem Rev **2004**; 104: 17-117.
57. *Freedman TB, Cao XL, Dukor RK, Nafie LA.* Absolute configuration determination of chiral molecules in the solution state using vibrational circular dichroism. Chirality **2003**; 15(9): 743-758.
58. *Mazzeo G, Santoro E, Andolfi A, Cimmino A, Troselj P, Petrovic AG, Superchi S, Evidente A, Berova N.* Absolute configurations of fungal and plant metabolites by chiroptical methods. ORD, ECD, and VCD studies on phyllostin, scytolide, and oxysporone. J Nat Prod **2013**; 76(4): 588-99.
59. *Bijvoet JM, Peerdeman AF, van Bommel AJ.* Determination of the absolute configuration of optically active compounds by means of X-rays. Nature **1951**; 168: 271-272.
60. *Thompson AL, Watkin DJ.* X-ray crystallography and chirality: understanding the limitations. Tetrahedron-Asymmetr **2009**; 20(6-8): 712-717.
61. *Kong LY, Wang P.* Determination of the absolute configuration of natural products. Chin J Nat Med **2013**; 11(3): 0193-0198.
62. *Xu JB, Zhang H, Gan LS, Han YS, Wainberg MA, Yue JM.* Logeracemin A, an anti-HIV daphniphyllum alkaloid dimer with a new carbon skeleton from *Daphniphyllum longeracemosum*. J Am Chem Soc **2014**; 136(21): 7631-7633.
63. *Wang GC, Zhang H, Liu HB, Yue JM.* Laevinoids A and B: two diterpenoids with an unprecedented backbone from *Croton laevigatus*. Org Lett **2013**; 15(18): 4880-3.
64. *Zhang B, Wang Y, Yang SP, Zhou Y, Wu WB, Wei T, Zuo JP, Li Y, Yue JM.* Ivorenolide A, an unprecedented immunosuppressive macrolide from *Khaya ivorensis*: structural elucidation and bioinspired total synthesis. J Am Chem Soc **2012**; 134(51), 20605-20608.
65. *Dale JA, Mosher HS.* Nuclear magnetic resonance enantiomer regents. Configurational correlations via nuclear magnetic resonance chemical shifts ofdiastereomeric mandelate, *O*-methylmandelate, and α-methoxy-α-trifluoromethyl phenylacetate (MTPA) esters. J Am Chem Soc **1973**; 95(2): 512-519.
66. *Latypov, SK, Seco, JM, Quiñoá E, Riguera R.* Are both the (*R*)- and the (*S*)-MPA esters really needed for the assignment of the absolute configuration of secondary alcohols by NMR? The use of a single derivative. J Am Chem Soc **1998**; 120(5): 877-882.
67. *García R, Seco JM, Vázquez SA, Quiñoá E, Riguera R.* Role of Barium (II) in the determination of the absolute configuration of chiral amines by ^{1}H NMR spectroscopy. J Org Chem **2006**; 71(3): 1119-1130.

68. *Li XC, Ferreira D, Ding YQ.* Determination of absolute configuration of natural products theoretical calculation of electronic circular dichroism as a tool. Curr Org Chem **2010**; 14(16): 1678-1697.
69. *Bringmann G, Bruhn T, Maksimenka K, Hemberger Y.* The assignment of absolute stereostructures through quantum chemical circular dichroism calculations. Eur. J Org Chem **2009**; 2717-2727.
70. *Sticher O.* Natural product isolation. Nat Prod Rep **2008**; 25: 517-554.
71. *Hostettmann K, Marston A, Hostettmann M.* Preparative chromatograaphy technuqes. 2nd Edition, Spronger Verlag, Berlin, **1998**.
72. *Marston A, Hostettmann K.* Developments in the application of countercurrent chromatography to plant analysis. J Chromatogr A **2006**; 1112: 181-194.
73. *Ito Y.* Golden rules and pitfalls in selecting optimum conditions for high-speed counter-current chromatography. J Chromatogr A **2005**; 1065: 145-168.
74. *Kerns EH, Di L.* Drug-like properties: concepts, structure design and methods. Academic Press, **2008**.
75. *Sanguinetti MC, Tristani-Firouzi M.* hERG potassium channels and cardiac arrhythmia. Nature **2006**; 440: 463-469.
76. *Polak S, Wiśniowska B, Brandys J.* Collation, assessment and analysis of literature in vitro data on hERG receptor blocking potency for subsequent modeling of drugs' cardiotoxic properties. J Appl Toxicol **2009**; 29: 183-206.
77. *Raschi E, Ceccarini L, De Ponti F, Recanatini M.* hERG related drug toxicity and models for predicting hERG liability and QT prolongation. Expert Opin. Drug Metab. Toxicol. **2009**, 5, 1005-1021.
78. *Scholz EP, Zitron E, Kiesecker C, Lück S, Thomas D, Kathöfer S, Kreye VAW, Katus HA, Kiehn J, Schoels W, Karle CA.* Inhibition of cardiac HERG channels by grapefruit flavonoid naringenin: implications for the influence of dietary compounds on cardiac repolarisation. Naunyn Schmiedebergs Arch Pharmacol **2005**; 371: 516-525.
79. *Lin CR, Ke XG, Ranade V, Somberg J.* The additive effects of the active component of grapefruit juice (naringenin) and antiarrhythmic drugs on hERG inhibition. Cardiology **2008**; 110: 145-152.
80. *Zitron E, Scholz E, Owen RW, Lück S, Kiesecker C, Thomas D, Kathöfer S, Niroomand F, Kiehn J, Kreye VAW, Katus HA, Schoels W, Karle CA.* QTc prolongation by grapefruit juice and its potential pharmacological basis-HERG channel blockade by flavonoids. Circulation **2005**; 111: 835-838.

81. *Schramm A, Saxena P, Chlebek J, Cahlíková L, Barburin I, Hering S, Hamburger M.* Natural products as potential Human ether-a-go-go-related gene channel inhibitors-screening of plant-derived alkaloids. Planta Med **2014**; 80: 740-746.

82. *Schramm A, Jähne EA, Baburin I, Hering S, Hamburger M.* Natural products as potential Human ether-a-go-go-related gene channel inhibitors-outcomes from a screening of widely used herbal medicines and edible plants. Planta Med **2014**; 80: 1045-1050.

83. Kvist T, Hansen KB, Bräuner-Osborne H. The use of *Xenopus oocytes* in drug screening. Expert Opin Drug Discov **2011**; 6:141-53.

84. *Baburin I, Beyl S, Hering S.* Automated fast perfusion of *Xenopus oocytes* for drug screening. Pflugers Arch Eur J Physiol 2006, **453**:117–123.

85. *Abreu AC, McBain AJ, Simoes M.* Plants as sources of new antimicrobials and resistance-modifying agents. Nat Prod Rep **2012**; 29: 1007-1021.

86. *Alekshun M N, Levy SB.* Molecular mechanisms of antibacterial multidrug resistance. Cell **2007**; 128: 1037-1050.

87. *Chan BCL, Ip M, Lau CBS, Lui SL, Jolivalt C, GanemElbaz C, Litaudon M, Reiner NE, Gong H, See RH, Fung KP, Leung PC.* Synergistic effects of baicalein with ciprofloxacin against NorA over-expressed methicillin-resistant *Staphylococcus aureus* (MRSA) and inhibition of MRSA pyruvate kinase. J Ethnopharmacol **2011**; 137: 767-773.

88. *Gibbons S.* Phytochemicals for bacterial resistance-stengths, weaknesses and opportunities. Planta Med **2008**; 74: 594-602.

89. *Simoes M, Bennett RN, Rosa EAS.* Understanding antimicrobial activities of phytochemicals against multidrug resistant bacteria and biofilms. Nat Prod Rep **2009**; 26: 746-757.

90. *Clardy J, Fischbach MA, Walsh CT.* New antibiotics from bacterial natural products. Nat Biotechnol **2006**; 24: 1541-1550.

91. *Butler MS.* Natural products to drugs: natural product-derived compounds in clinical trials. Nat Prod Rep **2008**; 25: 475-516.

92. *Dixon RA.* Natural products and plant disease resistance. Nature **2001**; 411: 834-847.

93. *Dangl JL, Jones JDG.* Plant pathogens and integrated defence responses to infection. Nature **2001**; 411: 826-832.

94. World Health Organization traditional medicine strategy 2002-2005, http://www.wpro.who.int/health_technology/book_who_traditional_medicine_strategy_2002_2005.pdf

95. *Joos S, Glassen K, Musselmann B.* Herbal medicine in primary healthcare in Germany: the patient's perspective. Evid Based Complement Alternat Med **2012**; DOI:10.1155/2012/294638.
96. *Van wyk BE, Gericke N.* People's plants, a guide to useful plants of Southern Africa. Briza, Pretoria, **2000**.
97. *Reiter E, Treadwell E, Cederstrom E, Reichardt PB, Clausen TP.* Diterpenes from *Colophospermum mopane*: ''Missing links'' in the biogenesis of 9,13-epoxylabdanes. J Nat Prod **2003**; 66, 30–33.
98. *Mebe PP.* Diterpenes from the bark and seeds of *Colophospermum mopane*. Phytochemistry **2001**; 57, 537–541.
99. *Englund BM, Griffeth L, Clausen TP.* A 9,13-epoxylabdane from *Colophospermum mopane*. Phytochem Lett **2009**; 2, 144–147.

2. RESULTS AND DISCUSSION

2.1. HPLC-Based Activity Profiling for hERG Channel Inhibitors in the South African Medicinal Plant *Galenia africana* (publication accepted by *Planta Medica*) (DOI: 10.1055/s-0035-1545929)

My contribution towards this publication: I collaborated closely with Dr Maria De Mieri on the manufacturing of the plant material extracts, HPLC microfractionation of the extract, isolation of pure compounds, recording spectroscopic and other data, structure elucidation including absolute configuration and preparation of the first draft of the manuscript.

Kun Du

HPLC-Based Activity Profiling for hERG Channel Inhibitors in the South African Medicinal Plant *Galenia africana**

Authors Kun Du[1#], Maria De Mieri[2#], Priyanka Saxena[3], Khanya V. Phungula[1], Anke Wilhelm[1], Madalina Marina Hrubaru[1], Elmarie van Rensburg[4], Pieter C. Zietsman[4,5], Steffen Hering[3], Jan H. van der Westhuizen[6], Matthias Hamburger[2]

Affiliations The affiliations are listed at the end of the article

Key words
- hERG channel inhibition
- herbal extract
- *Galenia africana*
- Aizoaceae
- HPLC-based activity profiling
- flavonoids

Abstract

The human ether-a-go-go-related gene channel is a voltage-activated K^+ channel involved in cardiac action potential. Its inhibition can lead to QT prolongation, and eventually to potentially fatal arrhythmia. Therefore, it is considered a primary antitarget in safety pharmacology. To assess the risk of human ether-a-go-go-related gene channel inhibition by medicinal plants, 700 extracts from different parts of 142 medicinal plants collected in Southern Africa were screened on *Xenopus laevis* oocytes. A CH_2Cl_2 extract from the stems and leaves of *Galenia africana* (Aizoaceae) reduced the peak tail human ether-a-go-go-related gene current by 50.4 ± 5.5% (n = 3) at a concentration of 100 µg/mL. By means of high-performance liquid chromatography-based activity profiling, nine flavonoids were identified in the active time windows. However, the human ether-a-go-go-related gene channel inhibition of isolated compounds was less pronounced than that of extract and active microfractions (human ether-a-go-go-related gene inhibition between 10.1 ± 5 and 14.1 ± 1.6 at 100 µM). The two major constituents, 7,8-methylenedioxyflavone (**1**) and 7,8-dimethoxyflavone (**13**), were quantified (4.3% and 9.4%, respectively, in the extract). Further human ether-a-go-go-related gene inhibition tests for compounds **1** and **13** at 300 µM showed a concentration-dependent inhibitory activity (33.2 ± 12.4 and 30.0 ± 7.4, respectively). In a detailed phytochemical profiling of the active extract, a total of 20 phenolic compounds, including six new natural products, were isolated and identified.

Abbreviations

hERG:	human ether-a-go-go-related gene
ECG:	electrocardiogram
TdP:	torsades de pointes

Supporting information available online at http://www.thieme-connect.de/products

received Dec. 19, 2014
revised March 9, 2015
accepted March 14, 2015

Bibliography
DOI http://dx.doi.org/10.1055/s-0035-1545929
Published online
Planta Med © Georg Thieme Verlag KG Stuttgart · New York · ISSN 0032-0943

Correspondence
Prof. Dr. Matthias Hamburger
University of Basel
Division of Pharmaceutical Biology
Klingelbergstrasse 50
4056 Basel
Switzerland
Phone: + 41 61 267 14 25
Fax: + 41 61 267 14 74
matthias.hamburger@unibas.ch

Introduction

The hERG channel is a voltage-gated potassium channel of the heart that conducts the repolarizing current I_{kr} in the action potential of cardiomyocytes. Inhibition of the human ether-a-go-go-related gene (hERG) K^+ channel by drugs can lead to QT prolongation, which is a risk factor for the development of torsades de pointes (TdP), a potentially fatal arrhythmia [1]. The hERG channel is considered a primary antitarget in safety pharmacology, since both cardiac and noncardiac drugs can potentially inhibit its repolarizing current I_{kr}. Several drugs, such as the widely used antitussive drug clobutinol have been withdrawn from the market due to proarrhythmic properties [1,2]. In industrial drug discovery, screening for a possible hERG liability is nowadays part of the early pharmacological/toxicological profiling of leads [3]. In contrast, comparably little is known about hERG channel inhibition by natural products. One case in point is naringenin in grape juice. The compound occurs at high concentrations, and an intake of 1 L of juice has been shown to lead to QT prolongation in healthy volunteers [4–6]. We recently screened a selection of widely

* Dedicated to Professor Dr. Dr. h.c. mult. Adolf Nahrstedt on the occasion of his 75th birthday.

# These authors contributed equally to this work.

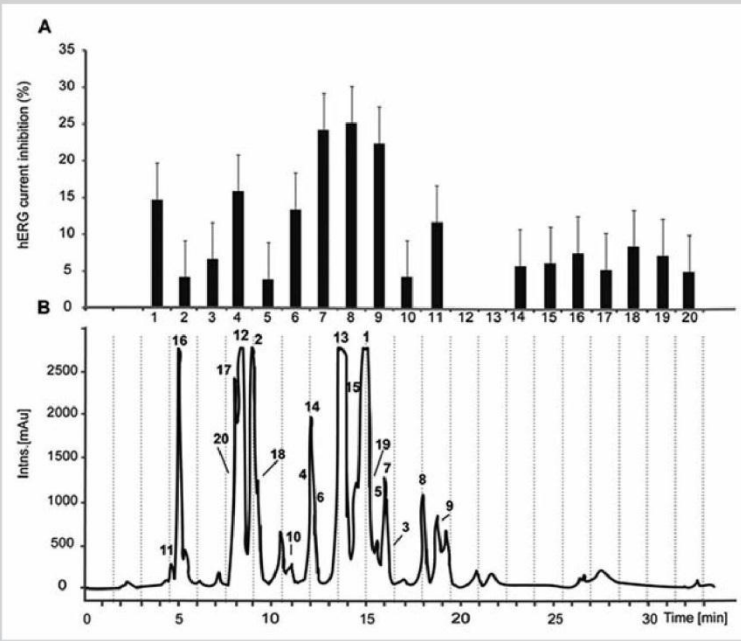

Fig. 1 HPLC-based activity profiling of the dichloromethane extract of the stems and leaves of *G. africana* for myocardic hERG channel inhibition. **A** Inhibition of hERG current by each microfraction (error bars correspond to SE). **B** HPLC chromatogram (254 nm) of semipreparative separation of the extract (5 mg). The 20 time-based fractions of 90 s each are indicated with dashed lines.

used food and medicinal plants [7], and identified the major alkaloid dihydroberberine in the traditional Chinese herbal drug Huanglian (rhizome of *Coptis chinensis* Franch., Ranunculaceae) as a compound with mild hERG inhibitory properties in the *Xenopus* oocyte assay [8].

To further assess the risk of hERG channel inhibition by medicinal plants, we screened a library of 142 South African medicinal plants. A total of 350 plant parts (roots, seeds, bark, fruits, pericarp, mesocarp, endocarp, bulb, flowers, stems, twigs, leaves, pods) were successively extracted with dichloromethane and methanol affording a library of 700 plant extracts. This library was screened in an automated functional two-microelectrode voltage-clamp assay on *Xenopus laevis* oocytes using our previously established methodology [8]. An initial concentration of 100 µg/mL was used, and extracts inhibiting the hERG current by ≥ 30% were selected for further investigation. Twelve extracts originating from seven species belonging to the Aizoaceae, Araliaceae, Fabaceae, and Thymelaeaceae families were found to be active. Among these, a CH_2Cl_2 extract of the stems and leaves of *Galenia africana* L. var. *africana* (Aizoaceae) induced 50.4 ± 5.5% (n = 3) inhibition of the peak tail hERG current at a concentration of 100 µg/mL.

G. africana is a shrub that is native to South Africa [9]. The aerial parts of the plant are traditionally used to treat venereal sores, asthma, cough, wounds, eye infections, tuberculosis, and skin diseases. Indigenous tribes chew the leaves to relieve toothaches [9,10]. Secondary metabolites such as chalcones and flavanones have been identified from the aerial parts of this plant [9,11]. We here report on the localization of hERG channel inhibitory activity in the CH_2Cl_2 extract with the aid of HPLC-based activity profiling [12,13], and on a detailed phytochemical profiling of the active extract.

Results and Discussion

The hERG channel inhibitory activity in the extract was tracked by HPLC-based activity profiling following a previously validated protocol [8,13], whereby time-based microfractions obtained from a single injection of 5 mg of extract into a semipreparative gradient HPLC was submitted to an off-line bioassay. The chromatogram (254 nm) of a semipreparative HPLC separation of the extract and the corresponding activity profile (20 microfractions of 90 s each) are shown in **Fig. 1**. hERG inhibition was assessed by a two-microelectrode voltage-clamp assay in *Xenopus* oocytes. By means of online (UV) and off-line (MS and microprobe NMR) spectroscopic analyses, the activity was correlated with peaks in the chromatogram. The strongest inhibition was observed in microfractions 7–9 that showed current inhibition values of 24.2 ± 2.5% (n = 2), 25.2 ± 3.4% (n = 2), and 22.3 ± 1.9% (n = 2), respectively. Rather unexpectedly, the hERG channel inhibition of these fractions was significantly weaker than that of the crude extract. For further pharmacological testing, compounds in the active time window were purified on a preparative scale.

Preparative medium-pressure liquid chromatography (MPLC) on silica gel afforded 13 subfractions (A–M). HPLC-ESIMS analysis on each subfraction under optimized separation conditions revealed that the extract was more complex than suggested by the time-based fractionation. Peaks with mass data and retention time fitting with the active microfractions 7–9 (**Fig. 1**) were detected in fractions F–M. Compounds **1, 3, 5–7, 13–15**, and **19** were isolated from the active time window, together with additional structurally related compounds **2, 4, 8–12, 16–18**, and **20** (**Fig. 2**). Structure elucidation was achieved by means of HRESIMS and 1D and 2D microprobe NMR spectroscopy, and the absolute configuration of compounds **4**–**7** was established by electronic circular dichroism (ECD) spectroscopy. The known compounds were identified as (+)-(2*R*,3*R*)-3-hydroxy-5-methoxy-6,7-methylenedioxyflavanone (**4**) [14], (*E*)-2′,4′-dihydroxychal-

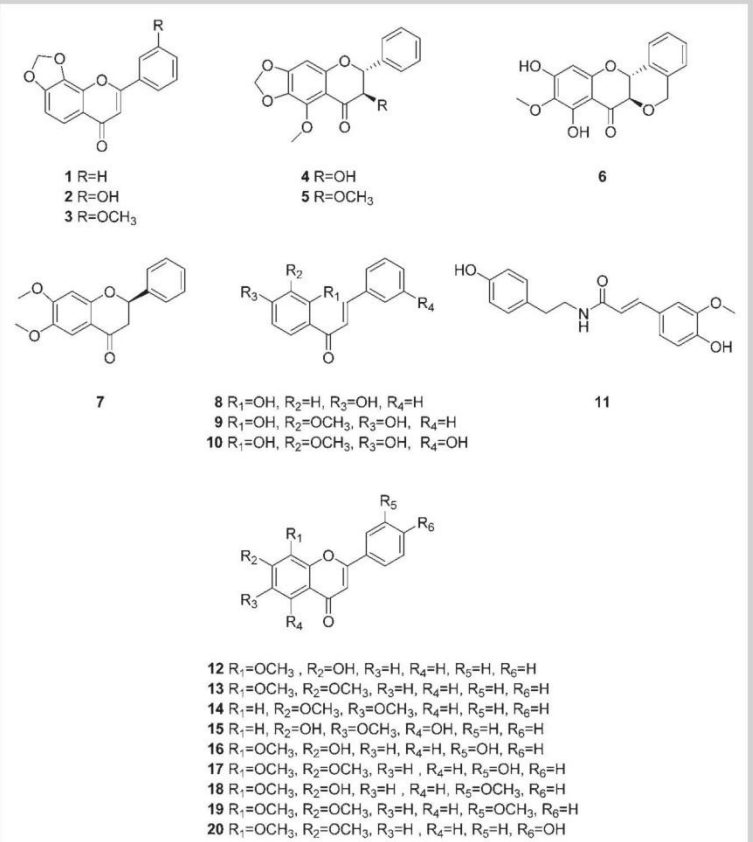

Fig. 2 Structures of compounds **1**–**20**.

cone (**8**) [15], (*E*)-2′,4′-dihydroxy-3′-methoxychalcone (**9**) [16], (*E*)-3,2′,4′-trihydroxy 3′-methoxychalcone (**10**) [11], *trans*-*N*-feruloyltyramine (**11**) [17], 7-hydroxy-8-methoxyflavone (**12**) [18], 7,8-dimethoxyflavone (**13**) [19], 6,7-dimethoxyflavone (**14**) [20], 5,7-dihydroxy-6-methoxyflavone (**15**) [21], 7,3′-dihydroxy-8-methoxyflavone (**16**) [18], and 4′-hydroxy 7,8-dimethoxyflavone (**20**) [18]. 7,8-Methylenedioxyflavone (**1**) [22,23], (2*S*)-6,7-dimethoxyflavanone (**7**) [24], and 3′-hydroxy-7,8-dimethoxyflavone (**17**) [25] have been previously described as synthetic products. Compounds **2, 3, 18**, and **19** were identified as new flavones, **5** as a new 2,3-dihydroflavonol, and **6** as a new peltogynoid. The structure elucidation of the new compounds is discussed below.

The NMR data of compounds **2** and **3** showed resonances of one olefinic methine (H-3), a carbonyl function (C-4), and a set of aromatic protons which, along with the UV maxima at 267 and 340 nm, suggested a flavonoid scaffold. Compound **2** had a molecular formula of $C_{16}H_{10}O_5$ based on HRESIMS (*m/z* 587.0976 [2 M + Na]$^+$; calculated for $C_{32}H_{20}O_{10}Na$: 587.0949) and ^{13}C NMR data. The ^1H NMR spectrum (**Table 1**) showed resonances of two vicinal aromatic methines, δ_H 7.60 (1H, d, J = 8.4 Hz, H-5) and 7.11 (1H, d, J = 8.4 Hz, H-6), and a resonance at δ_H 6.32 (2H, s), which was characteristic of oxymethylene protons. The HMBC correlation from H-5 (δ_H 7.60) to C-4 (δ_C 176.1) confirmed the location of the two *ortho*-coupled aromatic methines. Correlations from H-5 (δ_H 7.60) and H-6 (δ_H 7.11) to δ_C 152.3, and from H-6 (δ_H 7.11) to δ_C 134.6 confirmed that these carbon resonances belonged to C-7 and C-8, respectively. Correlations from oxymethylene proton δ_H 6.32 (2H, *s*) to C-7 (δ_C 152.3) and C-8 (δ_C 134.6) established the location of the methylenedioxy group. A four-proton spin system at δ_H 7.43 (1H, br d, J = 7.9 Hz, H-6′), 7.37 (1H, d, J = 2.0 Hz, H-2′), 7.35 (1H, t, J = 7.9 Hz, H-5′), and 7.00 (1H, dd, J = 7.9, 2.0 Hz, H-4′) indicated an *m*-substituted B ring and, hence, the location of a hydroxyl group at C-3′ (δ_C 158.0). This was supported by HMBC correlations from H-2′ and H-6′ to C-2 (δ_C 161.8). The structure of **2** was, therefore, established as 3′-hydroxy-7,8-methylenedioxyflavone.

Compound **3** had a molecular formula of $C_{17}H_{12}O_5$ based on HRESIMS (*m/z* 615.1296 [2 M + Na]$^+$; calculated for $C_{34}H_{24}O_{10}Na$: 615.1262) and ^{13}C NMR data. The ^1H and ^{13}C NMR spectra (**Table 1**) were similar to those of **2**, except for the presence of an additional methoxy group [δ_H 3.86 (3H, s, CH_3); δ_C 55.5]. Hence, **3** was identified as 3′-methoxy-7, 8-methylenedioxyflavone.

Compound **5** had a molecular formula of $C_{18}H_{16}O_6$, as established by HRESIMS data (*m/z* 679.1794 [2 M + Na]$^+$; calculated for $C_{36}H_{32}O_{12}Na$: 679.1786). Spectroscopic data for **5** (**Table 1**) resembled those of **4,** except for the presence of additional resonances [δ_H 3.31 (3H, *s*); δ_C 58.2] originating from a methoxy group. The attachment at C-3 (δ_C 80.5) was established by the presence of an HMBC correlation with δ_H 3.31 (3H, *s*). The remainder of the structure of **5** was supported by HMBC correlations, and was in agreement with the assignments for **4**. The large $^3J_{H,H}$ NMR coupling constant (9.2 Hz) between H-2 and H-3 in **5** indicated a *trans* configuration. The ECD spectra (**Fig. 3**) of compounds **4** and **5** were similar and exhibited the typical pat-

Table 1 ^{1}H and ^{13}C NMR spectroscopic data for compounds **2, 3, 5**, and **6** (DMSO-d_6; 500 MHz for δ_H, 125 MHz for δ_C).

	2		3		5[a]		6[c,d]	
Position	$\delta_{H\ multi}$ (*J*)	δ_C	$\delta_{H\ multi}$ (*J*)	δ_C	$\delta_{H\ multi}$ (*J*)	δ_C[a]	$\delta_{H\ multi}$ (*J*)	δ_C
2	–	161.8 106.3	–	161.5	5.38 (d, 9.2)	80.6	5.31 (d, 11.9)	74.5
3	6.78 (s)		6.95 (s)	106.8	4.24 (d, 9.2)	80.5	4.43 (d, 11.9)	75.1
4	–	176.1	–	176.2	–	188.9	–	194.1
5	7.60 (d, 8.4)	119.2	7.62 (d, 8.4)	119.3	–	142.4	–	154.4
6	7.11 (d, 8.4)	107.2	7.13 (d, 8.4)	107.4	–	132.5	–	128.8
7	–	152.3	–	152.4	–	155.4	–	157.8
8	–	134.6	–	134.7	6.42 (s)	92.5	6.24 (s)	95.0
9	–	140.3	–	140.4	–	[b]	–	157.5
10	–	119.3	–	120.0	–	[b]	–	102.3
1′	–	132.1	–	132.3	–	129.2	–	131.4
2′	7.37 (d, 2.0)	112.6	7.50 (t, 2.0)	111.3	7.47 (br d, 8.0)	126.7	–	133.7
3′	–	158.0	–	159.7	7.36–7.43 (m)	127.8	7. 10 (d, 7.5)	123.9
4′	7.00 (dd, 7.9, 2.0)	119.3	7.17 (dd, 8.0, 2.0)	117.7	7.36–7.43 (m)	128.0	7.35 (br t, 7.5)	128.5
5′	7.35 (t, 7.9)	130.3	7.49 (t, 8.0)	130.5	7.36–7.43 (m)	127.8	7.38 (br t, 7.5)	127.4
6′	7.43 (br d, 7.9)	116.9	7.58 (br d, 8.0)	118.4	7.47 (br d, 8.0)	126.7	7.70 (d, 7.5)	125.4
CH_2diox	6.32 (s)	103.7	6.32 (s)	103.7	6.05 (s)	101.4	–	–
3-OCH_2	–	–	–	–	–	–	5.03 and 5.08 (ABq, 15.2)	68.8
3-OCH_3	–	–	–	–	3.31 (s)	58.2	–	–
5-OCH_3	–	–	–	–	3.91 (s)	59.7	–	–
5-OH	–	–	–	–	–	–	11.81 (s)	–
6-OCH_3	–	–	–	–	–	–	3.97 (s)	61.0
3′-OCH_3	–	–	3.86 (s)	55.5	–	–	–	–

[a] Due to the low amount of sample, ^{13}C NMR shifts were obtained indirectly from HSQC and HMBC spectra; [b] not detected; [c] measured in $CDCl_3$; [d] semi-systematic numbering has been used; δ in ppm and *J* in Hz

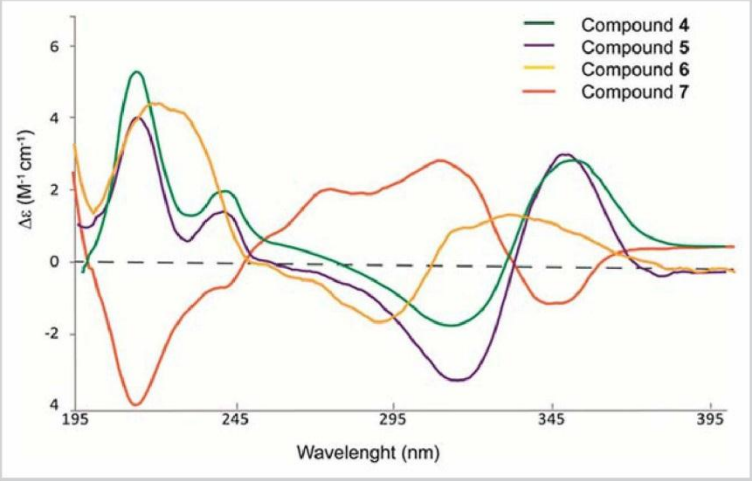

Fig. 3 Experimental ECD spectra of compounds **4**–**7**. (Color figure available online only.)

tern of (2*R*,3*R*)-dihydroflavonols, with a positive CE at 356 nm due to n→π* transitions [26]. The structure of compound **5** was, therefore, assigned as (2*R*,3*R*)-3,5-dimethoxy-6,7-methylenedioxyflavanone.

A molecular formula of $C_{17}H_{14}O_6$ was established for **6** based on HRESIMS (*m/z* 651.1524 [2 M + Na]$^+$; calculated for $C_{34}H_{28}O_{12}Na$: 651.1473) and ^{13}C NMR data. The NMR data of **6** (**Table 1**) showed resonances of two vicinal oxygenated methines at δ_H 5.31 (1H, d, *J* = 11.9 Hz, H-2) and 4.43 (1H, *d*, *J* = 11.9 Hz, H-3), a four-spin aromatic system δ_H 7.70 (1H, d, *J* = 7.5 Hz, H-6′), 7.38 (1H, br t, J = 7.5 Hz, H-5′) and 7.35 (1H, br t, *J* = 7.5 Hz, H-4′) and δ_H 7.10 (1H, d, *J* = 7.5 Hz, H-3′), two pyrano methylenic protons observed as an AB-quartet δ_H 5.08 and 5.03 (2H, J_{AB} = 15.2 Hz, CH_2-O). In addition, an isolated aromatic methine with *ortho*-oxy substituents (δ_H 6.24, s; δ_C 95.0), one aromatic methoxy group (δ_H 3.97, s; δ_C 61.0), and a carbonyl function (δ_C 194.1, C-4) were observed. Taken together, the NMR data suggested an uncommon tetracyclic dihydroflavanol skeleton. Connectivities were established by long-range H-C correlations, and corroborated by 2D NOESY (**Fig. 4**). The core A and C ring arrangement was supported by its characteristic ^{13}C NMR pattern and by a sharp singlet (δ_H 11.81) representing the hydrogen-bonded hy-

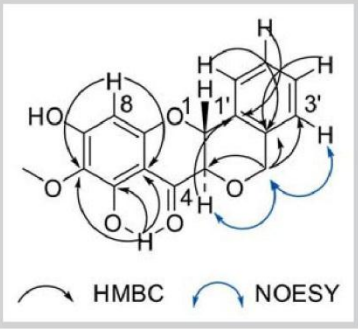

Fig. 4 Key HMBC and NOESY correlations for compound **6**. (Color figure available online only.)

droxyl proton at C-5. In the HMBC spectrum, this hydroxyl proton and the *O*-methyl protons all correlated to the carbon resonance at δ_C 128.8, thus confirming this carbon as C-6 and the location of the methoxy group. Also, correlations from both H-8 (δ_H 6.24, s) and the hydroxyl proton to δ_C 102.3 confirmed this carbon as C-10, and the location of this single resonance in ring A. The four-spin aromatic system was attributed to the protons in ring B. The linkage to ring C via an oxymethylene bridge was inferred by HMBC correlations of 3-OCH_2 to C-3 (δ_C 75.1), C-2′ (δ_C 133.7), and C-3′ (δ_C 123.9), and from H-3 to C-1′ (δ_C 131.4). This assignment was supported by the NOESY correlation between the pyrano methylene group with H-3 and H-3′. The *trans* configuration of H-2/H-3 was inferred from the large $^3J_{H,H}$ NMR coupling constant (11.9 Hz) (**Table 2**). In analogy with (2*R*,3*R*)-dihydroflavonols **4** and **5**, the ECD spectrum of **6** (**Fig. 3**) showed a negative CE at 290 nm, and a positive CE at 320–340 nm due to π→π* and n→π*transitions, respectively. Moreover, its specific optical rotation ($[\alpha]_D^{25}$ + 290.9 *c* 0. 13, $CHCl_3$) was similar to those reported for similar peltogynone derivatives [27]. The structure of **6** was, therefore, determined as (6a*R*,12a*R*)-8,10-dihydroxy-9-methoxy-6a,12a-dihydro-5*H*-isochromeno[4,3-*b*]chromen-7-one.

The structure of compound **7** matched with that of 6,7-dimethoxyflavanone, a synthetic product reported without an absolute configuration [24]. The large $^3J_{H,H}$ NMR coupling constant (11.8 Hz) between H-2 and H-3_{axial} indicated the equatorial disposition of the B ring. The ECD spectrum of **7** (**Fig. 4**), with a positive CE at 270–290 nm and a negative CE at 320–330 nm, together with a dextrorotatory optical rotation $[\alpha]_D^{25}$ + 43.8 (*c* 0. 74, $CHCl_3$), was indicative of a (2*R*)-flavanone [26]. Hence, compound **7** was identified as (2*R*)-6,7-dimethoxyflavanone.

Compound **17** had a molecular formula of $C_{17}H_{14}O_5$ based on HRESIMS (*m/z* 619.1654 [2 M + Na]$^+$; calculated for $C_{34}H_{28}O_{10}Na$: 619.1575). It was identified as 3′-hydroxy-7,8-dimethoxyflavone by analysis of its 1D and 2D NMR spectra (**Table 5S**, Supporting Information). The structure of **17** matched that of a compound reported in literature without physical-chemical characterization [25].

The UV and NMR spectra of compounds **18** and **19** also exhibited characteristic features of flavonoids. Compound **18** had a molecular formula of $C_{17}H_{14}O_5$ based on HRESIMS (*m/z* 619.1630 [2 M + Na]$^+$; calculated for $C_{34}H_{28}O_{10}Na$: 619.1575) and ^{13}C NMR data. In the ^1H NMR spectrum (**Table 2**), one olefinic methine, δ_H 6.86 (s, H-3), two vicinal aromatic methines at δ_H 7.62 (1H, d, *J* = 8.5 Hz, H-5) and 6.96 (1H, d, *J* = 8.5 Hz, H-6), a four aromatic proton spin system, δ_H 7.57 (1H, *d*, *J* = 8.0 Hz, H-6′), 7.55 (1H, d, *J* = 2.0 Hz, H-2′), 7.50 (1H, *t*, *J* = 8.0 Hz, H-5′), and 7.16 (1H, dd, *J* = 8.0, 2.0 Hz, H-4′), and two methoxy groups, δ_H 3.95 (3H, *s*) and 3.87 (3H, *s*), were observed. An HMBC correlation from H-5 to C-4 (δ_C 176.6) and C-7 (δ_C 156.7) confirmed the location of the two vicinal aromatic methines and, hence, the aromatic spin system at the B ring. The location of the methoxy group at δ_H 3.95 was assigned via a mutual HMBC correlation with H-6 to the highly shielded quaternary carbon δ_C 135.1 (C-8). The attachment at C-3′ of the methoxy function resonating at a higher field (δ_H 3.87) was confirmed through the HMBC correlation H-5′/C-3′. The structure of **18** was, therefore, established as the new compound 7-hydroxy-8,3′-dimethoxyflavone.

Compound **19** had a molecular formula of $C_{18}H_{16}O_5$ based on HRESIMS (*m/z* 647.1916 [2 M + Na]$^+$; calculated for $C_{36}H_{32}O_{10}Na$: 647.1888) and thus differed from **18** by 12 units. NMR data for **19** (**Table 2**) resembled those of **18**, except for the presence of additional resonances at δ_H 3.96 (3H, s) and δ_C 56.6 of a methoxy

Table 2 ^1H and ^{13}C NMR spectroscopic data for compounds **18** and **19** (DMSO-d_6; 500 MHz for δ_H, 125 MHz for δ_C).

	18		**19**	
Position	**$\delta_{H\ multi}$ (*J*)**	**δ_C**	**$\delta_{H\ multi}$ (*J*)**	**δ_C**
2	–	161.3 106.6	–	161.9
3	6.86 (s)		6.96 (s)	106.7
4	–	176.6	–	176.9
5	7.62 (d, 8.5)	120.1	7.78 (d, 9.0)	120.3
6	6.96 (d, 8.5)	115.9	7.27 (d, 9.0)	110.9
7	–	156.7	–	156.6
8	–	135.1	–	136.4
9	–	150.7	–	149.9
10	–	116.8	–	118.0
1′	–	133.0	–	132.7
2′	7.55 (d, 2.0)	111.2	7.55 (dd, 2.0, 1.5)	111.3
3′	–	159.7	–	159.7
4′	7.16 (dd, 8.0, 2.0)	117.3	7.17 (ddd, 8.0, 2.0, 0.7)	117.6
5′	7.50 (t, 8.0)	130.5	7.51 (t, 8.0)	130.5
6′	7.57 (d, 8.0)	118.3	7.63 (ddd, 8.0, 1.5, 0.7)	118.0
R_1	3.95 (s)	60.8	3.96 (s)	61.2
R_2	–	–	3.96 (s)	56.6
R_5	3.87 (s)	55.4	3.86 (s)	55.4

δ in ppm and *J* in Hz

group. Thus, compound **19** was identified as 7,8,3′-trimethoxyflavone.

Among the compounds isolated from the active time window, compounds **1, 7, 13, 14**, and **15** were obtained in sufficient amounts for testing in the oocyte assay at a concentration of 100 µM. All compounds displayed weak and comparable hERG blocker activity [13.1 ± 0.2% (**1**); 11.4 ± 3.3% (**7**); 10.1 ± 5.0% (**13**); 14.1 ± 1.6% (**14**); 12.6 ± 1.5% (**15**)]. Considering that compounds **1** and **13** were the by far the most abundant compounds in the active time window and corresponded to the two dominant peaks in the UV chromatogram of the extract (t_{Rs} = 13.5 and 14.8 min) (**Fig. 1B**), we hypothesized that the pronounced activity of the extract was imputable to their high concentration.

The content of compounds **1** and **13** in the DCM extract was determined by HPLC (Supporting Information) and found to be 43.02 ± 0.01 mg/g extract (4.3%) and 94.31 ± 0.02 mg/g extract (9.4%), respectively. Additional experiments were performed with **1** and **13** at 300 µM (**Fig. 5**), which confirmed hERG inhibitory activity for both compounds [inhibition by 33.2 ± 12.4% (**1**) and 30.0 ± 7.4% (**13**)]. One has, however, to consider that drugs are generally less potent on ion channels expressed in *Xenopus* oocytes compared to channels expressed in either mammalian cells or even native tissues. This decrease in potency is likely due to the presence of a large amount of yolk particles inside the oocyte membrane which may absorb the drugs, thereby reducing the effective intracellular free drug concentration [28, 29]. Compounds **1** and **13** induced only about a 30% block when applied at a high concentration (300 µM). Higher concentrations were considered to be less relevant and, therefore, were not tested. The known hERG blocker propofenone, used as a positive control, showed an IC_{50} of 3.8 ± 0.2 µM in the *Xenopus* oocyte model [30]. Proarrhythmic properties of different flavonoids due to hERG inhibitory activity have been recently reported. Naringenin, the major flavonoid in pink grapefruit juice, was identified as a hERG channel blocker in a *Xenopus* oocyte assay among several dietary flavonoids. Naringenin blocked the current with an IC_{50} of 102.3 uM [4] suggesting, however, a comparably low affinity of the hERG channel for this compound [6]. The prolongation of the QT interval observed in volunteers after consumption of grapefruit juice was due to the very high amount of naringenin ingested by this means.

Our study provided further evidence on the potential effect of flavonoids on cardiac electrophysiology. Flavonoids in *G. africana* showed a low-affinity block *in vitro*, suggesting a low risk for hERG-mediated cardiotoxicity for this medicinal plant. However, similar to naringenin, the concentration-dependent inhibition of **1** and **13** emphasizes the need for a more extensive safety assessment of traditional herbal remedies, considering that additive effects of natural products like naringenin and antiarrhythmic drugs have been reported [5].

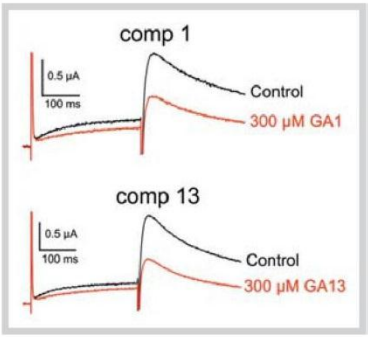

Fig. 5 Representative current traces illustrating the inhibition of the hERG potassium current by 300 µM of compounds **1** and **13**. (Color figure available online only.)

Materials and Methods

Chemicals and general experimental procedures

HPLC grade methanol (MeOH), acetonitrile (MeCN) (Scharlau Chemie S.A.), and water (obtained by an EASY-pure II from Barnstead water-purification system, Dubuque) were used for HPLC separations. For analytical separations, HPLC solvents contained 0.1% HCOOH (Scharlau). Dimethylsulfoxide (DMSO) (Scharlau) was used for dissolving the samples. Chloroform-*d* (100 atom% D) and DMSO-d_6 (100 atom% D) for NMR were purchased from Armar Chemicals. Solvents used for extraction were of analytical grade (Romil Pure Chemistry). HPLC-PDA-MS analyses were performed with an Agilent 1100 system consisting of a degasser, a quaternary pump, a column oven, and a PDA detector connected to a Gilson 215 injector and an Esquire 3000 plus ion trap mass spectrometer (Bruker Daltonics). Data acquisition and processing were performed using HyStar 3.0 software (Bruker Daltonics). Flash chromatography was carried out with a PuriFlash® 4100 chromatography system (Interchim) controlled by InterSoft V5.0 software. Preparative HPLC was carried out on a Shimadzu LC-8A instrument equipped with an SCL-10A VP system controller, an LC-8A pump, an SPD-M10A VP PDA detector, and VP 6.14 SP2A control software. Semipreparative HPLC was performed with an Agilent 1100 series instrument equipped with a PDA detector. Data acquisition and processing were done with HyStar 3.2 software (Bruker Daltonics). For HR-ESIMS, a micrOTOF ESI-MS system (Bruker Daltonics) was used. Mass calibration was performed with a solution of formic acid 0.1% in 2-propanol/water (1 : 1) containing 5 mM NaOH. Mass spectra were recorded in the range of *m/z* 150–1500 in the positive ion mode with the aid of micrOTOF control software 1.1 (Bruker Daltonics). NMR spectra were recorded on a Bruker AVANCE III™ 500 MHz spectrometer equipped with a 1-mm TXI microprobe (^{1}H and 2D NMR) or a 5-mm BBO probe (^{13}C NMR) (Bruker BioSpin) operating at 500.13 (^{1}H) and 125.77 MHz (^{13}C). All measurements were carried out at 291.15 K. Chemical shifts are reported as δ values (ppm) with the residual solvent signal as the internal reference. *J* in Hz standard pulse sequences from Topspin 3.0 software package were used. Further spectroscopic data were acquired on a Hewlett Packard 8453 Photometer (UV) and a Chirascan CD spectrometer, and analyzed with Pro-Data V2.4 software (CD) and a Perkin Elmer polarimeter (model 341) equipped with a 1 dm microcell (OR).

Plant material

The stems and leaves of *G. africana* were collected in the Nossob river between Molopo Lodge and Twee Rivieren, Gordonia Magisterial District (Northern Cape Province), South Africa, in March 2010 by Dr Pieter C. Zietsman, Natural History Museum and University of the Free State, Bloemfontein, South Africa. A voucher specimen (NMB 26707) was deposited in the herbarium of the National Museum, Bloemfontein, South Africa (NMB).

Extraction

The air-dried stems and leaves (290 g) were frozen with liquid nitrogen and ground with a ZM1 ultracentrifugal mill (Retsch). The powdered plant material was percolated at room temperature

with DCM. Evaporation under reduced pressure afforded a crude extract (15.0 g).

Microfractionation and activity profiling

Time-based microfractionation for HPLC-activity profiling was performed as previously described [4], with minor modifications. Separation was done on a SunFire™ C18 column (5 µm, 10 × 150 mm, Waters) with H_2O (A) and MeCN (B) using the following gradient profile: 30% → 40% B (0–5 min), 40% → 60% B (5–25 min), 60% → 100% B (25–26 min), 100% B (26–35 min). The flow rate was 4 mL/min. 100 µL of a stock solution of the extract (50.3 mg/mL in DMSO) was injected. Twenty time-based microfractions of 90 s each were collected by the aid of an F204 fraction collector (Gilson). After solvent removal (GeneVac EZ-2 Plus evaporator), the dried films were redissolved in methanol, transferred to a 4-mL glass vial, and dried again under N_2 gas prior to dissolution in DMSO for the bioassay.

Isolation of compounds 1–20

The DCM extract (13.5 g) was separated by flash chromatography on a silica gel (60–200 µm) column (5 × 35 cm) with a gradient [n-hexane (A) and ethyl acetate (B); 5% → 100% B (0–3 h) and 100% B (3–3.5 h); collection 22 mL each] at a flow rate of 50 mL/min. The combination of fractions was based on TLC analysis [Fr. A (1.636 g), Fr. B (0.883 g), Fr. C (1.404 g), Fr. D (0.890 g), Fr. E (0.814 g), Fr. F (1.382 g), Fr. G (0.261 g), Fr. H (0.159 g), Fr. I (0.843 g), Fr. J (0.249 g), Fr. K (0.222 g), Fr. L (1.643 g), Fr. M (1.559 g)]. Fractions A–M were analyzed by HPLC-PDA-MS on a SunFire™ RP-C18 column (3.5 µm, 3.0 mm × 150 mm, Waters) with a gradient [0.1% formic acid in H_2O (A) and MeCN (B); 30% → 40% B (0–5 min), 40% → 60% B (5–25 min), 60% → 100% B (25–26 min), 100% B (26–35 min); flow rate 0.4 mL/min]. Fractions F to M were found to contain the compounds of the active time window.

Fraction E (469 mg) was separated by open column chromatography (18 × 2 cm) on silica gel (60–200 µm) with $CHCl_3$ to give E_1–E_{16}. The purification of the subfraction E_4 (32 mg) was done by semipreparative HPLC [SunFire™ C18 column (5 µm, 10 × 150 mm, Waters)] with a gradient [H_2O (A) and MeCN (B); 30% → 40% B (0–5 min), 40% → 60% B (5–25 min), 60% → 100% B (25–26 min), 100% B (26–35 min); flow rate 4 mL/min; sample conc. 32 mg/mL in DMSO; injection volume 200 µL] to give **7** (9.5 mg, t_R 17.0 min). The purification of subfractions E_7 (9.6 mg) [sample concentration (48 mg/mL) and injection volume (100 µL)] and E_{11} (9.0 mg) [sample concentration (45 mg/mL) and injection volume (100 µL)] was done as for subfraction E_4 to afford **9** (6.6 mg, t_R 21.5 min) and **8** (6.6 mg, t_R 19.5 min), respectively.

Fraction I (150 mg) was separated on a Sephadex LH-20 column (31 × 4 cm) with EtOAc (flow rate 0.6 mL/min) to afford subfractions I_1-I_8 based on TLC analysis. Purification of I_2 (18.0 mg) by semipreparative HPLC [SunFire™ C18 column (5 µm, 10 × 150 mm, Waters)] with a gradient [H_2O (A) and MeCN (B); 20% → 50% B (0–10 min), 50% B (10–35 min), 50% → 100% B (35–40 min), 100% B (40–43 min); flow rate 2 mL/min; sample conc. 36 mg/mL in DMSO; injection volume 150 µL] gave **5** (1 mg, t_R 28.0 min). Fraction I (50 mg) was again purified by semipreparative HPLC [SunFire™ C18 column (5 µm, 10 × 150 mm, Waters)] with a gradient [0.1% formic acid in H_2O (A) and MeCN (B); 20% → 35% B (0–5 min), 35% B (5–40 min); flow rate 4 mL/min; sample conc. 50 mg/mL in DMSO; injection volume 100 µL] to afford **10** (5 mg, t_R 20.0 min), **4** (1 mg, t_R 23.5 min), **6** (1 mg, t_R 24.5 min), **15** (5 mg, t_R 31.0 min), **1** (8.1 mg, t_R 34.0 min), and subfraction I_9 (2.0 mg, t_R 39.0 min). The precipitate (1 mg) from an MeOH solution of I_9 was subjected to semipreparative HPLC [SunFire™ C18 column (5 µm, 10 × 150 mm, Waters)] with a gradient [H_2O (A) and MeCN (B); 20% → 30% B (0–5 min), 30% → 50% B (5–25 min), 50% → 100% B (25–26 min), 100% B (26–35 min); flow rate 4 mL/min; sample conc. 5 mg/mL in DMSO; injection volume 50 µL] to give **3** (0.6 mg, t_R 26.5 min).

Fraction L (200 mg) was separated by preparative HPLC [SunFire™ C18 column (5 µm, 30 × 150 mm, Waters)] with a gradient [H_2O (A) and MeCN (B); 30% → 40% B (0–10 min), 40% B (10–15 min), 40% → 50% B (15–20 min), and 50% → 100% B (20–30 min); flow rate 20 mL/min; sample conc. 50 mg/mL in DMSO; injection volume 1 mL] to afford subfractions L_1-L_4. The purification of L_3 (70 mg) using the same conditions as for fraction L afforded **13** (50 mg, t_R 32.0 min). The purification of subfraction L_1 (50 mg) by preparative HPLC [SunFire™ C18 column (5 µm, 30 × 150 mm, Waters)] with a gradient [H_2O (A) and MeCN (B); 30% B (0–25 min), 30% → 100% B (25–27 min), 100% B (27–30 min); flow rate 15 mL/min; sample conc. 50 mg/mL in DMSO; injection volume 1 mL]) gave **12** (7.9 mg, t_R 22.5 min), **2** (2.2 mg, t_R 23.3 min), and **18** (1.5 mg, t_R 24.0 min).

Fraction M (935 mg) was separated on a Sephadex LH-20 column (31 × 4 cm) with EtOAc (flow rate 0.8 mL/min) to give M_1-M_{17}, according to TLC analysis. The purification of subfraction M_3 (22 mg) by semipreparative HPLC [SunFire™ C18 column (5 µm, 10 × 150 mm, Waters)] with a gradient [H_2O (A) and MeCN (B); 30% → 40% B (0–5 min), 40% → 45% B (5–14 min), 45% B (14–25 min), 45% → 100% B (25–26 min), 100% B (26–35 min); flow rate 4 mL/min; sample conc. 50 mg/mL in DMSO; injection volume 60 µL] gave **19** (1 mg, t_R 18.5 min). The purification of M_4 (50 mg) by semipreparative HPLC [SunFire™ C18 column (5 µm, 10 × 150 mm, Waters)] with a gradient [H_2O (A) and MeCN (B); 20% → 30% B (0–5 min), 30% → 50% B (5–25 min), 50% → 100% B (25–26 min), 100% B (26–35 min); flow rate 4 mL/min; sample conc. 50 mg/mL in DMSO; injection volume 100 µL] gave **7** (5 mg, t_R 21.0 min), **13** (16.7 mg, t_R 23.0 min), and **3** (1 mg, t_R 26.5 min). The purification of M_{10} (40 mg) by semipreparative HPLC [SunFire™ C18 column (5 µm, 10 × 150 mm, Waters)] with a gradient [H_2O (A) and MeCN (B); 5% → 30% B (0–6 min), 30% B (6–37 min), 30% → 100% B (37–40 min); flow rate 4 mL/min; sample conc. 57 mg/mL in DMSO; injection volume 100 µL] gave **20** (1 mg, t_R 21.2 min), **17** (5 mg, t_R 25.0 min), and **2** (6 mg, t_R 30.0 min). The purification of M_{11} (40 mg) by semipreparative HPLC [SunFire™ C18 column (5 µm, 10 × 150 mm, Waters)] with a gradient [H_2O (A) and MeCN (B); 5% → 25% B (0–5 min), 25% B (5–37 min), 25% → 100% B (37–40 min); flow rate 4 mL/min; sample conc. 54 mg/mL in DMSO; injection volume 100 µL] gave **11** (1 mg, t_R 17.0 min) and subfraction $M_{11.1}$ (t_R 19.0 min, 2 mg). Compound **16** (2 mg) was precipitated from an MeOH solution of subfraction $M_{11.1}$.

3′-Hydroxy-7,8-methylenedioxyflavone (**2**): yellow amorphous solid, UV (MeOH) λ_{max} (log ε) 206 (1.77), 267 (1.60), 340 (*sh*) nm; ^1H and ^{13}C NMR data, see **Table 1**; HRESIMS *m/z* 587.0976 [2 M + Na]$^+$ (calculated for $C_{32}H_{20}O_{10}Na$: 587.0949). NMR spectra of **2** are available as Supporting Information.

3′-Methoxy-7,8-methylenedioxyflavone (**3**): yellow amorphous solid, UV (MeOH) λ_{max} (log ε) 205 (1.78), 267 (1.45), 336 (*sh*) nm; ^1H and ^{13}C NMR data, see **Table 1**; HRESIMS *m/z* 615.1296 [2 M + Na]$^+$ (calculated for $C_{34}H_{24}O_{10}Na$: 615.1262). NMR spectra of **3** are available as Supporting Information.

(+)-(2R,3R)-3,5-Dimethoxy-6,7-methylenedioxydihydroflavonol (**5**): yellow amorphous solid, UV (MeOH) λ_{max} (log ε) 243 (2.03), 285 (1.84), 338 (1.37) nm; $[\alpha]_D^{25}$ + 21.7 (*c* 0. 04, MeOH); CD (MeOH, *c* 8.23 × 10^{-4} M, 0.1 cm path length): $[\theta]_{215}$ + 5598, $[\theta]_{243}$ + 2372, $[\theta]_{320}$ − 3626, $[\theta]_{356}$ + 4423; ^{1}H and ^{13}C NMR data, see **Table 1**; HRESIMS *m/z* 679.1794 [2 M + Na]$^+$ (calculated for $C_{36}H_{32}O_{12}Na$: 679.1786). NMR spectra of **5** are available as Supporting Information.

(6aR,12aR)-8,10-Dihydroxy-9-methoxy-6a,12a-dihydro-5H-isochromeno[4,3-b]chromen-7-one (**6**): yellow amorphous solid, UV (MeOH) λ_{max} (log ε) 210 (*sh*), 240 (*sh*), 297 (2.01), 336 (1.73) nm; $[\alpha]_D^{25}$ 290.93 (*c* 0. 13, $CHCl_3$); CD (MeOH, *c* 7.0 × 10^{-4} M, 0.1 cm path length): $[\theta]_{221}$ + 6749, $[\theta]_{290}$ − 1617, $[\theta]_{330}$ + 2687; ^{1}H and ^{13}C NMR data, see **Table 1**; HRESIMS *m/z* 651.1524 [2 M + Na]$^+$ (calculated for $C_{34}H_{28}O_{12}Na$: 651.1473).

7-Hydroxy-8,3′-dimethoxyflavone (**18**): yellow amorphous solid, UV (MeOH) λ_{max} (log ε) 209 (1.93), 232 (*sh*), 262 (1.68), 275 (1.64), 311 (1.49) nm; ^{1}H and ^{13}C NMR data, see **Table 2**; HRESIMS *m/z* 619.1630 [2 M + Na]$^+$ (calculated for $C_{34}H_{28}O_{10}Na$: 619.1575). NMR spectra of **3** are available as Supporting Information.

7,8,3′-Trimethoxyflavone (**19**): yellow amorphous solid, UV (MeOH) λ_{max} (log ε) 208 (2.55), 241 (2.24), 260 (2.29), 310 (2.19) nm; ^{1}H and ^{13}C NMR data, see **Table 2**; HRESIMS *m/z* 647.1916 [2 M + Na]$^+$ (calculated for $C_{34}H_{28}O_{10}Na$: 647.1888). NMR spectra of **19** are available as Supporting Information.

Electrophysiological bioassay

cDNAs of hERG (accession number NP000229) were kindly provided by Prof. Sanguinetti (University of Utah, UT, USA). Synthesis of capped run-off complementary ribonucleic acid (cRNA) transcripts from linearized complementary deoxyribonucleic acid (cDNA) templates and the injection of cRNA were performed as described previously [32]. Oocytes from the South African clawed frog *X. laevis*, (NASCO, Fort Atkinson, WI, USA) were isolated as follows: After 15 min exposure of female *X. laevis* to the anesthetic (0.2% solution of MS-222, the methane sulfonate salt of the 3-aminobenzoic acid ethyl ester; Sigma), parts of the ovary tissue were surgically removed. Defolliculation was achieved by enzymatic treatment with 2 mg/mL collagenase type 1A (Sigma) and partly by mechanical removal of the follicular layer using forceps. Stage V–VI oocytes were selected and injected with WT hERG-encoding cRNA. Injected oocytes were stored at 18 °C in ND96 bath solution (96 mM sodium chloride, 2 mM potassium chloride, 1 mM magnesium chloride, 5 mM HEPES, 1.8 mM CaCl2; pH 7.5, titrated with NaOH) containing a 1% penicillin-streptomycin solution. All chemicals used were purchased from Sigma-Aldrich Chemie GmbH, Taufkirchen, Germany.

Currents through the hERG channels were measured one to three days after microinjection of the cRNA using the two-microelectrode voltage-clamp technique. ND96 was used as an extracellular recording solution. Voltage-recording and current-injecting microelectrodes were filled with 3 M KCl, and had resistances between 0.3 and 2 MΩ. Endogenous currents (estimated in oocytes injected with DEPC water) did not exceed 0.15 µA. Currents > 5 µA were discarded to minimize voltage-clamp errors. Ionic currents were recorded with a Turbo Tec 03X Amplifier (npi electronic, GmbH, Tamm, Germany) and digitized with a Digidata 1322A (Axon Instruments, Inc.). The pClamp software package version 9.2 (Axon Instruments, Inc.) was used for data acquisition. Microcal Origin 7.0 was employed for analysis. A precondition for all measurements was the achievement of stable peak current amplitudes over periods of 10 min after an initial "run-up" period. Compounds were applied by means of a fast perfusion system enabling the solution exchange within 100 ms [30]. The oocytes were incubated for 3 min in the presence of a studied compound at a holding potential of − 100 mV to equilibrate the compound diffusion. The following voltage protocol was used: From a holding potential of − 100 mV, the cell membrane was initially depolarized to + 20 mV (300 ms) in order to ensure channel activation and subsequent rapid inactivation. During the following repolarization to − 50 mV (300 ms), the channels recovered from the inactivation and elicit peak tail current. A final step to the holding potential ensured that the channels returned to the closed state. The protocol was applied at 3-s intervals (0.3 Hz pulse frequency). Decreases in tail current amplitudes were taken as a measure of use-dependent block development during repetitive pulsing. Data are presented as means ± SE from at least three oocytes from ≥ 2 batches. The studied compounds were dissolved in DMSO to prepare a 10-mM stock on the day of the experiments. Compound stock solution was further diluted to the required concentration using ND96 recording solution. The final maximum DMSO concentration (1%) in the test solutions did not affect the hERG currents (data not shown). Propafenone was used as a positive control and exhibited an IC_{50} of 3.8 ± 0.2 µM [30].

Supporting information

NMR spectra (1D and 2D) of new compounds **2, 3, 5, 6, 18**, and **19**, ^{1}H and ^{13}C NMR data for known compounds **1, 4, 7**–**17**, and **20**, and experimental details for quantitative analysis of **1** and **13** are available as Supporting Information.

Acknowledgements

This project was carried out within the International Research Staff Exchange Scheme (IRSES) project "hERG Related Risk Assessment of Botanicals" PIRSES-GA-2011–295 174 Marie Curie Actions funded under the 7th Framework Programme of the European Commission. Thanks are due to Mrs. Jeanne Van der Westhuizen for proofreading the manuscript.

Conflict of Interest

The authors declare no conflict of interest.

Affiliations

[1] Department of Chemistry, University of the Free State, Bloemfontein, South Africa
[2] Division of Pharmaceutical Biology, University of Basel, Basel, Switzerland
[3] Institute of Pharmacology and Toxicology, University of Vienna, Vienna, Austria
[4] National Museum, Bloemfontein, South Africa
[5] Centre for Environmental Management, University of the Free State, Bloemfontein, South Africa
[6] Directorate Research Development, University of the Free State, Bloemfontein, South Africa

References

1 *Vasina V, De Ponti F.* The hERG K$^+$ channel: target and antitarget strategies in drug development. Pharmacol Res 2008; 57: 181–195
2 *Deisemann H, Ahrens N, Schlobohm I, Kirchhoff C, Netzer R, Möller C.* Effects of common antitussive drugs on the hERG potassium channel current. J Cardiovasc Pharmacol 2008; 52: 494–499
3 *Polak S, Wiśniowska B, Brandys J.* Collation, assessment and analysis of literature *in vitro* data on hERG receptor blocking potency for subse-

quent modeling of drugs' cardiotoxic properties. J Appl Toxicol 2009; 29: 183–206
4 *Scholz EP, Zitron E, Kiesecker C, Lück S, Thomas D, Kathöfer S, Kreye VAW, Katus HA, Kiehn J, Schoels W, Karle CA.* Inhibition of cardiac HERG channels by grapefruit flavonoid naringenin: implications for the influence of dietary compounds on cardiac repolarisation. Naunyn Schmiedebergs Arch Pharmacol 2005; 371: 516–525
5 *Lin CR, Ke XG, Ranade V, Somberg J.* The additive effects of the active component of grapefruit juice (naringenin) and antiarrhythmic drugs on HERG inhibition. Cardiology 2008; 110: 145–152
6 *Zitron E, Scholz E, Owen RW, Lück S, Kiesecker C, Thomas D, Kathöfer S, Niroomand F, Kiehn J, Kreye VAW, Katus HA, Schoels W, Karle CA.* QTc prolongation by grapefruit juice and its potential pharmacological basis – HERG channel blockade by flavonoids. Circulation 2005; 111: 835–838
7 *Schramm A, Jähne EA, Barburin I, Hering S, Hamburger M.* Natural products as potential hERG channel inhibitors – outcomes from a screening of widely used herbal medicines and edible plants. Planta Med 2014; 80: 1045–1050
8 *Schramm A, Baburin I, Hering S, Hamburger M.* hERG channel inhibitors in extracts of Coptidis rhizoma. Planta Med 2011; 77: 692–697
9 *Vries FA, Bitar HEL, Green IR, Klassen JA, Mabusela WT, Bodo B, Johnson Q.* An antifungal active extract from the aerial parts of *Galenia africana*. 11th Napreca Symposium Book of Proceedings. Antananarivo: Napreca; 2005: 123–131
10 *Watt C, Breyer-Brandwijk MG.* The medicinal and poisonous plants of southern and eastern Africa. Edinburg: E & S Livingstone Ltd.; 1962: 449
11 *Mativandlela SPN, Muthivhi T, Kikuchi H, Oshima Y, Hamilton C, Hussein AA, van der Walt ML, Houghton PJ, Lall N.* Antimycobacterial flavonoids from the leaf extract of *Galenia africana*. J Nat Prod 2009; 72: 2169–2171
12 *Potterat O, Hamburger M.* Concepts and technologies for tracking bioactive compounds in natural product extracts: generation of libraries, and hyphenation of analytical processes with bioassays. Nat Prod Rep 2013; 30: 546–564
13 *Potterat O, Hamburger M.* Combined use of extract libraries and HPLC-based activity-profiling for lead discovery. Planta Med 2014; 80: 1171–1181
14 *Kuroyanagi M, Yamamoto Y, Fukushima S, Ueno A, Noro T, Miyase T.* Chemical studies on the constituents of *Polygonum nodosum*. Chem Pharm Bull 1982; 30: 1602–1608
15 *Huan Y, Dong W, Li T, Baochang C.* Flavonoid aglycones of *Oxytropis falcata*. Chem Nat Comp 2009; 45: 239–241
16 *Tran VH, Druke RK, Abu-Mellal A, Duke CC.* Propolis with high flavonoid content collected by honey bees from *Acacia paradoxa*. Phytochemistry 2012; 81: 126–132
17 *Al-Taweel AM, Perveen S, El-Shafae AM, Fawzy GA, Malik A, Afza N, Iqbal L, Latif M.* Bioactive phenolic amides from *Celtis africana*. Molecules 2012; 17: 2675–2682
18 *Herath W, Mikell JR, Khan IA.* Microbial metabolism. Part 10: Metabolites of 7,8-dimethoxyflavone and 5-methoxyflavone. Nat Prod Res 2009; 23: 1231–1239
19 *Bernard-Gautier V, Boudjemeline M, Rosa-Neto P, Thiel A, Shirrmacher R.* Towards tropomyosin-related kinase B (trKB) receptors ligands for brain imaging with PET: radiosynthesis and evaluation of 2-(4-[^{18}F]fluorophenyl)-7,8-dihydroxy-4*H*-chromen-4-one and 2-(4-([N-methyl-^{11}C]-dimethylamino)phenyl)-7,8-dihydroxy-4*H*-chromene-4-one. Bioorg Med Chem 2013; 21: 7816–7829
20 *Yoon H, Eom S, Hyun J, Jo G, Hwang D, Lee S, Yong Y, Park JC, Lee YH, Lim Y.* ^{1}H and ^{13}C NMR data on hydroxy/methoxy flavonoids and the effects of substituents on chemical shifts. Bull Korean Chem Soc 2011; 32: 2101–2104
21 *Zhang Q, Guo WJ, Fu CL, Ma S, Zhu MQ.* Chemical constituents from an endophyte *Cercosporella sp.* Chem Nat Comp 2013; 49: 117–118
22 *Visweswara Rao K, Viswanadham N.* A note on 7, 8-dimethoxy flavones. Proc Indian Acad Sci 1949; 29: 218–220
23 *Wang QA, Liao TG, Tang JG, Fan HF.* [Improved synthesis and structure modification of 7-hydroxyflavone and 7,8-dihydroxyflavone.] Hunan Daxue Xuebao (Ziran Kexueban) 2004; 31: 1–4
24 *Anjaneyulu ASR, Sudha Rani G, Mallavadhani UV, Murthy YLN.* Synthesis and characterization of some new chalcones and flavanones. Indian J Heterocycl Chem 1994; 4: 9–14
25 *Bhattacharya RK, Pyrozi PR.* Effect of plant flavonoids on microsome catalyzed reactions of aflatonine B_1 leading to activation and DNA adduct formation. Cancer Lett 1988; 39: 85–91
26 *Dlade D, Ferreira D, Marajs LPJ.* Circular dichroism, a powerful tool for the assessment of absolute configuration of flavonoids. Phytochemistry 2005; 66: 2167–2215
27 *Brandt EV, Ferreira D, Roux DG.* Ring expansion of crombeone, a natural 5-hydroxypeltogynone. J Chem Soc Chem Commun 1971; 116–117
28 *Clare JJ, Trezise DJ.* Expression and analysis of recombinant ion channels: from structural studies to pharmacological screening. Weinheim: Wiley-VCH Verlag; 2006: 1–25
29 *Witchel HJ, Milnes JT, Milcheson JS, Anchox JC.* Troubleshooting problems with *in vitro* screening of drugs for QT interval prolongation using HERG K^+ channels expressed in mammalian cell lines and *Xenopus* oocytes. J Pharmacol Toxicol Methods 2002; 48: 45–80
30 *Windisch A, Timin EN, Schwarz T, Stork-Riedler D, Erker T, Ecker GF, Hering S.* Trapping and dissociation of propafenone derivatives in HERG channels. Br J Pharmacol 2011; 162: 1542–1552
31 *Stork D, Timin EN, Berjukow S, Huber C, Hohaus A, Auer M, Hering S.* State dependent dissociation of HERG channel inhibitors. Br J Pharmacol 2007; 151: 1368–1376
32 *Baburin I, Beyl S, Hering S.* Automated fast perfusion of *Xenopus* oocytes for drug screening. Pflugers Arch 2006; 453: 117–123

HPLC-Based Activity Profiling for hERG Channel Inhibitors in the South African Medicinal Plant *Galenia Africana* (Supporting Information)

Kun Du[1]*, Maria De Mieri[2]*, Priyanka Saxena[3], Khanya V. Phungula[1], Anke Wilhelm[1], Madalina Marina Hrubaru[1], Elmarie van Rensburg[4], Pieter C. Zietsman[4,5], Steffen Hering[3], Jan H. van der Westhuizen[6] and Matthias Hamburger[2]

Affiliation

[1] Department of Chemistry, University of the Free State, Nelson Mandela Avenue, Bloemfontein 9301, South Africa

[2] Division of Pharmaceutical Biology, University of Basel, Klingelbergstrasse 50, CH-4056 Basel, Switzerland

[3] Institute of Pharmacology and Toxicology, University of Vienna, Althanstrasse 14, A-1090 Vienna, Austria

[4] National Museum, P.O. Box 266, Bloemfontein 9300, South Africa

[5] Centre for Environmental Management, University of the Free State, P.O. Box 339, Bloemfontein 9301, South Africa

[6] Directorate Research Development, University of the Free State, Nelson Mandela Avenue, Bloemfontein 9301, South Africa

Correspondence

Prof. Dr Matthias Hamburger, Division of Pharmaceutical Biology, University of Basel, Klingelbergstrasse 50, CH-4056 Basel, Switzerland.

E-mail: matthias.hamburger@unibas.ch

Phone: +41 61 267 14 25 Fax: +41 61 267 14 74

*These authors contributed equally to this work

Dedicated to Professor Dr. Dr. h.c. mult. Adolf Nahrstedt on the occasion of his 75th birthday

Table 1S. ^{1}H and ^{13}C NMR data (500 MHz for ^{1}H, 125 MHz for ^{13}C) for compounds **1**, **4**, and **7** ($CDCl_3$ for **1**, DMSO-d_6 for **4** and **7**).

	1		**4**		**7**	
	$\delta_{H\ multi}$ (*J*)	δ_C	$\delta_{H\ multi}$ (*J*)	δ_C [a]	$\delta_{H\ multi}$ (*J*)	δ_C [a]
2	-	162.5	5.12 (d, 11.4)	83.2	5.58 (dd,12.9, 3.0)	79.4
3	6.19 (s)	106.9	4.41 (d, 11.4)	72.9	2.76 (d, 16.7, 3.0)	43.1
					3.10 (d, 16.7, 12.9)	
4	-	177.3	-	191.0	-	190.0
5	7.83 (d, 8.5)	120.0	-	142.5	7.18 (s)	106.3
6	6.97 (d, 8.5)	107.1	-	132.7	-	144.3
7	-	152.4	-	155.0	-	156.1
8	-	134.7	6.40 (s)	93.5	6.68 (s)	100.8
9	-	141.1	-	159.0	-	157.5
10	-	119.9	-	107.3	-	112.6
1'	-	131.3	-	137.6	-	139.1
2'	7.93 (m)	126.1	7.50 (m)	128.2	7.53 (br d, 7.5)	126.6
3'	7.55-7.50 (m)	129.0	7.43-7.37 (m)	128.5	7.43-7.37 (m)	128.5
4'	7.55-7.50 (m)	131.6	7.43-7.37 (m)	128.9	7.43-7.37 (m)	128.6
5'	7.55-7.50 (m)	129.0	7.43-7.37 (m)	128.5	7.43-7.37 (m)	128.5
6'	7.93 (m)	126.1	7.50 (m)	128.2	7.53 (br d, 7.5)	126.6
CH_2diox	6.23 (s)	103.2	6.05 (s)	102.2	-	-
5- OCH_3	-	-	3.93 (s)	60.3	-	-
6- OCH_3	-	-	-	-	3.76 (s)	55.7
7- OCH_3	-	-	-	-	3.83 (s)	56.2

[a] ^{13}C NMR signals were extracted from HSQC and HMBC spectra.

Table 2S. ^{1}H and ^{13}C NMR data for compounds **8**, **9** and **10** (DMSO-d_6, 500 MHz for ^{1}H, 125 MHz for ^{13}C).

	8		9		10	
Position	$\delta_{H\ multi}$ (*J*)	δ_C [a]	$\delta_{H\ multi}$ (*J*)	δ_C [a]	$\delta_{H\ multi}$ (*J*)	δ_C [a]
1	-	134.9	-	134.9	-	136.3
2	7.89 (m)	129.4	7.88 (m)	129.4	7.22 (t, 1.5)	115.0
3	7.50-7.44 (m)	129.4	7.50-7.42 (m)	129.3	-	158.0
4	7.50-7.44 (m)	130.9	7.50-7.42 (m)	130.9	6.88 (ddd, 7.7, 1.5, 1.0)	117.5
5	7.50-7.44 (m)	129.4	7.50-7.42 (m)	129.3	7.25 (t, 7.7)	129.5
6	7.89 (m)	129.4	7.88 (m)	129.4	7.29 (dt, 7.7, 1.0)	119.5
1'	-	113.4	-	114.3	-	113.8
2'	-	166.5	-	158.2	-	[b]
3'	6.32 (d, 2.3)	102.9	-	135.4	-	135.2
4'	-	166.0	-	158.9	-	158.8
5'	6.44 (dd, 8.8, 2.3)	108.7	6.50 (d, 9.0)	108.5	6.48 (d, 8.9)	108.1
6'	8.17 (dd, 8.8)	133.4	7.97 (d, 9.0)	127.5	7.89 (d, 8.9)	126.6
3'- OCH_3	-	-	3.76 (s)	60.1	3.74 (s)	59.2
A	7.95 (d, 15.5)	121.9	7.95 (d, 15.5)	121.7	7.83 (d, 15.5)	120.9
B	7.79 (d, 15.5)	143.8	7.81 (d, 15.5)	144.2	7.68 (d, 15.5)	143.3
C=O	-	191.9	-	192.5	-	191.9

[a] ^{13}C NMR signals were extracted from HSQC and HMBC spectra, [b] not detected due to low S/N.

Table 3S. ^{1}H and ^{13}C NMR data (DMSO-d_6, 500 MHz for ^{1}H, 125 MHz for ^{13}C) for compound **11**.

	11	
position	**$\delta_{H\ multi}$ (*J*)**	**δ_C [a]**
1	-	126.4
2	7.10 (brs)	110.6
3	-	147.8
4	-	148.0
5	6.78 (d, 8.2)	115.3
6	6.98 (bd, 8.2, 1.8)	121.5
7	7.31 (d, 15.5)	138.4
8	6.42 (d, 15.5)	118.5
9	-	165.1
1'	-	129.2
2'	7.01 (d, 8.4)	128.9
3'	6.69 (d, 8.4)	114.8
4'	-	155.7
5'	6.69 (d, 8.4)	114.8
6'	7.01 (d, 8.4)	128.9
7'	2.65 (t, 7.2)	34.1
8'	3.34 (q like, 7.2, 5.8)	40.3
3- OCH_3	3.80 (s)	55.3
N-H	7.92 (t, 5.8)	-

[a] ^{13}C NMR signals were extracted from HSQC and HMBC spectra.

Table 4S. ^{1}H and ^{13}C NMR data (DMSO-d_6, 500 MHz for ^{1}H, 125 MHz for ^{13}C) for compounds **12**, **13**, **14** and **15**.

	12		**13**		**14**		**15**	
position	$\delta_{H\ multi}$ (*J*)	δ_C [a]	$\delta_{H\ multi}$ (*J*)	δ_C [a]	$\delta_{H\ multi}$ (*J*)	δ_C [a,b]	$\delta_{H\ multi}$ (*J*)	δ_C [a]
2	-	162.0	-	161.5	-	162.5	-	163.5
3	6.83 (s)	108.0	6.92 (s)	105.9	6.77 (s)	106.6	6.90 (s)	105.1
4	-	176.9	-	175.7	-	177.7	-	182.4
5	7.65 (d, 8.7)	121.1	7.78 (d, 9.0)	119.7	7.53 (s)	104.4	-	[c]
6	7.00 (d, 8.7)	116.2	7.27 (d, 9.0)	110.4	-	147.6	-	132.1
7	-	155.5	-	155.6	-	154.0	-	158.1
8	-	135.2	-	135.5	6.97 (s)	99.5	6.62 (s)	94.8
9	-	151.0	-	149.2	-	151.8	-	152.9
10	-	117.4	-	117.2	-	117.2	-	104.7
1'	-	131.7	-	130.6	-	131.5	-	131.3
2'	8.00 (m)	126.8	8.06 (m)	125.5	7.87 (m)	126.2	8.05 (m)	126.6
3'	7.56-7.52 (m)	130.2	7.62-7.57 (m)	128.9	7.36-7.43 (m)	128.6	7. 63-7.54 (m)	129.5
4'	7.56-7.52 (m)	132.1	7.62-7.57 (m)	131.2	7.36-7.43 (m)	131.0	7. 63-7.54 (m)	132.3
5'	7.56-7.52 (m)	130.2	7.62-7.57 (m)	128.9	7.36-7.43 (m)	128.6	7. 63-7.54 (m)	129.5
6'	8.00 (m)	126.8	8.06 (m)	125.5	7.87 (m)	126.2	8.05 (m)	126.6
6- OCH_3	-	-	-	-	3.94 (s)	56.1	3.77 (s)	60.2
7- OCH_3	-	-	3.97 (s)	56.0	3.99 (s)	56.1	-	-
8- OCH_3	3.96 (s)	135.2	3.96 (s)	60.5	-	-	-	-

[a] ^{13}C NMR signals were extracted from HSQC and HMBC spectra, [b] measured in $CDCl_3$, [c] not detected due to low S/N.

Table 5S. ^{1}H and ^{13}C NMR data (DMSO-d_6, 500 MHz for ^{1}H, 125 MHz for ^{13}C) for compounds **16**, **17** and **20**.

	16		**17**		**20**	
position	$\delta_{H\ multi}$ (*J*)	δ_C	$\delta_{H\ multi}$ (*J*)	δ_C	$\delta_{H\ multi}$ (*J*)	δ_C [a]
2	-	161.8	-	162.2	-	162.5
3	6.78 (s)	106.0	6.78 (s)	106.0	6.72 (s)	104.8
4	-	176.0	-	176.7	-	[b]
5	7.64 (d, 8.9)	119.7	7.76 (d, 8.9)	120.0	7.75 (d, 8.8)	120.6
6	7.02 (d, 8.9)	114.7	7.25 (d, 8.9)	110.6	7.24 (d, 8.8)	111.4
7	-	154.1	-	156.5	-	157.0
8	-	134.5	-	136.7	-	136.8
9	-	150.1	-	149.9	-	[b]
10	-	116.5	-	118.4	-	118.2
1'	-	132.1	-	132.2	-	[b]
2'	7.44 (t, 2.2)	112.3	7.41 (dd, 2.0, 1.5)	112.5	7.88 (d, 8.7)	128.9
3'	-	157.8	-	158.1	6.92 (d, 8.7)	117.2
4'	7.00 (ddd, 8.2, 2.2, 0.9)	118.3	7.00 (dd, 8.0, 2.0)	117.4	-	[b]
5'	7.32 (t, 8.0)	129.9	7.37 (t, 7.9)	130.3	6.92 (d, 8.7)	117.2
6'	7.48 (ddd, 8.0, 2.2, 0.9)	116.5	7.46 (dd, 8.0, 1.5)	116.8	7.88 (d, 8.7)	128.7
7- OCH_3	-	-	3.93 (s)	56.2	3.96 (s)	57.7
8- OCH_3	3.96 (s)	60.7	3.93 (s)	61.1	3.95 (s)	61.8

[a] ^{13}C NMR signals were extracted from HSQC and HMBC spectra, [b] not detected due to low S/N.

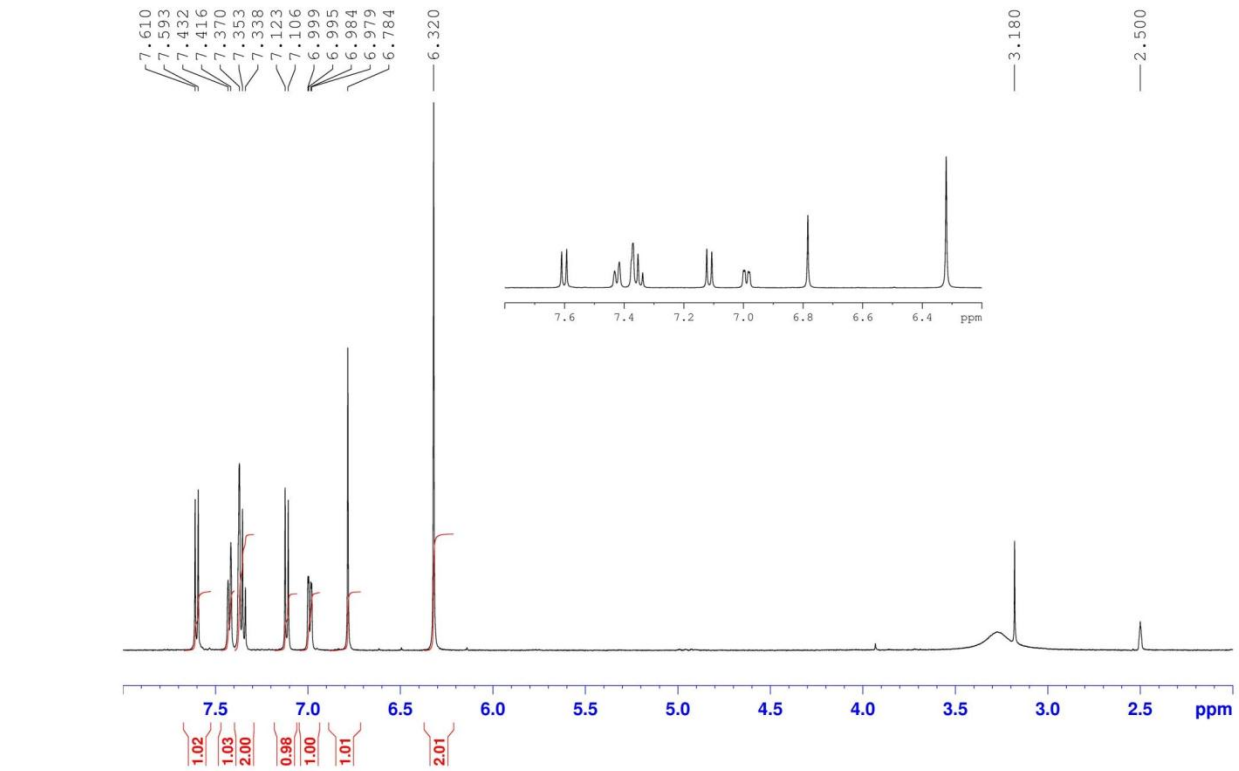

Fig. 1S. ^{1}H NMR spectrum of compound **2** in DMSO-d_6.

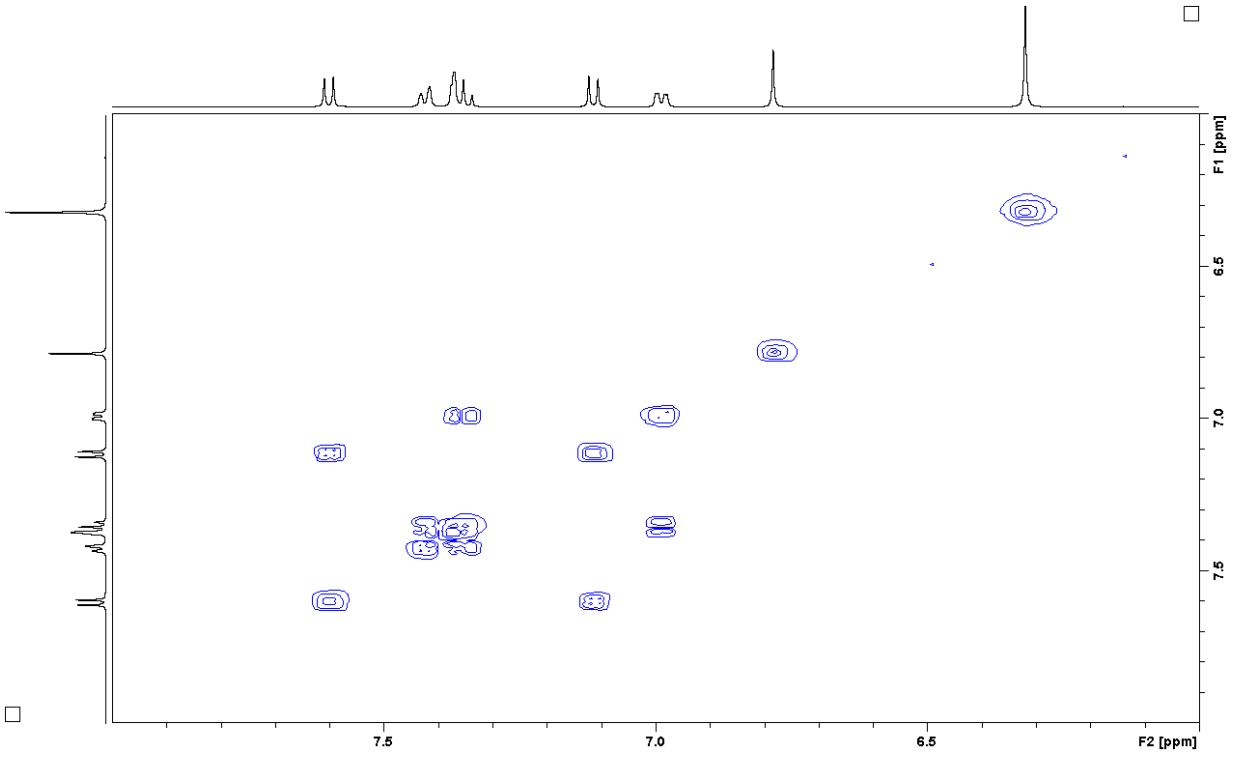

Fig. 2S. ^{1}H-^{1}H COSY NMR spectrum of compound **2** in DMSO-d_6.

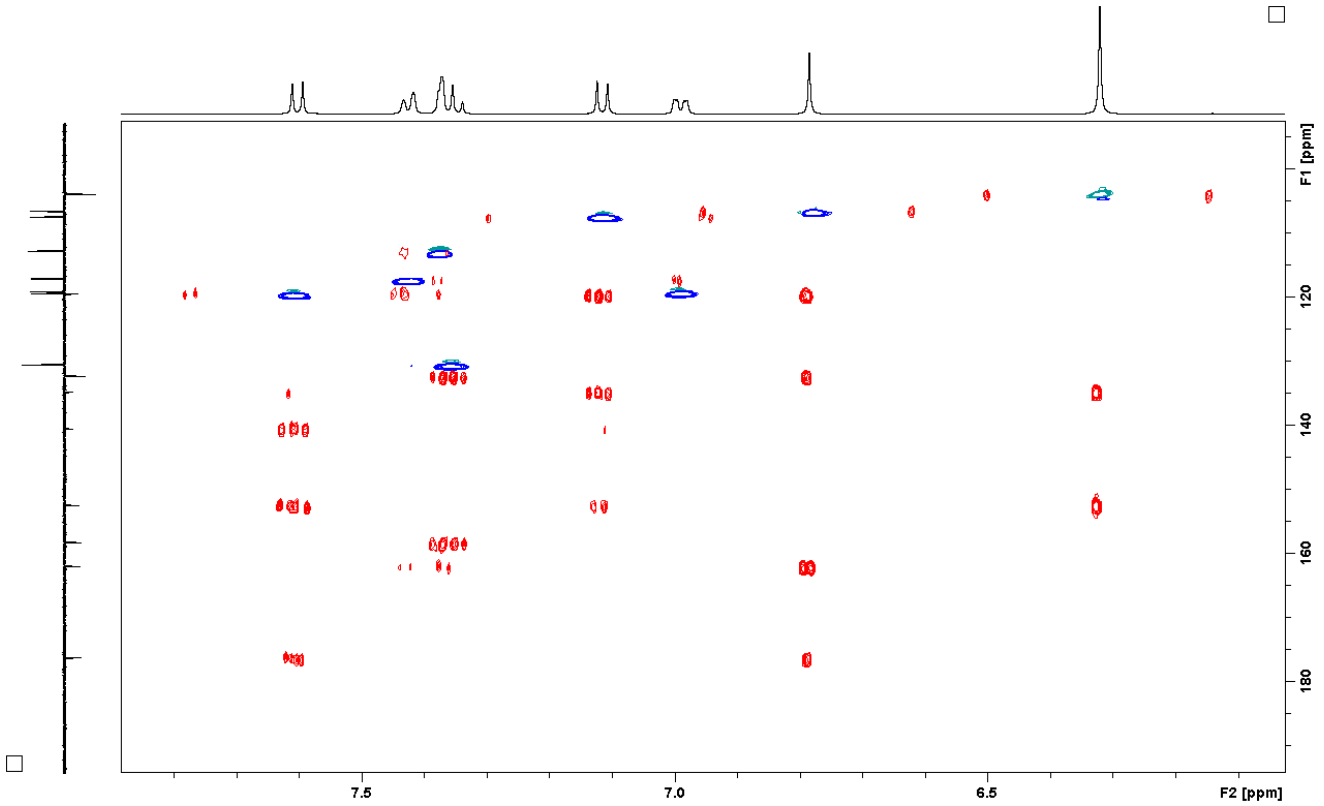

Fig. 3S. HSQC-DEPT (light green/blue) and HMBC (red) overlaid spectra of compound **2** in DMSO-d_6.

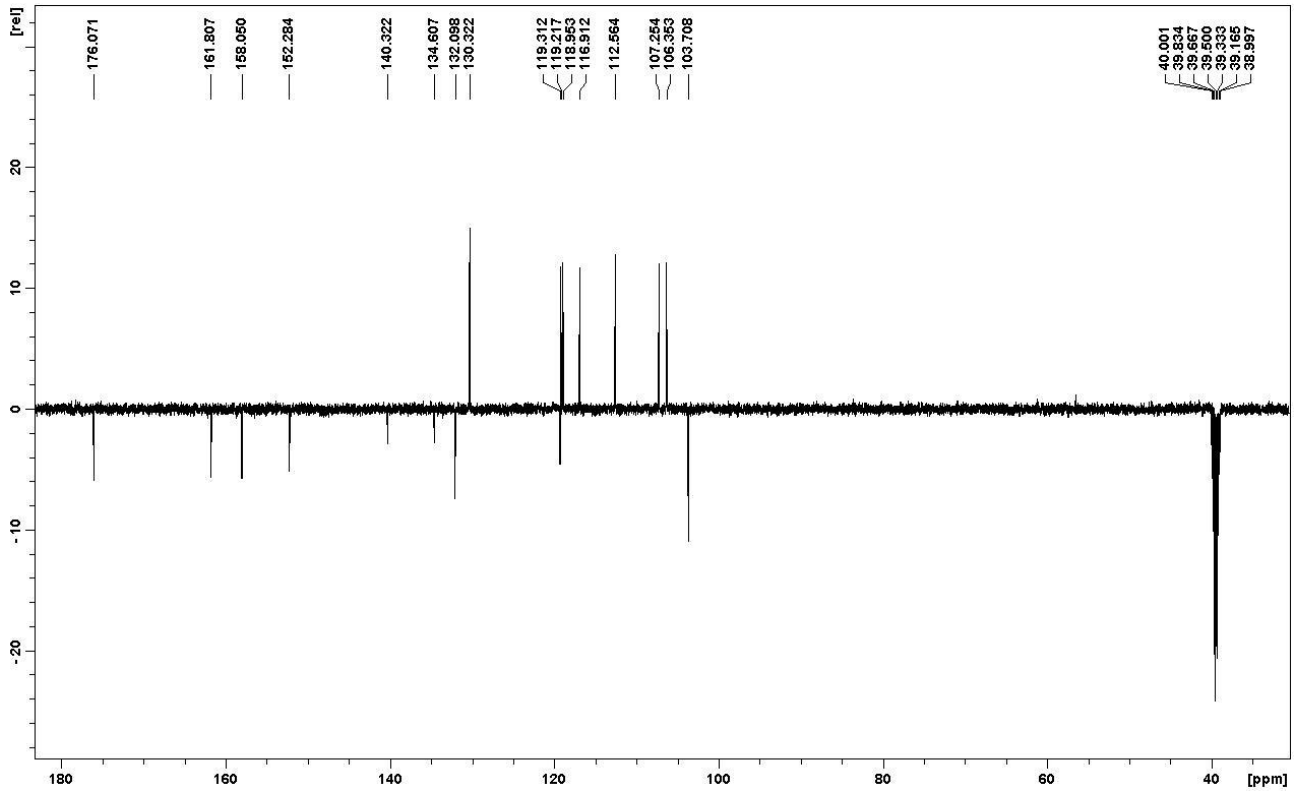

Fig. 4S. DEPTQ spectrum of compound **2** in DMSO-d_6.

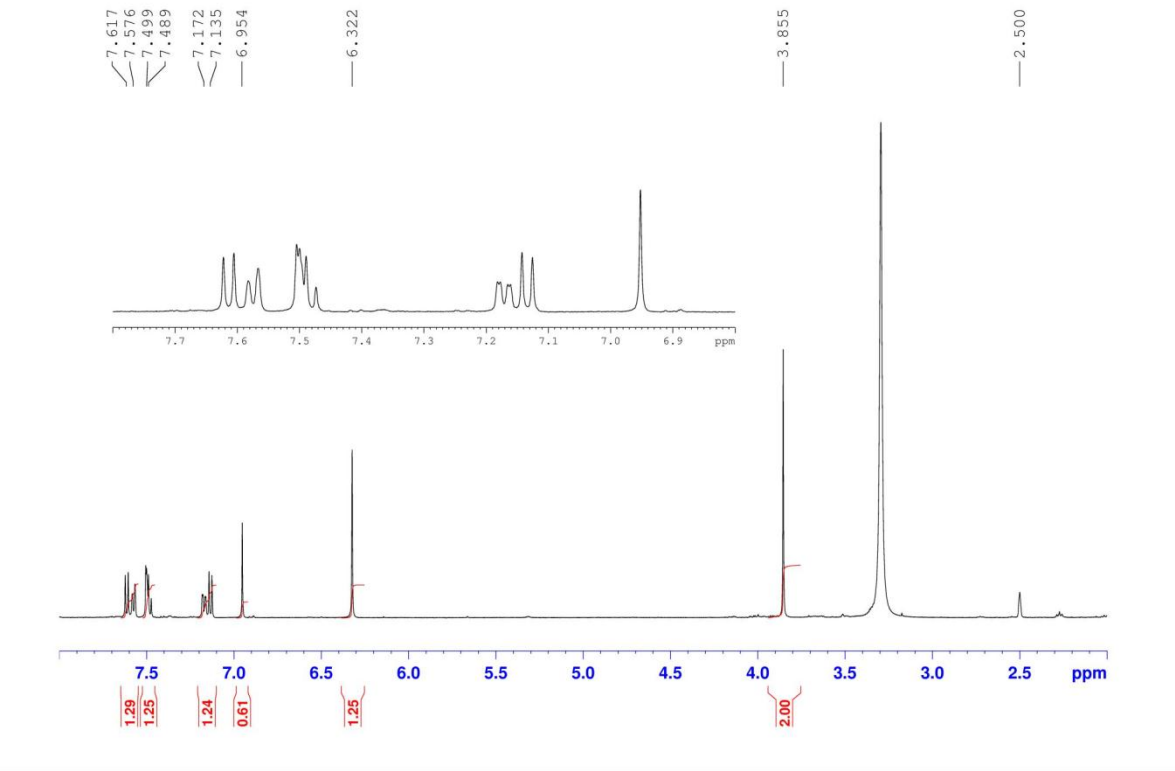

Fig. 5S. ^{1}H NMR spectrum of compound **3** in DMSO-d_6.

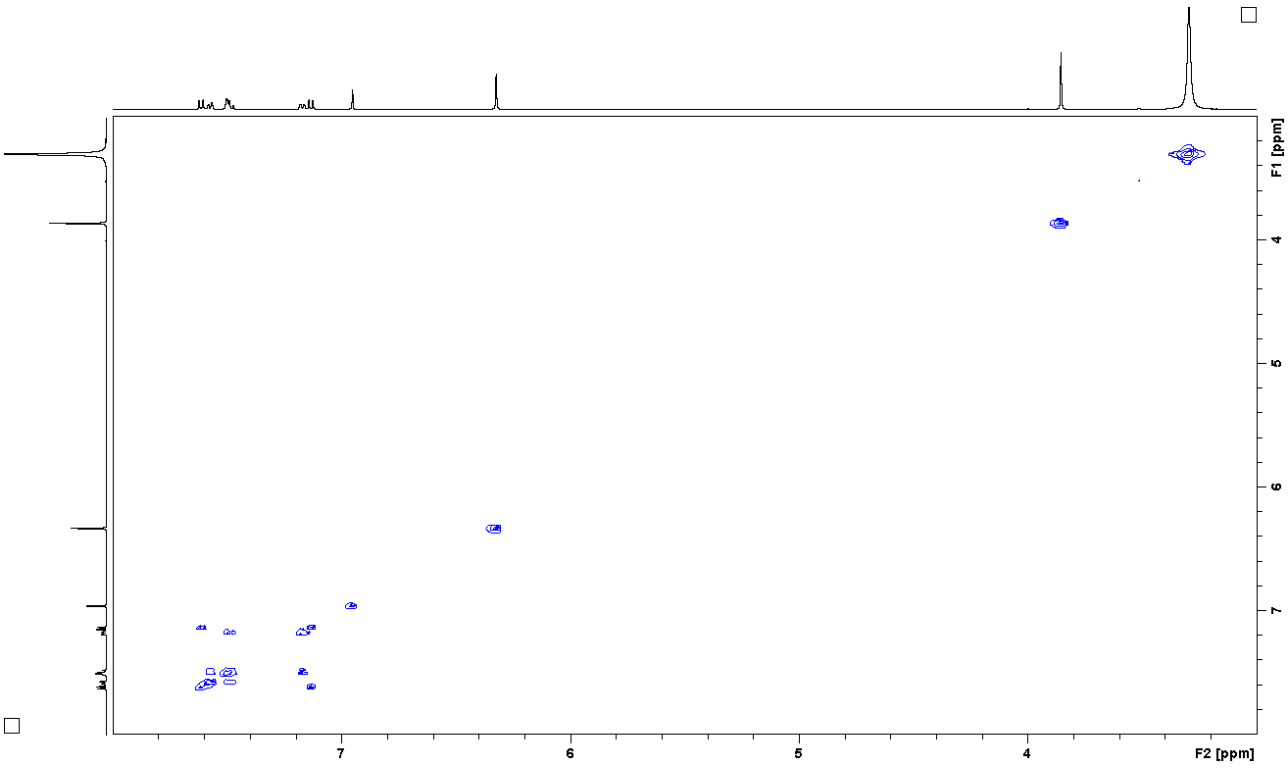

Fig. 6S. ^{1}H-^{1}H COSY NMR spectrum of compound **3** in DMSO-d_6.

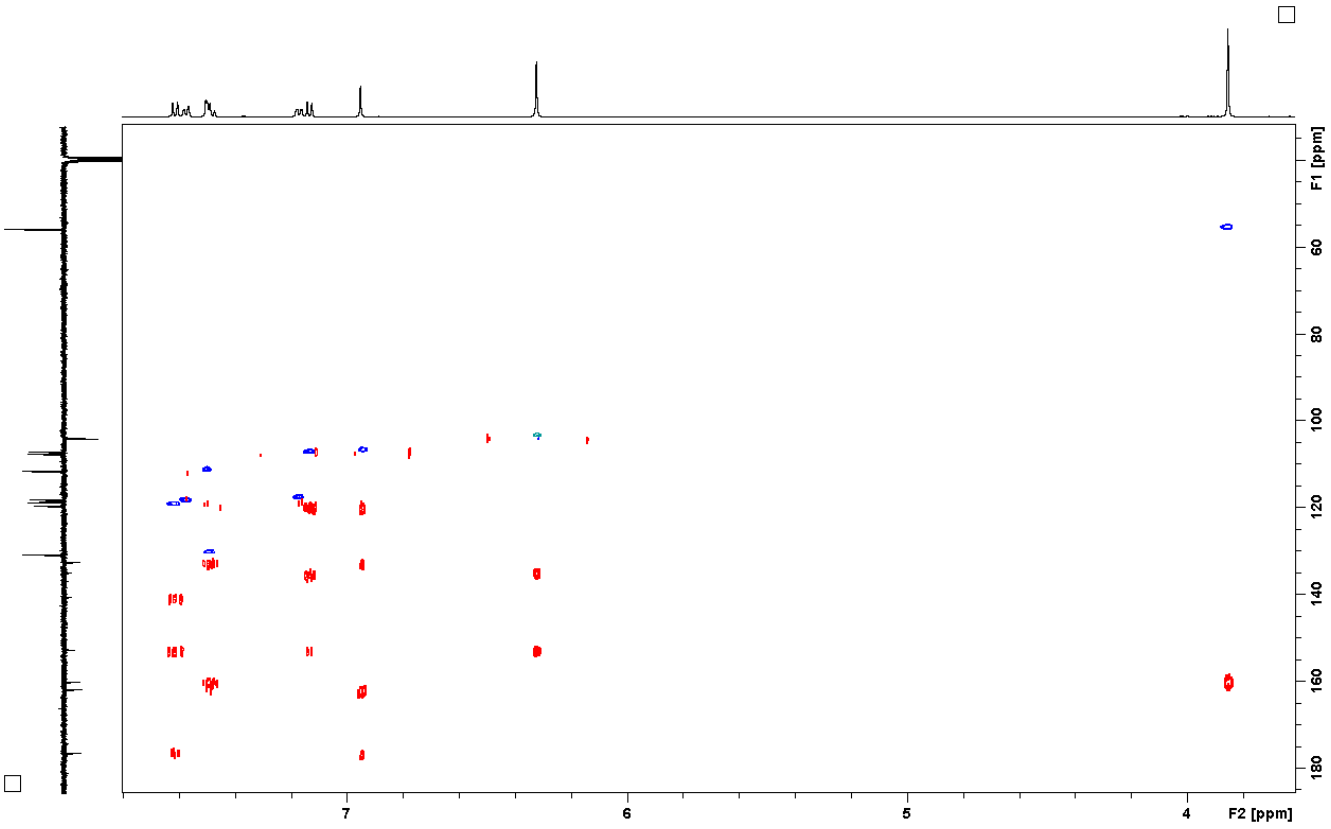

Fig. 7S. HSQC-DEPT (light green/blue) and HMBC (red) overlaid spectra of compound **3** in DMSO- d_6.

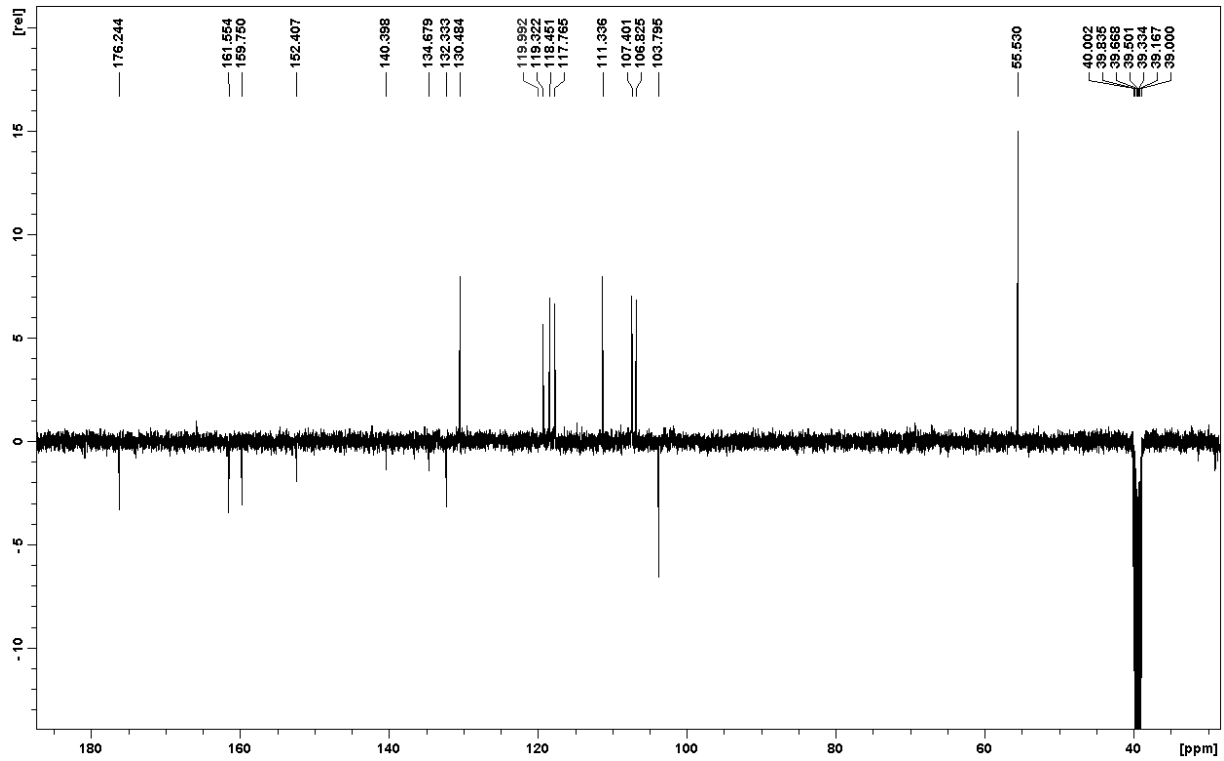

Fig. 8S. DEPTQ spectrum of compound **3** in DMSO-d_6.

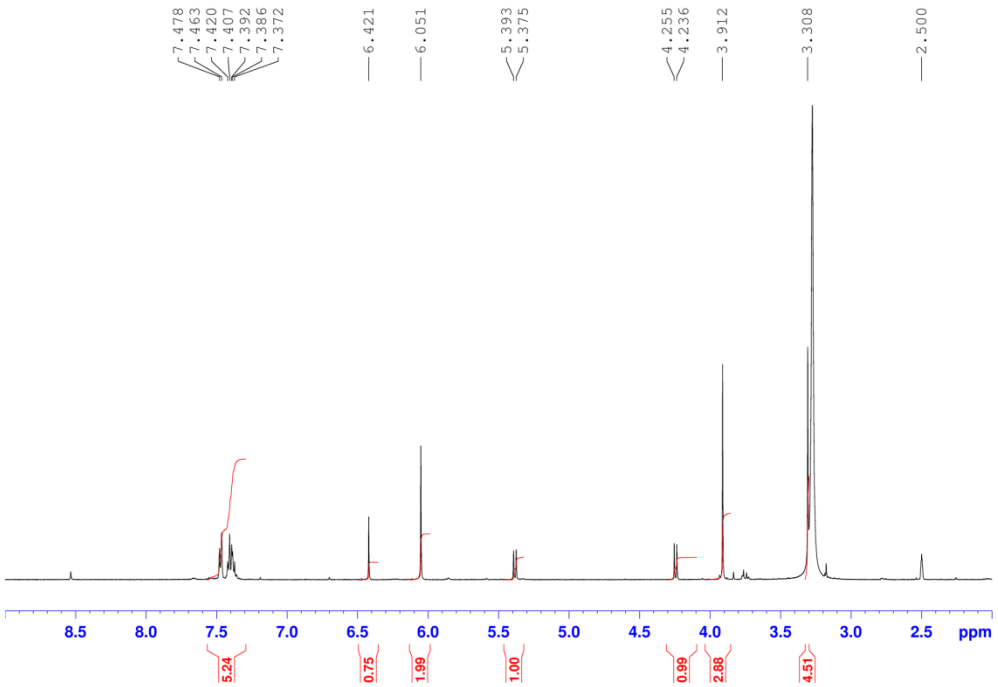

Fig. 9S. ^{1}H NMR spectrum of compound **5** in DMSO-d_6.

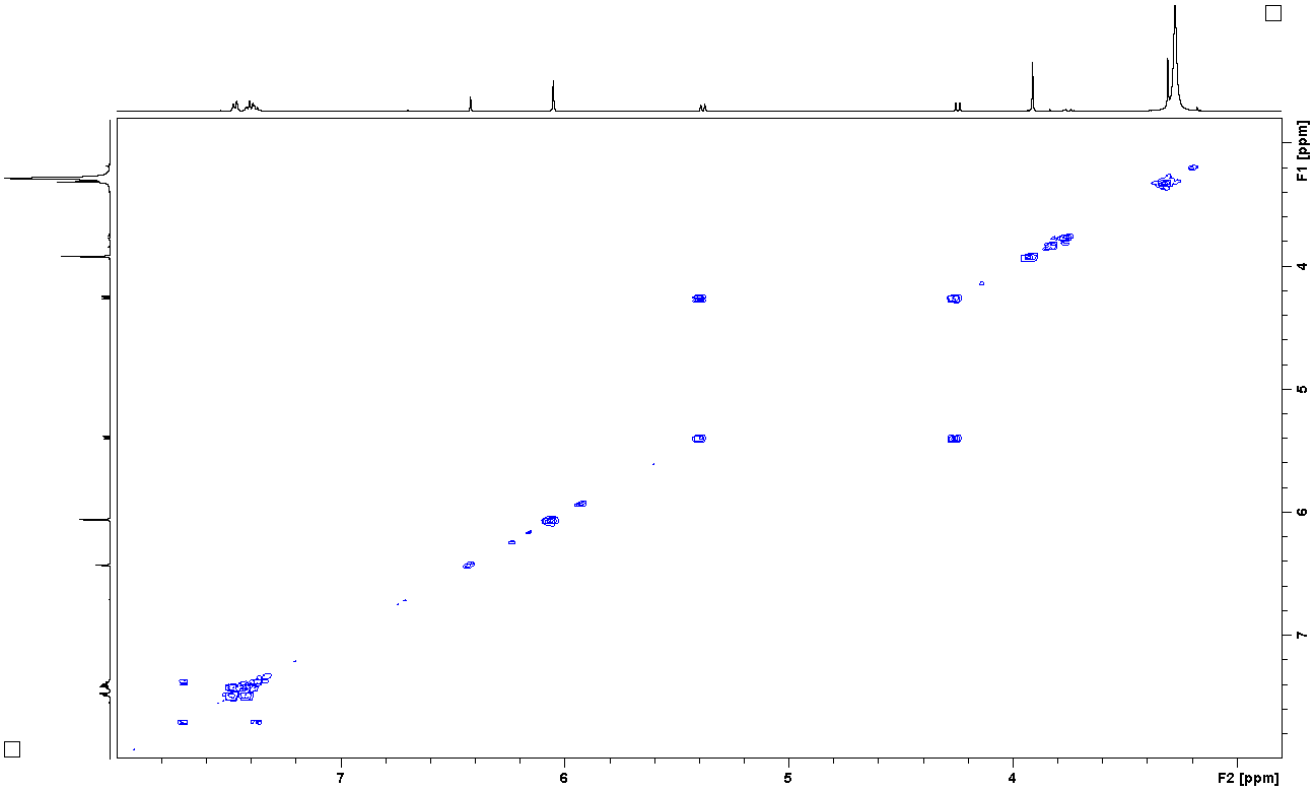

Fig. 10S. ^{1}H-^{1}H COSY NMR spectrum of compound **5** in DMSO-d_6.

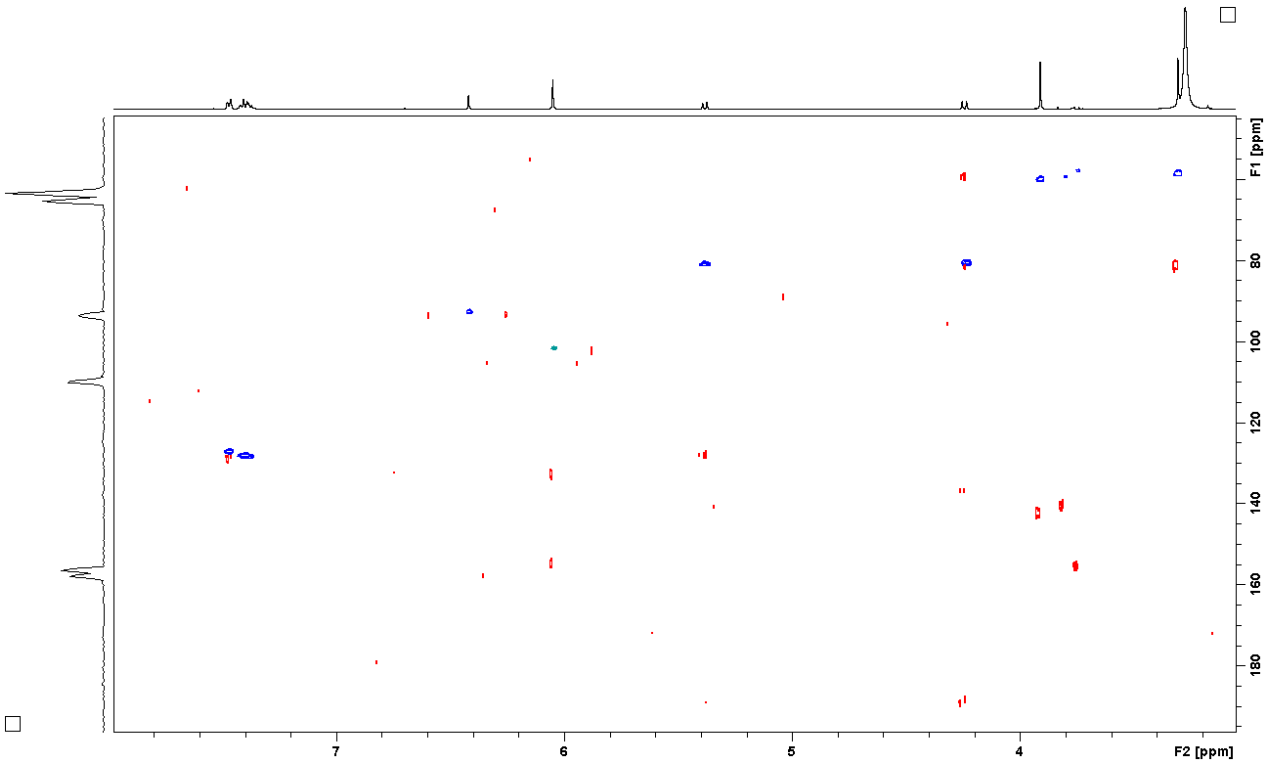

Fig. 11S. HSQC-DEPT (light green/blue) and HMBC (red) overlaid spectra of compound **5** in DMSO- d_6.

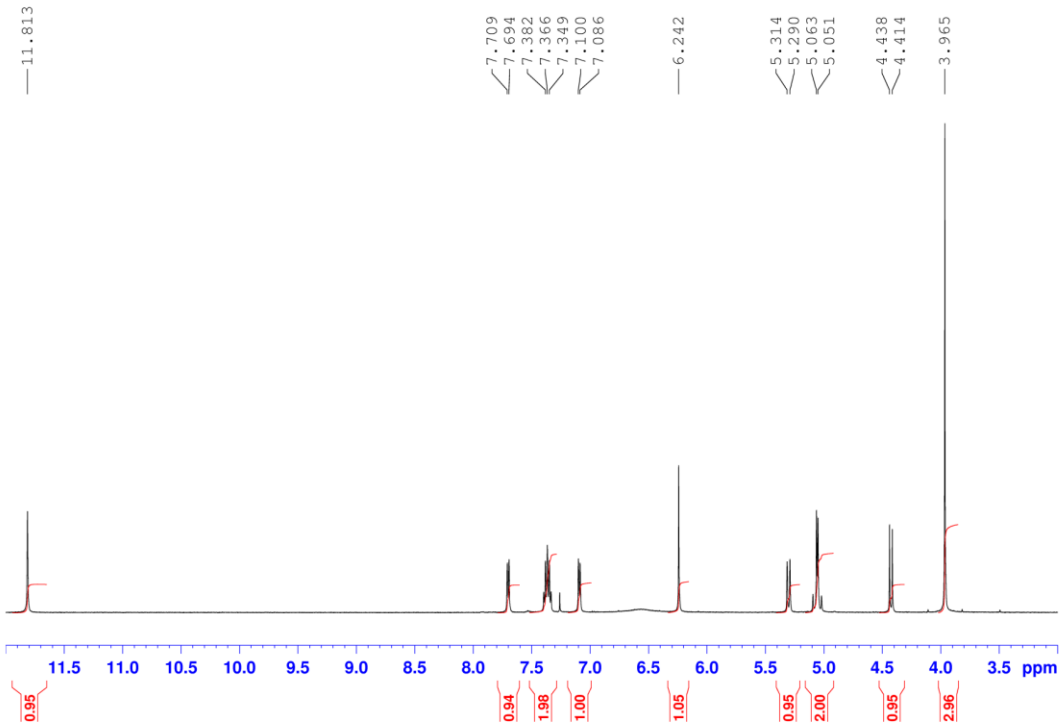

Fig. 12S. ^{1}H NMR spectrum of compound **6** in $CDCl_3$.

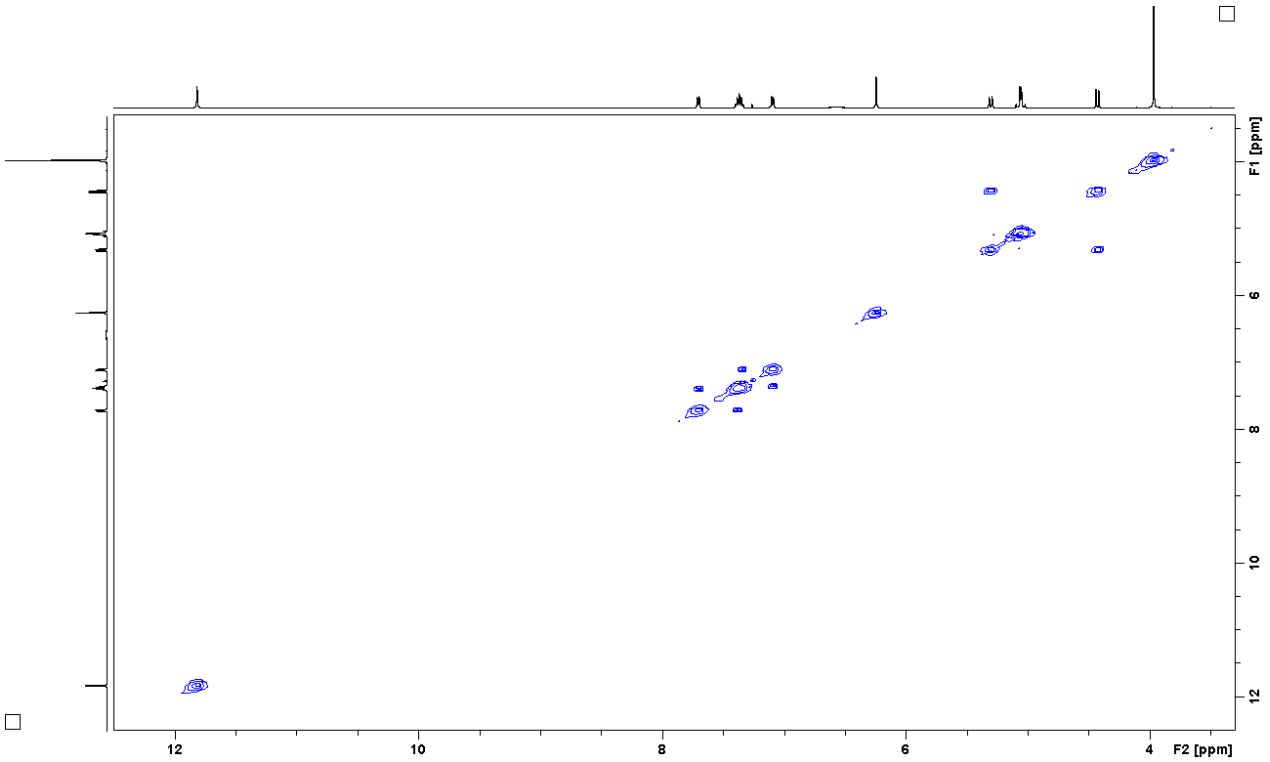

Fig. 13S. ^{1}H-^{1}H COSY NMR spectrum of compound **6** in $CDCl_3$.

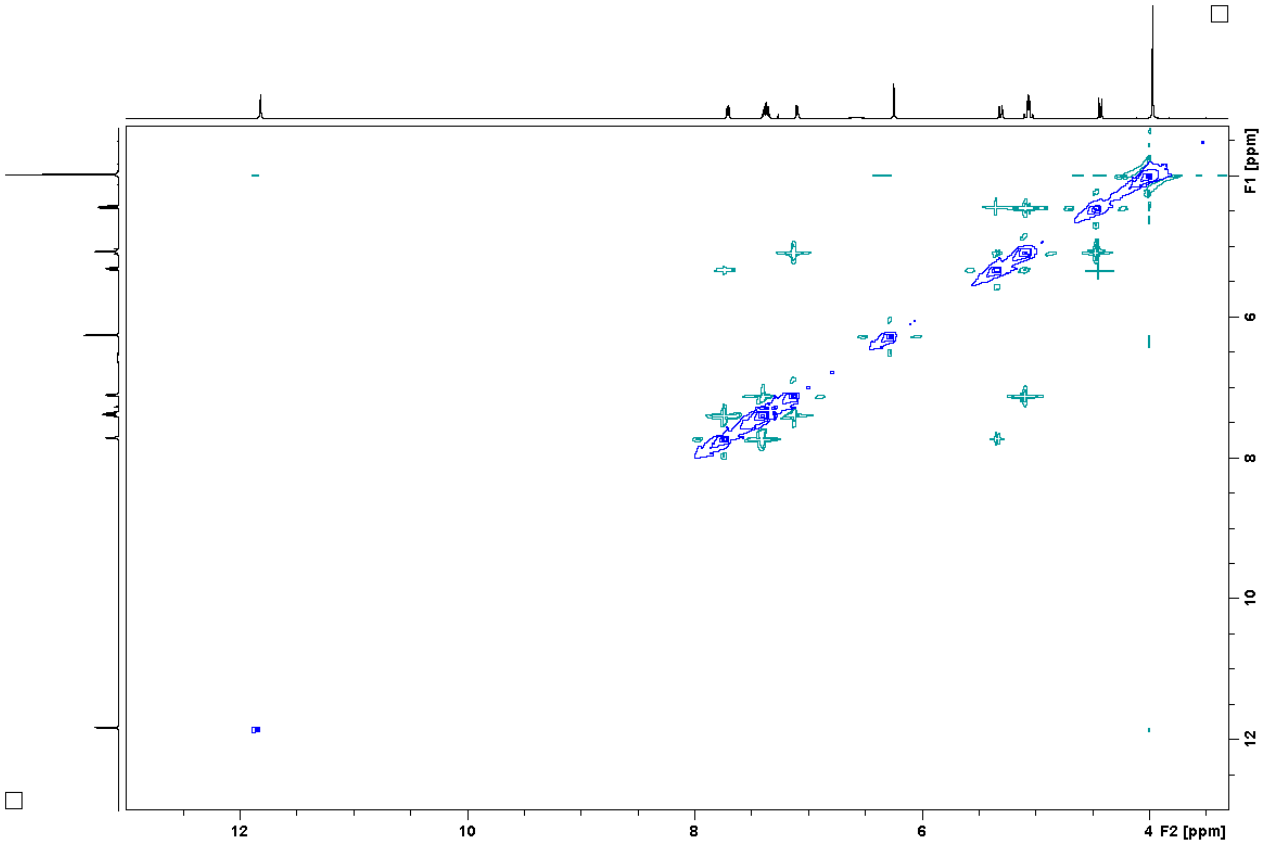

Fig. 14S. ^{1}H-^{1}H NOESY NMR spectrum of compound **6** in $CDCl_3$.

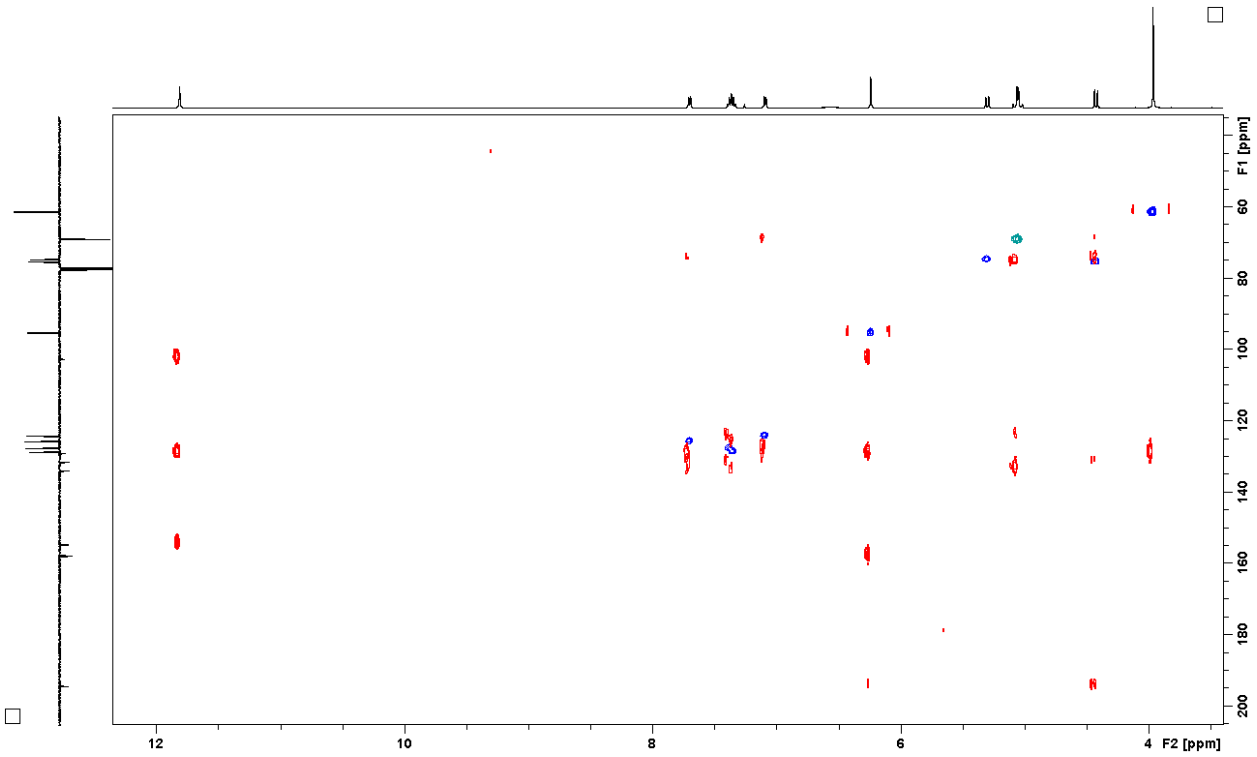

Fig. 15S. HSQC-DEPT (light green/blue) and HMBC (red) overlaid spectra of compound **6** in $CDCl_3$.

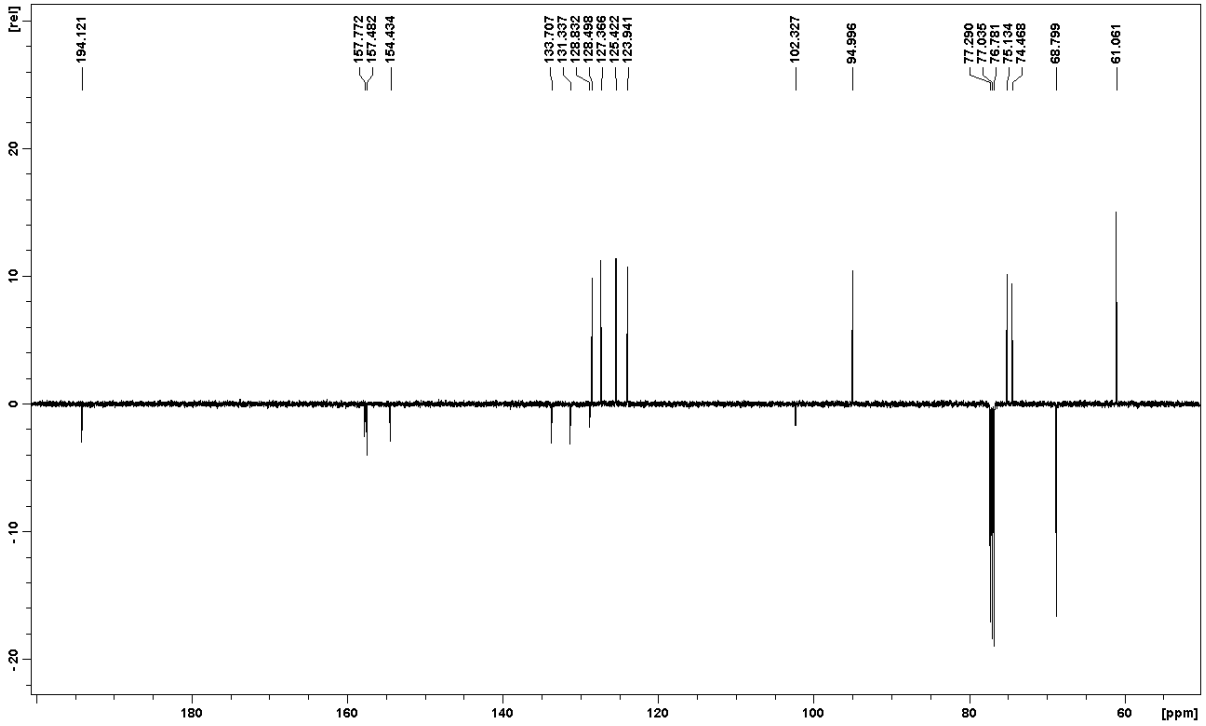

Fig. 16S. DEPTQ spectrum of compound **6** in $CDCl_3$.

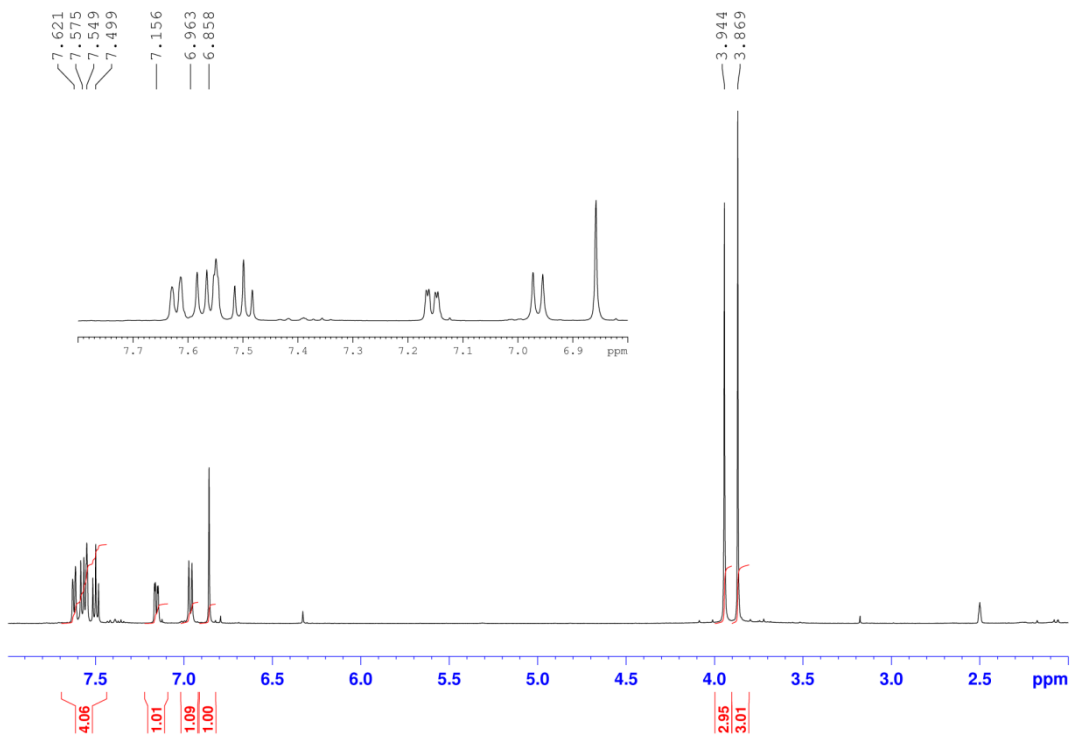

Fig. 17S. ^{1}H NMR spectrum of compound **18** in DMSO-d_6.

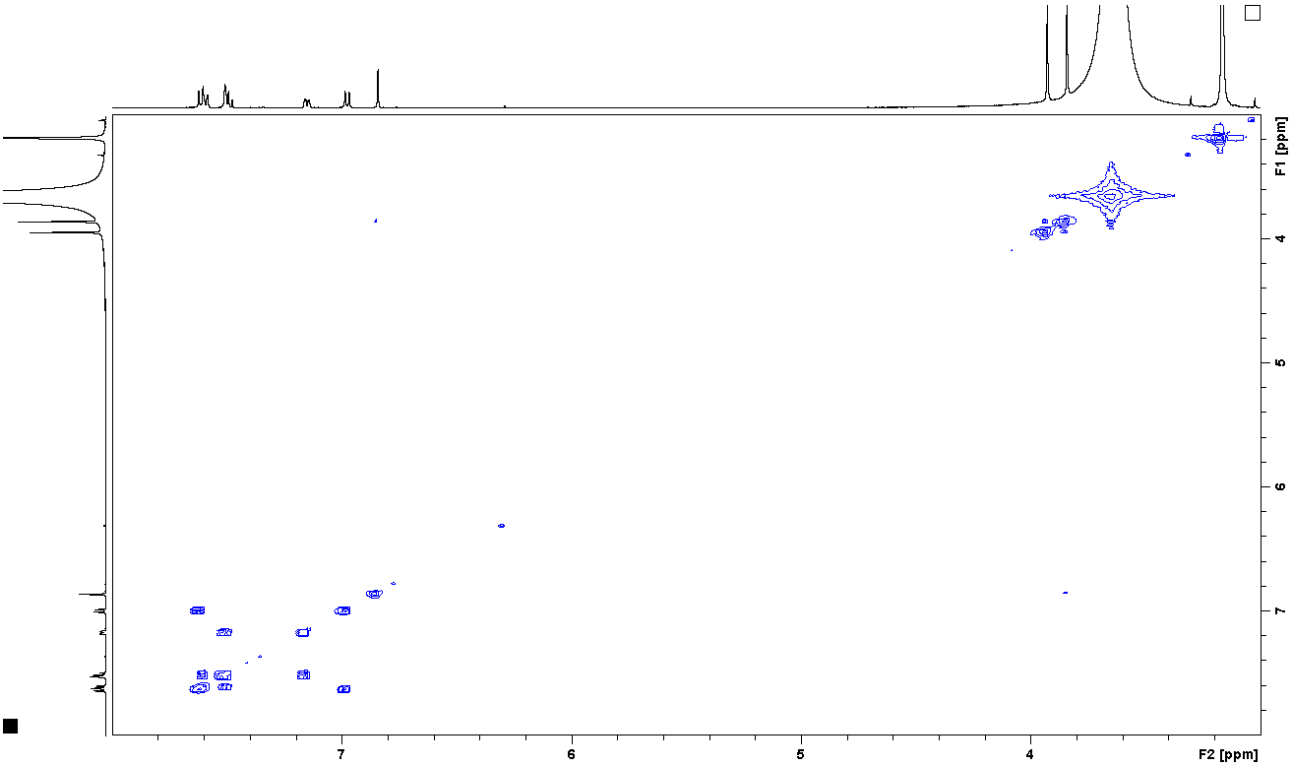

Fig. 18S. ^{1}H-^{1}H COSY NMR spectrum of compound **18** in DMSO-d_6.

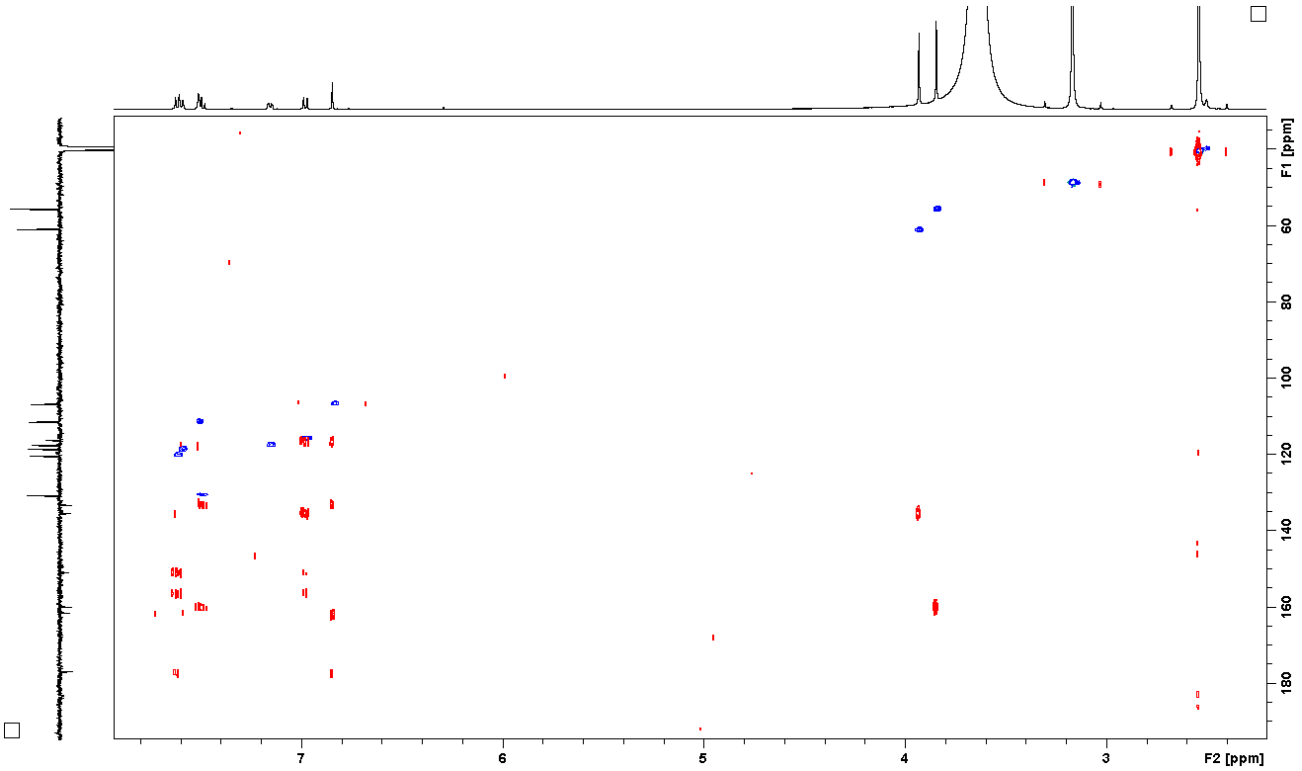

Fig. 19S. HSQC-DEPT (light green/blue) and HMBC (red) overlaid spectra of compound **18** in DMSO-d_6.

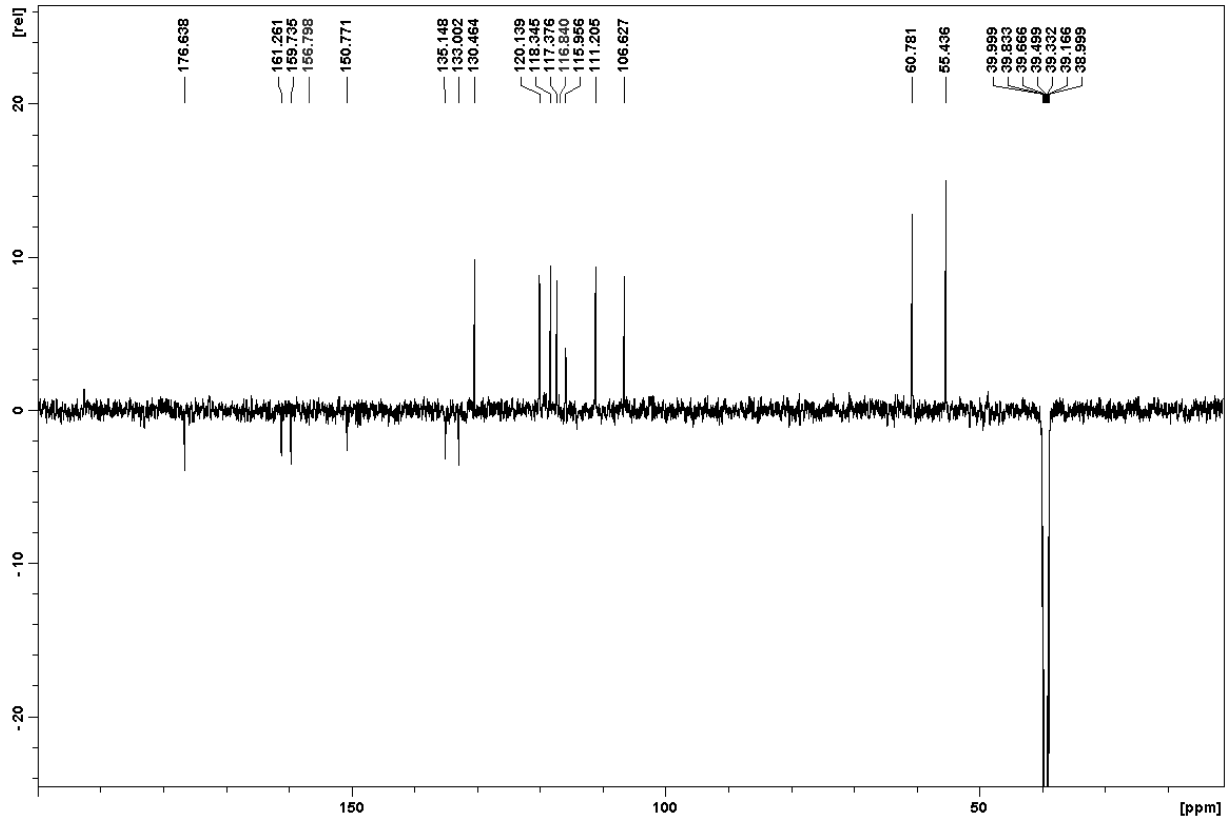

Fig. 20S. DEPTQ spectrum of compound **18** in DMSO-d_6.

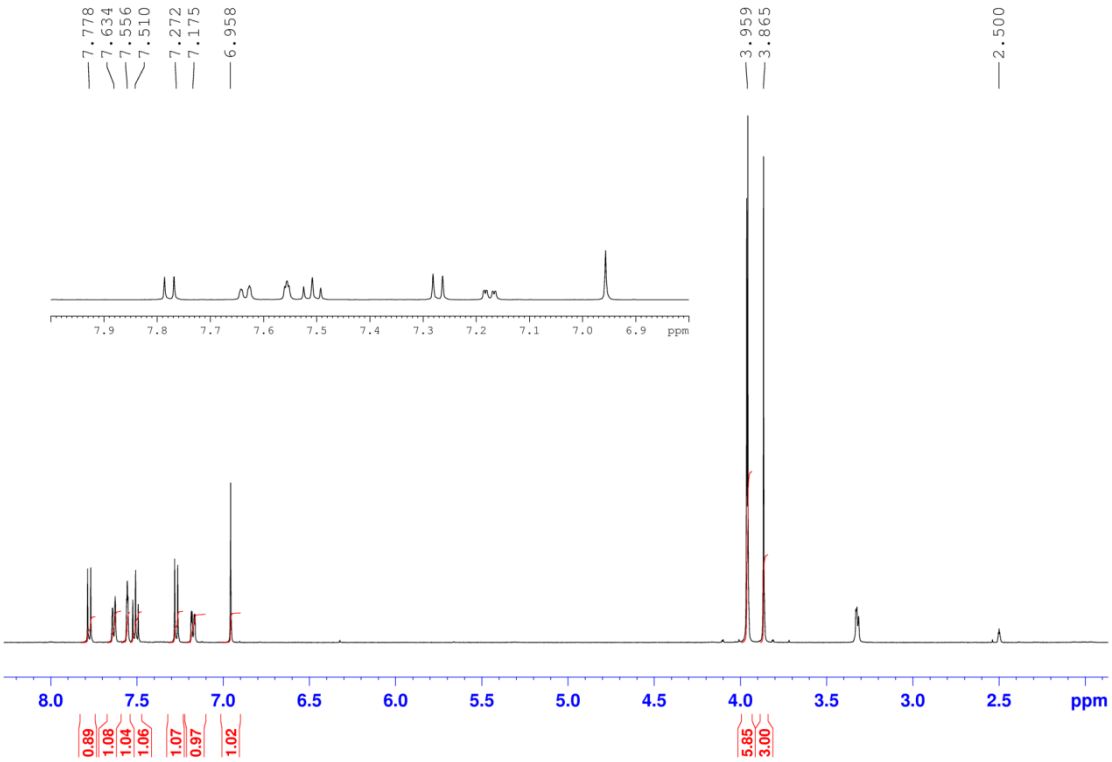

Fig. 21S. ^{1}H NMR spectrum of compound **19** in DMSO-d_6.

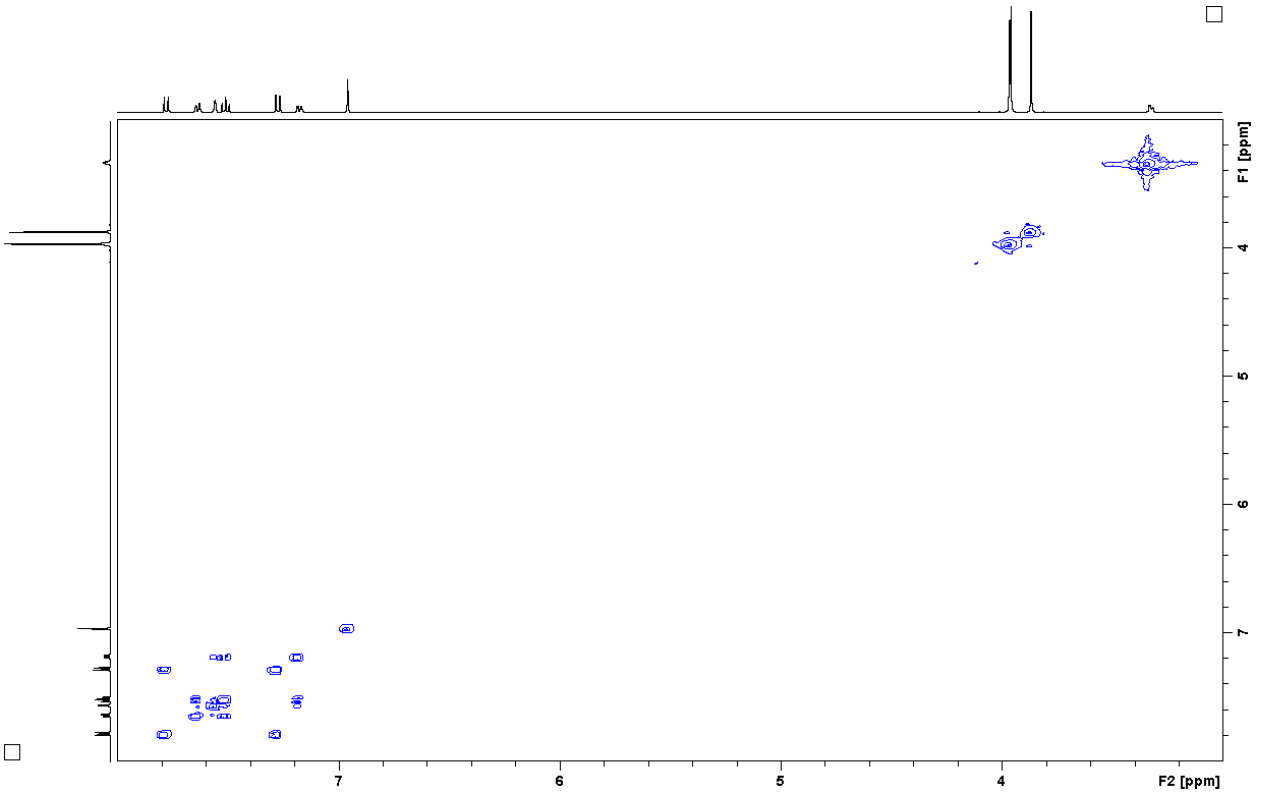

Fig. 22S. ^{1}H-^{1}H COSY NMR spectrum of compound **19** in DMSO-d_6.

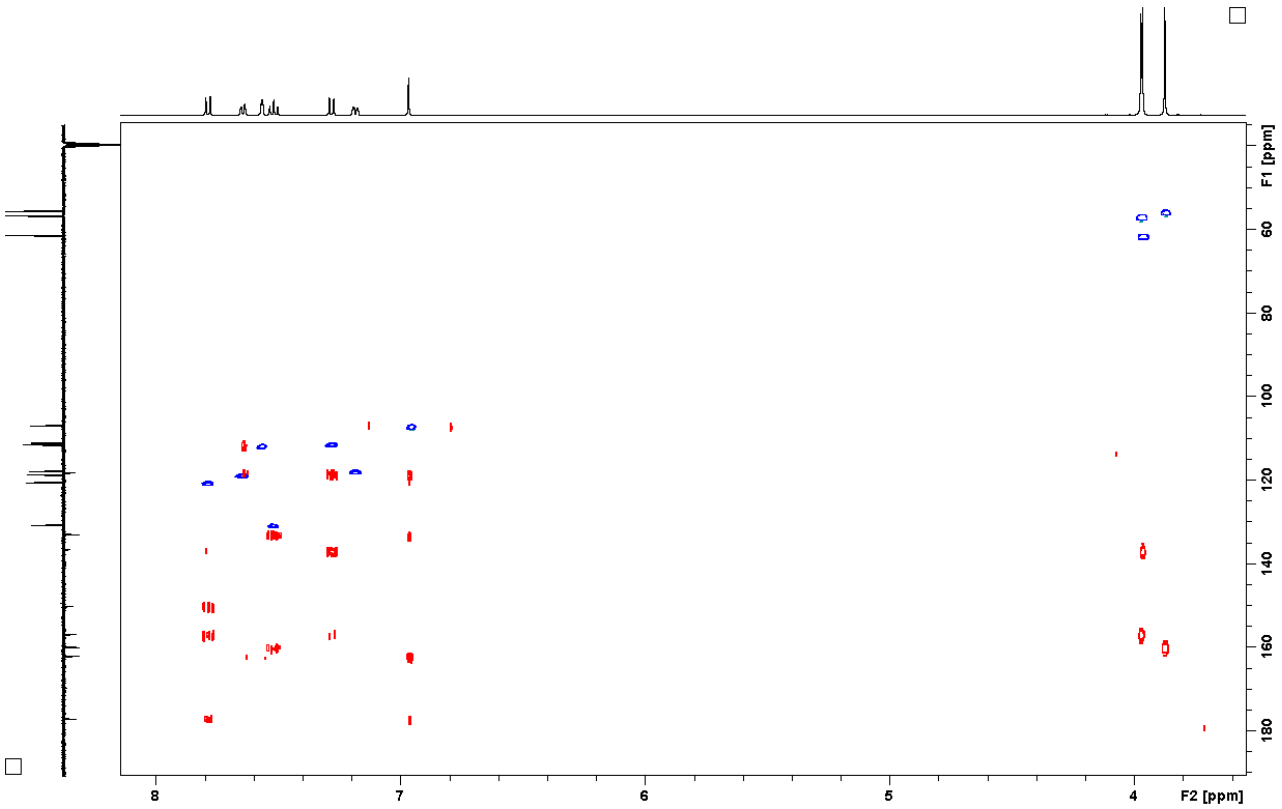

Fig. 23S. HSQC-DEPT (light green/blue) and HMBC (red) overlaid spectra of compound **19** in DMSO-d_6.

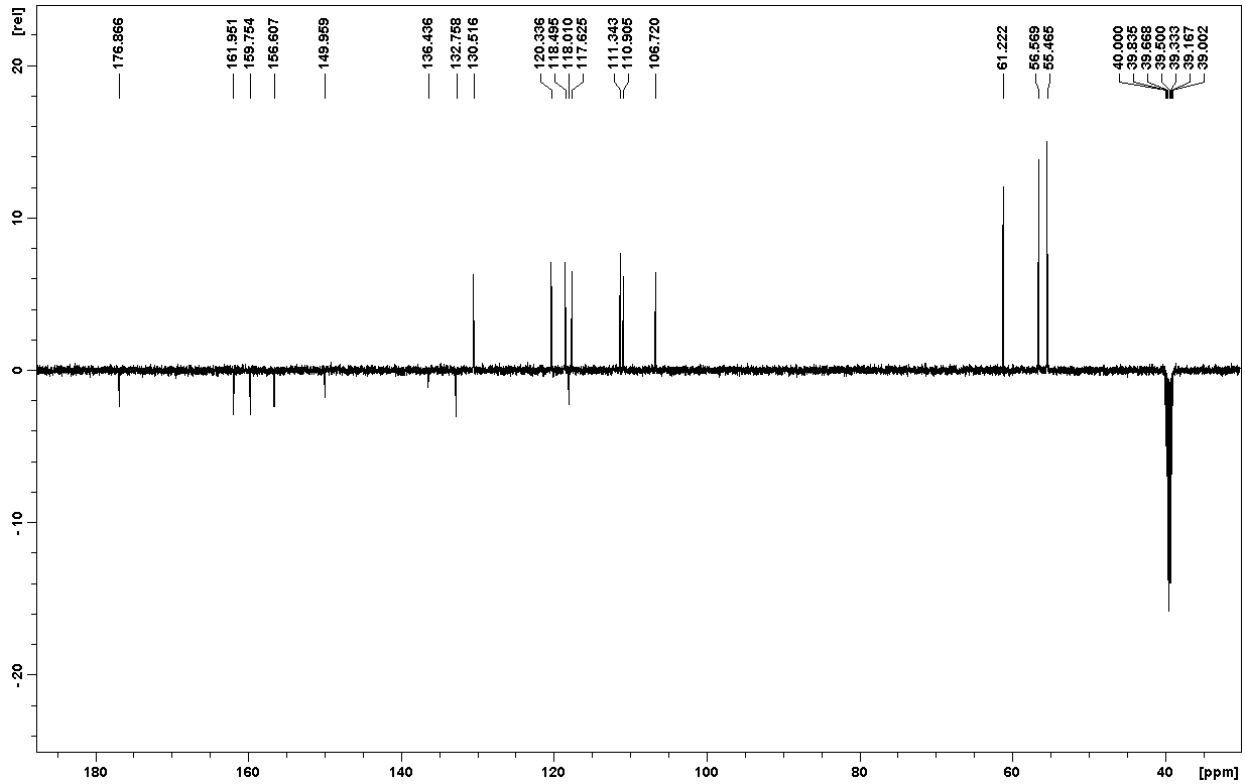

Fig. 24S. DEPTQ spectrum of compound **19** in DMSO-d_6.

Quantification of compounds 1 and 13

HPLC analyses were performed in triplicate on an Alliance 2695 instrument (Waters) equipped with a 996 PDA detector. Separations were performed on a SunFire C18 column (3.5 µm, 150 x 3.0 mm i.d., Waters) equipped with a guard column (10.0 x 3.0 mm i.d.). The flow rate was 0.4 mL/min. The mobile phase consisted of water with 0.1% formic acid (solvent A), and acetonitrile with 0.1% formic acid (solvent B). A gradient of 30% → 40% B (0 – 10 min), 40% B (10 – 30 min), 50% → 100% B (30 – 31 min), 100% B (31 – 45 min) was used to achieve best separation of compounds **1** and **13**. Detection was at 266 and 258 nm for compounds **1** and **13**, respectively. Equilibration time between injections was 6 min. The injections volume was 5 µl. All samples were prepared in DMSO. Quantification of compound **1** and **13** was performed on the same batch of the CH_2Cl_2 extract used for the HPLC-time based fractionation prepared at concentration of 6.294 mg/ml and 3.147 mg/ml, respectively. References **1** and **13** were isolated from *Galenia africana* in the course of this study, and their purity was ≥95% by ^{1}H NMR. Six calibrator solutions for each reference were prepared at concentrations of 0.035-0.800 mg/ml. Calibration curves were used to determine the concentration of the respective compounds in the extracts. Compound **1** $y = 4.7\ 10^7\ x + 6\ 10^5 (r^2 = 1)$; compound **13** $y = 6.6\ 10^7 x + 4.8\ 10^4$ ($r^2 = 1$). The content of compound **1** was 43.02 ± 0.01 mg/g extract (4.3%). The content of compound **13** was 94.31 ± 0.02 mg/g extract (9.4%). The limits of detection (LOD) and quantification (LOQ) were 0.0003 mg/ml and 0.0008 mg/ml for compound **1** and 0.0005 mg/ml and 0.001 mg/ml for compound **13,** respectively.

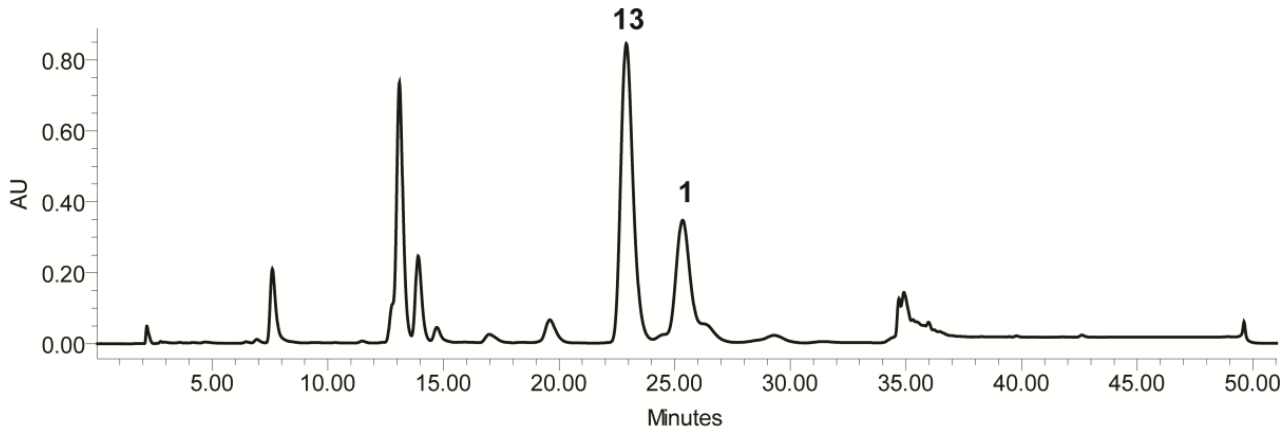

Fig 25S. HPLC chromatogram (254 nm) of *Galenia africana* CH_2Cl_2 extract (6.294 mg/ml) with conditions used for quantification of **1** and **13**.

2.2. hERG Channel Inhibitory Daphnane Diterpenoid Orthoesters, and Polycephalones A and B with Unprecedented Skeletons from *Gnidia polycephala* (manuscript and supporting information submitted to *Journal of Natural Products*)

(Manuscript ID: np-2015-003447)

My contribution towards this manuscript: I collaborated closely with Dr Maria De Mieri on the manufacturing of the plant material extracts, HPLC microfractionation of the extract, isolation of pure compounds, recording spectroscopic and other data, crystallization, structure elucidation including absolute configuration and preparation of the first draft of the manuscript.

Kun Du

hERG Channel Inhibitory Daphnane Diterpenoid Orthoesters, and Polycephalones A and B with Unprecedented Skeletons from *Gnidia polycephala*

Maria De Mieri[†,1], Kun Du[‡,1], Markus Neuburger[§], Priyanka Saxena[⊥], Pieter C. Zietsman[∥,▽], Steffen Hering[⊥], Jan H. van der Westhuizen[°] and Matthias Hamburger[†,*]

[†]Division of Pharmaceutical Biology, University of Basel, Klingelbergstrasse 50, CH-4056 Basel, Switzerland

[‡]Department of Chemistry, University of the Free State, Nelson Mandela Avenue, Bloemfontein 9301, South Africa

[§]Division of Inorganic Chemistry, Department of Chemistry, University of Basel, Basel, Switzerland

[⊥]Institute of Pharmacology and Toxicology, University of Vienna, Althanstrasse 14, A-1090 Vienna, Austria

[∥]National Museum, P.O. Box 266, Bloemfontein 9300, South Africa

[▽]Centre for Enviromental Management, University of the Free State, P.O. Box 339, Bloemfontein 9301, South Africa

[°]Directorate: Research Development, University of the Free State, Nelson Mandela Avenue,

Bloemfontein 9301, South Africa

*Corresponding author. Tel.: +41-61-2671425; fax: +41-61-2671474.
E-mail: matthias.hamburger@unibas.ch

[1]These authors contributed equally to this work

ABSTRACT

The hERG channel is an important anti-target in safety pharmacology. Several drugs have been withdrawn from the market or received severe restrictions on use because of hERG-related cardiotoxicity. In a screening of medicinal plants for hERG channel inhibition using a two-microelectrode voltage clamp assay with *Xenopus laevis* oocytes, a DCM extract of the roots of *Gnidia polycephala* (Thymelaeaceae) reduced the peak tail hERG current by 58.8 ± 13.4% (n = 3) at a concentration of 100 μg/mL. By means of HPLC-based activity profiling daphnane-type diterpenoid orthoesters (DDOs) **1**, **4** and **5** were identified as the active compounds [55.4 ± 7.0% (n = 4); 42.5 ± 16.0% (n = 3) and 51.3 ± 9.4% (n = 4) respectively, at 100 μM]. In a detailed phytochemical profiling of the active extract, a total of sixteen compounds were isolated and characterized, including two 2-phenyl-pyranones **15** and **16** with an unprecedented tetrahydro-4*H*-5,8-epoxypyrano[2,3-*d*]oxepine-4-one skeleton, two new DDOs (**3** and **4**), two new guaiane sesquiterpenoids (**11** and **12**), and ten known compounds (**1**-**2**, **5**-**10**, **13** and **14**). Structure elucidation was achieved by extensive spectroscopic analysis (1D and 2D NMR, HRMS and ECD), computational methods and X-ray crystallography.

INTRODUCTION

The human ether-a-go-go-related gene (hERG) encodes the inner pore-forming α-subunit of a voltage-gated potassium (K^+) channel which plays a pivotal role in cardiac action potential repolarization. It gates the flow of K^+ ions out of the cell that creates the rapidly activating delayed rectifier K^+ current (I_{Kr}) which accelerates repolarization.[1] Inhibition of the hERG channel by drugs leads to delayed repolarization and, consequently, to QT prolongation in the electrocardiogram (ECG) that may trigger life-threatening torsades de pointes (TdP) arrhythmia.[2] Therefore, hERG channel blockage is nowadays considered a major safety liability in preclinical

drug development and clinical practice.[3] The hERG channel is a promiscuous drug target that can be blocked by structurally diverse molecules, and this characteristic has led to withdrawals or restrictions of use of a series of noncardiac drug substances.[4,5] Surprisingly little is known about hERG-related cardiotoxicity of medicinal plants and finished herbal products (*viz.* phytomedicines) although they are widely used as complementary medicines and continue to increase in popularity. [6] Thus, there is an urgent need to critically assess the potential risks of these botanical products, and to identify hERG channel blocking secondary metabolites in these herbal medicines. In recent years, natural products belonging to the class of flavonoids, (e.g. naringenin) and alkaloids (e.g. reserpine and lobeline) have been identified as hERG blockers *in vitro*.[7-9] Also, it was shown that consumption of 1 L of pink grapefruit juice (containing naringenin) led to prolongation of the QT-interval in healthy volunteers and cardiac patients.[7] For a broader risk assessment, we recently screened a selection of widely used food and medicinal plants,[10] and identified the major alkaloid dihydroberberine in the traditional Chinese herbal drug Huanglian (rhizome of *Coptis chinensis* Franch., Ranunculaceae) as a compound with mild hERG-inhibitory properties in the *Xenopus* oocyte assay.[11] As a follow-up, we then screened a diverse collection of alkaloids found in medicinal plants and identified additional alkaloids with in vitro hERG blocking properties.[8]

We then extended the assessment of possible hERG liabilities by a screening of an extract library generated from 142 medicinal plants used in southern Africa. Extracts were tested in an automated functional two-microelectrode voltage-clamp assay on *Xenopus laevis* oocytes at a concentraction of 100 μg/mL. Among the extracts in this library, a DCM extract of the roots of *Gnidia polycephala* (Thymelaeaceae) induced 58.8 ± 13.4% (n = 3) inhibition of the peak tail hERG current. *G. polycephala* is a densely tufted bush native to Southern Africa. Its roots are used in Botswana to treat a variety of ailments.[12] However, the species is also documented as a poisonous plant responsible for loss of livestock.[13] Previous phytochemical studies of stems and roots of *G. polycephala* revealed the presence of phenolic acids and their derivatives.[14] We here report daphnane-type diterpenoid orthoesters (DDOs) as a new scaffold for hERG channel inhibitors, identified *via* HPLC-based activity profiling of the root extract. In addition, we performed a detailed phytochemical profiling of the extract that led to the characterization of 2-phenyl pyranones with an unprecedented tetrahydro-4*H*-5,8-epoxypyrano[2,3-*d*]oxepine-4-one

skeleton (**15** and **16**), two new DDOs (**3** and **4**), two new guaiane sesquiterpenoids (**11** and **12**), and eleven known compounds (**1**-**2**, **5**-**10**, **13** and **14**).

RESULT AND DISCUSSION

The hERG channel inhibitory activity in the DCM extract was tracked by means of HPLC-based activity profiling using a previously validated protocol, whereby time-based microfractions (20 fractions; 90 s each) obtained from a single injection of 5 mg of extract into a semi-preparative gradient-HPLC were submitted to an off-line bioassay with two-microelectrode voltage-clamp in *Xenopus laevis* oocytes transiently expressing the hERG channel.[15] The chromatogram (254 nm) of a semi-preparative HPLC separation and the corresponding activity profile of the time-based microfractionation are shown in Figure 1. By means of on-line (UV) and off-line (MS and microprobe NMR) spectroscopic analysis bioactivity was correlated with peaks in the chromatogram. The strongest inhibition was observed in microfractions 17 and 18 that showed current inhibition values of 60.5 % ± 2.5% (n = 2) and 55.5 ± 2.5% (n = 2), respectively. However, HPLC peaks in this time window were unresolved. LC-PDA-MS analysis of microfractions 17 and 18 under optimized conditions resolved the previously overlapping peaks (Figure 2). UV spectra (Figure 2A) combined with mass spectrometry (Figure 2B and C) revealed one major compound (**1**, *m/z* $[M+H]^+$ 529.5) in microfraction 17 corresponding to the dominant UV peak (**1**, t_R = 18.9 min), and two major compounds (**4**, *m/z* $[M+H]^+$ 649.6; **5**, *m/z* $[M+H]^+$ 649.6) in microfraction 18 corresponding to the two dominant UV peaks (**4**, t_R = 23.5 min; **5**, t_R = 25.5 min; respectively). Considering that the three compounds were the most abundant in the two active microfractions (17 and 18), we hypothesized that they were likely responsible for the hERG channel inhibitory effect of the extract.

For further pharmacological testing, compounds **1**, **4** and **5** were purified at preparative scale, using open column and flash chromatography on silica gel, gel fitration on Sephadex LH-20, and semipreparative HPLC. At the same time, minor compounds **2** and **3** were obtained. Chromatographic separation of other fractions led to additional compounds **6**-**16**. Structure elucidation was achieved by means of ESI-TOF-MS, and 1D and 2D microprobe NMR spectroscopy. The absolute configuration of compound **15** was established by comparison of experimental and calculated ECD spectra, and corroborated by X-ray crystallography. Known

compounds were identified as daphnane ester **1**,[16] excoecariatoxin **2**,[17,18] yuanhuacine **5**,[19] 2'-hydroxy-3'-methoxyflavone **6**,[20] 2'-3'-dimethoxyflavone **7**,[21] 6-hydroxy-2'-3'-dimethoxyflavone **8**,[22] 7,7'-dimethoxy-6,6'-biscoumarin **9**,[23] lisiocephalin **10**,[23] daphnauranol A **13**,[24] and chamaejasmone D **14**.[25] Compounds **3** and **4** were new DDOs, **11** and **12** new sesquiterpenes, and **15** and **16** were 2-phenyl-pyran-4-ones with an unprecedented tetrahydro-4*H*-5,8-epoxypyrano[2,3-*d*]oxepine-4-one skeleton. Structure elucidation of the new compounds is discussed below.

Compound **3** had a molecular formula of $C_{35}H_{40}O_{10}$, based on HRESIMS (*m/z* 643.2569 $[M+Na]^+$; calculated for $C_{35}H_{40}O_{10}Na$: 643.2514) and ^{13}C NMR data. The ^1H and ^{13}C NMR data of **3** (Table 1) were virtually identical to those of yuanhuacine **5**. The only difference was in the absence of resonances at δ_H 1.30-1.28 and δ_C 31.4 and 22.6 (positions 8' and 9' in **5**) in the spectra of **3**. Thus, the new daphane ester **3** was identified as shown in Fig. 1 and named yuanhuacine A.

Compound **4**, named as yuanhuacine B, showed the same molecular formula as **5** [$C_{37}H_{44}O_{10}$ according to an $[M + Na]^+$ ion at *m/z* 671.2827 (calcd for $C_{37}H_{44}O_{10}Na$, 671.2876) in the HRESIMS spectrum]. The ^1H NMR of **4** revealed that it was the *cis*-C-4'/C-5' geometrical isomer of **5**, as deduced from a $^3J_{H4', H5'}$ value of 11.3 Hz ($^3J_{H4', H5'}$ = 15.4 Hz in **5**). The ROESY spectra of **3** and **4** (Supporting Information), and their positive optical rotation confirmed their stereochemistry as reported.[26]

Compound **11** showed a molecular formula of $C_{15}H_{22}O_2$, based on HRESIMS (*m/z* 257.1520 $[M+Na]^+$; calculated for $C_{15}H_{22}O_2Na$: 257.1512) and ^{13}C NMR data. The UV absorption maximum at 247 nm, and three downfield shifted quaternary carbons (δ_C 208.1, C-3; δ_C 133.3, C-4; δ_C 173.9, C-5) indicated the presence of a conjugated system. The ^1H NMR displayed three diastereotopic methylenes [δ_H 2.68 (dd, *J* = 13.4 and 2.2 Hz, H-6a) and 2.38 (dd, *J* = 13.4 and 10.8 Hz, H-6b), δ_H 1.76 (overlapped, H-8a) and 1.59 (overlapped, H-8b), δ_H 1.58 (overlapped, H-9b) and 1.49 (m, H-9a)] and three methines [δ_H 2.31 (br m, H-1), 2.10 (br m, H-7), 1.76 (overlapped, H-10)] which, according to a ^1H-^1H COSY spectrum, belonged to a cycloheptane ring. Additional resonances were assigned to an oxygenated methine [δ_H 3.78 (d, *J* = 3.2 Hz, H-2)], an isopropenyl group (δ_C 149.1, C-11; δ_C 110.0, CH_2-12; δ_C 20.6 CH_3-13), a secondary

methyl group [δ_H 1.16 (d, J = 7.0 Hz)] and an upfield shifted vinylic methyl group [δ_H 1.62 (s), δ_C 7.9]. These spectroscopic data were readily assigned to a guaiane-type sesquiterpene with the same planar structure as 2β-hydroxy-1βH,7αH,10βH-guaia-4,11-(12)-dien-3-one reported from roots of *Ligularia narynensis* (Asteraceae).[27] However, slight differences in NMR shifts of **11** compared to reported data suggested that the compound was a diastereomer. The relative stereochemistry of **11** was assigned by detailed analysis of ^{1}H-^{1}H J couplings and of critical NOEs, and was confirmed through conformational analysis and geometrical optimization of the putative stereoisomer (Figure 4A). Similarly to previous reports,[27, 28] the anti-orientation of H-1 and H-2 was assigned on the basis of the $^3J_{H1\text{-}H2}$ value of 3.2 Hz, corresponding to a dihedral angle of approx 130 °. In a similar way, the equatorial orientation of the isopropenyl group was inferred by a $^3J_{H6,\ H7}$ value of 10.8 Hz. On the other hand, key NOESY contacts of H-6axial (δ_H 2.38) with H-1 (δ_H 2.31) and CH_3-14 (δ_H 1.16) suggested their cofacial orientation (Figure S15). Conformational analysis followed by geometrical optimization of the compound revealed an equilibrium between three conformations (C1 36.5%, C2 59.8% and C3 3.6%; Figure S30) for the cycloheptane ring that could explain the NOESY contacts H-1/$CH_3$14, H-10, and H-2/$CH_3$14, H-10, and the critical dipolar coupling between H-2 and H-9α that was only possible for the C1 conformer (distance H-2/H-9α 2.73Å). Hence, the structure of **11** was assigned as 2β-hydroxy-1βH,7αH,10αH-guaia-4,11-(12)-dien-3-one, the epimer at C-10 of the previously isolated stereoisomer.[27]

Compound **12** had a molecular formula of $C_{15}H_{22}O_3$ (HRESIMS *m/z* 273.1451 $[M+Na]^+$; calculated for $C_{15}H_{22}O_3Na$: 273.1416). NMR data of **12** were similar to those of **11**. The only marked difference was in the presence of an additional hydroxyl group due to oxidation of the allylic methylene group at C-6 [δ_H 4.59 (1H, d, J = 9.3 Hz) in compound **12**; δ_H 2.68 and 2.38 (CH_2-6) in **11**]. ^{1}H-^{1}H J coupling and NOESY contacts confirmed the same relative stereochemistry at carbons C-1, C-2, C-7 and C-10 as in **11** (Figure 4B). The α-orientation of the hydroxyl function at C-6 was inferred from a $^3J_{H6,\ H7}$ value of 9.3 Hz that implied an anti-diaxial orientation of these protons. NOESY contacts H-6/H-10, H_3-14 further proved this structural assignment. Thus, the structure of **12** was established as 2β,6α-dihydroxy-1βH,7αH,10αH-guaia-4,11-(12)-dien-3-one.

A molecular formula of $C_{17}H_{16}O_6$ was assigned to compound **15** based on an $[M + Na]^+$ ion at *m/z* 339.0866 (calcd for $C_{17}H_{16}O_6Na$, 339.0839) in its HRESIMS spectrum, indicating ten indices of hydrogen deficiency. The UV spectrum displayed absorption bands at 216 and 269 nm that were diagnostic of a conjugated benzene chromophore. DEPTQ, HSQC and HMBC spectra showed seven sp^2 quaternary carbons at δ_C 123.2, 125.4, 146.7, 153.0, 160.7, 161.5, including a carbonyl at δ_C 174.6, four aromatic carbons (CH) at δ_C 114.7, 115.7, 120.4 and 124.5, three oxygen-bearing sp^3 carbons at δ_C 67.1 (CH), 73.0 (CH_2) and 98.9 (CH), two methoxy groups at δ_C 56.0 and 60.6, and one methylene at δ_C 35.7. Subsequent scrutiny of the ^1H NMR, DEPTQ, ^1H-^1H COSY, HSQC, and HMBC spectra (Table 3) allowed the identification of two substructures (Figure 5). The sp^2 carbon and proton resonances were indicative of a 2-phenyl-pyran-4-one moiety (substructure a, rings B and C), with a tri-substituted B ring bearing an ABC spin system. Characteristic HMBC correlation from the ABC protons to oxygenated carbons at δ_C 146.7 (C-2') and δ_C 153.0 (C-3') unequivocally established the substitution pattern of the B ring (Figure 5). Moreover, diagnostic HMBC correlations from H-6' δ_H 7.21 and H-3 δ_H 6.67 to C-2 δ_C 161.5 confirmed the attachment of the B-ring at C-2. The remaining atoms forming substructure b (ring A in Figure 5) consisted of two spin systems contained three aliphatic protons each, as deduced by vicinal scalar couplings of H-5/H_2-6 and H-7/H_2-8 in the COSY spectrum. Attachment of fragment H-5/H_2-6 at C-10 (δ_C 123.2), was established *via* HMBC correlations from H-5 (δ_H 5.41) to C-4 (δ_C 174.6) and C-9 (δ_C 160.7), and from H_2-6 (δ_H 3.95 and 3.79) to C-10 (δ_C 123.2). Similarly, HMBC correlations from H_2-8 (δ_H 3.14 and 2.65) to C-10, and from H-7 (δ_H 5.91) to C-9 (δ_C 160.7) inferred the attachment of the H-7/H_2-8 spin system at C-9. The final connectivity of substructure b was established considering the two degrees of unsaturation and the two oxygen atoms that were still needed according to the molecular formula. The chemical shifts of CH-7 (δ_H 5.91 and δ_C 98.9) were indicative of an acetal proton that, consequently, dictated the need of an oxygen bridgehead between carbons C-7 and C-5. This structural assignment was supported by HMBC connectivities (H-5/C-7, H-7/C-5, H-7/C-6, and a weak H_2-8/C-6 correlation). Thus, the gross structure of **15** was established as reported in Figure 5, and the new compound was named polycephalone A. Based on geometric considerations, the attachment of the epoxy bridge at carbons C-5 and C-7 should be *syn*, and this was supported by a weak NOESY correlation between H-5 and H-7. The proximity of stereogenic centers at C-5 and C-7 to the pyran-4-one chromophore allowed the absolute configuration of **15** to be established as 5(*R*),7(*S*) by electronic circular dichroism (ECD)

(Figure 6). Furthermore, after several attempts, colorless needles of **15** were obtained from MeOH that were analyzed by X-ray crystallography. The ORTEP drawing (Figure 7) confirmed the structure and absolute configuration of **15** as above.

Compound **16** had a molecular formula of $C_{16}H_{14}O_6$ based on HRESIMS (*m/z* 325.0683 $[M+Na]^+$; calculated for $C_{16}H_{14}O_6Na$: 325.0683), and thus differed from **15** by 14 units. NMR data for **16** (Table 3) resembled those of **15**, but lacked a resonance of the methoxy group at C-3' [δ_H 3.86 (3H, s); δ_C 56.0] in compound **15**. Positive optical rotation, and an ECD spectrum (Figure S36) similar to that of **15** confirmed the stereochemistry of **16**. Thus, compound **16** was identified as depicted in Figure 3 and named polycephalone B.

To the best of our knowledge this is the first report on natural products containing a tetrahydro-4*H*-pyran[2,3-d]oxepine-4-one moiety. Considering the 2-phenyl-pyran-4-one scaffold it is reasonable to assume that **15** and **16** derive from a polyketide precursor [Figure 8 (1)]. A Baeyer-Villiger oxidation would be the key step that causes the A ring expansion [Figure 8 (2)]. Subsequent Michael-type nucleophilic addiction and reduction steps [Figure 8 (3)], followed by nucleophilic attack of the secondary alcohol to the hemiacetal group [Figure 8 (4)] would afford the tetrahydro-4*H*-5,8-epoxypyrano[2,3-*d*]oxepine-4-one ring and, thus, lead to structure **15**.

Compounds **1**, **4** and **5** were obtained in sufficient amounts for testing in the oocyte assay at a concentration of 100 μM. All three compounds displayed hERG channel inhibition [55.4 ± 7.0%, n = 4 (**1**); 42.5 ± 16.0%, n = 3 (**4**) and 51.3 ± 9.4%, n = 4 (**5**)] (Figure 9), thereby corroborating our assumption that they were largely responsible for the activity of the extract. DDOs occur only in the plant families of Thymelaeaceae and Euphorbiaceae. This class of compounds possesses a broad range of biological activities, whereby anticancer and TRPV1 activities have been studied in more detail.[29] More recently, DDOs have also been identified as potent and selective *in vitro* HIV inhibitors.[17] Although some DDOs possess interesting biological activities, only few compounds have been submitted to more advanced pharmacological evaluation. The most common undesirable effects associated with DDOs were irritant and tumor promoting activities, and general toxicity. However, hERG channel blocking properties are reported here for the first time for this class of compounds. With respect to the general aims of this project, the discovery of

hERG inhibition by DDOs is relevant beyond southern African traditional medicine, considering that DDO containing plants, e.g. *Daphne genkwa*, are used in Traditional Chinese Medicine.[30] Further toxicological studies are needed to evaluate in more detail the cardiotoxicity of this compound class, and the clinical relevance of our finding. However, our outcomes emphasize the need for more extensive safety assessment of traditional herbal remedies, in particular, of cardiac safety.

EXPERIMENTAL SECTION

General experimental procedures. Optical rotation was measured with a Perkin Elmer 341 polarimeter using a 10 cm microcell and MeOH (1mg/mL) as solvent. UV and CD spectra were recorded in MeOH (120 μg/mL) on a Chirascan CD spectrometer, and analyzed with Pro-Data V2.4 software. NMR spectra were recorded on a Bruker AVANCE III^{TM} 500 MHz spectrometer equipped with a 1 mm TXI microprobe (^{1}H and 2D NMR) or a 5 mm BBO probe (^{13}C NMR) (Bruker BioSpin) operating at 500 (^{1}H) and 125 MHz (^{13}C). All measurements were carried out at 291.15 K. Chemical shifts are reported as δ values (ppm) with the residual solvent signal as internal reference, *J* in Hz. Standard pulse sequences from Topspin 3.0 software package were used. For HR-ESIMS a micrOTOF ESI-MS system (Bruker Daltonics) was used. Mass calibration was performed with a solution of formic acid 0.1% in 2-propanol/water (1:1) containing 5 mM NaOH. Mass spectra were recorded in the range of *m/z* 150 – 1500 in positive ion mode with the aid of micrOTOF control software 1.1 (Bruker Daltonics). HPLC-PDA-MS analyses were performed with an Agilent 1100 system consisting of a degasser, a quaternary pump, a column oven, a PDA detector connected to a Gilson 215 injector and to an Esquire 3000 plus ion trap mass spectrometer (Bruker Daltonics). Data acquisition and processing were performed using HyStar 3.0 software (Bruker Daltonics). Flash chromatography was carried out with a PuriFlash® 4100 chromatography system (Interchim) controlled by InterSoft V5.0 software. Semi-preparative HPLC was performed with an Agilent 1100 series instrument equipped with a PDA detector. Data acquisition and processing were performed using HyStar 3.2 software (Bruker Daltonics). HPLC-grade methanol (MeOH), acetonitrile (MeCN) (Scharlau Chemie S.A.), and water (obtained by an EASY-pure II from Barnstead water purification system, Dubuque) were used for HPLC separations. HPLC solvents contained 0.1% HCOOH (Scharlau) for analytical separations. Dimethylsulfoxide (DMSO) (Scharlau) was used for dissolving the samples. Chloroform-*d* (100

atom% D) and DMSO-d_6 (100 atom% D) for NMR were purchased from Armar Chemicals. Solvents used for extraction were of analytical grade (Romil Pure Chemistry).

Plant material. The roots of *G. polycephala* were collected from the Postmasburg Magisterial District (Northern Cape Province), South Africa, in September 2013 by P.C. & L. Zietsman. A voucher specimen (NMB 26166) was deposited in the herbarium of the National Museum, Bloemfontein, South Africa (NMB).

Extraction. The air-dried roots (180 g) of *G. polycephala* were ground into powder, and percolated with DCM (3 x 24 h) at room temperature. The solvent was evaporated under reduced pressure to yield 3.2 g of crude extract.

Microfractionation and activity profiling. Time-based microfractionation for HPLC-activity profiling was performed as previously described,[8] with minor modifications: separation was done on a SunFire™ C18 column (5 μm, 10 × 150 mm, Waters) with H_2O (A) and MeCN (B) using the following gradient profile: 20% → 30% B (0 – 5 min), 30% → 54% B (5 – 22 min), 54% → 100% B (22 – 25 min), 100% B (25 – 32 min). The flow rate was 4 mL/min. 100 μL of a stock solution of the extract (50 mg/mL in DMSO) were injected. A total of 20 microfractions of 90 s each were collected with the aid of a F204 fraction collector (Gilson). After solvent removal (GeneVac EZ-2 Plus evaporator), the dried films were re-dissolved in methanol, transferred to 4-mL glass vial, and dried again under N_2 gas prior to dissolution in DMSO for bioassay.

Optimized separation of active microfractions. Separation was achieved on a SunFire™ C18 column (3.5 μm, 3 × 150 mm, Waters) with 0.1% formic acid in H_2O (A) and 0.1% formic acid in MeCN (B) using the following gradient profile: 50% → 80% B (0 – 15 min), 80% B (15 – 40 min), 80% → 100% B (40 – 42 min), 100% B (42 – 50 min). The flow rate was 0.4 mL/min.

Isolation of compounds 1-16. The DCM extract (3.0 g) was separated by open column chromatography (34.5 × 4 cm) on silica gel (0.04-0.063 mm, 200 g) with a step-gradient *n*-hexane (A), EtOAc (B): 5% B (100 mL), 10% B (100 mL), 15% B (100 mL), 25% B (100 mL), 35% B (100 mL), 40% B (100 mL), 45% B (100 mL), 50% B (1.4 L), 60% B (200 mL), 100% B (1.0 L),

and final wash with EtOAc-MeOH 1:1 (2.0 L). The extract was dissolved in 10 mL DCM for loading, and the flow rate was 15 mL/min. Fractions A-K were combined based on TLC analysis [A (82.6 mg), B (57.6 mg), C (30.7 mg), D (458.0 mg), E (185.2 mg), F (228.6 mg), G (797.7 mg), H (80.2 mg), I (113.6 mg), J (481.1 mg), and K (513.0 mg)].

Fraction D (382 mg) was separated by open column chromatography (36 x 2.5 cm) on silica gel (0.04-0.063 mm) with the following step gradient: DCM (1.7 L), *n*-hexane-EtOAc 1:1 (1 L) and EtOAc (2 L), at a flow rate of 6 mL/min. Fractions D_1-D_6 were combined based on TLC analysis [D_1 (56.8 mg), D_2 (84.7 mg), D_3 (277.1 mg), D_4 (34.0 mg), D_5 (44.0 mg), and D_6 (58.2 mg)].

Fraction E (164.4 mg) was separated on a Sephadex LH-20 column (31 x 4 cm) with EtOAc, at a flow rate of 1.5 mL/min. Fractions E_1-E_9 were combined based on TLC analysis [E_1 (69.7 mg), E_2 (5 mg), E_3 (8.8 mg), E_4 (13.7 mg), E_5 (30.5 mg), E_6 (4.8 mg), E_7 (21.8 mg), E_8 (7.9 mg), E_9 (10.0 mg)].

Purification of subfraction E_7 (19.8 mg) by semiprep HPLC [SunFire™ C18 column (5 μm, 10 × 150 mm, Waters)] with a gradient [H_2O (A), MeCN (B); 40% B (0-30 min), 40% → 100% B (30-31 min), 100% B (31-35 min); flow rate 4 mL/min; sample conc. 39.6 mg/mL in DMSO; injection volume 200 μL] gave **11** (8.4 mg, t_R 23.0 min).

Fraction F (149.8 mg) was separated by flash chromatography on a C18 cartridge (30 g, RediSep®Rf; Teledyne Isco, Nebraska, USA) [H_2O (A), MeCN (B); 50% → 80% B (0-1 h), 80% B (1-2 h), 80% → 100% B (2 h-2 h 10 min), 100% B (2 h 10 min-3 h); flow rate 10 mL/min; sample dissolved in 1 mL DMSO for injection; fractions of 10 mL each]. Fractions F_1-F_7 were combined based on TLC analysis [F_1 (16.4 mg), F_2 (17.2 mg), F_3 (10.1 mg), F_4 (10.4 mg), F_5 (7.2 mg), F_6 (7.8 mg), F_7 (20.8 mg)].

Subfraction F_2 (17.2 mg) was separated by flash chromatography on a silica cartridge (15 μm, 40 g, puriFlash®) [EtOAc (A), *n*-hexane (B); 100% → 80% B (0-1 h), 80% → 70% B (1-2 h), 70% → 50% B (2-3 h) and 50% → 0% B (3-4 h); flow rate 10 mL/min; sample dissolved in 1.5 mL DCM for injection; fractions of 10 mL each]. Fractions $F_{2.1}$- $F_{2.6}$ were combined based on TLC

analysis [$F_{2.1}$ (2.8 mg), $F_{2.2}$ (6.1 mg), $F_{2.3}$ (2.6 mg), $F_{2.4}$ (1.8 mg), $F_{2.5}$ (3.6 mg), $F_{2.6}$ (3.1 mg)]. Fractions $F_{2.2}$ and $F_{2.5}$ consisted of **11** and **7**, respectively.

Fraction G (697.7 mg) was separated on a Sephadex LH-20 column (19 x 3 cm) with EtOAc, at a flow rate 2 mL/min. Fractions G_1- G_8 were combined based on TLC analysis [G_1 (101.0 mg), G_2 (122.0 mg), G_3 (34.0 mg), G_4 (141.0 mg), G_5 (33.0 mg), G_6 (30.0 mg), G_7 (98.0 mg), G_8 (97.0 mg)].

After washing with hexane to remove the lipophilic products, subfraction G_4 was combined with G_3 and G_5. The combined fraction (150 mg) was then separated by flash chromatography on a C18 cartridge (30 g, RediSep®Rf) [H_2O (A), MeCN (B); 50% → 80% B (0-1 h), 80% B (1-2 h), 80% → 100% B (2 h-2 h 10 min) and 100% B (2 h 10 min-3 h); flow rate 10 mL/min; sample dissolved in 1 mL DMSO for injection; fractions of 10 mL each]. Fractions $G_{4.1}$- $G_{4.8}$ were combined based on TLC analysis [$G_{4.1}$ (45.4 mg), $G_{4.2}$ (17.3 mg), $G_{4.3}$ (1.2 mg), $G_{4.4}$ (3.1 mg), $G_{4.5}$ (8.6 mg), $G_{4.6}$ (9.5 mg), $G_{4.7}$ (3.9 mg), $G_{4.8}$ (3.9 mg)].

Repeated injections of subfraction $G_{4.2}$ (17.0 mg) onto a semiprep HPLC column [SunFire™ C18 column (5 μm, 10 × 150 mm, Waters)] [H_2O (A) and MeCN (B); 50% → 67% B (0-15 min), 67% B (15-30 min), 67% → 100% B (30-35 min), 100% B (35-40 min); flow rate 4 mL/min; sample conc. 34 mg/mL in DMSO; injection volume 50-80 μL each] gave **1** (6.2 mg, t_R 24.5 min), **3** (1.3 mg, t_R 25.9 min) and **2** (3.7 mg, t_R 27.5 min). Purification of subfraction $G_{4.5}$ (8.6 mg) by repeated injections onto semiprep HPLC [SunFire™ C18 column (5 μm, 10 × 150 mm, Waters)] with a gradient [H_2O (A) and MeCN (B); 70% → 80% B (0-20 min), 80% B (20-30 min), 80% → 100% B (30-35 min), 100% B (35-40 min); flow rate 4 mL/min; sample conc. 21.5 mg/mL in DMSO; injection volume 200 μL] gave **4** (3.3 mg, t_R 19.5 min). Purification of subfraction $G_{4.6}$ (9.5 mg) [sample concentration (31.6 mg/mL) and injection volume (300 μL)] with the same conditions afforded **5** (5.4 mg, t_R 21.5 min).

Subfraction G_7 (93.5 mg) was separated by flash chromatography on a C18 cartridge (30 g, RediSep®Rf) [H_2O (A), MeCN (B); 50% → 80% B (0-2 h), 80% B (2-3 h), 80% → 100% B (3 h-4 h) and 100% B (4 h-5 h); flow rate of 10 mL/min; sample dissolved in 1 mL DMSO for

injection; fractions of 10 mL each] . Fractions $G_{7.1}$- $G_{7.11}$ were combined based on TLC analysis [$G_{7.1}$ (15.4 mg), $G_{7.2}$ (9.3 mg), $G_{7.3}$ (4.1 mg), $G_{7.4}$ (4.5 mg), $G_{7.5}$ (6.2 mg), $G_{7.6}$ (10.7 mg), $G_{7.7}$ (6.5 mg), $G_{7.8}$ (2.9 mg), $G_{7.9}$ (6.2 mg), $G_{7.10}$ (2.5 mg), $G_{7.11}$ (33.9 mg)]. Compound **10** (5.3 mg) was precipitated from $G_{7.6}$.

Purification of subfraction $G_{7.2}$ (9.3 mg) by semiprep HPLC [SunFire™ C18 column (5 μm, 10 × 150 mm, Waters)] [H_2O (A) and MeCN (B); 20% → 30% B (0-30 min), 30% → 100% B (30-35 min); flow rate 4 mL/min; sample conc. 18.6 mg/mL in DMSO; injection volume 300 μL] gave **15** (3.0 mg, t_R 29.5 min).

Subfraction G_8 (91.7 mg) was separated by flash chromatography on a C18 cartridge (30 g, RediSep®Rf) [H_2O (A), MeCN (B); 10% → 50% B (0-1 h), 50% → 80% B (1 h-3 h), 80% → 100% B (3 h-3 h 30 min) and 100% B (3 h 30 min-4 h); flow rate 10 mL/min; sample dissolved in 1 mL DMSO for injection; fractions of 10 mL each] . Fractions $G_{8.1}$-$G_{8.1}$ were combined based on TLC analysis [$G_{8.1}$ (11.6 mg), $G_{8.2}$ (9.1 mg), $G_{8.3}$ (7.0 mg), $G_{8.4}$ (7.1 mg), $G_{8.5}$ (21.0 mg), $G_{8.6}$ (2.9 mg), $G_{8.7}$ (14.4 mg), $G_{8.8}$ (1.5 mg), $G_{8.9}$ (2.8 mg), $G_{8.10}$ (46.8 mg), $G_{8.11}$ (2.0 mg), $G_{8.12}$ (19.8 mg)].

Subfractions $G_{8.2}$ and $G_{8.3}$ (16.1 mg) were combined and separated by flash chromatography on a silica cartridge (30 μm, 4 g, puriFlash®) [*n*-hexane (A), EtOAc (B), 0% → 40% B (0-0.5 h), 40% B (0.5 h-1 h), 40% → 100% B (1 h-1.5 h) and 100% B (1.5 h-2 h); flow rate 5 mL/min; sample dissolved in 0.5 mL DCM for injection; fractions of 5 mL each]. Fractions $G_{8.2.1}$- $G_{8.2.10}$ were combined based on TLC analysis [$G_{8.2.1}$ (1.9 mg), $G_{8.2.2}$ (0.7 mg), $G_{8.2.3}$ (0.4 mg), $G_{8.2.4}$ (0.4 mg), $G_{8.2.5}$ (2.0 mg), $G_{8.2.6}$ (1.2 mg), $G_{8.2.7}$ (0.3 mg), $G_{8.2.8}$ (3.3 mg), $G_{8.2.9}$ (2.6 mg), $G_{8.2.10}$ (1.7 mg)]. Fractions $G_{8.2.2}$, $G_{8.2.5}$ and $G_{8.2.9}$ consisted of **12**, **13** and **16**, respectively.

Subfraction. $G_{8.7}$ (13.0 mg) was separated by flash chromatography on a silica cartridge (30 μm, 4 g, puriFlash®) with a gradient [*n*-hexane (A), EtOAc (B); 0% → 60% B (0-0.5 h), 60% B (0.5 h-1 h), 60% → 100% B (1 h-1.5 h); flow rate 5 mL/min; sample dissolved in 0.5 mL DCM for injection; fractions of 5 mL each] . Fractions were combined based on TLC analysis [$G_{8.7.1.1}$ (5.9 mg), $G_{8.7.1.2}$ (0.9 mg), $G_{8.7.1.3}$ (2.5 mg), $G_{8.7.1.4}$ (0.8 mg)]. Fractions $G_{8.7.1.1}$ and $G_{8.7.1.3}$ consisted of **14** and **8**, respectively.

Purification of subfraction $G_{8.10}$ (46.8 mg) by semiprep HPLC [SunFire™ C18 column (5 μm, 10 × 150 mm, Waters)] [H_2O (A), MeCN (B); 30% → 35% B (0-10 min), 35% B (10-30 min), 35% → 100% B (30-35 min); flow rate 4 mL/min; sample conc. 58.5 mg/mL in DMSO; injection volume 200-300 μL] gave **6** (2.7 mg, t_R 18.5 min) and **9** (0.6 mg, t_R 25.5 min).

(+)Yuanhuacine A (**3**): yellow amorphous solid; $[\alpha]_D$= +43.9 ° (c 0.11 $CHCl_3$); UV (MeOH) λ_{max} (log ε) 232 (3.52) nm.; ^1H and ^{13}C NMR data, see Table 1; HRESIMS *m/z* 643.2569 $[M+Na]^+$ (calculated for $C_{35}H_{40}O_{10}Na$: 643.2514). NMR and ECD spectra of **3** are available as Supporting Information.

(+)Yuanhuacine B (**4**): off-white amorphous solid; $[\alpha]_D$= +52.7 ° (c 0.30 $CHCl_3$); UV (MeOH) λ_{max} (log ε) 235 (3.63) nm; ^1H and ^{13}C NMR data, see Table 1; HRESIMS *m/z* 671.2876 $[M+Na]^+$ (calculated for $C_{37}H_{44}O_{10}Na$: 671.2827). NMR and ECD spectra of **4** are available as Supporting Information.

(-)2β-Hydroxy-1βH,7αH,10αH-guaia-4,11-(12)-dien-3-one(**11**): colorless oil; $[\alpha]_D$= -70.8 ° (c 0.13 $CHCl_3$); UV (MeOH) λ_{max} (log ε) 247 (3.37) nm; ^1H and ^{13}C NMR data, see Table 2; HRESIMS *m/z* 257.1520 $[M+Na]^+$ (calculated for $C_{15}H_{22}O_2Na$: 257.1512). NMR and ECD spectra of **11** are available as Supporting Information.

(-)2β,6α-Dihydroxy-1βH,7αH,10αH-guaia-4,11-(12)-dien-3-one (**12**): white amorphous solid; $[\alpha]_D$= -36.5 ° (c 0.04 $CHCl_3$); UV (MeOH) λ_{max} (log ε) 238 (3.15), 313 (2.73) nm; ^1H and ^{13}C NMR data, see Table 2; HRESIMS *m/z* 273.1451 $[M+Na]^+$ (calculated for $C_{15}H_{22}O_3Na$: 273.1416). NMR and ECD spectra of **12** are available as Supporting Information.

(+)Polycephalone A (**15**): colorless needle-type crystals; $[\alpha]_D$= +29.5 ° (c 0.12 in $CHCl_3$); UV (MeOH) λ_{max} (log ε) 216 (3.17), 269 (3.00) nm; ^1H and ^{13}C NMR data, see Table 3; HRESIMS *m/z* 339.0866 $[M+Na]^+$ (calculated for $C_{17}H_{16}O_6Na$: 339.0839). NMR and ECD spectra of **15** are available as Supporting Information.

(+)*Polycephalone B* (**16**): white amorphous solid; $[\alpha]_D$ = +4.7 ° (c 0.05 $CHCl_3$); UV (MeOH) λ_{max}

(log ε) 226 (3.19), 272 (3.07) nm; ^{1}H and ^{13}C NMR data, see Table 3; HRESIMS *m/z* 325.0683 $[M+Na]^{+}$ (calculated for $C_{16}H_{14}O_6Na$: 325.0683). NMR and ECD spectra of **16** are available as Supporting Information.

X-ray crystallography of compound 15. Polycephalone A **15** was crystallized by slow evaporation at 4 ℃ from a solution of MeOH. The crystal was measured on a Bruker Kappa Apex2 diffractometer at 123K using graphite-monochromated Cu K_α-radiation with λ = 1.54180 Å, Θ_{max} = 68.979 °. Minimal/maximal transmission 0.95/0.96, μ = 0.937 mm^{-1}. The Apex2 suite[31] has been used for data collection and integration. From a total of 19540 reflections, 5420 were independent (merging r = 0.024). From these, 5391 were considered as observed (I>2.0σ(I)) and were used to refine 434 parameters. The structure was solved by the charge flipping method using the program Superflip.[32] Least-squares refinement against F was carried out on all non-hydrogen atoms using the program CRYSTALS.[33] R = 0.0282 (observed data), wR = 0.0324 (all data), GOF = 1.0988. Minimal/maximal residual electron density = -0.43/0.23 e Å^{-3}. Chebychev polynomial weights[34] were used to complete the refinement. The asymmetric unit of the structure contains one molecule of water which is disordered. Attempts to localize the hydrogen atoms were not successful. Plots were produced using Mercury.[35] Crystallographic data (excluding structure factors) for the structure in this paper have been deposited with the Cambridge Crystallographic Data Center, the deposition number is 1060525. Copies of the data can be obtained, free of charge, on application to the CCDC, 12 Union Road, Cambridge CB2 1EZ, UK [fax: +44-1223-336033 or e-mail: deposit@ccdc.cam.ac.uk].

*Crystal data of polycephalone A (**15**)*: formula $C_{34}H_{34}O_{13}$ ($2(C_{17}H_{16}O_6)$, H_2O), M = 650.64, F(000) = 1360, colourless needle, size 0.04 ·0.06 ·0.25 mm^3, monoclinic, space group C 2, Z = 4, a = 26.954(3) Å, b = 7.9731(7) Å, c = 14.5563(16) Å, α = 90°, β = 106.331(3)°, γ = 90°, V = 3002.0(3) Å^3, $D_{calc.}$ = 1.435 Mg m^{-3}.

Computational Methods. Conformational analysis of **11**, **12** and **15** was performed with Schrödinger MacroModel 9.8 (Schrödinger, LLC, New York) employing the OPLS2005 (optimized potential for liquid simulations) force field in H_2O. Conformers within a 2 Kcal/mol energy window from the global minimum were selected for geometrical optimization and energy

calculation applying DFT with the Becke's nonlocal three parameter exchange and correlation functional, and the Lee-Yang-Parr correlation functional level (B3LYP) using the B3LYP/6-31 G** basis set in the gas phase with the Gaussian 09 program package.[36] Vibrational evaluation was done at the same level to confirm minima. For compound **15** excitation energy (denoted by wavelength in nm), rotator strength dipole velocity (R_{vel}), and dipole length (R_{len}) were calculated in MeOH by TD-DFT/CAM-B3LYP/6-31 G**, using the SCRF method, with the CPCM model. ECD curves were obtained on the basis of rotator strengths with a half-band of 0.3 eV using SpecDis v1.61.[37] ECD spectra were calculated from the spectra of individual conformers according to their contribution calculated by Boltzmann-weighting.

Electrophysiological bioassay: expression of human ether-a-go-go-related gene channels in *Xenopus* oocytes and voltage-clamp experiment.

cDNAs of hERG (accession number NP000229) were kindly provided by Prof. Sanguinetti (University of Utah, UT, USA). Synthesis of capped run-off complementary ribonucleic acid (cRNA) transcripts from linearized complementary deoxyribonucleic acid (cDNA) templates and injection of cRNA were performed as described previously.[38] Oocytes from the South African clawed frog, *Xenopus laevis*, (NASCO, Fort Atkinson, WI, USA) were isolated as following. After 15 min exposure of female *Xenopus laevis* to the anesthetic (0.2 % solution of MS-222; the methane sulfonate salt of 3- aminobenzoic acid ethyl ester; Sigma), parts of the ovary tissue were surgically removed. Defolliculation was achieved by enzymatic treatment with 2 mg/mL collagenase type 1A (Sigma) and partly by mechanical removal of follicular layer using forceps. Stage V–VI oocytes were selected and injected with the WT hERG-encoding cRNA. Injected oocytes were stored at 18 ℃ in ND96 bath solution (96 mM sodium chloride, 2 mM potassium chloride, 1 mM magnesium chloride, 5 mM HEPES, 1.8 mM $CaCl_2$; pH 7.5, titrated with NaOH) containing 1% penicillin-streptomycin solution. All chemicals used were purchased from Sigma-Aldrich Chemie GmbH, Taufkirchen, Germany.

Currents through hERG channels were measured one to three days after microinjection of the cRNA using the two-microelectrode voltage clamp technique. ND96 was used as extracellular recording solution. Voltage-recording and current-injecting microelectrodes were filled with 3 M

KCl, and had resistances between 0.3 and 2 MΩ. Endogenous currents (estimated in oocytes injected with DEPC water) did not exceed 0.15 μA. Currents > 5 μA were discarded to minimize voltage clamp errors. Ionic currents were recorded with a Turbo Tec 03X Amplifier (npi electronic, GmbH, Tamm, Germany) and digitized with a Digidata 1322A (Axon Instruments Inc., Union City, CA, USA). The pClamp software package version 9.2 (Axon Instruments Inc.) was used for data acquisition. Microcal Origin 7.0 was employed for analysis. A precondition for all measurements was the achievement of stable peak current amplitudes over periods of 10 min after an initial 'run-up' period. Compounds were applied by means of a fast perfusion system enabling solution exchange within 100 ms.[39] The oocytes were incubated for 3 min in the presence of studied compound at a holding potential of - 100 mV to equilibrate compound diffusion. The following voltage protocol was used: From a holding potential of - 100 mV, the cell membrane was initially depolarized to + 20mV (300 ms) in order to ensure channel activation and subsequent rapid inactivation. During following repolarization to - 50mV (300ms), channels recover from inactivation and elicit peak tail current. A final step to the holding potential ensured that channels returned to the closed state. The protocol was applied every 3-s intervals (0.3 Hz pulse frequency). Decreases in tail current amplitudes were taken as a measure of use-dependent block development during repetitive pulsing. Data are presented as means ± s.e. from at least three oocytes from ≥ 2 batches. The studied compounds were dissolved in DMSO to prepare a 10 mM stock on the day of experiments. Compound stock solution was further diluted to the required concentration using ND96 recording solution. The final maximum DMSO concentration (1%) in test solutions did not affect hERG currents (data not shown). Propafenone was used as a positive control and exhibited an of IC_{50} of 3.8 ± 0.2 μM.[40]

ASSOCIATED CONTENT

Supporting Information

NMR spectra (1D and 2D) and ECD spectra of new compounds **3**, **4**, **11**, **12**, **15** and **16**; ^{1}H and ^{13}C NMR data for known compounds **1**, **2**, **5**-**10**, **13** and **14**.

ACKNOWLEDGMENT

ECD spectra were measured at the Biophysics Facility, Biozentrum, University of Basel. The project was carried out within the International Research Staff Exchange Scheme (IRSES) project

"hERG Related Risk Assessment of Botanicals" PIRSES-GA-2011–295174 Marie Curie Actions funded under the 7th Framework Programme of the European Commission.

REFERENCES

(1) Kerns, E. H.; Di, L. *Drug-like Properties: Concepts, Structure Design and Methods: from ADME to Toxicity Optimazation;* Academic Press: Burlington, MA, 2008; pp 209.

(2) Hancox, J. C.; McPate, M. J.; El Harchi, A.; Zhang, Y. H. *Pharmacol. Ther.* **2008**, 119, 118-132.

(3) Polak, S.; Wiśniowska, B.; Brandys, J. *J. Appl. Toxicol.* **2009**, 29, 183-206.

(4) Yap, Y. G.; Camm, A. J. *Heart* **2003**, 89, 1363-1372.

(5) Sanguinetti, M. C.; Tristani-Firouzi, M. *Nature* **2006**, 440, 463-469.

(6) Blumenthal, M.; Lindstrom, A.; Ooyen, C.; Lynch, M. E. *Herbal Gram* **2012**, 95, 60-64.

(7) Zitron, E.; Scholz, E.; Owen, R. W.; Lück, S.; Kiesecker, C.; Thomas, D.; Kathöfer, S.; Niroomand, F.; Kiehn, J.; Kreye, V. A. W.; Katus H. A.; Schoels, W.; Karle, C. A. *Circulation* **2005**, 111, 835-838.

(8) Schramm, A.; Saxena, P.; Chlebek, J.; Cahlíková, L.; Barburin, I.; Hering, S.; Hamburger, M. *Planta Med.* **2014**, 80, 740-746.

(9) Jeong, I.; Choi, B. H.; Hahn, S. J. *Pflugers Arch* **2010**, 460, 851-862.

(10) Schramm, A.; Jähne, E. A.; Baburin, I.; Hering, S.; Hamburger, M. *Planta Med.* **2014**, 80, 1045-1050.

(11) Schramm, A.; Baburin, I.; Hering, S.; Hamburger, M. *Planta Med.* **2011**, 77, 692-697.

(12) Van Wyk, B-E.; Van Oudtshoorn, B.; Gericke, N. *Medicinal Plants of South Africa;* Briza Publications: Pretoria, 2009; pp156.

(13) Van Wyk, B-E.; Van Heerden, F; Van Oudtshoorn, B. *Poisonous Plants of South Africa;* Briza Publications: Pretoria, 2002; pp120.

(14) Munkombwe, N. M.; Galebotswe, P.; Modibesane, K.; Morebodi, N. *Phytochemistry* **2003**, 64, 1401-1404.

(15) Potterat, O.; Hamburger, M. *Planta Med.* **2014**, 80, 1171-1181.

(16) Ohigashi, H.; Katsumata, H.; Kawazu K.; Koshimizu K.; Mitsu T. *Agr. Biol. Chem.* **1974**, 38, 1093-1095.

(17) Vidal, V.; Potterat, O.; Louvel, S.; Hamy, F.; Mojarrab, M.; Sanglier, J-J.; Klimkait, T.; Hamburger, M. *J. Nat. Prod.* **2012**, 75, 414-419.

(18) Powell, R. G.; Weisleder, D.; Smith Jr, C. R. *J. Nat. Prod.* **1985**, 48, 102-107.

(19) Zhou, B. N.; Xue, L.; Lin, L. Z.; Lin, L. J.; Johnson M. E.; Cordell, G. A. *Magn. Reson. Chem.* **1993**,

31, 194–199.

(20) Chang, C. Y.; Huang, L. J.; Wang, J. P.; Teng, C. M.; Chen, S. C.; Kuo, S. C. *Chem. Pharm. Bull.* **2000**, 48, 964-973.

(21) Munekazu, I.; Shin, M.; Kousuke, K. *Chem. Pharm. Bull.* **1980**, 28, 708-716.

(22) Habsaoui, A.; Cami, J. L. F.; Wallet, J. C.; Gaydou, E. M. *Heterocycles* **1998**, 48, 1759-1767.

(23) Tanemossu, S. A. F.; Franke, K.; Arnold, N.; Schmidt, J.; Wabo, H. K.; Tane, P.; Wessjohann, L. A. *Phytochemistry* **2014**, 105, 171-177.

(24) Huang, S. Z.; Li, X. N.; Ma, Q. Y.; Dai, H. F.; Li, L. C.; Cai, X. H.; Liu, Y. Q.; Zhou, J.; Zhao, Y. X. *Tetrahedron Lett.* **2014**, 55, 3693-3696.

(25) Liu, L. P.; Han, K.; Chen, W.; Zhang, Y. Y.; Tong, L. J.; Peng, T.; Xie, H.; Ding, J.; Wang, H. B. *Bioorg. Med. Chem.* **2014**, 22, 4198-4203.

(26) Sakata, K.; Kawazu, K.; Mitsui, T. *Tetrahedron Lett.* **1971**, 16, 1141-1144.

(27) Gao, X.; Xie, W. D.; Jia, Z. J. *J. Asian Nat. Prod. Res.* **2008**, 10, 185-192.

(28) Blaj, G.; Garcia, B.; Molina, E.; Pedro, J.R. *Tetrahedron* **2005**, 61, 1156-1162.

(29) Liao, S. G.; Chen, H. D.; Yue, J. M. *Chem. Rev.* **2009**, 109, 1092-1140.

(30) Zhou, B. N.; *Mem. Inst.Oswaldo Cruz* **1991**, 86, 219-226.

(31) Bruker Analytical X-ray Systems, Inc., 2006. *Apex2*, Version 2 User Manual, M86-E01078, Madison, WI.

(32) Palatinus, L. & Chapuis, G. (2007). J. Appl. Cryst. 40, 786-790.

(33) Betteridge, P.W., Carruthers, J.R., Cooper, R.I., Prout, K. & Watkin, D.J. (2003). J. Appl. Cryst. 36, 1487.

(34) Watkin D.J. (1994). Acta Cryst, A50, 411-437.

(35) C. F. Macrae, I. J. Bruno, J. A. Chisholm, P. R. Edgington, P. McCabe, E. Pidcock, L. Rodriguez-Monge, R. Taylor, J. van de Streek and P. A. Wood, J. Appl. Cryst., 41, 466-470, 2008

(36) Frisch, M. J.; Trucks, G. W.; Schlegel, H. B.; Scuseria, G. E.; Robb, M. A.; Cheeseman, J. R.; Scalmani, G.; Barone, V.; Mennucci, B.; Petersson, G. A.; Nakatsuji, H.; Caricato, M.; Li, X.; Hratchian, H. P.; Izmaylov, A. F.; Bloino, J.; Zheng, G.; Sonnenberg, J. L.; Hada, M.; Ehara, M.; Toyota, K.; Fukuda, R.; Hasegawa, J.; Ishida, M.; Nakajima, T.; Honda, Y.; Kitao, O.; Nakai, H.; Vreven, T.; Montgomery Jr., J. A.; Peralta, J. E.; Ogliaro, F.; Bearpark, M. J.; Heyd, J.; Brothers, E. N.; Kudin, K. N.; Staroverov, V. N.; Kobayashi, R.; Normand, J.; Raghavachari, K.; Rendell, A. P.; Burant, J. C.; Iyengar, S. S.; Tomasi, J.; Cossi, M.; Rega, N.; Millam, N. J.; Klene, M.; Knox, J. E.; Cross, J. B.; Bakken, V.; Adamo, C.; Jaramillo,

J.; Gomperts, R.; Stratmann, R. E.; Yazyev, O.; Austin, A. J.; Cammi, R.; Pomelli, C.; Ochterski, J. W.; Martin, R. L.; Morokuma, K.; Zakrzewski, V. G.; Voth, G. A.; Salvador, P.; Dannenberg, J. J.; Dapprich, S.; Daniels, A. D.; Farkas, Ö.; Foresman, J. B.; Ortiz, J. V.; Cioslowski, J.; Fox, D. J. *Gaussian 09*, Gaussian, Inc.: Wallingford, CT, USA, 2009.

(37) Bruhn, T.; Hemberger, A. S. Y.; Bringmann, G. *SpecDis version 1.61*, University of Wuerzburg, Germany, 2014.

(38) Stork, D.; Timin, E.N.; Berjukow, S.; Huber, C.; Hohaus, A.; Auer, M.; Hering, S. *Br J Pharmacol* **2007**, 151, 1368-1376.

(39) Baburin, I.; Beyl, S.; Hering, S. *Pflügers Arch Eur J Physiol* **2006**, 453, 117-123.

(40) Windisch, A.; Timin, E.N.; Schwarz, T.; Stork-Riedler, D.; Erker, T.; Ecker, G.F.; Hering, S. *Br J Pharmacol* **2011**, 162, 1542-1552.

Abbreviations

hERG: human ether-a-go-go-related gene

ECG: electrocardiogram

TdP: torsades de pointes

DDOs: daphnane-type diterpene orthoesters

TRPV1: Transient Receptor Potential Vanilloid 1

ECD: electronic circular dichroism

Table 1. ^{1}H and ^{13}C NMR spectroscopic data for compounds **3** and **4** ($CDCl_3$, 500 MHz for ^{1}H, and 125 MHz for ^{13}C NMR, δ in ppm).

	3		**4**	
Position	δ_H (J in Hz)	δ_C [b], type	δ_H (J in Hz)	δ_C, type
1	7.57 [a]	160.9, CH	7.55 (m)	160.4, CH
2	-	136.8, C	-	137.1, C
3	-	210.2, C	-	209.5, C
4	-	72.3, C	-	72.3, C
5	4.21 (s)	72.2, CH	4.19 (s)	72.0, CH
6	-	61.4, C	-	60.8, C
7	3.63 (s) [a]	64.5, CH	3.62 (s)	64.1, CH
8	3.63 (d, 2.4) [a]	36.8, CH	3.64 (d, 2.5)	35.9, CH
9	-	78.5, C	-	78.4, C
10	3.86 (quint, 2.5) [d]	48.0, CH	3.84 [a]	47.6, CH
11	2.56 (q, 7.0)	44.5, CH	2.58 (q, 7.2)	44.2, CH
12	5.23 (br s)	79.5, CH	5.24 (br s)	79.9, CH
13	-	84.6, C	-	84.0, C
14	4.90 (d, 2.4)	81.1, CH	4.91 (d, 2.5)	80.7, CH
15	-	143.2, C	-	143.1, C
16	5.02 (br m)	114.0, CH_2	5.04 (br m)	113.8, CH_2
	4.99 (br m)		5.00 (br m)	
17	1.87 (br s)	19.2, CH_3	1.88 (br s)	18.9, CH_3
18	1.39 (d, 7.0)	18.9, CH_3	1.40 (d, 7.2)	18.5, CH_3
19	1.77 (br s)	10.3, CH_3	1.76 (br s)	10.0, CH_3
20	3.91 and 3.83 (ABq, 12.4)	65.0, CH_2	3.86 [a]	64.8, CH_2
1'	-	117.7, C	-	117.2, C
2'	5.68 (d, 15.5)	122.9, CH	5.77 (d, 15.4)	124.4, CH
3'	6.70 (dd, 15.5, 10.5)	135.6, CH	7.00 (ddd, 15.4, 11.3, 0.9)	127.0, CH
4'	6.07 (dd, 15.2, 10.5)	129.2, CH	6.03 (br t, 11.3)	130.0, CH
5'	5.87 (dt, 15.2, 7.2)	139.4, CH	5.62 (br dt, 11.3, 7.2)	136.6, CH
6'	2.01 (q, 7.2)	35.2, CH_2	2.23 (qd, 7.2, 1.0)	28.0, CH_2
7'	1.33 (sex, 7.2)	22.8, CH_2	1.41 (sex, 7.2)	29.2, CH_2
8'	0.91 (t, 7.2)	14.2, CH_3	1.36 [a]	31.5, CH_2
9'	-	-	1.36 [a]	22.6, CH_2
10'	-	-	0.90 (t, 7.0)	14.2, CH_3
1"	-	166.0, C	-	165.6, C
2"	-	[c], C	-	129.8, C
3"-7"	7.89 (br d, 8.0)	129.9, CH	7.89 (br d, 8.0)	129.6, CH

4"-6"	7.44 (br t, 8.0)	128.9, CH	7.43 (br t, 8.0)	128.8, CH
5"	7.57 (t, 8.0)	133.6, CH	7.56 [a]	133.5, CH

[a] overlapping signals; [b] from inverse detected experiments HSQC and HMBC due to low amount of sample; [c] not detected; [d] apparent.

Table 2. ^{1}H and ^{13}C NMR spectroscopic data for compounds **11** and **12** ($CDCl_3$, 500 MHz for ^{1}H, and 125 MHz for ^{13}C NMR, δ in ppm).

	11		**12**	
Position	δ_H (J in Hz)	δ_C, type	δ_H (J in Hz)	δ_C [b], type
1	2.31 (br m)	57.5, CH	2.40 (br m)	55.3, CH
2	3.78 (d, 3.2)	78.5, CH	3.78 (d, 2.5)	78.2, CH
3	-	208.1, C	-	208.0, C
4	-	133.3, C	-	135.5, C
5	-	173.9, C	-	172.3, C
6	2.68 (dd, 13.4, 2.2)	34.1, CH_2	4.59 (d, 9.3)	71.3, CH
	2.38 (dd, 13.4, 10.8)		-	-
7	2.10 (br m)	44.6, CH	2.46 (ddd, 9.3, 6.4, 6.3)	51.4, CH
8	1.76 [a]	30.0, CH_2	1.84 (m)	26.7, CH_2
	1.59 [a]		1.72 (m)	
9	1.58 [a]	31.6, CH_2	1.55 (m)	30.5, CH_2
	1.49 (m)		-	-
10	1.76 [a]	35.7, CH	1.74 [a]	38.0, CH
11	-	149.1, C	-	146.2, C
12	4.67 (br m)	110.0, CH_2	4.98 (br m)	113.7, CH_2
	4.65 (br s)		4.84 (br s)	
13	1.69 (br s)	20.6, CH_3	1.80, (br s)	19.6, CH_3
14	1.16 (br d, 7.0)	22.1, CH_3	1.19 (d, 7.0)	21.8, CH_3
15	1.62 (d, 2.0)	7.9, CH_3	1.94 (d, 2.0)	9.3, CH_3

[a] overlapping signals; [b] from inverse detected experiments HSQC and HMBC due to low amount of sample.

Table 3. ^{1}H and ^{13}C NMR spectroscopic data for compounds **15** and **16** (DMSO-d_6 for **15**, $CDCl_3$ for **16**, 500 MHz for ^{1}H, and 125 MHz for ^{13}C NMR, δ in ppm).

	15		**16**	
Position	δ_H (J in Hz)	δ_C, type	δ_H (J in Hz)	δ_C [b], type
2	-	161.5, C	-	161.5, C
3	6.67 (s)	114.7, CH	7.11 (s)	119.7, CH
4	-	174.6, C	-	176.4, C
5	5.41 (d, 4.0)	67.1, CH	5.59 (d, 4.0)	68.2, CH
6	3.95 (d, 7.0)	73.0, CH_2	4.08 (d, 7.0)	74.0, CH_2
	3.79 (dd, 7.0, 4.0)		3.92 (ddd, 7.0, 4.5,1.2)	
7	5.91 (d, 2.0)	98.9, CH	5.89 (br d, 2.5)	99.5, CH
8	3.14 (br d, 18.0)	35.7, CH_2	3.10 (ddd, 17.6, 2.5, 1.2)	36.5, CH_2
	2.65 (d, 18.0)		2.69 (br d, 17.6)	
9	-	160.7, C	-	160.8, C
10	-	123.2, C	-	124.1, C
1’	-	125.4, C	-	124.7, C
2’	-	146.7, C	-	145.5, C
3’	-	153.0, C	-	150.2, C
4’	7.24 [a]	115.7, CH	7.13-7.07 [a]	115.3, CH
5’	7.21 [a]	124.5, CH	7.13-7.07 [a]	125.4, CH
6’	7.21 [a]	120.4, CH	7.13-7.07 [a]	120.0, CH
2’-OCH_3	3.78 (s)	60.6, CH_3	3.76 (s)	61.3, CH_3
3’-OCH_3	3.86 (s)	56.0, CH_3	-	-

[a] overlapping signals.

Legends for Figures

Figure 1. HPLC-based activity profiling of the dichloromethane extract of *Gnidia polycephala*, for hERG channel inhibition. (A) Inhibition of hERG current during 0.3 Hz pulsing by microfractions (error bars correspond to SE); (B) HPLC chromatogram (254 nm) of a semipreparative separation (5 mg of extract). The 20 time-based fractions of 90 s each are indicated with dashed lines.

Figure 2. Optimized analytical HPLC separation of microfractions 17 and 18. (A) UV chromatogram (254 nm); (B) ESI (+) base peak mass chromatogram; (C) extracted mass spectra.

Figure 3. Structures of compounds **1**-**16**.

Figure 4. Key NOESY correlations of compounds **11**(A) and **12** (B).

Figure 5. Structure assignment of compound **15**, with diagnostic COSY, HMBC and NOESY connectivities.

Figure 6. Experimental and calculated (cam-b3lyp/6-31g(d,p) ECD spectra for the 5*R*,7*S* stereoisomer of compound **15** in MeOH.

Figure 7. Ellipsoid plot of structure **15**. There are two molecules present in the asymmetric unit which are not related by symmetry. For clarity reasons only one out of the two is shown here. The two molecules have the same stereochemistry, but show slightly different conformations in the peripherical substituents. Also the disordered water molecule present in the structure has been omitted.

Figure 8. Proposed biosynthesis of compounds **15** and **16**.

Figure 9. Representative current traces illustrating inhibition of hERG potassium current by 100 μM of compounds **1** (A), **4** (B) and **5** (C). The current trace recorded in absence of the drug (control) is superimposed with a trace illustrating steady state inhibition during 0.3 Hz pulsing (D). Inhibition of hERG current (in %) by compounds **1**, **4** and **5**.

Figure 1.

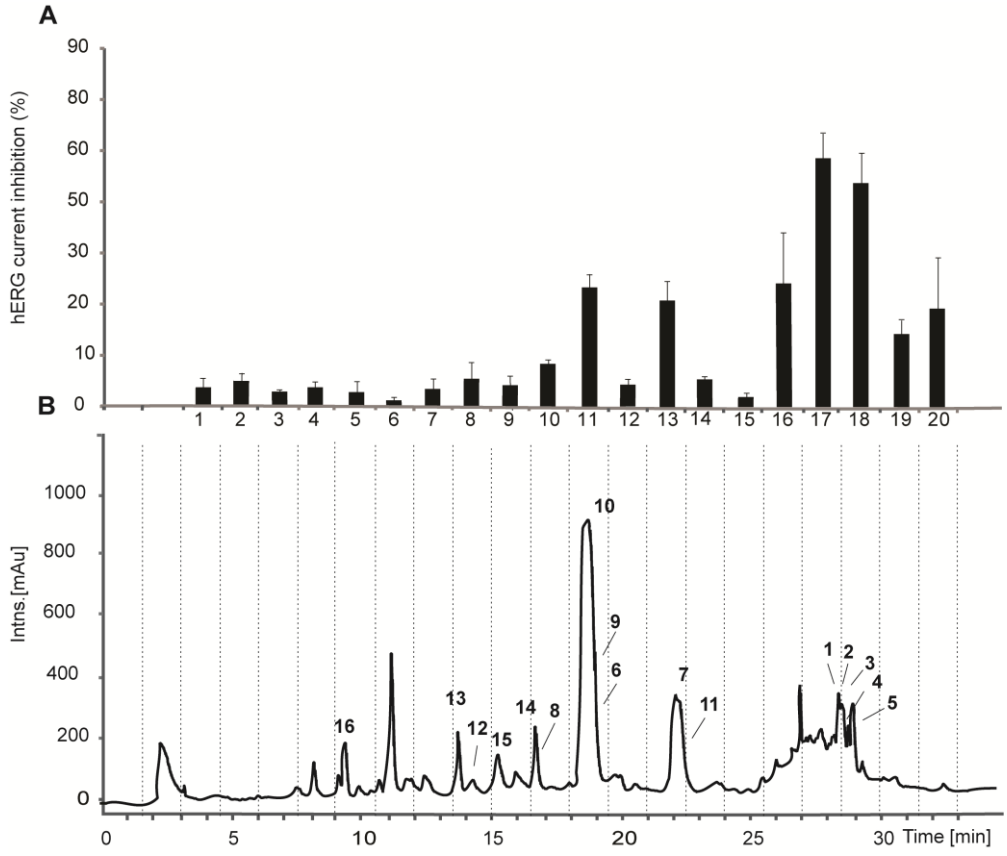
A
hERG current inhibition (%)
90
80
60
50
30
20
10
0
1 2 3 4 5 6 7 8 9 10 11 12 13 14 15 16 17 18 19 20
B
Intns.[mAu]
1000
800
600
400
200
0
16
13
12
15
14
8
10
9
6
7
11
1
2
3
4
5
0 5 10 15 20 25 30 Time [min]

Figure 2.

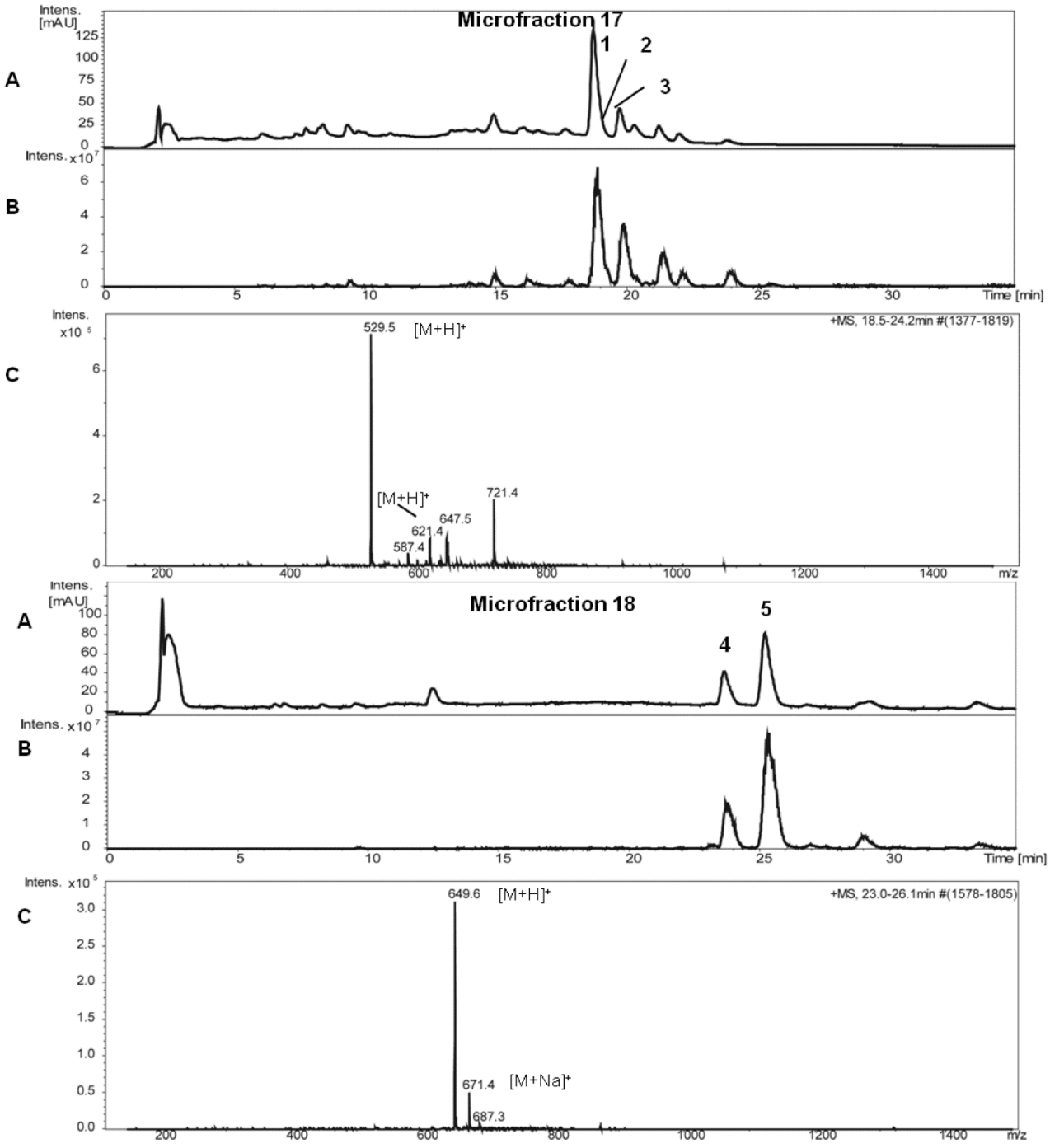
Microfraction 17
A
Intens. [mAU]
1
2
3
B
Intens. x10 7
Time [min]
C
Intens. x10 5
529.5 [M+H]+
+MS, 18.5-24.2min #(1377-1819)
[M+H]+
721.4
647.5
621.4
587.4
m/z
Microfraction 18
A
Intens. [mAU]
4
5
B
Intens. x10 7
Time [min]
C
Intens. x10 5
649.6 [M+H]+
+MS, 23.0-26.1min #(1578-1805)
671.4 [M+Na]+
687.3
m/z

Figure 3

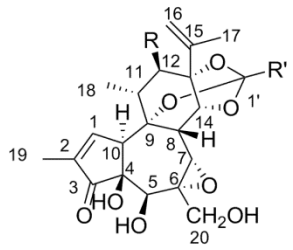

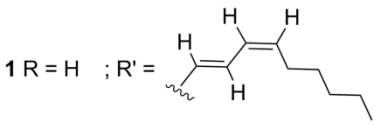

1 R = H ; R' =

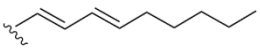

2 R = H ; R' =

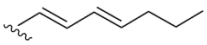

3 R = OBenzoyl ; R' =

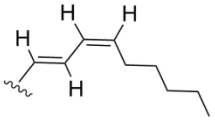

4 R = OBenzoyl ; R' =

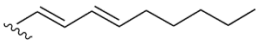

5 R = OBenzoyl ; R' =

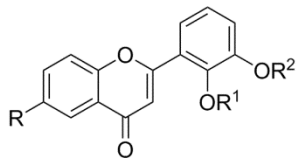

6 R = H; R^1 = H; R^2 = CH_3

7 R = H; R^1 = CH_3; R^2 = CH_3

8 R = OH; R^1 = CH_3; R^2 = CH_3

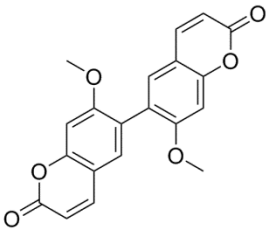

9

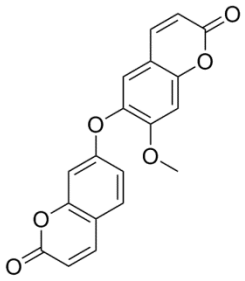

10

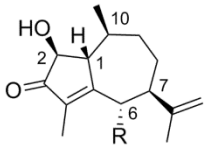

11 R = H
12 R = OH

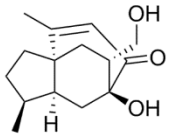

13

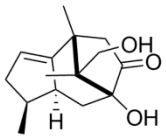

14

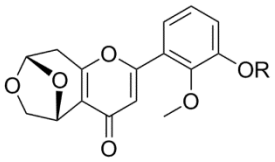

15 R = CH_3
16 R = H

Figure 4

Figure 5

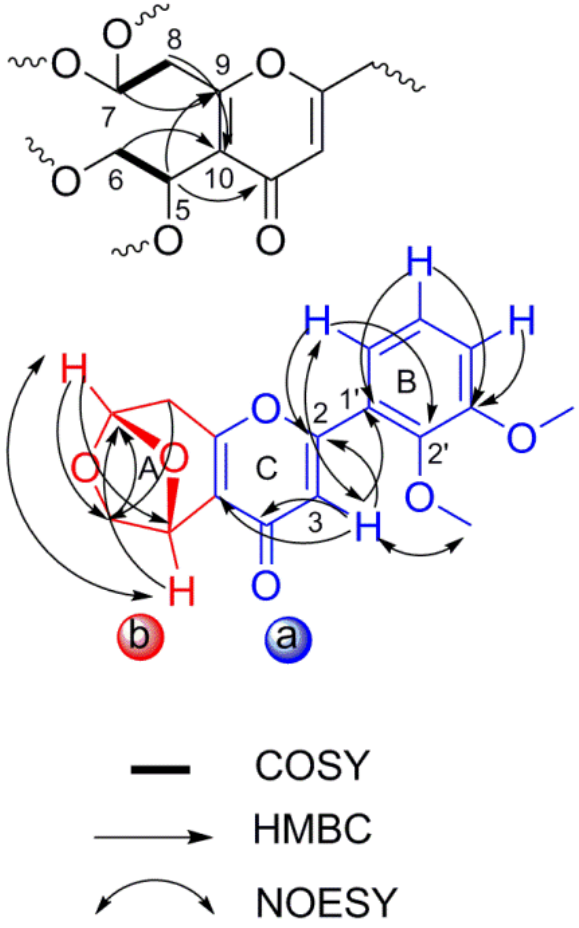

Figure 6.

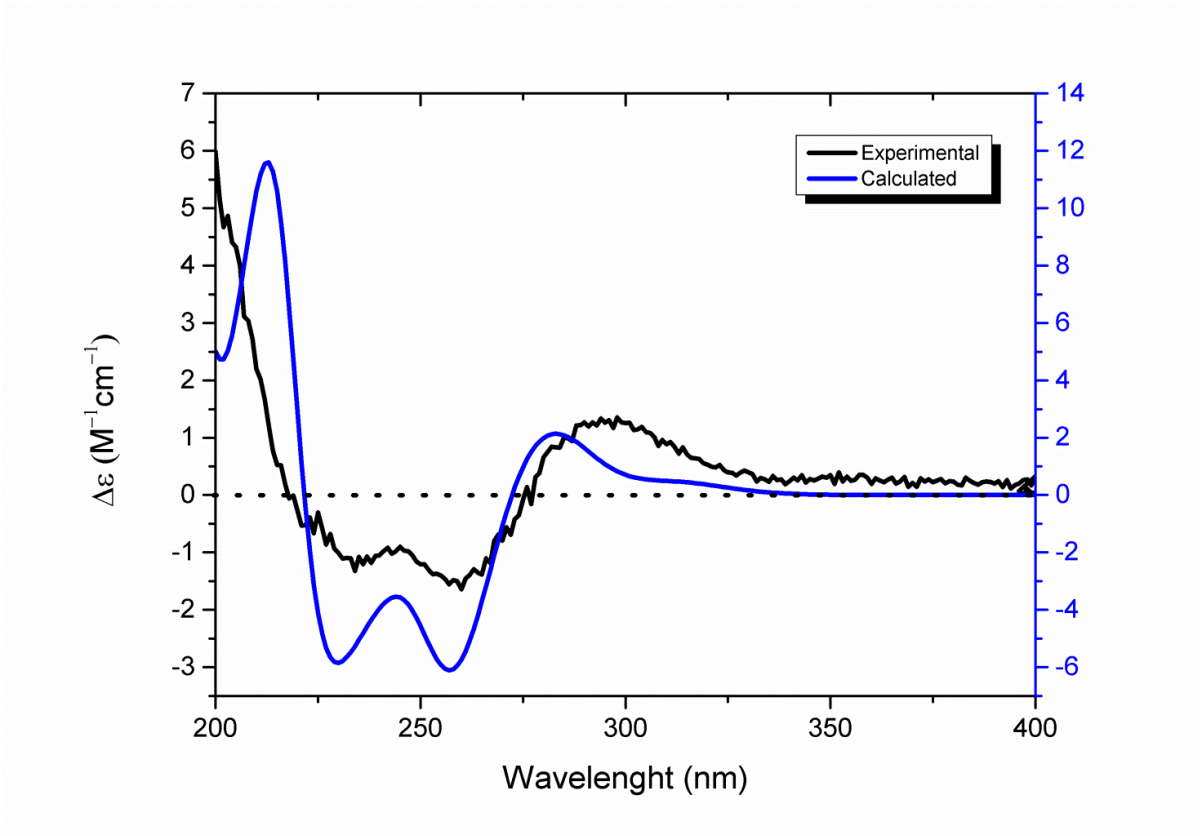

Figure 7

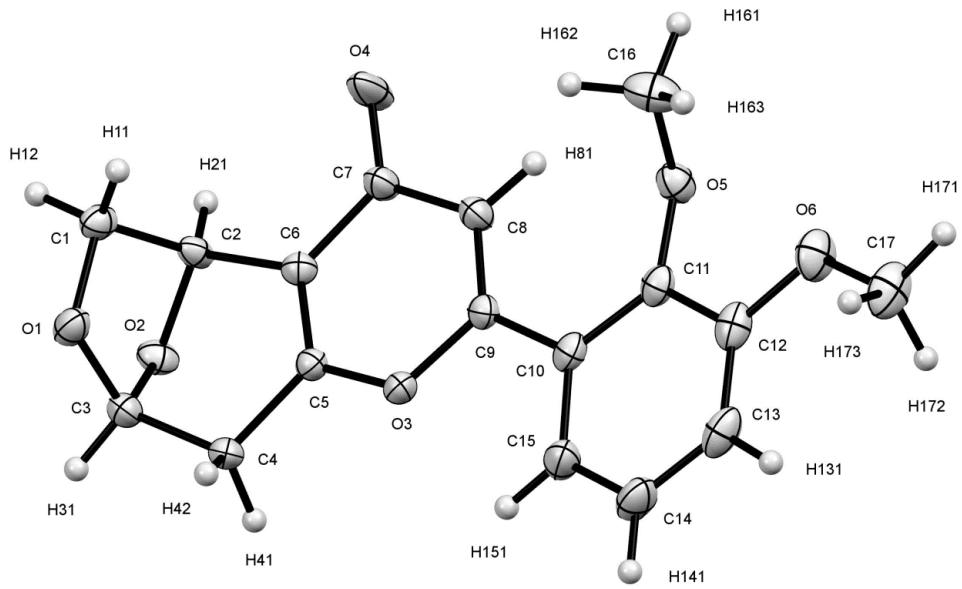

Figure 8

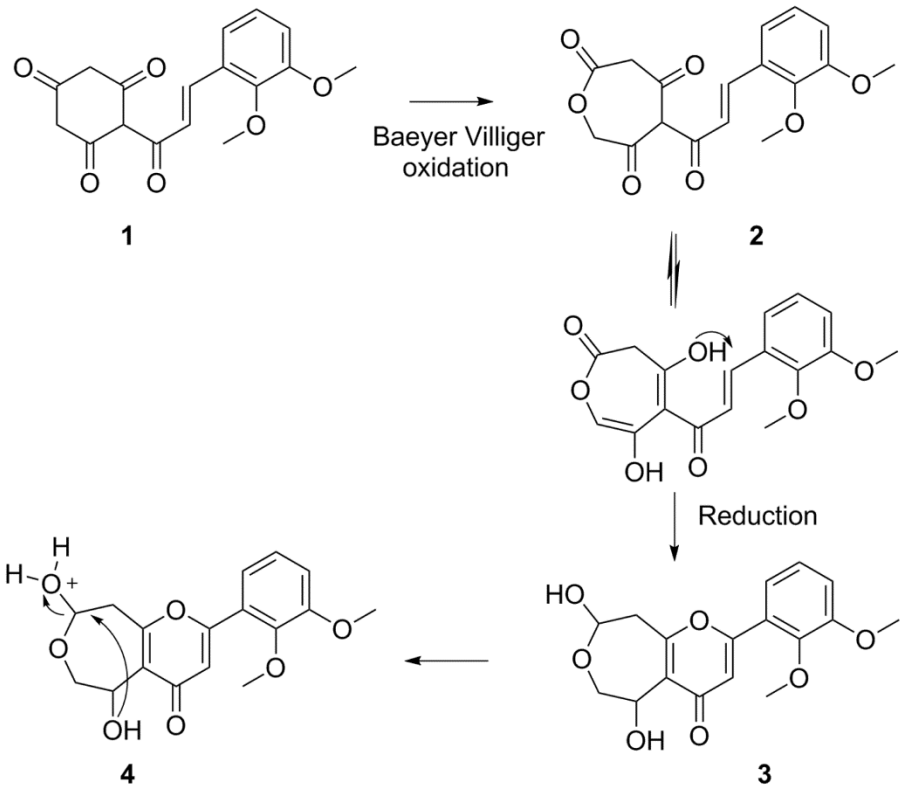

Figure 9

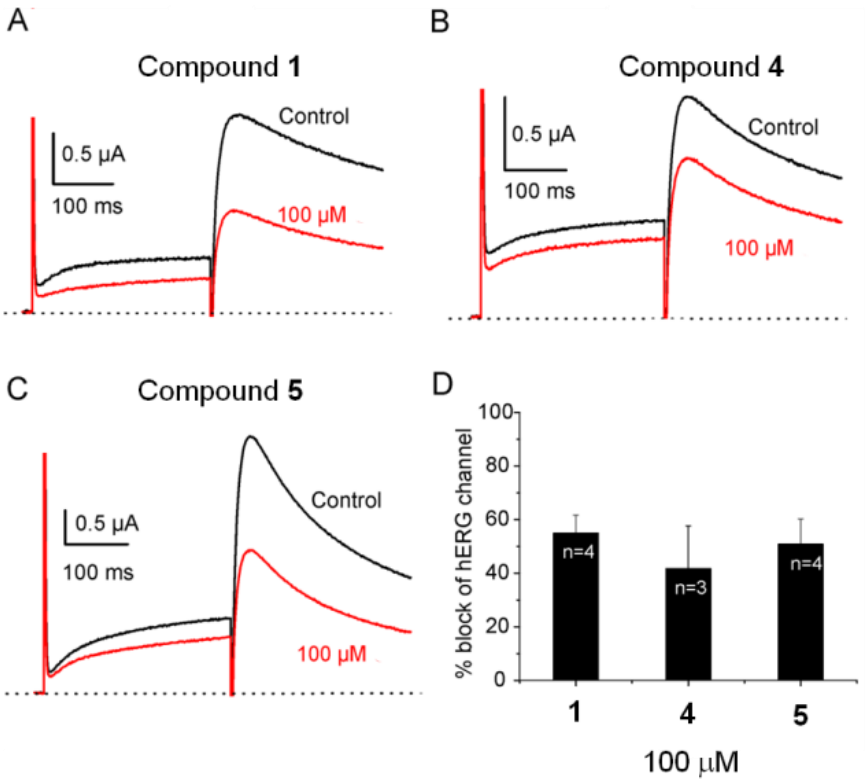

hERG Channel Inhibitory Daphnane Diterpenoid Orthoesters, and Polycephalones A and B with Unprecedented Skeletons from *Gnidia polycephala*

(Supporting Information)

Maria De Mieri[†,1], Kun Du[‡,1], Markus Neuburger[§], Priyanka Saxena[⊥], Pieter C. Zietsman[∥,▽], Steffen Hering[⊥], Jan H. van der Westhuizen[○] and Matthias Hamburger[†,*]

[†]Division of Pharmaceutical Biology, University of Basel, Klingelbergstrasse 50, CH-4056 Basel, Switzerland

[‡]Department of Chemistry, University of the Free State, Nelson Mandela Avenue, Bloemfontein 9301, South Africa

[§]Division of Inorganic Chemistry, Department of Chemistry, University of Basel, Basel, Switzerland

[⊥]Institute of Pharmacology and Toxicology, University of Vienna, Althanstrasse 14, A-1090 Vienna, Austria

[∥]National Museum, P.O. Box 266, Bloemfontein 9300, South Africa

[▽]Centre for Enviromental Management, University of the Free State, P.O. Box 339, Bloemfontein 9301, South Africa

[○]Directorate: Research Development, University of the Free State, Nelson Mandela Avenue, Bloemfontein 9301, South Africa

*Corresponding author. Tel.: +41-61-2671425; fax: +41-61-2671474.

E-mail: matthias.hamburger@unibas.ch

[1]These authors contributed equally to this work

Content

Figure S26. ^{13}C NMR spectrum of compound **16** (125 MHz, $CDCl_3$).

Figure S27. ^{1}H-^{1}H COSY spectrum of compound **16** (500MHz, $CDCl_3$).

Figure S28. Overlay of HSQC and HMBC spectra of compound **16** (500MHz, $CDCl_3$).

Figure S29. 2D ^{1}H-^{1}H NOESY spectrum of compound **16** (500MHz, $CDCl_3$).

Figure S30. Conformers of compound **11**.

Figure S31. Superimposed conformers of compound **12**.

Figure S32. Superimposed conformers of compound **15**.

Figure S33. ECD spectra of compounds **3** and **4** in MeOH.

Figure S34. ECD spectra of compounds **11** and **12** in MeOH.

Figure S35. Calculated and experimental UV spectra of compound **15** in MeOH.

Figure S36. ECD spectra of compound **16** in MeOH.

Table S1. ^{1}H and ^{13}C NMR spectroscopic data for compounds **1** and **2** ($CDCl_3$, 500 MHz for ^{1}H, and 125 MHz for ^{13}C NMR, δ in ppm).

	1		**2**	
Position	δ_H (J in Hz)	δ_C, type	δ_H (J in Hz)	δ_C, type
1	7.50 br s	161.2, CH	7.61 (m)	161.3, CH
2	-	136.8, C	-	136.8, C
3	-	209.9, C	-	210.0, C
4	-	72.4, C	-	72.4, C
5	4.19 (s)	71.9, CH	4.25 (s)	72.0, CH
6	-	60.6, C	-	60.5, C
7	3.36 (s)	64.2, CH	3.43 (s)	64.3, CH
8	2.87 (br s)	36.8, CH	2.93 (d, 2.5)	36.8, CH
9	-	79.7, C	-	79.7, C
10	3.76 (quint[a], 2.5)	48.2, CH	3.81 [b]	48.2, CH
11	2.44 (quint[a], 7.0)	35.0, CH	2.49 (dq, 8.7, 7.0)	35.0, CH
12	2.18 [b]	36.5, CH_2	2.23 (dd, 14.3, 8.7)	36.5, CH_2
	1.59 (d, 14.0)		1.67 (d, 14.3)	
13	-	84.5, C	-	84.5, C
14	4.39 (br s)	82.2, CH	4.42 (d, 2.5)	82.1, CH
15	-	146.2, C	-	146.2, C
16	4.96 (br m)	111.5, CH_2	5.01(br quint, 1.4)	111.5, CH_2
	4.83 (br m)		4.90 (quint, 1.4)	
17	1.73 (br s)	19.1, CH_3	1.78 (t, 1.4)	19.1, CH_3
18	1.10 (d, 7.0)	20.5, CH_3	1.17 (d, 7.0)	20.5, CH_3
19	1.70 (br s)	10.1, CH_3	1.80 (br s)	10.0, CH_3
20	3.67 and 3.81 (ABq, 12.2)	65.2, CH_2	3.82 [b]	65.2, CH_2
1´	-	116.6, C	-	116.6, C
2´	5.72 (d, 15.0)	125.0, CH	5.70 (d, 15.4)	122.9, CH
3´	6.95 (dd, 15.0, 10.0)	128.7, CH	6.69 (dd, 15.4, 10.6)	134.9, CH
4´	5.95 (t, 10.0)	127.2, CH	6.06 (br dd, 15.0, 10.6)	128.9, CH
5´	5.51 (m)	136.2, CH	5.84 (dt, 15.0, 7.2)	139.1, CH

6´	2.14 [b]	28.0, CH_2	2.10 (br q, 7.2)	32.8, CH_2
7´	1.33 (m)	29.2, CH_2	1.39 (quint, 7.2)	28.9, CH_2
8´	1.22 [b]	31.5, CH_2	1.28 [b]	31.4, CH_2
9´	1.23 [b]	22.6, CH_2	1.31 [b]	22.6, CH_2
10´	0.82 (t, 7.0)	14.2, CH_3	0.88 (t, 7.0)	14.2, CH_3

[a] apparent; [b] overlapping signals

Table S2. ^{1}H and ^{13}C NMR spectroscopic data for compound **5** ($CDCl_3$, 500 MHz for ^{1}H, and 125 MHz for ^{13}C NMR, δ in ppm).

	5	
Position	δ_H (J in Hz)	δ_C, type
1	7.57 (m) [a]	160.4, CH
2	-	137.0, C
3	-	209.5, C
4	-	72.3, C
5	4.19 (s)	71.8, CH
6	-	60.8, C
7	3.61 (s)[a]	64.1, CH
8	3.62 (d, 2.5) [a]	35.9, CH
9	-	78.3, C
10	3.84 (quint[d], 2.5)[a]	47.6, CH
11	2.56 (q, 7.2)	44.2, CH
12	5.23 (br s)	79.0, CH
13	-	84.0, C
14	4.89 (d, 2.5)	80.6, CH
15	-	143.0, C
16	5.02 (br m)	113.8, CH_2
	4.99 (br m)	
17	1.87 (br s)	18.9, CH_3
18	1.38 (d, 7.2)	18.5, CH_3
19	1.76 (br m)	10.0, CH_3
20	3.88 and 3.81 (ABq,	64.8, CH_2

	12.4)[a]	
1'	-	117.0, C
2'	5.68 (d, 15.4)	122.3, CH
3'	6.69 (ddd, 15.4, 10.6)	135.3, CH
4'	6.06 (br dd, 15.4, 10.6)	128.7, CH
5'	5.87 (br dt, 15.4, 7.1)	139.6, CH
6'	2.11 (q, 7.2)	32.8, CH_2
7'	1.39 [a]	28.8, CH_2
8'	1.28 [a]	31.4, CH_2
9'	1.30 [a]	22.6, CH_2
10'	0.89 (t, 7.0)	14.2, CH_3
1"	-	165.4, C
2"	-	129.8, C
3"-7"	7.88 (br d, 7.5)	129.6, CH
4"-6"	7.43 (br t, 7.5)	128.7, CH
5"	7.55 (br t, 7.5)[a]	133.5, CH

[a] overlapping signals

Table S3. ^{1}H and ^{13}C NMR spectroscopic data for compounds **6-8** (DMSO-d_6 for **6** and **8**, $CDCl_3$ for **7**; 500 MHz for ^{1}H, and 125 MHz for ^{13}C NMR, δ in ppm).

	6		**7**		**8**	
Position	δ_H (*J* in Hz)	δ_C [b], type	δ_H (*J* in Hz)	δ_C [b], type	δ_H (*J* in Hz)	δ_C [b], type
2	-	161.4, C	-	161.5, C	-	161.6, C
3	7.20 (s)	110.5, CH	6.95 (s)	112.0, CH	6.67 (s)	110.6, CH
4	-	177.5, C	-	178.3, C	-	177.2, C
5	8.04 (dd, 8.0,1.2)	124.4, CH	8.21 (dd, 8.0, 1.2)	125.5, CH	7.36 (d, 3.0)	107.9, CH
6	7.45 (t, 7.5)	124.8, CH	7.37 (t, 7.5)	124.9, CH	-	155.4, C
7	7.78 (td, 8.0, 1.2)	133.7, CH	7.63 (td, 8.0, 1.2)	133.4, CH	7.24 [a]	123.5, CH
8	7.68 (d, 8.0)	117.4, CH	7.50 (d, 8.0)	117.8, CH	7.55 (d, 7.0)	120.0, CH
9	-	155.6, C	-	155.9, C	-	150.1, C
10	-	123.0, C	-	123.1, C	-	124.8, C
1’	-	117.6, C	-	126.1, C	-	126.2, C
2’	-	147.2, C	-	147.8, C	-	147.0, C
3’	-	148.3, C	-	153.2, C	-	153.7, C
4’	7.12 (br d, 8.0)	113.8, CH	7.06 (br d, 8.0)	115.1, CH	7.24 [a]	116.2, CH
5’	6.90 (t, 8.0)	117.8, CH	7.15 (t, 8.0)	123.9, CH	7.20 (dd, 8.0, 7.5)	124.7, CH
6’	7.46 (br d, 8.0)	119.6, CH	7.33 (br d, 8.0)	120.6, CH	7.31 (dd, 7.5, 1.6)	120.9, CH
2’-OCH_3	-	-	3.88 [a]	60.7, CH_3	3.81[a]	61.0, CH_3
3’-OCH_3	3.86 (s)	55.7, CH_3	3.88 [a]	55.9, CH_3	3.87 [a]	56.5, CH_3

[a] overlapping signals; [b] from inverse detected experiments HSQC and HMBC due to low amount of sample

Table S4. ^{1}H and ^{13}C NMR spectroscopic data for compounds **9** and **10** ($CDCl_3$ for **9**, DMSO-d_6 for **10**; 500 MHz for ^{1}H, and 125 MHz for ^{13}C NMR, δ in ppm).

	9		10	
	Position δ_H (J in Hz)	δ_C[a], type	δ_H (J in Hz)	δ_C[a], type
2	-	160.3, C	-	160.3, C
3	6.31 (d, 9.5)	113.2, CH	6.36 (d, 9.5)	113.7, CH
4	7.98 (d, 9.5)	144.6, CH	7.96 (d, 9.5)	144.1, CH
5	7.52 (s)	130.3, CH	7.58 (s)	121.2, CH
6	-	123.0, C	-	139.9, C
7	-	160.4, C	-	155.0, C
8	7.15 (s)	100.2, CH	7.29 (s)	102.1, CH
9	-	155.7, C	-	153.0, C
10	-	112.6, C	-	112.3, C
2’	-	160.3, C	-	160.3, C
3’	6.31 (d, 9.5)	113.2, CH	6.34 (d, 9.5)	113.9, CH
4’	7.98 (d, 9.5)	144.6, CH	8.00 (d, 9.5)	144.6, CH
5’	7.52 (s)	130.3, CH	7.67 (d, 8.6)	130.0, CH
6’	-	123.0, C	6.92 (dd, 8.6, 2.4)	113.3, C
7’	-	160.4, C	-	161.3, C
8’	7.15 (s)	100.2, CH	6.84 (d, 2.4)	103.4, CH
9’	-	155.7, C	-	155.3, C
10’	-	112.6, C	-	114.4, C
7-OCH_3	3.85 (s)	57.1, CH_3	3.85 (s)	57.1, CH_3
7’-OCH_3	3.85 (s)	57.1, CH_3	-	-

[a] From inverse detected experiments HSQC and HMBC.

Table S5. ^{1}H and ^{13}C NMR spectroscopic data for compounds **13** and **14** ($CDCl_3$; 500 MHz for ^{1}H, and 125 MHz for ^{13}C NMR, δ in ppm).

	13		**14**	
Position	δ_H (*J* in Hz)	δ_C, type	δ_H (*J* in Hz)	δ_C, type
1	-	51.9, C	-	148.5, C
2	1.87 [a]	35.1, CH_2	5.23 (br m)	118.9, CH
	1.60 ddd (12.5, 6.5, 2.0)		-	-
3	1.93 [a]	33.3, CH_2	2.53 [a]	41.0, CH_2
	1.39 (dddd, 12.5, 11.0, 8.5, 6.5)		1.92 (br d, 16.0)[a]	
4	2.25 [a]	35.0, CH	2.39 (sext, 7.3)	33.4, CH
5	2.06 [a]	45.8, CH	2.66 (m)	42.6, CH
6	1.92 [a]	33.6, CH_2	1.97 (dd ,12.3, 10.5)	32.9, CH_2
	1.51 (dd, 13.3, 10.6)		1.42 (dd, 12.3, 8.2)	
7	-	83.2, C	-	83.8, C
8	-	202.3, C	-	220.2, C
9	6.13 (br m)	127.3 CH	2.53 and 2.06 (d, 19.0)	47.2, CH_2
10	-	175.0, C	-	41.6, C
11	2.29 (m)	43.5, CH	-	49.3, C
12	2.05 [a]	33.0, CH_2	0.84 (s)	12.4, CH_3
	1.28 (ddd, 14.5, 4.2, 1.5)		-	-
13	3.46 (dd, 10.6, 6.2)	65.8, CH_2	3.66 and 3.62 (ABq, 11.7)	65.5, CH_2
	3.24 (dd, 10.6, 7.5)		-	-
14	2.02 (d, 1.0)	23.5, CH_3	1.21 (s)	16.5, CH_3
15	1.01 (d, 7.2)	18.8, CH_3	0.87 (d, 7.3)	17.5, CH_3
7-OH	4.68 (br s)	-	-	-

[a] overlapping signals

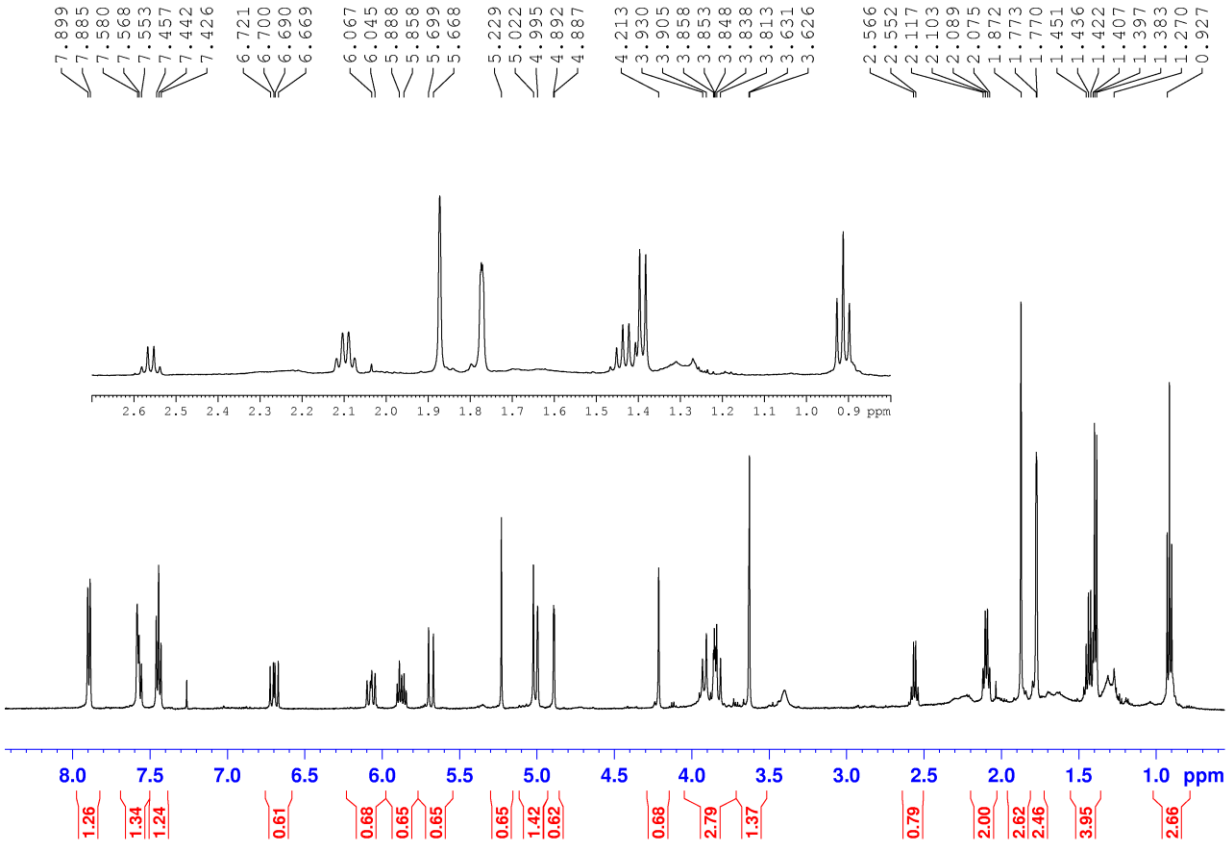

Figure S1. ^{1}H NMR spectrum of compound **3** (500 MHz, $CDCl_3$).

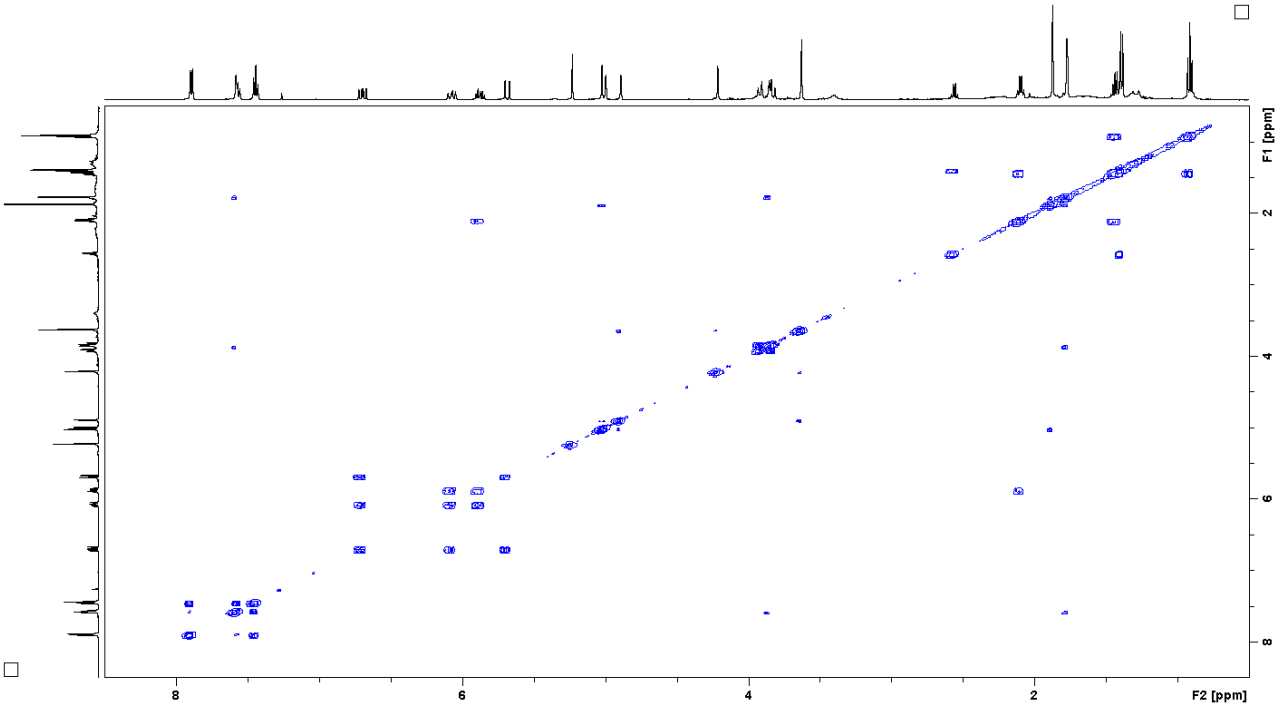

Figure S2. ^{1}H-^{1}H COSY spectrum of compound **3** (500 MHz, $CDCl_3$).

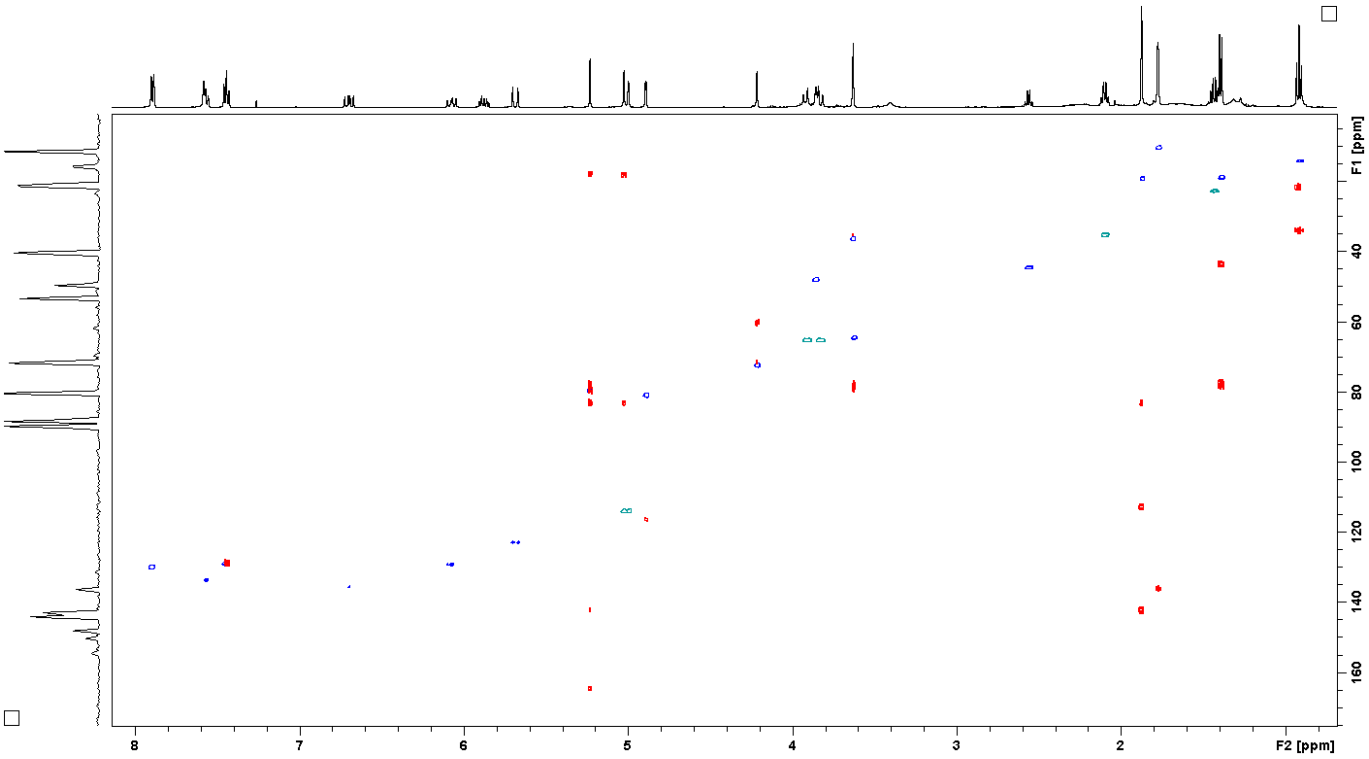

Figure S3. Overlay of HSQC-DEPT (blue/light green) and HMBC (red) spectra of compound **3** (500 MHz, $CDCl_3$).

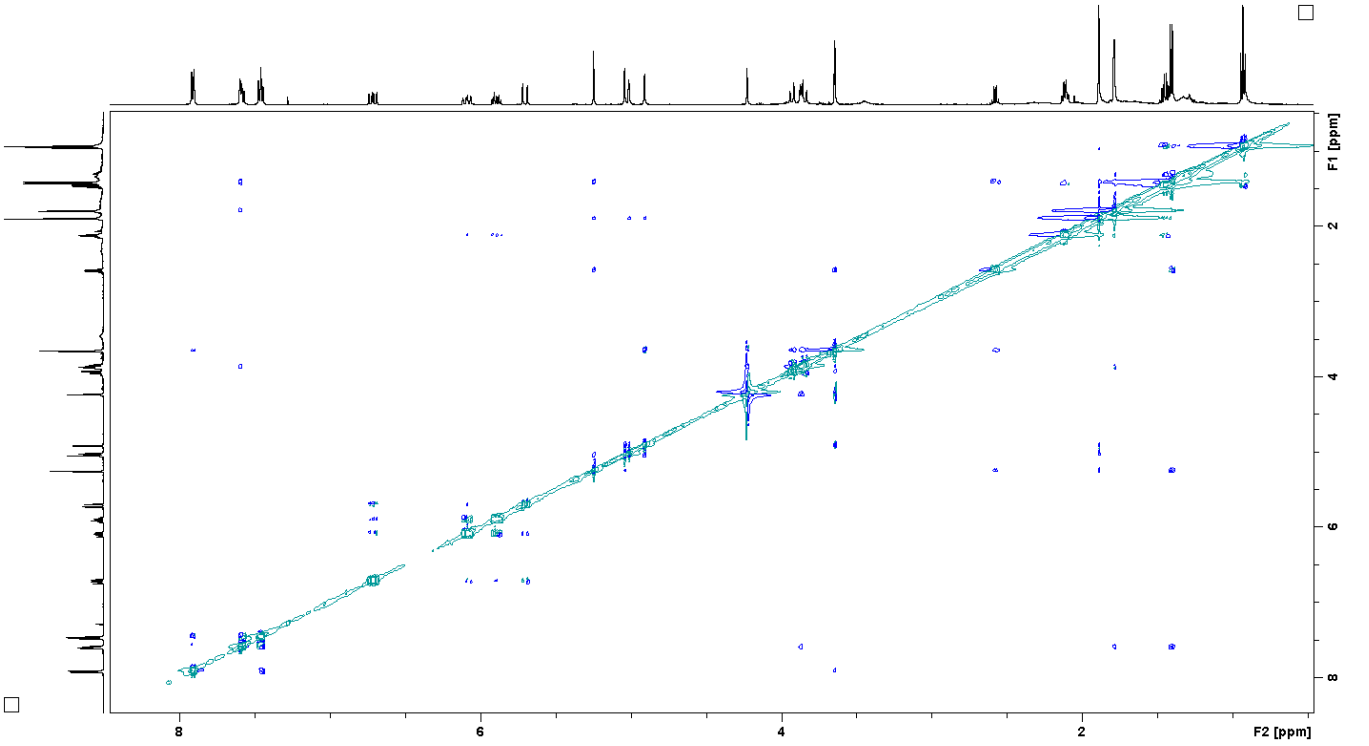

Figure S4. 2D ^{1}H-^{1}H ROESY spectrum of compound **3** (500 MHz, $CDCl_3$).

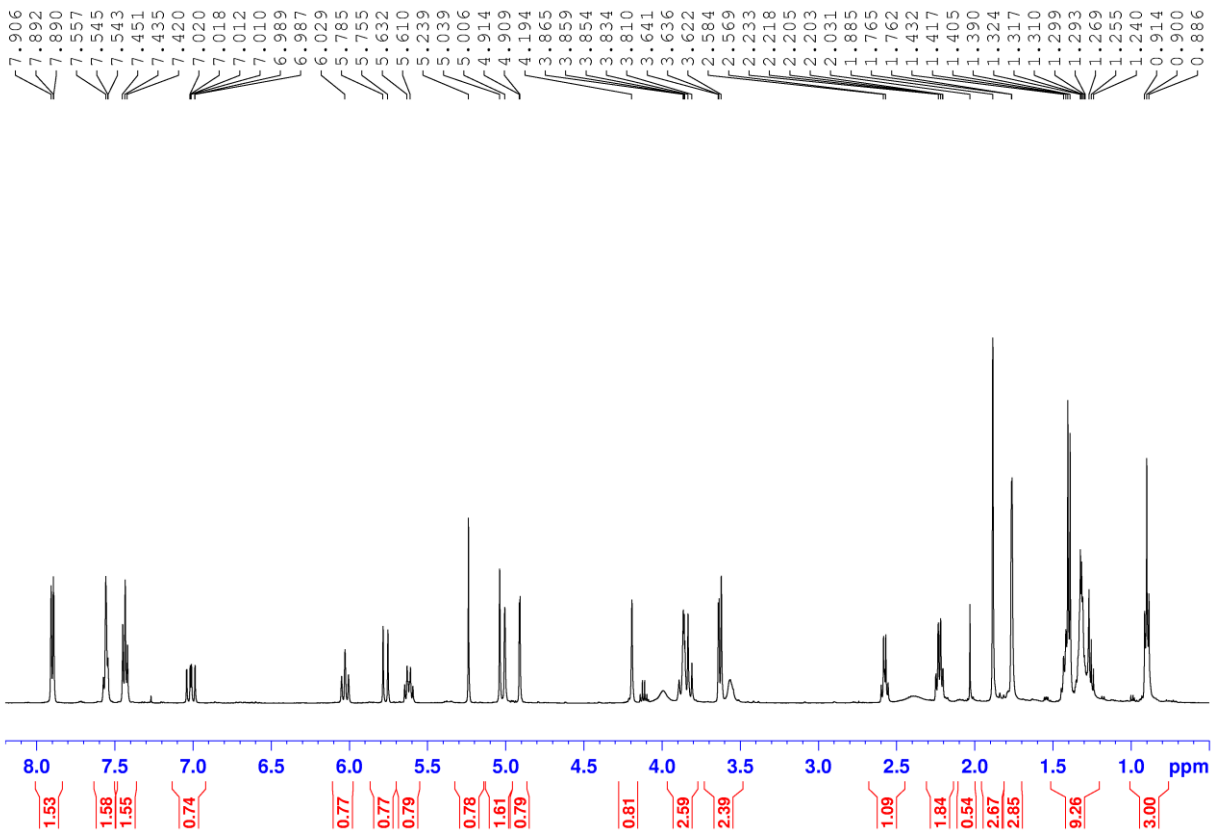

Figure S5. ^{1}H NMR spectrum of compound **4** (500 MHz, $CDCl_3$).

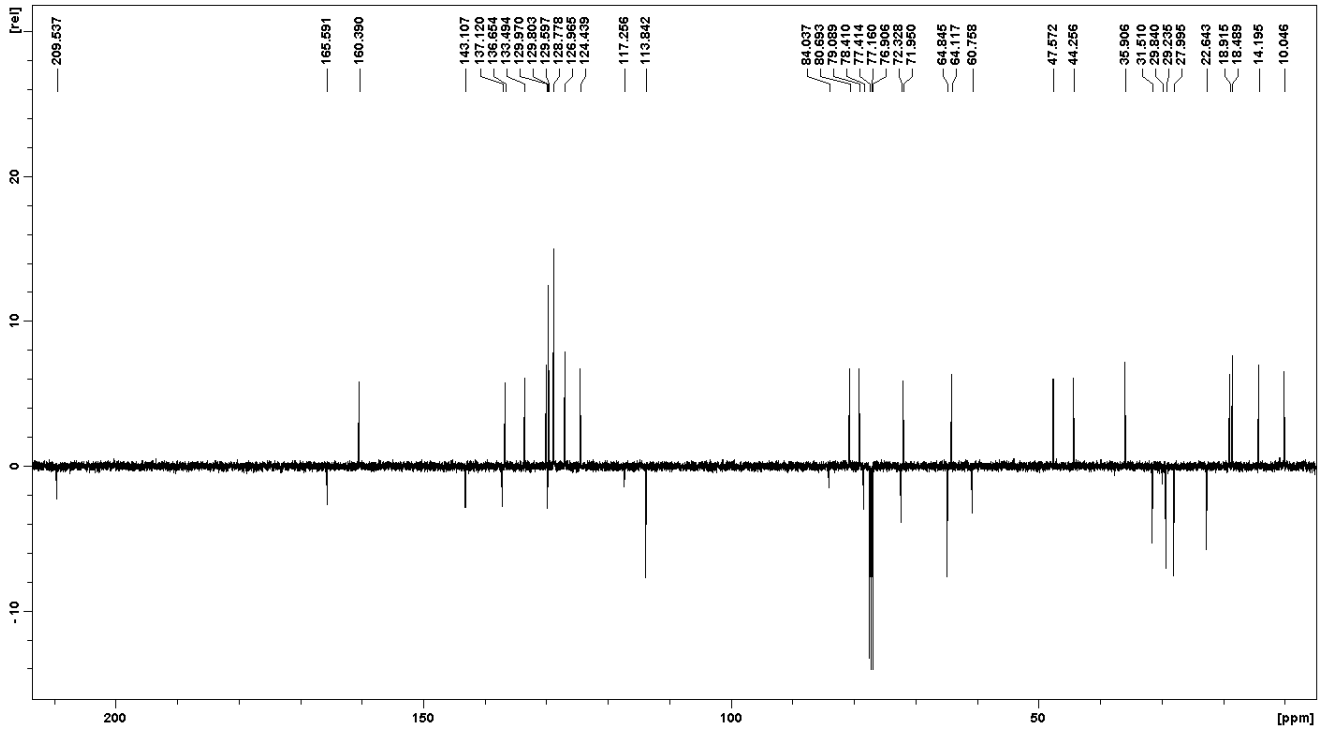

Figure S6. DEPTQ spectrum of compound **4** (500 MHz, $CDCl_3$).

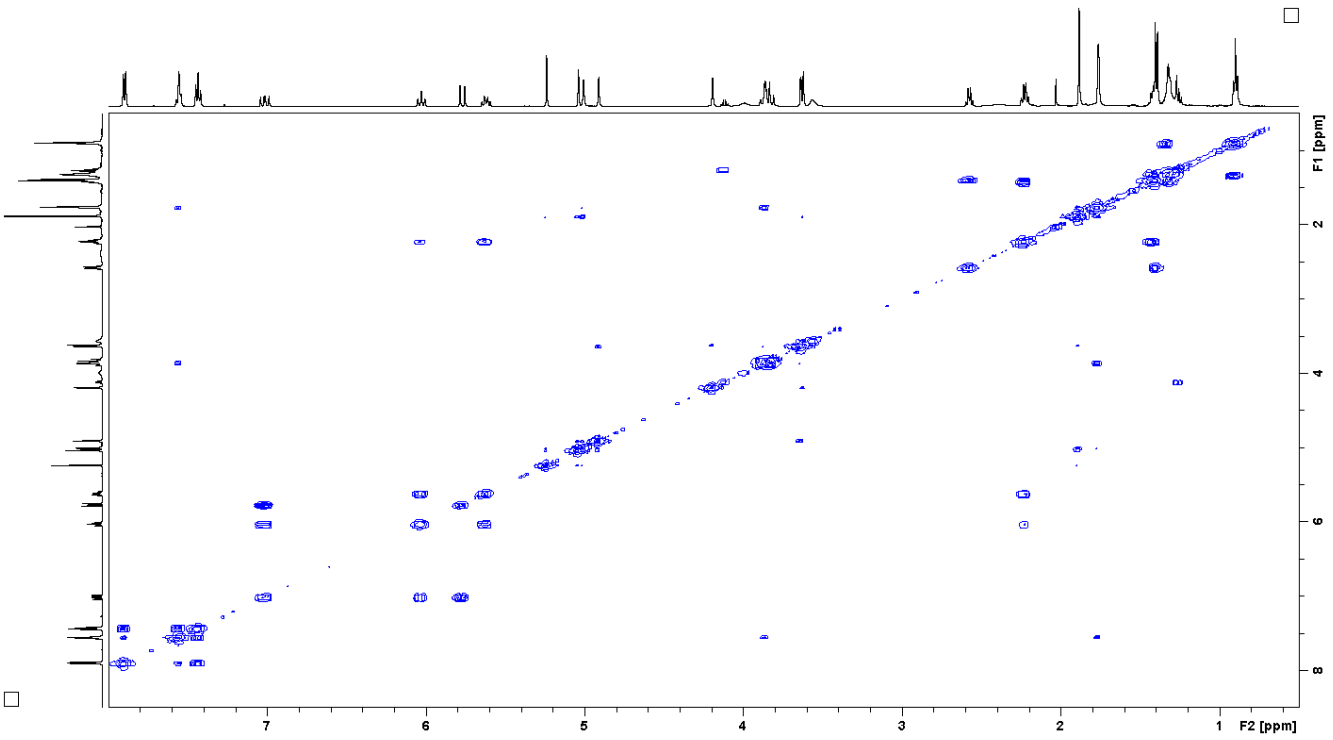

Figure S7. ^{1}H-^{1}H COSY spectrum of compound **4** (500 MHz, $CDCl_3$).

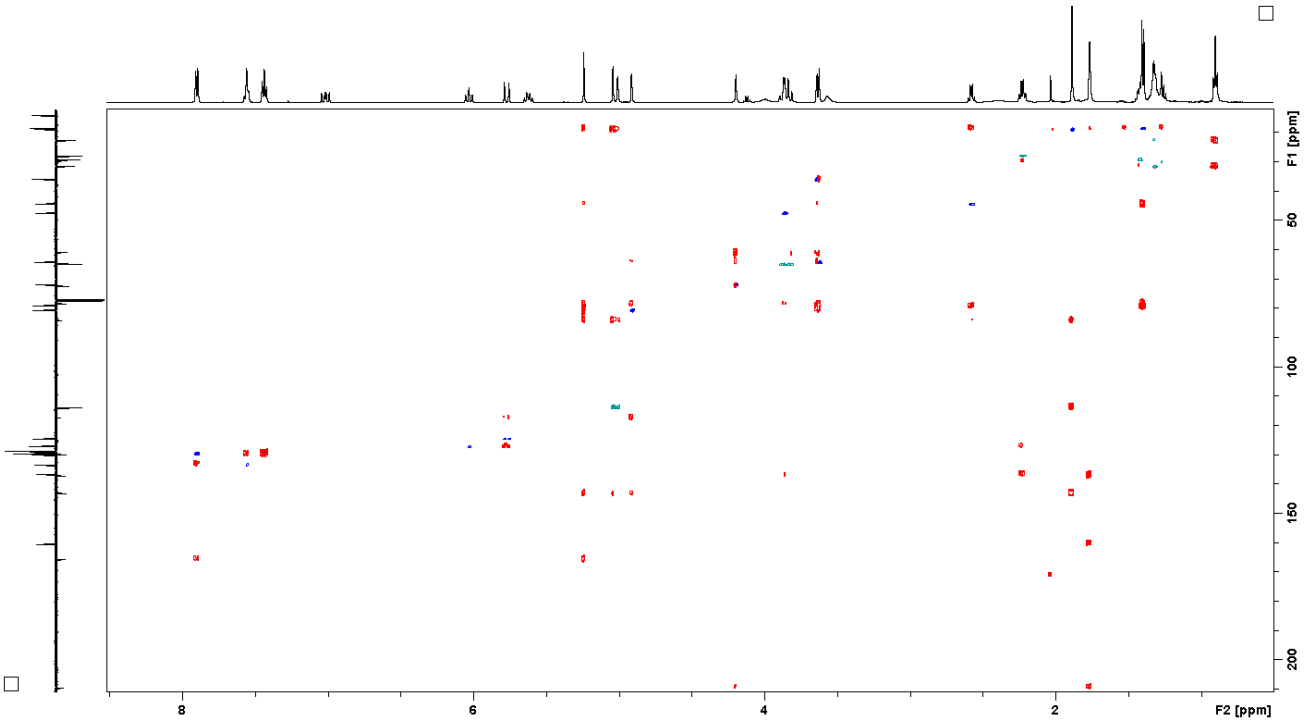

Figure S8. Overlay of HSQC-DEPT (blue/light green) and HMBC spectra of compound **4** (500 MHz, $CDCl_3$).

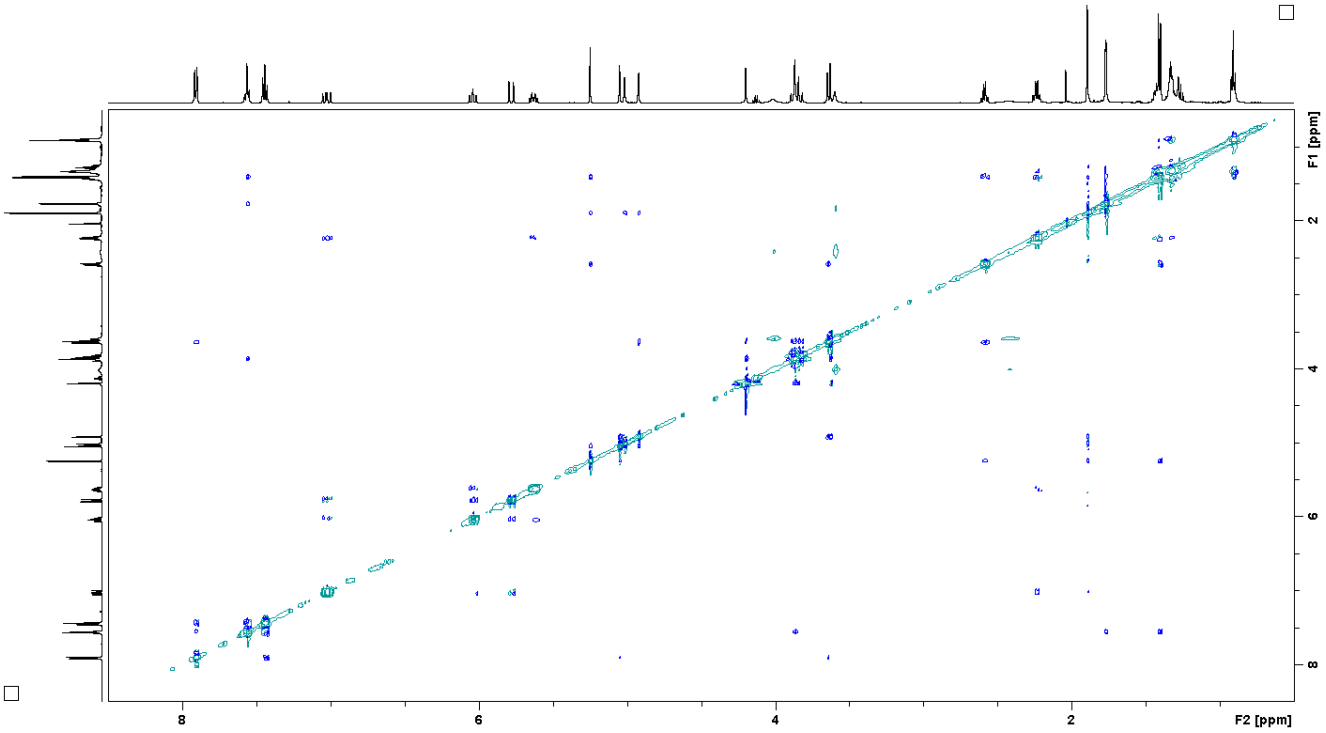

Figure S9. 2D ^{1}H-^{1}H ROESY spectrum of compound **4** (500 MHz, $CDCl_3$).

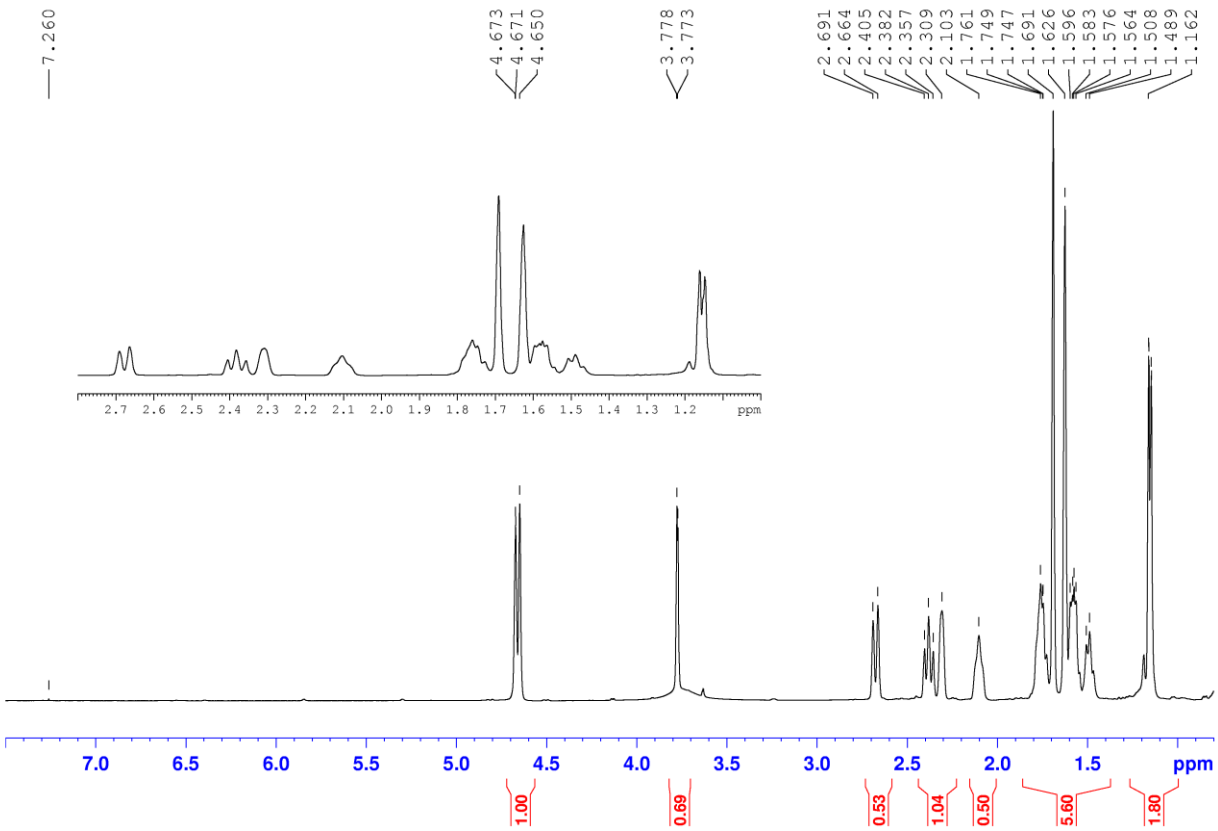

Figure S10. ^{1}H NMR spectrum of compound **11** (500MHz, $CDCl_3$).

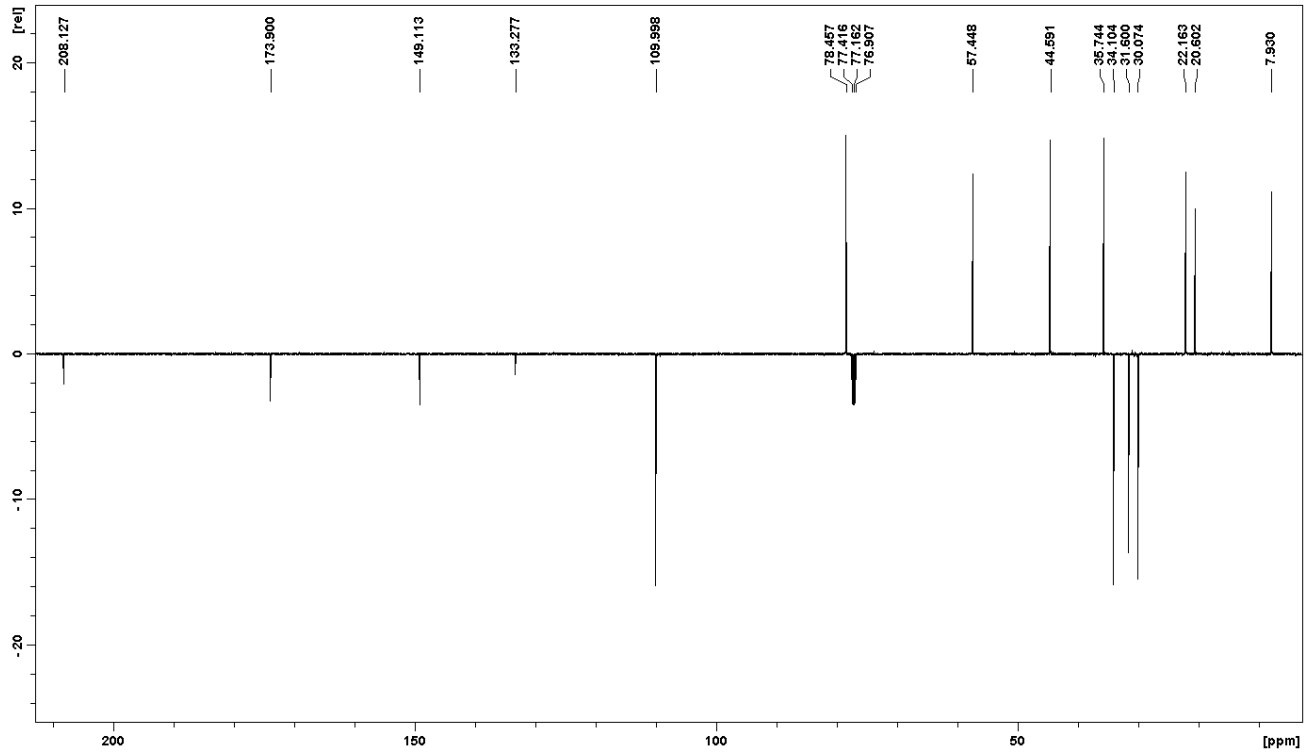

Figure S11. DEPTQ spectrum of compound **11** (500 MHz, $CDCl_3$).

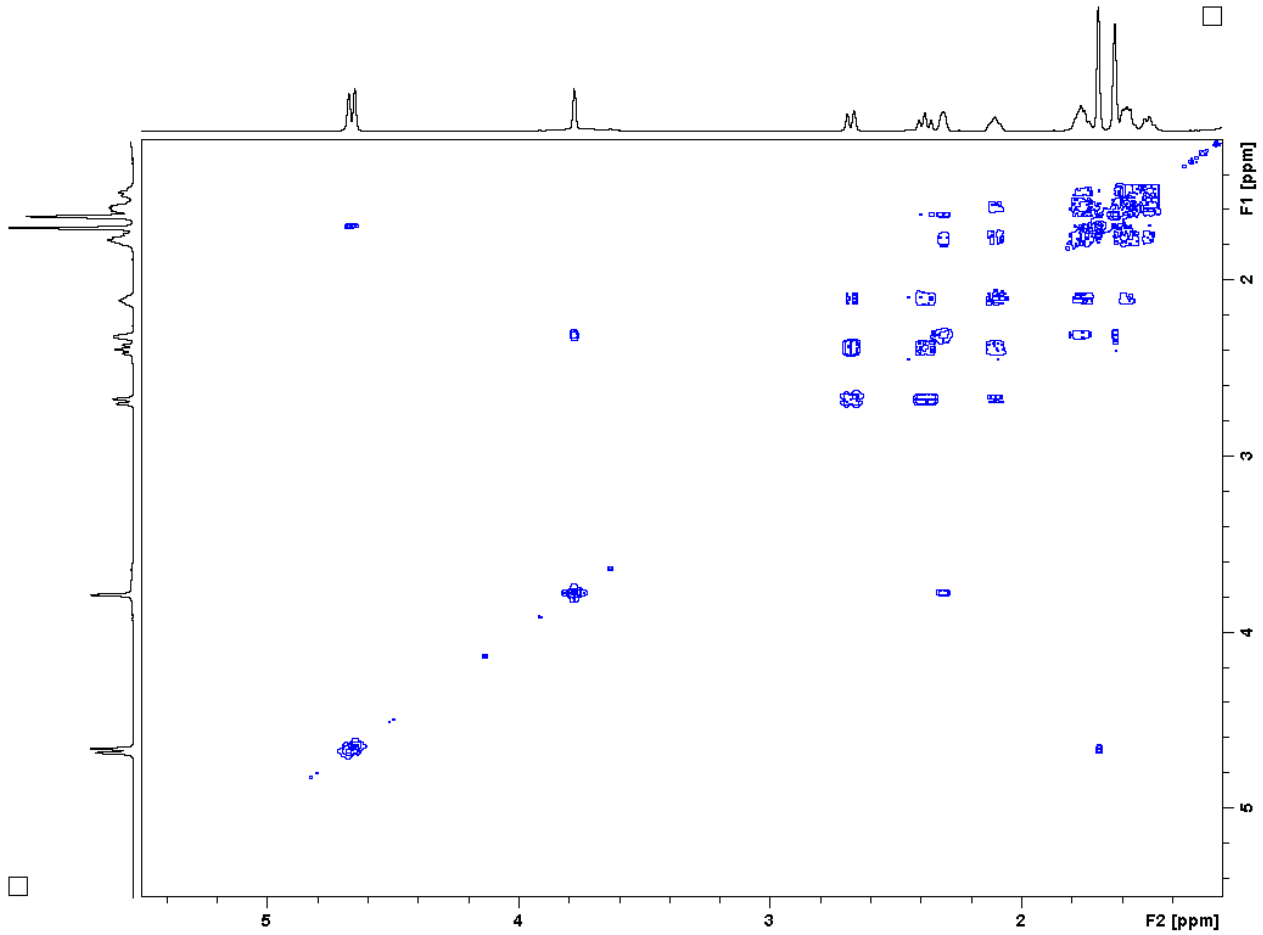

Figure S12. ^{1}H-^{1}H COSY spectrum of compound **11** (500 MHz, $CDCl_3$).

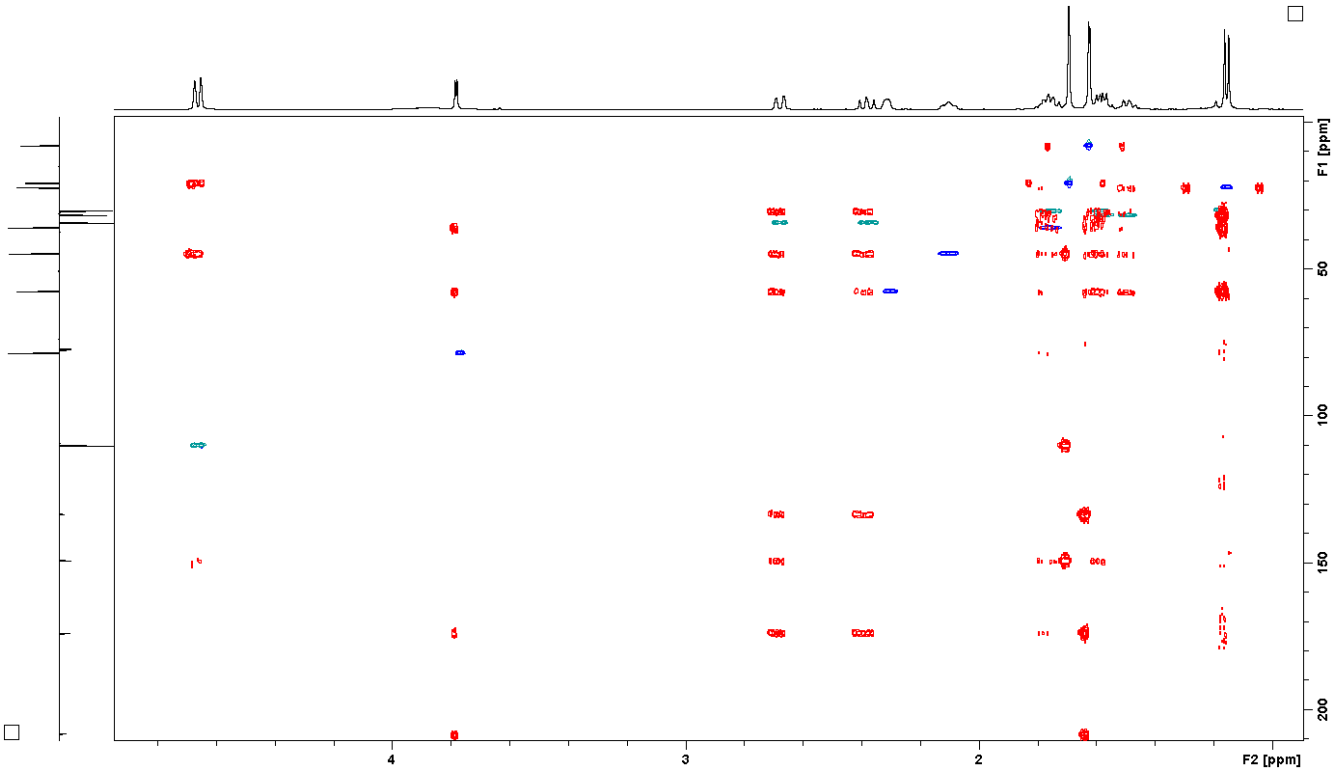

Figure S13. Overlay of HSQC-DEPT (blue/light green) and HMBC spectra of compound **11** (500 and 125 MHz, $CDCl_3$).

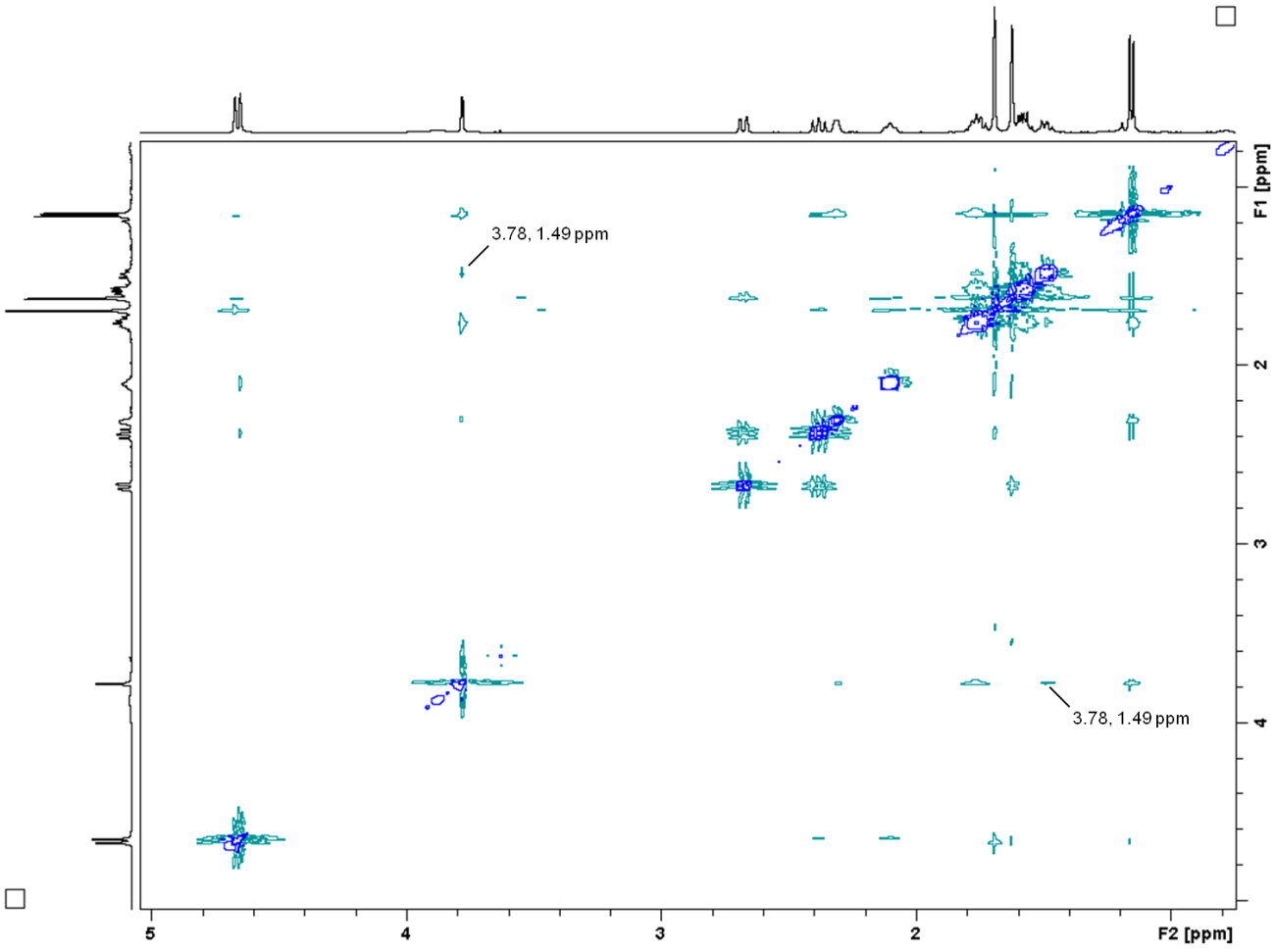

Figure S14. 2D ^{1}H-^{1}H NOESY spectrum of compound **11** (500MHz, $CDCl_3$).

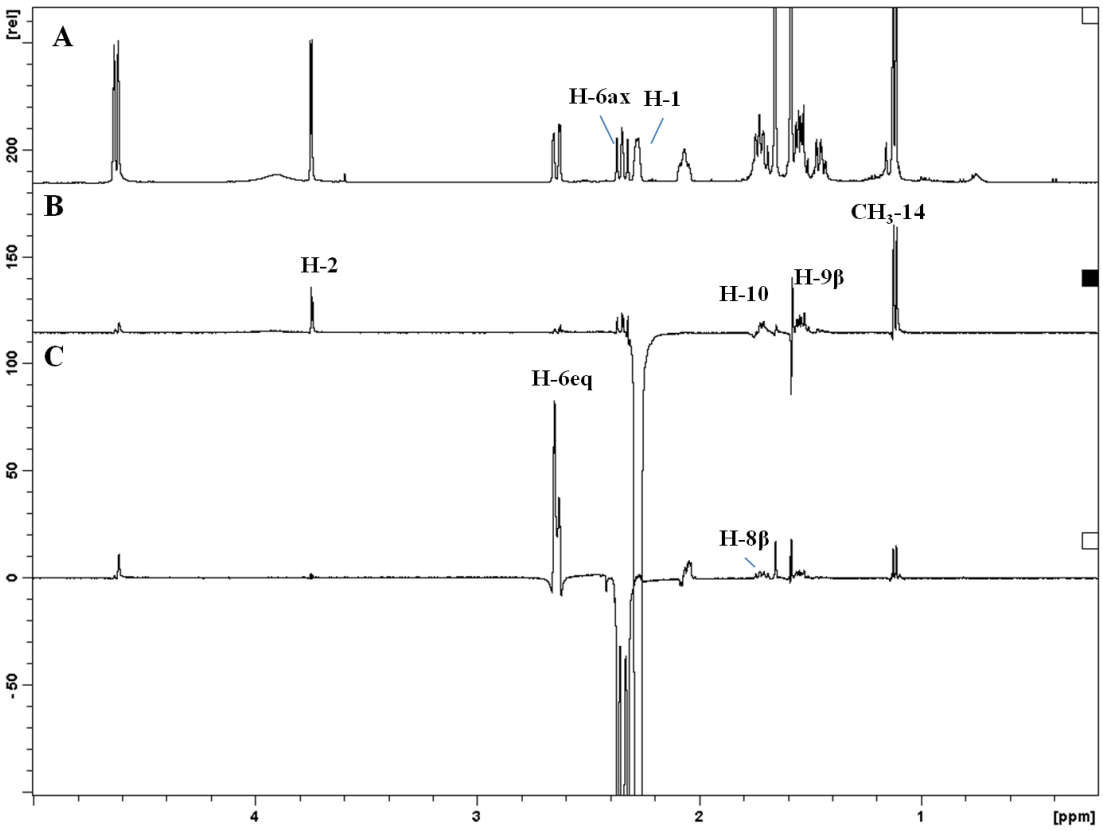

Figure S15. 1D Selective NOESY spectra of compound **11** (500MHz, $CDCl_3$; D8 = 0.5 sec) (**A**) Full ^{1}H NMR spectrum (**B**-**C**) Selective irradiations of H-1 and H-6, respectively.

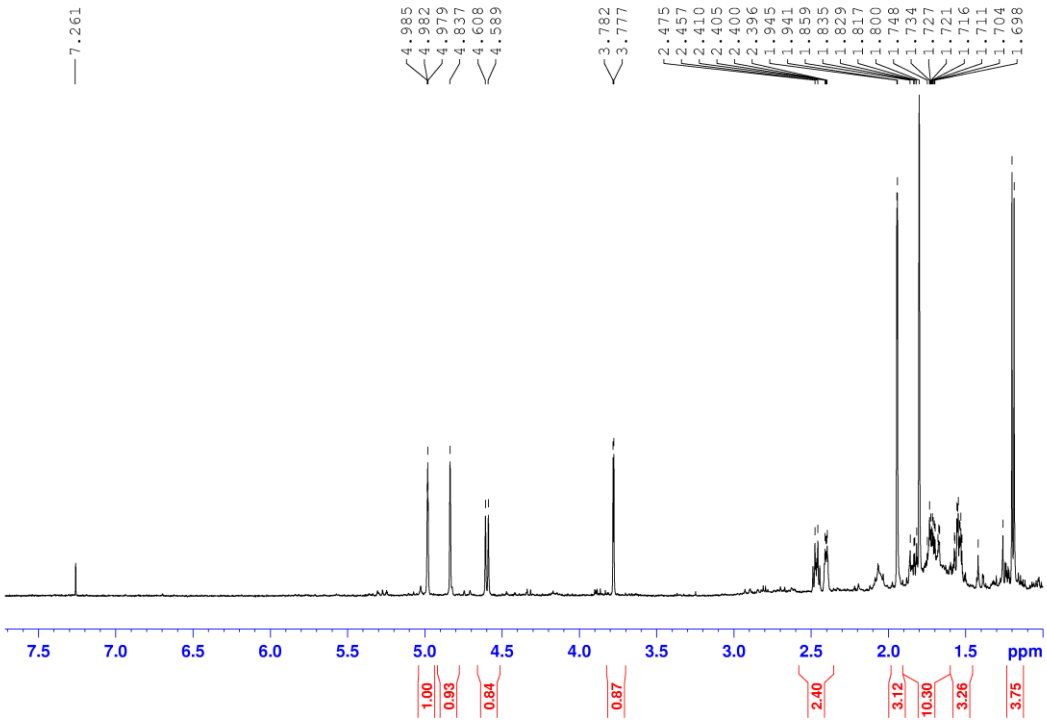

Figure S16. ^{1}H NMR spectrum of compound **12** (500MHz, $CDCl_3$).

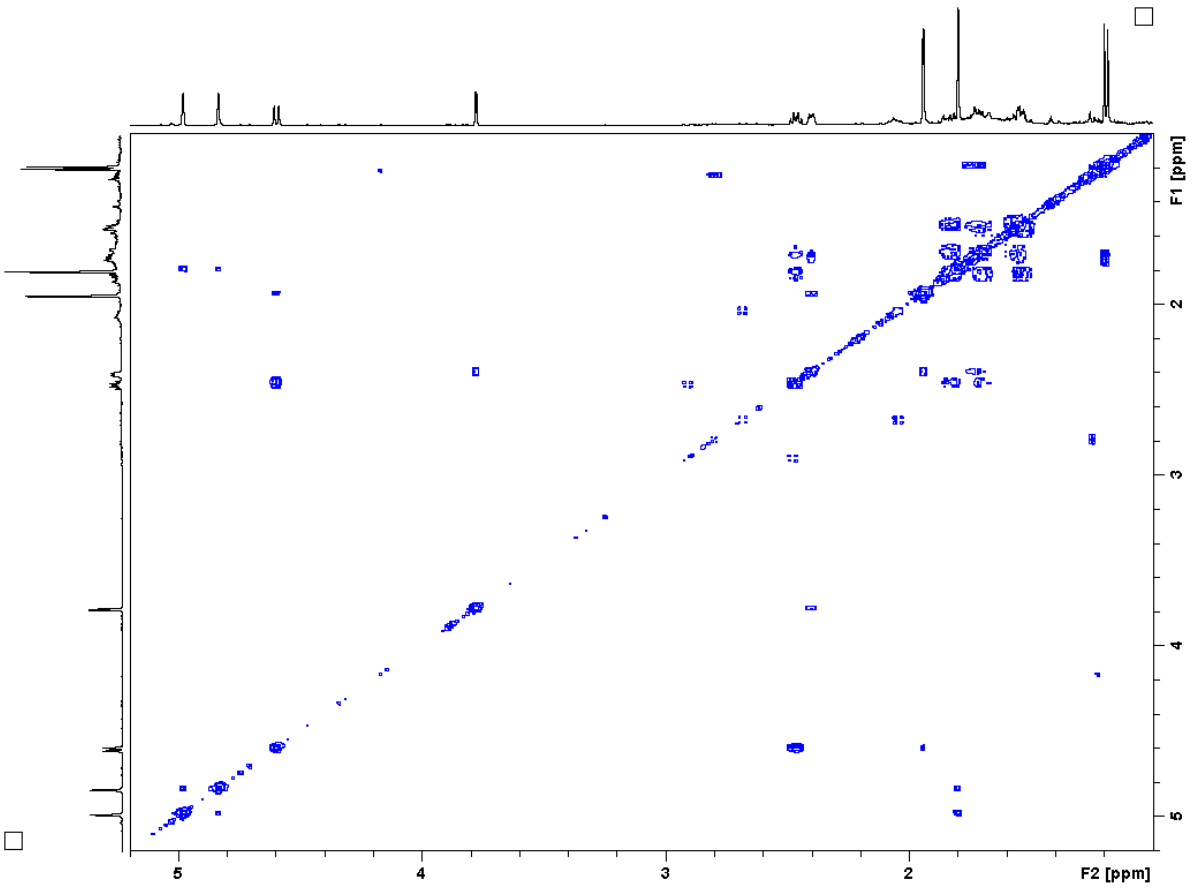

Figure S17. ^{1}H-^{1}H COSY spectrum of compound **12** (500MHz, $CDCl_3$).

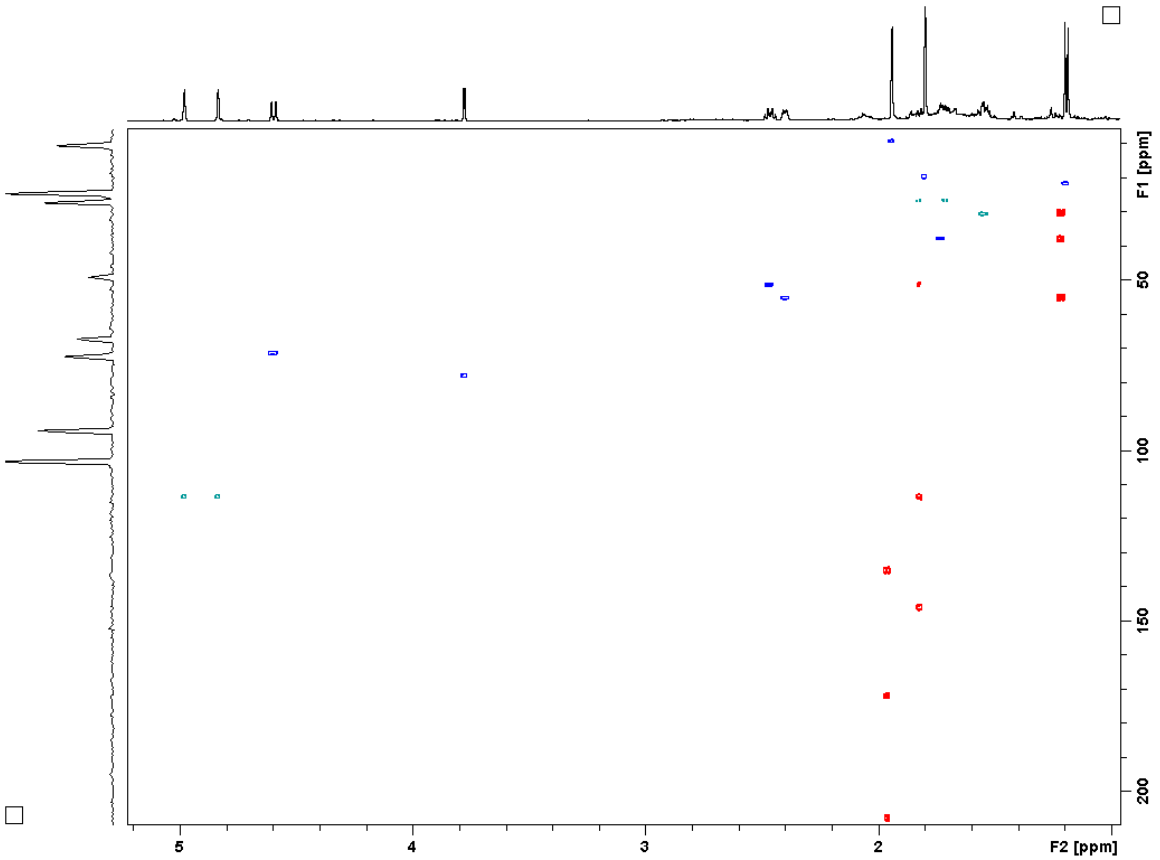

Figure S18. Overlay of HSQC-DEPT (blue/light green) and HMBC spectra of compound **12** (500MHz, $CDCl_3$).

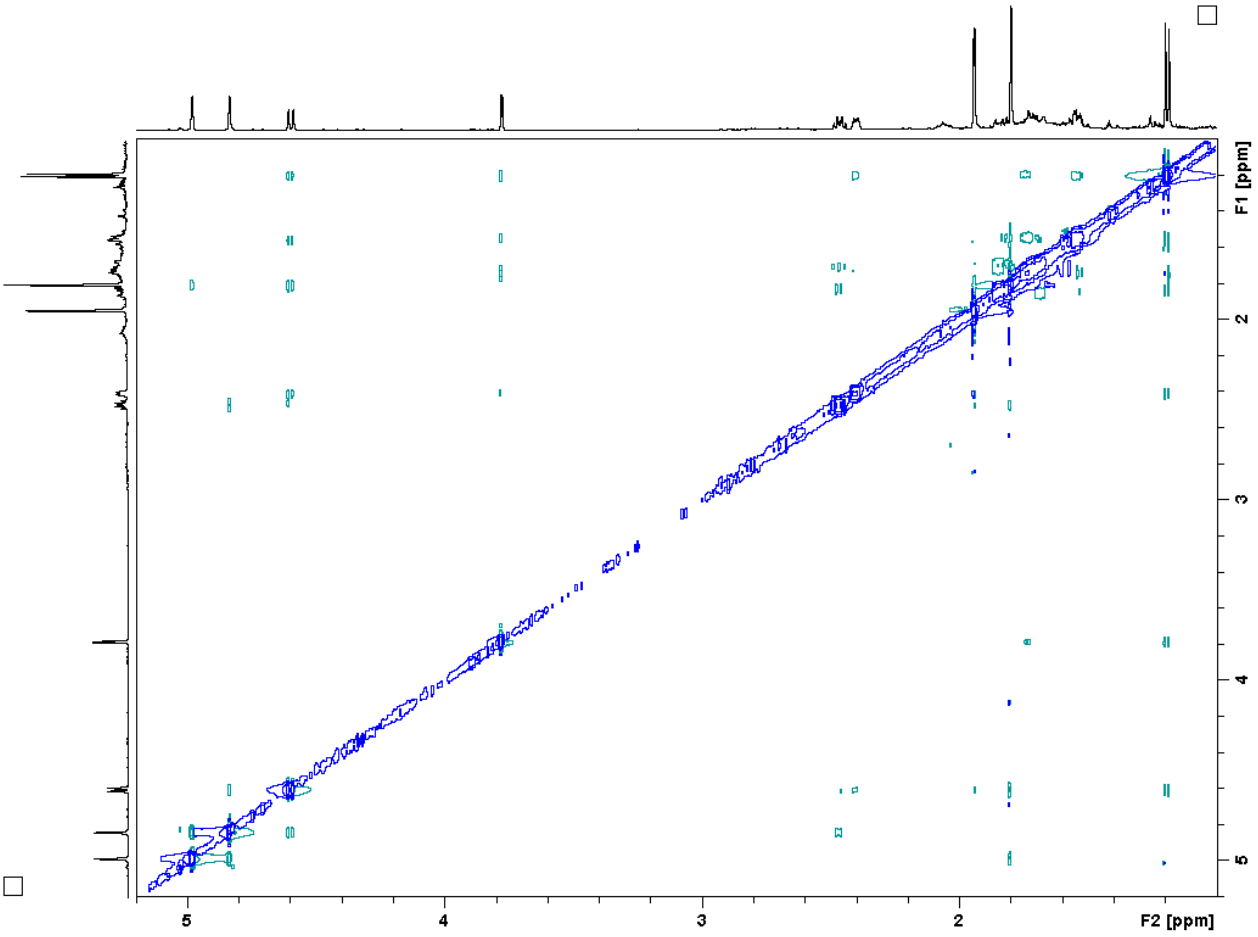

Figure S19. 2D ^{1}H-^{1}H NOESY spectrum of compound **12** (500MHz, $CDCl_3$).

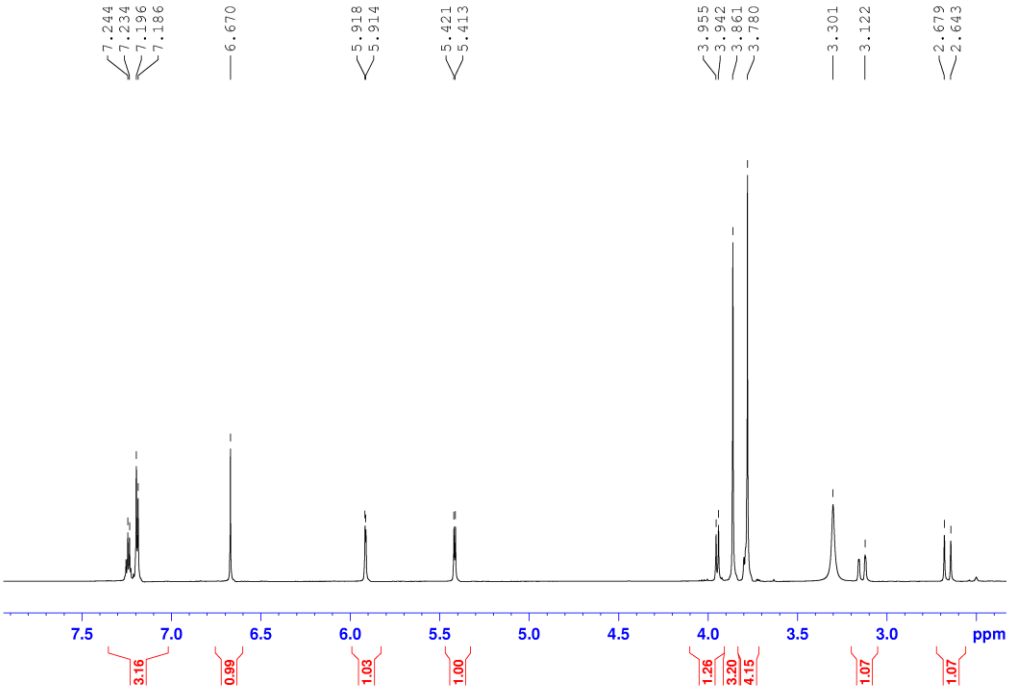

Figure S20. ^{1}H NMR spectrum of compound **15** (500MHz, DMSO-d_6).

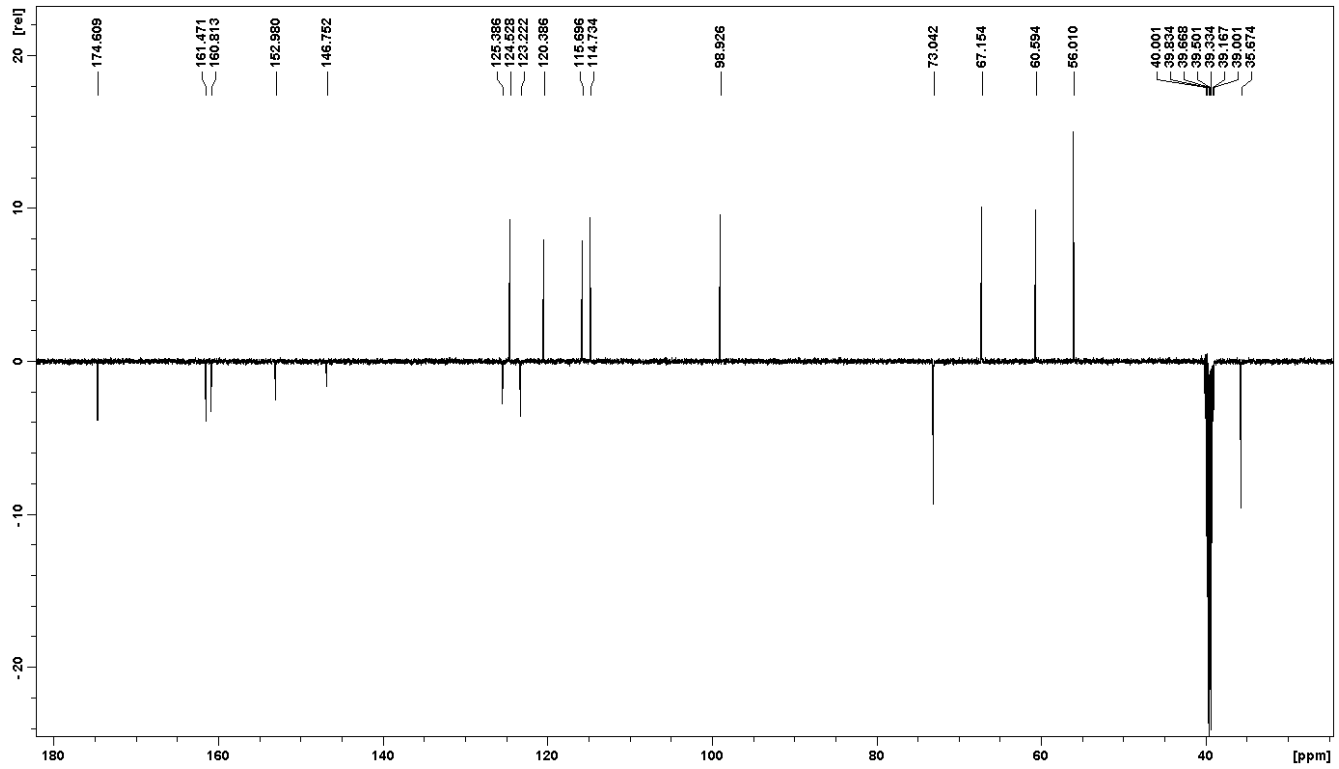

Figure S21. ^{13}C NMR spectrum of compound **15** (125 MHz, DMSO-d_6).

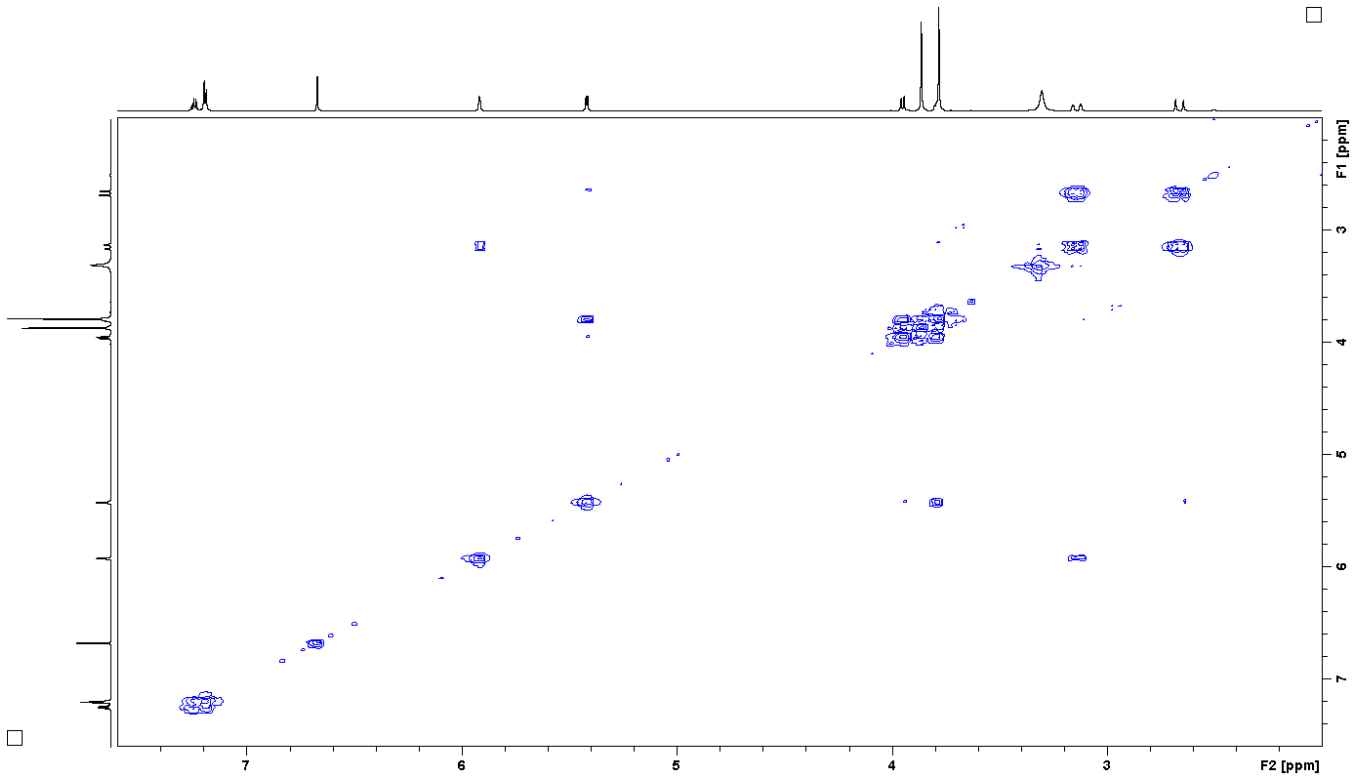

Figure S22. ^{1}H-^{1}H COSY spectrum of compound **15** (500MHz, DMSO-d_6).

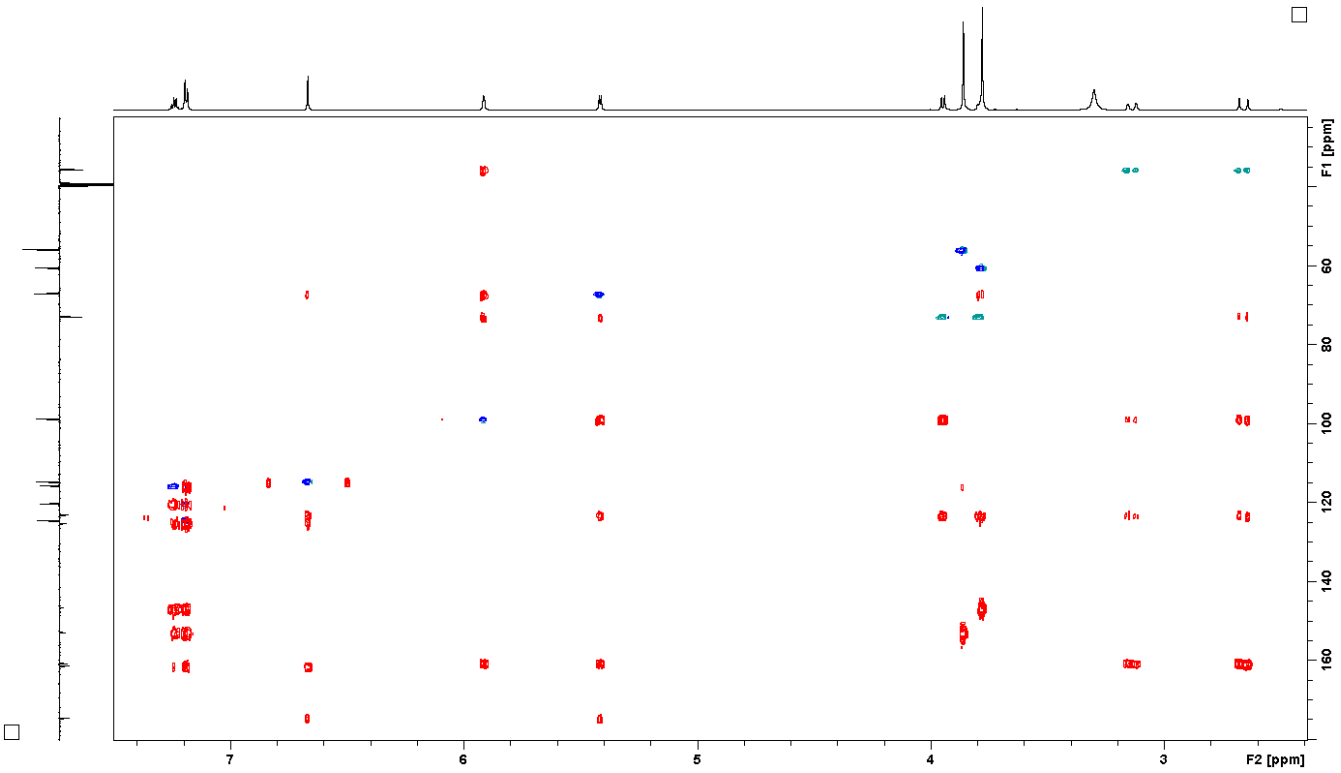

Figure S23. Overlay of HSQC-DEPT (blue/light green) and HMBC spectra of compound **15** (500MHz, DMSO-d_6).

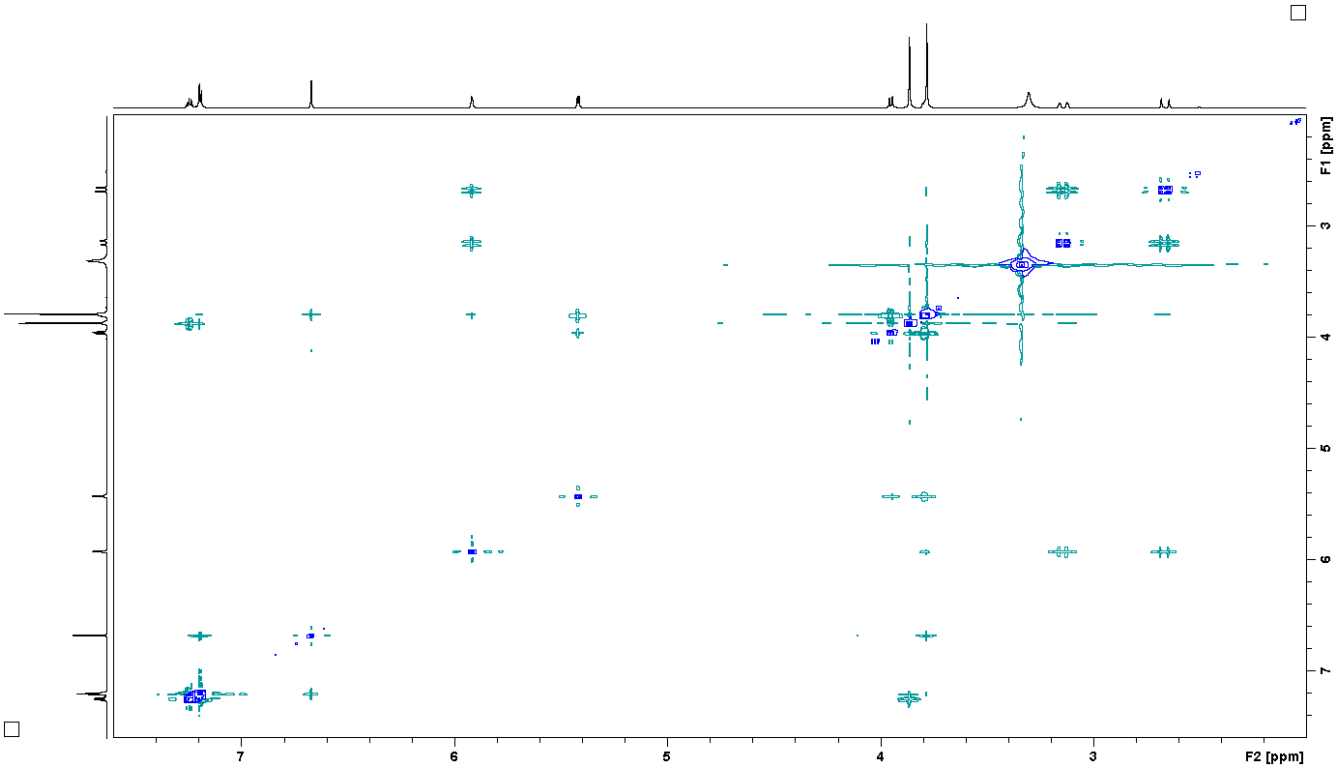

Figure S24. 2D ^{1}H-^{1}H NOESY spectrum of compound **15** (500MHz, DMSO-d_6).

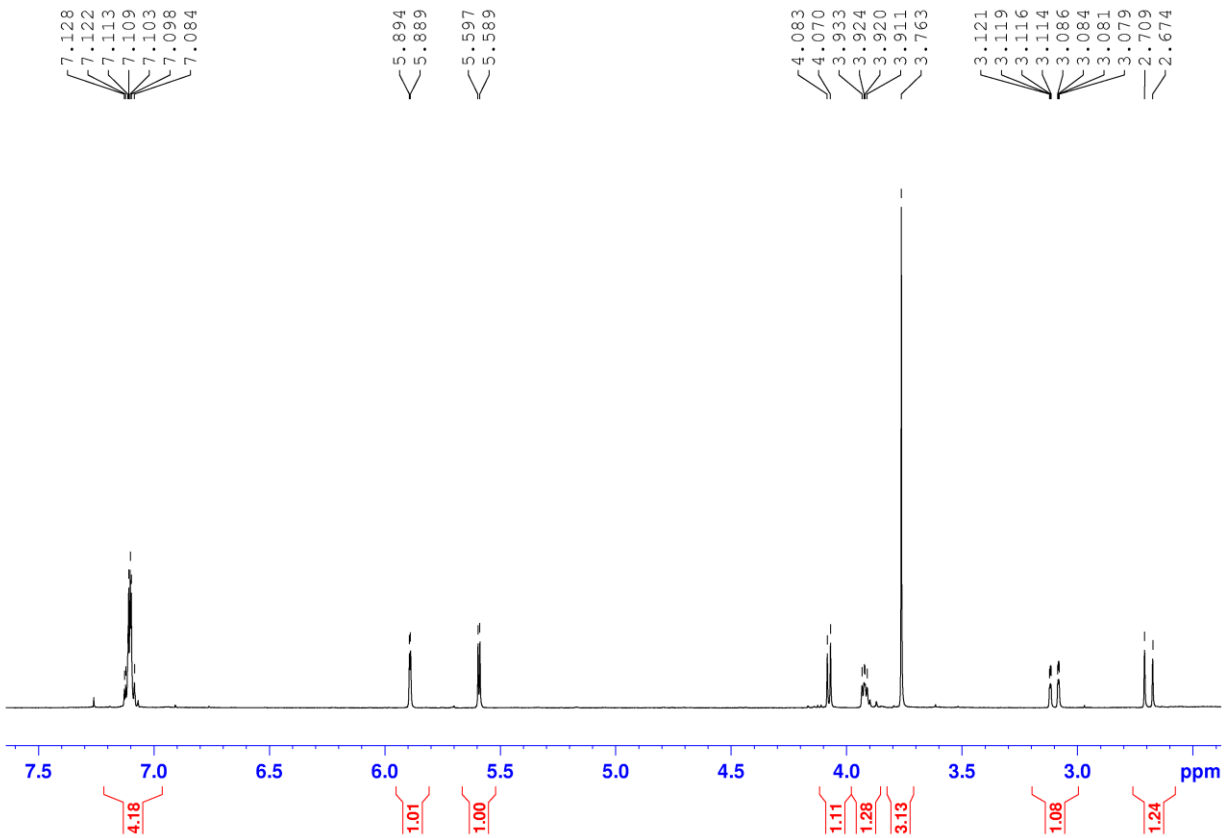

Figure S25. ^{1}H NMR spectrum of compound **16** (500MHz, $CDCl_3$).

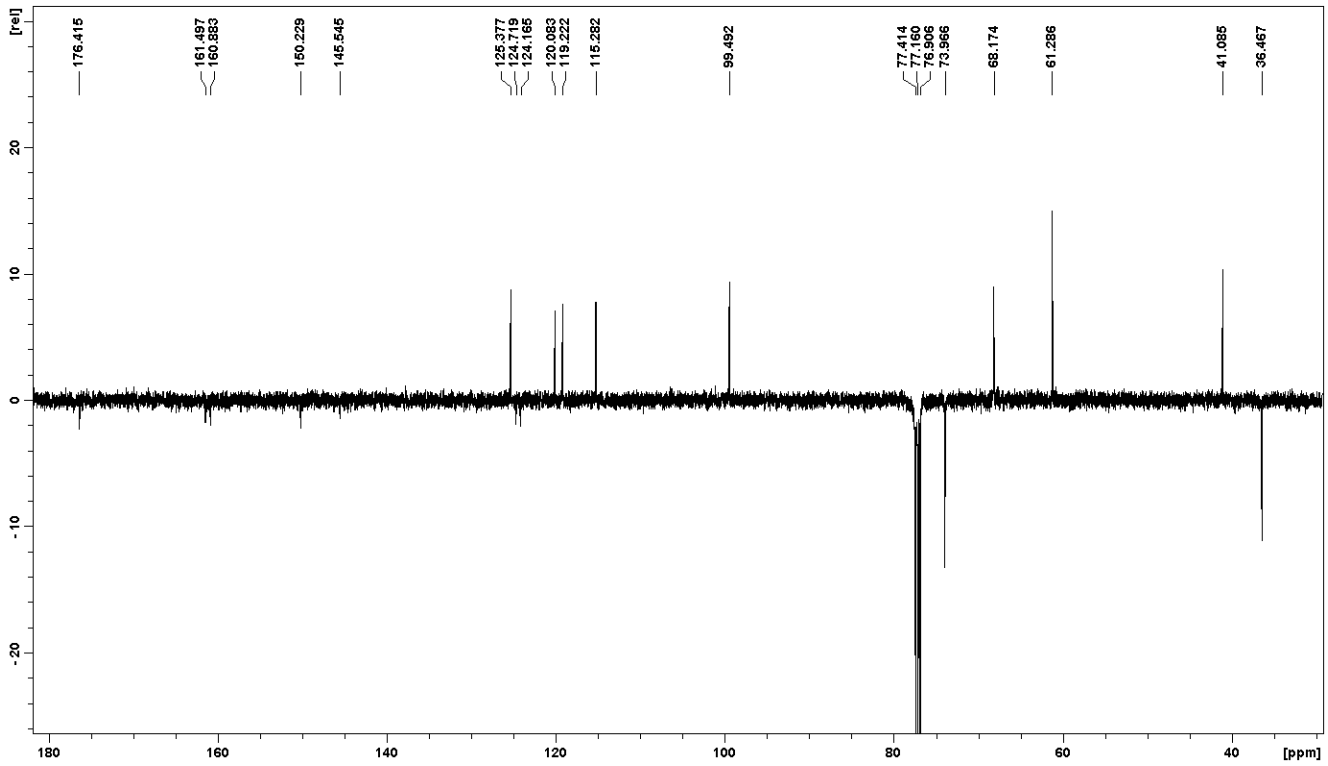

Figure S26. ^{13}C NMR spectrum of compound **16** (125 MHz, $CDCl_3$).

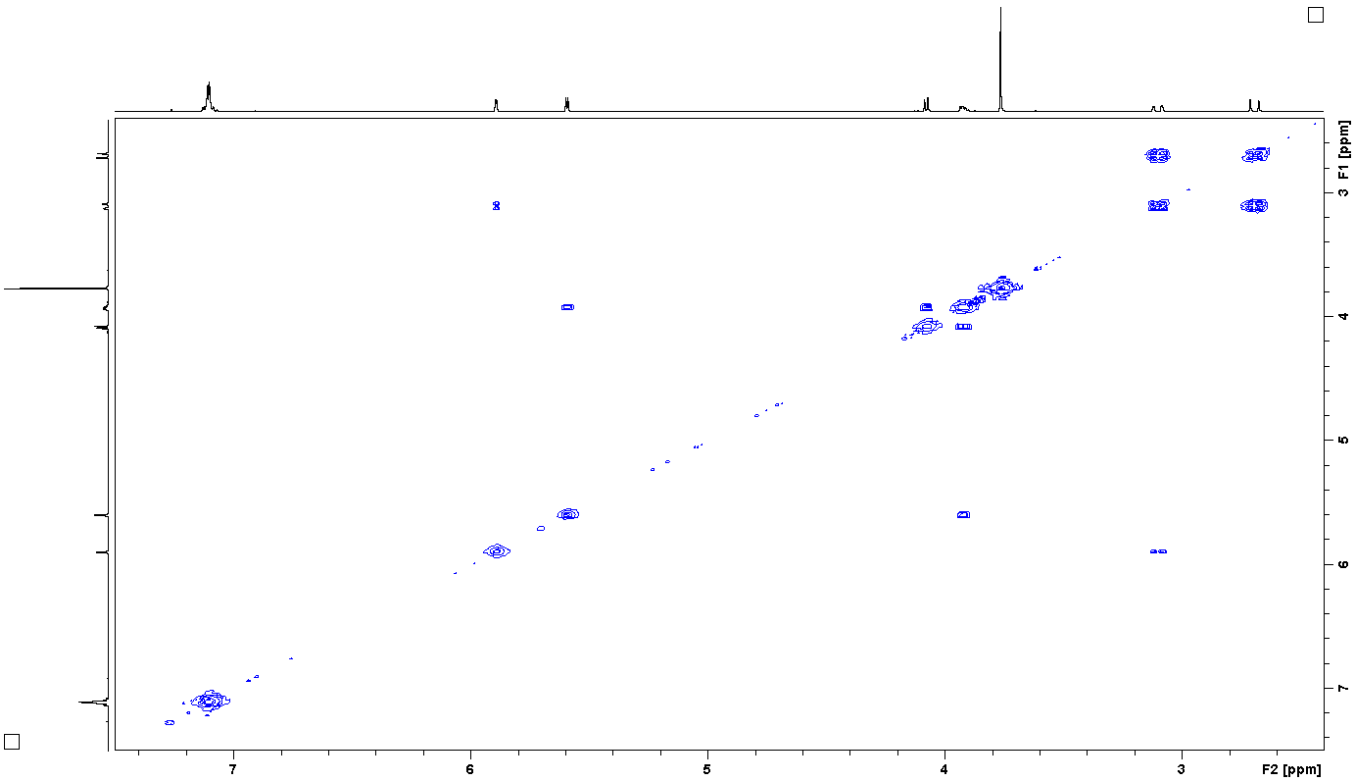

Figure S27. ^{1}H-^{1}H COSY spectrum of compound **16** (500MHz, $CDCl_3$).

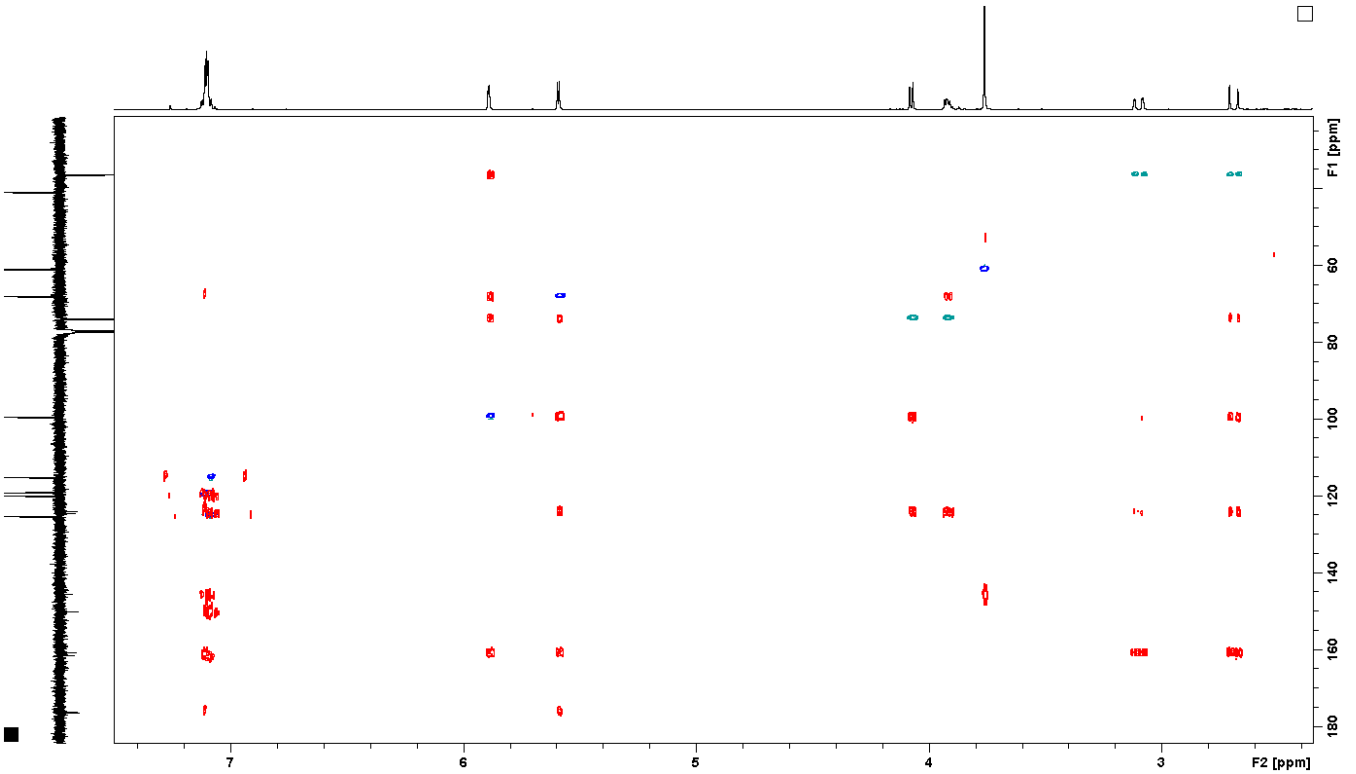

Figure S28. Overlay of HSQC-DEPT (blue/light green) and HMBC spectra of compound **16** (500MHz, $CDCl_3$).

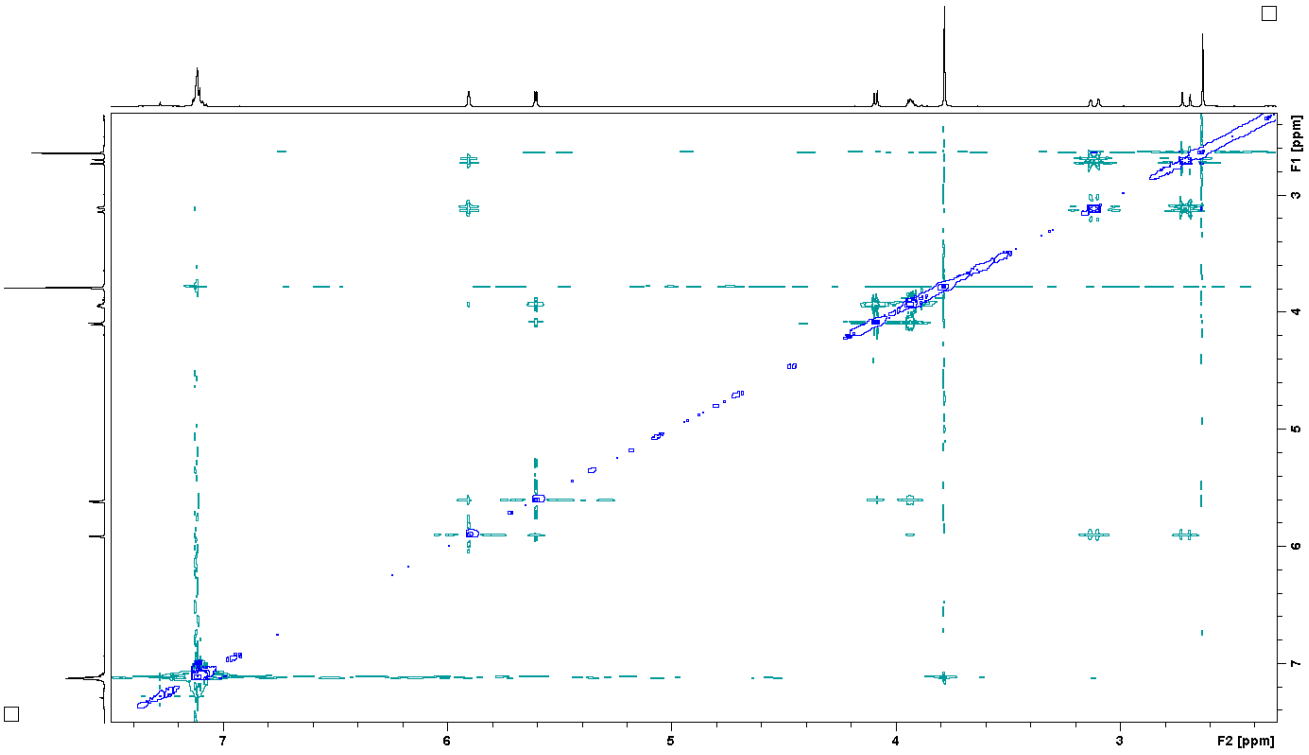

Figure S29. 2D ^{1}H-^{1}H NOESY spectrum of compound **16** (500MHz, $CDCl_3$).

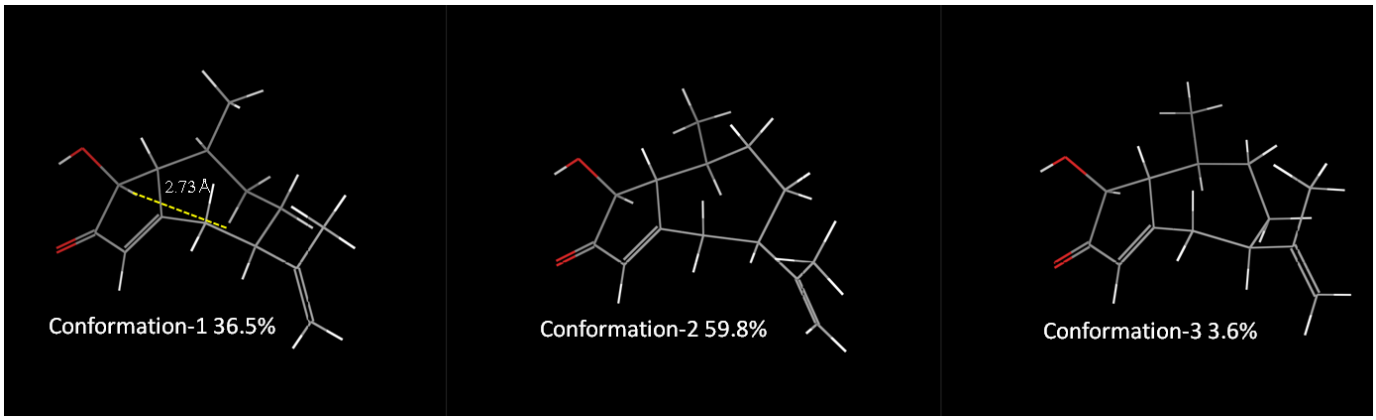

Figure S30. Major conformers of compound **1**, according to their weight in the Boltzmann distribution after geometrical optimization (b3lyp/6-31g(d,p)) in gas phase.

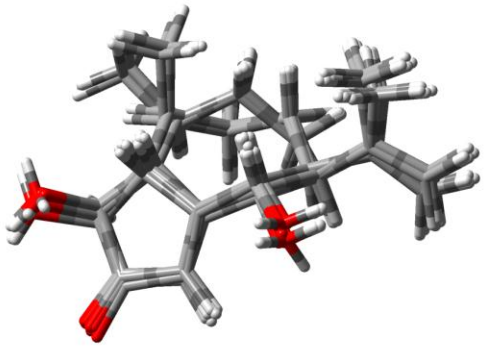

Figure S31. Superimposed conformers of compound **11** found within 2 Kcal/mol from the global minimum **(**Schrödinger MacroModel 9.8; OPLS2005 in water).

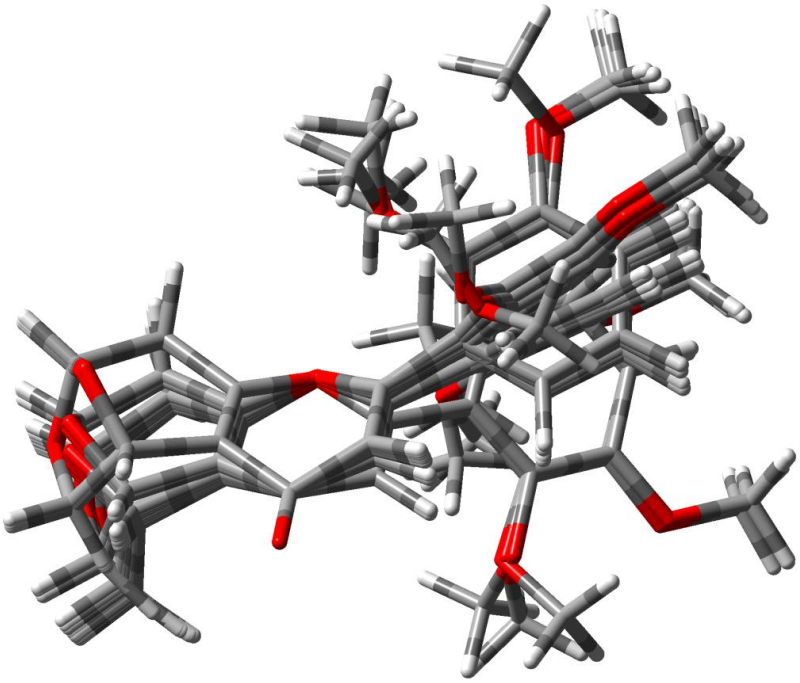

Figure S32. Superimposed conformers of compound **15** found within 2 Kcal/mol from the global minimum **(**Schrödinger MacroModel 9.8 ;OPLS2005 in water).

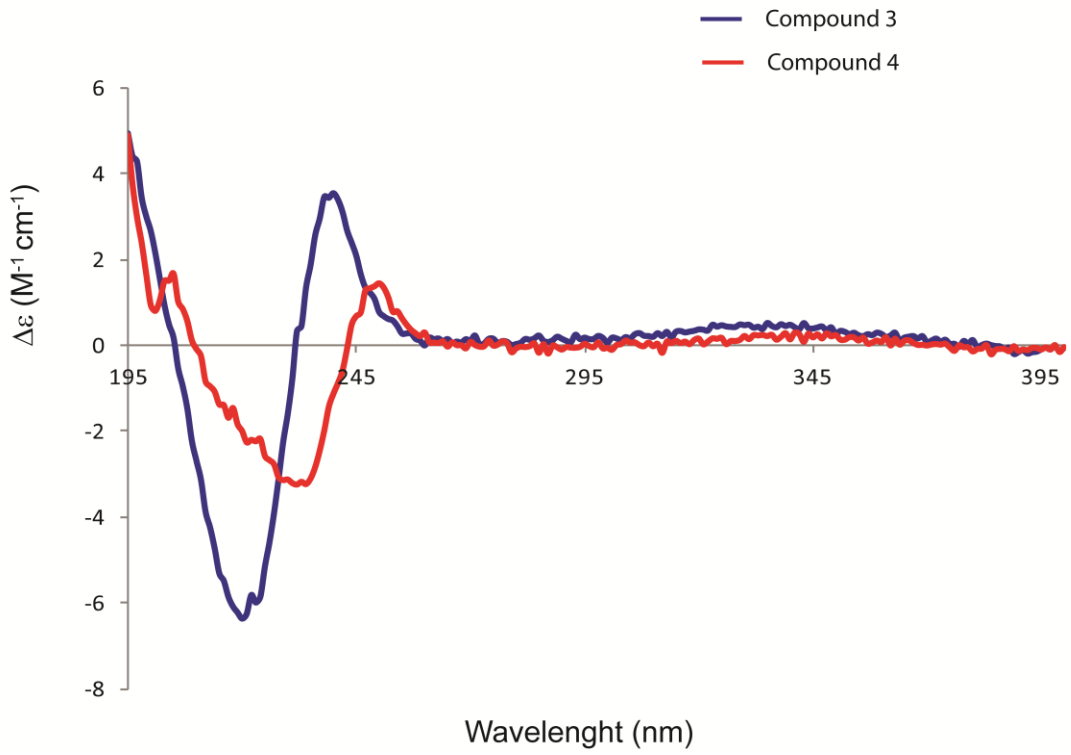

Figure S33. ECD spectra of compounds **3** and **4** in MeOH.

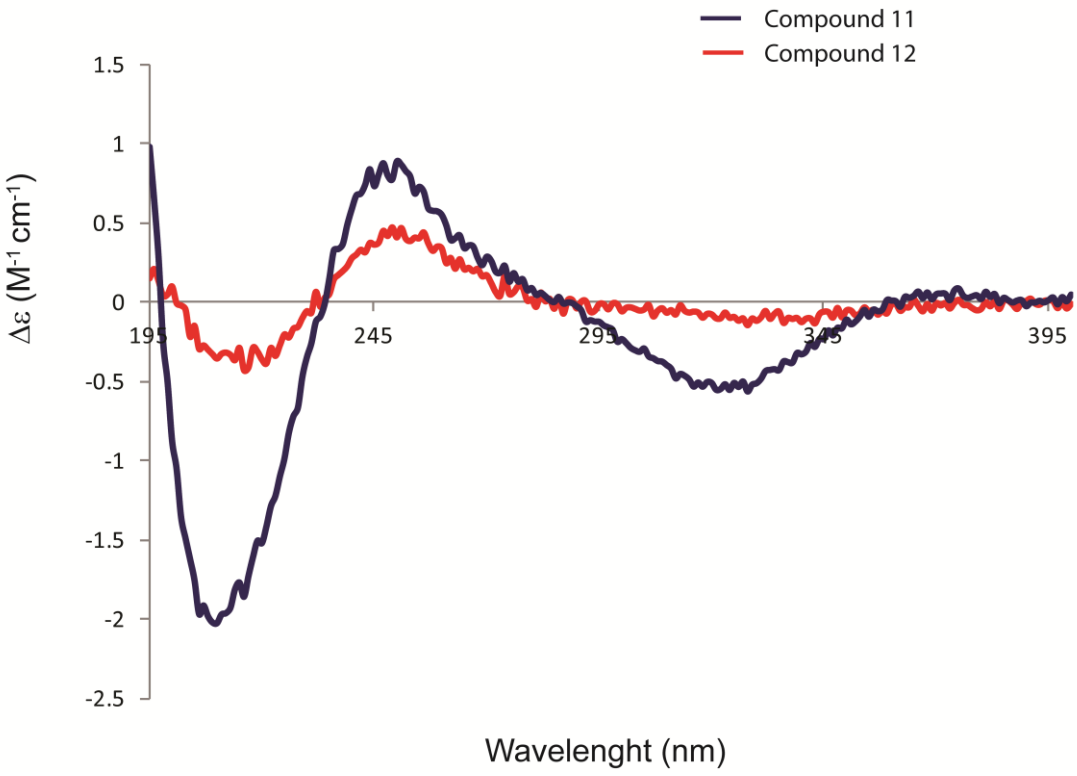

Figure S34. ECD spectra of compounds **11** and **12** in MeOH.

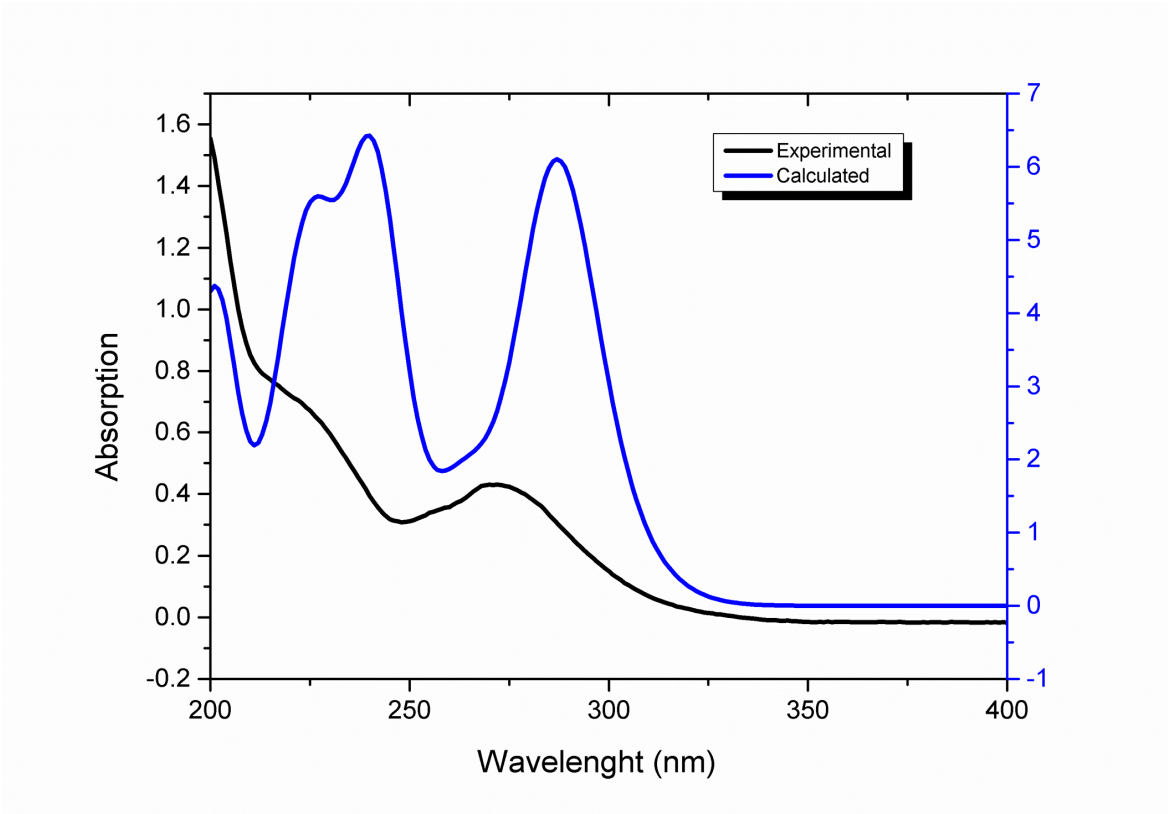

Figure S35. Experimental and calculated (cam-b3lyp/6-31g(d,p) UV spectra for the 5*R*,7*S* stereoisomer of compound **15** in MeOH.

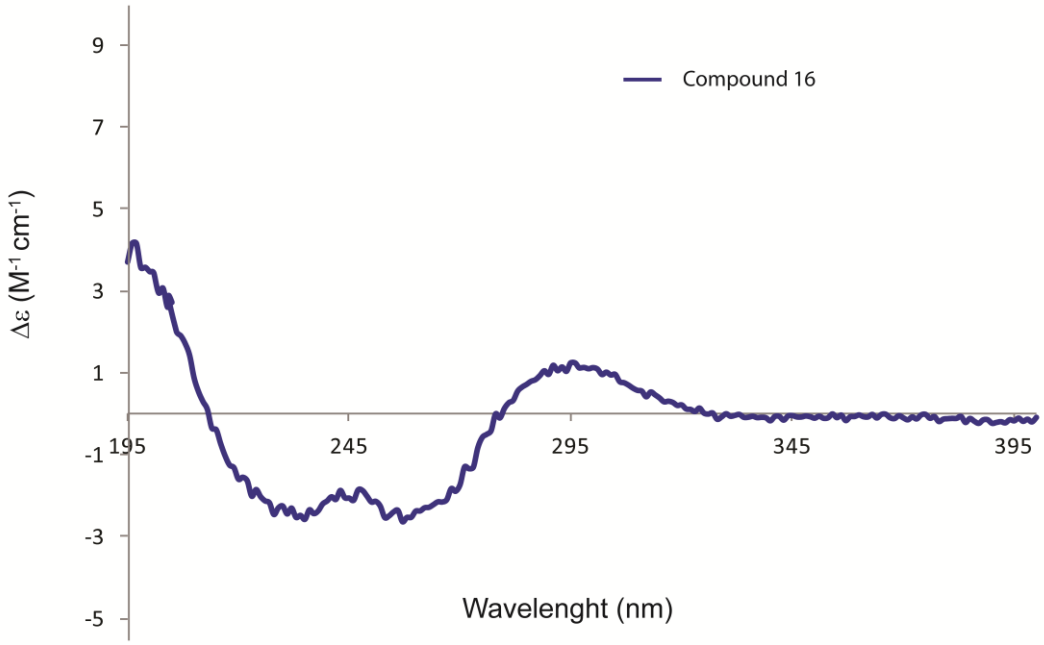

Figure S36. ECD spectra of compound **16** in MeOH.

2.3. Labdane and Clerodane Diterpenoids from *Colophospermum mopane* (manuscript and supporting information submitted to *Phytochemistry*)

(Manuscript ID: PHYTOCHEM-D-15-00239)

My contribution towards this manuscript: I prepared extracts and pure samples with countercurrent chromatography in Bloemfontein. Dr Maria De Mieri assisted me in Basel with further purification, recording of spectroscopic and other data, crystallization, structure elucidation including absolute configuration and preparation of the first draft of the manuscript.

Kun Du

Labdane and clerodane diterpenoids from *Colophospermum mopane*

Kun Du [a,1], Maria De Mieri [b,1], Markus Neuburger [c], Pieter C. Zietsman [d,e], Andrew Marston [a,#], Sandy F. van Vuuren [f], Matthias Hamburger [b,*], and Jan H. van der Westhuizen [g,*]

[a]Department of Chemistry, University of the Free State, Nelson Mandela Avenue, Bloemfontein 9301, South Africa

[b]Division of Pharmaceutical Biology, University of Basel, Klingelbergstrasse 50, 4056 Basel, Switzerland

[c]Division of Inorganic Chemistry, Department of Chemistry, University of Basel, Basel, Switzerland

[d]National Museum, P. O. Box 266, Bloemfontein 9300, South Africa

[e]Centre for Environmental Management, University of the Free State, P.O. Box 339, Bloemfontein, 9301, South Africa

[f]Department of Pharmacy and Pharmacology, Faculty of Health Sciences, University of the Witwatersrand, Parktown, South Africa

[g]Directorate Research Development, University of the Free State, Nelson Mandela Avenue, Bloemfontein 9301, South Africa

[*]Corresponding authors at:

Prof. Jan H. van der Westhuizen, Department of Chemistry, University of the Free State, Bloemfontain 9301, South Africa.

Prof. Matthias Hamburger, Division of Pharmaceutical Biology, University of Basel, Klingelbergstrasse 50, CH-4056 Basel, Switzerland.

[1]These authors contributed equally to this work

[#] Deceased

E-mail addresses: vdwestjh.@ufs.ac.za, Phone: +27 828935113

matthias.hamburger@unibas.ch, Phone: +41 61 267 14 25 Fax: +41 61 267 14 74

ABSTRACT

Five labdane **1-5**, one isolabdane **6** and five clerodane diterpenoids **7-11**, were isolated from seeds, husks and leaves of *Colophospermum mopane*. Compounds **1-3** and **6-9** were new, and their structures were elucidated by means of spectroscopic analysis (1D and 2D NMR, HRESIMS). The absolute configuration of **1**, **7** and **10** were determined by single-crystal X-ray diffraction with Cu K*α* radiation. For compounds **2** and **6** absolute configuration was established by modified Mosher's method, and corroborated by comparison of experimental and calculated ECD spectra of their 3-*p*-bromobenzoate derivatives. The crude extracts and compounds were evaluated for antimicrobial activity. The leaf extract was the most active against *Staphylococcus aureus* (125 µg/ml). Compound **11** showed the best inhibitory activity with minimum inhibitory values of 15.6 µg/ml against *Escherichia coli* and *Staphylococcus aureus*, and 31.3 µg/ml against *Enterococcus faecalis*.

Keywords

Leguminosae/ *Colophospermum mopane*/ Labdane diterpenoids/ Clerodane diterpenoids/ Antibacterial activity

1. Introduction

Colophospermum mopane Kirk ex J. Leonard (previously *Copaifera mopane* Kirk ex Benth), belonging to a monotypic genus in Caesalpinioideae (Laeguminosae subfamily) (Lewis, 2005), is one of the dominant trees in the dry regions of Southern Africa. It is one of the most distinctive vegetation groups, often forming pure stands. These have given rise to the now accepted term 'mopane woodland' or '*Colophospermum* woodland' which has an atmosphere entirely of its own (Palgrave, 1983). *C. mopane* leaves and pods provide an important food source for many animals,

while the roasted caterpillars of the mopane moth, commonly known as ‘mopane worms’, are an important delicacy and protein source in the diet of local Africans. In addition, plant infusions are used in traditional medicine to treat syphilis, dysentery, diarrhea and inflamed eyes (Watt and Breyer-Brandwijl, 1962). *C. mopane* has unique habitat in the dry low-lying areas with extreme climatic conditions, where it is exposed to shallow, poorly drained, often alkaline soils, thus increasing the chances of finding original metabolites that are indispensable for drug development (Venter and Venter, 2002).

The phytochemistry of *C. mopane* has been poorly studied, and a more detailed survey of its constituents is thus of high interest. Previous investigations revealed the presence of phenolic compounds in the heartwood (Ferreira et al., 2003), and a few diterpenoids in the bark, seeds, husks and leaves (Englund et al., 2009; Mebe, 2001; Reiter et al., 2003). As part of our ongoing search for novel bioactive compounds from medicinal plants in Southern Africa (Du et al., 2014; Hata et al., 2014; Hata et al., 2013), we focused on *C. mopane*, one of the most easily recognized trees because of its distinctive bifoliolate leaves and widespread distribution.

Fractionation of the DCM extracts of seeds, husks and leaves, respectively, afforded three new (**1**-**3**) and two known (**4**-**5**) labdane diterpenoids, one new isolabdane **6**, three new (**7**-**9**) and two known (**10**-**11**) clerodane diterpenoids in total (Fig.1). Herein, we report on the isolation and structure elucidation of these diterpenoids, and on the testing of these compounds for antibacterial activity.

2. Results and discussion

The metabolites reported here were isolated from seeds, leaves and husks of *Colophospermum mopane* by using similar isolation methods. The three dichlomethane extracts were submitted to a preliminary fractionation by open column chromatography on silica gel. Fractions were combined on the basis of their TLC patterns, and were further purified by semipreparative HSCCC, semipreparative HPLC, and chromatography on ODS and Sephadex LH-20 columns. Seeds afforded compounds **1**-**3**, **5**, **7**, **10** and **11** (Fig.1). Compounds **4**, **6** and **9** were isolated from leaves, while husks yielded compound **8** (Fig.1). The structures of known compounds were determined by comparing their spectroscopic data with literature values. They were identified as mopaneol A (**4**)

(Reiter et al., 2003) and *rel*-8(S),13(*R*)-dihydrogrindelic acid[1] (**5**) (Englund et al., 2009). Compounds **10** and **11** were identified as *cis*-clerodane diterpenoids previously reported from aerial parts of *Haploppapus paucidentatu,* (Borquez et al., 1995; Jakupovic et al., 1986) and stems of *Aristolochia brasiliensis* (Lopes et al., 1987), respectively. Both compounds were previously reported with no absolute configuration assignment and no optical rotation. The absolute configuration of **10** was assigned by X-ray as 5*R*,8*S*,9*R*,10*S* (Fig. 2). Compound **11** had the same relative configuration and similar optical rotation ($[\alpha]^{25}_{D}$ -19.1, *c* 0.41, MeOH) as **10** ($[\alpha]^{25}_{D}$ -29.7, *c* 0.18, MeOH). Thus, we propose the absolute configuration of **11** as 5*R*,8*S*,9*R*,10*S*. Structure elucidation of the new compounds is discussed in the following paragraphs.

Compound **1**, obtained as colorless crystals, showed a *quasi*-molecular-ion peak $[M+Na]^+$ at *m/z* 343.2257 in its HRESIMS spectrum. Together with the ^{13}C-NMR data this indicated a molecular formula of $C_{20}H_{32}O_3$ (calcd for $C_{20}H_{32}NaO_3$, 343.2244) which was consistent with five indices of hydrogen deficiency. Assignments of the ^{1}H and ^{13}C NMR spectra of **1** (Table 1) were supported by 2D-NMR (^{1}H-^{1}H COSY, HSQC and HMBC) experiments. In the ^{13}C NMR spectrum (Table 1), 20 carbon signals were observed, which were assigned to four methyls, eight methylenes (including one oxygenated, δ_C 73.2), three methines (including one olefinic δ_C 115.0), and five quaternary carbons (including one carbonyl, δ_C 174.2, one olefinic, δ_C 171.6 and one oxygenated, δ_C 78.4). The HMBC correlations of H_2-16 (δ_H 4.77) to C-13 (δ_C 171.6), C-14 (δ_C 115.0), C-15 (δ_C 174.2), and of H-14 (δ_H 5.84) to C-13 (δ_C 171.6), C-15 (δ_C 174.2), and C-16 (δ_C 73.2) suggested the presence of an *α,β*-unsaturated *γ*-lactone moiety. Hence, three of the indices of hydrogen deficiency were accounted for. The two remaining indices were attributed to two ring systems. The ^{1}H NMR spectrum (Table 1) displayed singlets for two geminal methyl groups at δ_H 0.86 and 0.91, one tertiary (δ_H 1.03) and one secondary methyl group at δ_H 1.06 (d, J = 7.7 Hz), and were diagnostic of a labdane-type diterpenoid. The HMBC correlations from H-8 (δ_H 1.87), H-11b (δ_H 1.70), H_3-17 (δ_H 1.06) and H_3-20 (δ_H 1.04) to an oxygenated quaternary carbon (δ_C 78.4) established the location of an OH group at C-9. Thus, the gross structure of **1** was established (Fig. 1). The absolute configuration was assigned as 5*S*,8*S*,9*R*,10*S* on the basis of low-temperature (100K) Cu K*α*

[1] ^{1}H and ^{13}C shifts of **5** were slightly different to reported values. The relative strereochemistry of **5** was assigned as 8(*S*),13(*R*)-dihydrogrindelic acid by 1D and 2D NOESY (Supporting information, Figures S23 and S24). The same *rel*-stereoisomer as **5** has been erroneously denominated as 8(*S*),13(*S*)-dihydrogrindelic acid in the previous report (Englund, 2009).

radiation X-ray diffraction data (Fig. 3). Compound **1** is an isomer of viterulin which has been previously reported from *Vitex rotundifolia* (Lee et al., 2013).

Compound **2**, obtained as a white powder, had a molecular formula of $C_{20}H_{34}O_4$ according to an $[M+Na]^+$ ion at *m/z* 361.2359 (calcd for $C_{20}H_{34}NaO_4$, 361.2359) in its HRESIMS spectrum. The ^1H and ^{13}C NMR data of **2** (Table 1) were similar to those of dihydrogrindelic acid **5**. The only remarkable difference was the presence of an oxygenated methine (δ_H 3.43, dd, J = 2.5 and 1.0 Hz, δ_C 76.4). HMBC correlations from the *gem*-dimethyl group (δ_H 0.83 and 0.96; H_3-19 and H_3-18, respectively) to the latter oxygenated carbon (δ_C 76.4) established the planar structure of **2**. A severe overlapping of critical resonances in the ^1H spectrum of **2** precluded the relative configuration to be assigned by NOESY. The presence of the stereogenic alcohol at C-3 prompted us to prepare the 3-*p*-bromobenzoyl-15-methylester **2a**. Its NOESY spectrum provided a better signal dispersion that allowed assignment of the relative configuration (Fig. 4). Selective irradiation of H_3-20 enhanced H_3-17, H_3-19 and H_2-11, thus establishing their *syn*-orientation, arbitrarily assigned as β (Fig. S14). On the other hand, the β-equatorial orientation of H-3 (δ_H 4.78) was inferred by its J coupling constant (dd, $J_{H3\text{-}H2equatorial}$ = 3.4 and $J_{H3\text{-}H2axial}$ = 3.0 Hz), and corroborated by dipolar coupling with both H_3-18 and H_3-19. NOESY contacts between H-5 and H_3-19 confirmed the *trans*-junction of the decaline ring. Finally, the 13-*rel*-(*R*)-stereochemistry of **2** was confirmed by NOESY cross peaks between H_2-14 and the *ortho*-aromatic protons of the benzoyl ring (Fig. 4). The absolute stereochemistry of **2** was established by the modified Mosher's method (Hoye et al., 2007). Esterification of the 15-methyl ester of **2** with (*S*)-and (*R*)-MTPA-Cl afforded 3-O-(*R*)-MTPA and 3-O-(*S*)-MTPA esters, respectively. Compared to parent compound **2**, the resonances of protons at positions 2, 1 and 14 were shifted upfield in the (*R*)-MTPA derivative, while resonances belonging to H_3-18, H-5 and H_2-6 moved downfield. The reverse was observed for the (*S*)-MTPA ester, suggesting the *R* configuration at C-3 (Fig. 5). The absolute stereochemistry assigned by the modified Mosher's method was further corroborated by electronic circular dichroism (ECD). The ECD spectrum of **2a** showed a positive Cotton effect at 245 nm owing to the $\pi \rightarrow \pi^*$ transition of the *p*-bromobenzoate, and perfectly matched with the ECD curve calculated for the 3*R*,5*S*,7*R*,8*S*,9*R*,10*S* stereoisomer (Fig. 6).

Compound **3**, obtained as colorless crystals, showed a molecular formula of $C_{22}H_{36}O_5$ according to

an $[M+Na]^+$ ion at *m/z* 403.2473 (calcd for $C_{22}H_{36}NaO_5$, 403.2455) in its HRESIMS spectrum. The ^1H and ^{13}C data of NMR data of **3** were similar to those of **2** (Table 1). The only difference was the hydroxyl group at C-3 in **2** that was replaced by an acetoxy group in **3**, as deduced from the HMBC correlation of H-3 (δ_H 4.62 t, J = 2.6 Hz) with an ester carbonyl (δ_C 171.2). According to the observed NOESY correlation the relative configuration of **3** was identical with that of **2** (Fig. 4). On the basis of a levorotatory optical rotation ($[\alpha]^{25}_D$ -50.0, *c* 0.10, MeOH) as for **2** ($[\alpha]^{25}_D$ -21.1, *c* 0.11, MeOH) we propose the absolute configuration of **3** as 3*R*,5*S*,7*R*,8*S*,9*R*,10*S*.

The molecular formula of compound **6** was determined as $C_{20}H_{30}O_3$, based on a pseudomolecular ion in the HRESIMS at *m/z* 341.2102 $[M+Na]^+$ (calcd for $C_{20}H_{30}NaO_3$, 341.2087). This implied six indices of hydrogen deficiency. In analogy with **1**, inspection of the NMR spectra of **6** (Table 1) showed the presence of a 3-ethyl-α,β-butenolide moiety. The remaining resonances were i) three tertiary methyl groups at δ_H 0.64 (s, H_3-20), 0.91 (s, H_3-19), and 1.10 (s, H_3-18); ii) a six-proton spin system composed of two vicinal diastereotopic methylene groups (δ_H 1.14/1.65, H_2-1and δ_H 1.78/1.49, H_2-2) that were linear coupled to an angular methine (δ_H 2.05, brd, J = 13.3, H-10) and an oxygenated methine (δ_H 3.19, dd, J = 11.5, 4.2 Hz, H-3); iii) a four proton spin-system composed of a methylene group (δ_H 1.77/1.88, H_2-7) scalar coupled to a tertiary methine (δ_H 1.49, m, H-8), and an olefinic methine at δ_H 5.52 (d, J = 4.0 Hz, H-6). These spectral features, along with the remaining three degree of unsaturation needed for the molecular formula, suggested an isolabdane-type structure. ^1H-^{13}C HMBC correlations of the geminal dimethyl group H_3-18 and H_3-19 to the oxygenated methine (δ_C 76.6, C-3) and to a sp^2 quaternary carbon at δ_C 144.7 confirmed the C-3 to C-6 connectivity. The relative configuration of the four stereocenters of **6** was deduced from NOESY correlations (Fig. 7) and J coupling analysis. The J couplings of H-3 (δ_H 3.19, dd, J = 11.5, 4.2 Hz) and H-10 (δ_H 2.05, br d, J = 13.3 Hz) together with their NOESY correlations (H-3/H-2eq, H-3/H-1axial, H-3/H_3-19; H-10/H-1equatorial, H-10/H-2axial, H-10/ H_3-18) clearly indicated their axial antifacial orientation, and a chair-like conformation for ring A. The NOESY contacts of H-10/H_2-12 and H_3-17/H_3-20 supported the α-orientation of the side chain at C-9, and a β-cis orientation of the vicinal methyls H_3-17/H_3-20. Stereoisomers of **6** have been previously synthesized from labdane diterpenes isolated from *Solidago* species (McCrindle and Nakamura, 1974; McCrindle et al., 1976). The absolute stereochemistry of compound **6** was inferred by the modified Mosher's method. Similar to **2**, the protons in **6** for positions 2, 1, 10 and

12 were shielded in the (*R*)-MTPA, while resonances belonging to H_3-19 and H_2-6 were shifted downfield. The reverse was observed for the (*S*)-MTPA-ester, suggesting *R* configuration at C-3. This stereochemical assignment was further corroborated by the good match of the ECD specta of 3-*p*-bromobenzoate derivatives **2a** and **6a** (Fig. 6). Thus, the absolute configuration of **6** was assigned as 3*R*,8*S*,9*R*,10*S*.

Compound **7** was obtained as colorless crystals. The HRESIMS exhibited a $[M+Na]^+$ ion at *m/z* 343.2260 (calcd for $C_{20}H_{32}NaO_3$, 343.2244), suggesting a molecular formula of $C_{20}H_{32}O_3$ and five indices of hydrogen deficiency. The ^1H and ^{13}C NMR spectra of **7**, in addition to resonances characteristic for a clerodane diterpene, revealed the presence of a trisubstituted double bond (δ_H 5.65, br s, δ_C 115.4 C-14; δ_C 160.9 C-13) conjugated with a carboxyl group (δ_C 168.9). These spectroscopic data showed close similarities to those of 5α,8α-2-oxokolavenic acid, a 3,4-epoxyclerodan-13*E*-en-15-oic acid reported from *D. microcarpum* fruits (Cavin et al., 2006). However, slight differences in chemical shifts of the resonances belonging to the decaline system suggested that **6** was a diastereoisomer of the latter. Crystals suitable for X-ray diffraction analysis of **6** were obtained by crystallization from methanol-d_4 (Fig. 8). Hence, the absolute configuration of **7** was assigned as 3*R*,4*S*,5*R*,8*S*,9*R*,10*S*. The crystal structure of **7** showed that 2 molecules of **7** are linked via a hydrogen bond involving the acidic proton of the carboxylic acid and the carbonyl oxygen.

Compound **8** was obtained as a colorless oil. The HRESIMS exhibited a $[M + Na]^+$ peak at *m/z* 341.2101 (calcd for $C_{20}H_{30}NaO_3$, 341.2087) that differed from that of **7** by 2 mass units. ^1H and ^{13}C NMR resonances of **8** closely resembled those of **7** (Table 2). The only remarkable difference was the absence of the resonance of H_3-16 [δ_H 2.14 (d, J = 1.1 Hz), δ_C 17.8 in **7**] that was replaced by an hydroxymethylene group [δ_H 4.75 (d, J = 1.6 Hz), δ_C = 73.1 in **8**]. Long range HMBC correlations from the latter to δ_C 115.1 (H-14), 171.1 (C-13), 174.1 (C-15) and 22.3 (H_2-12) indicated the presence of an *α,β*-unsaturated *γ*-lactone moiety. Thus, the planar structure of **8** was assigned as depicted in Fig.1. The *cis*-stereochemistry of the decaline ring was inferred by the *J* coupling value of H-10 (δ_H 1.08, t, J = 4.5 Hz), indicative of dihedral angles of approx 60 ° with H-1_{axial} and H-$1_{equatorial}$. NOESY correlations of H-10 and H-8 with H_2-12 indicated their cofacial β-orientation (Fig. 9) and established the stereochemistry at C-8 and C-9. On the other hand, NOESY contacts

H-3/H_3-18, H-3/H_3-20, H_3-18/H_3-20, and the *J* value (d, 3.5 Hz) of H-3 indicated an α-equatorial orientation of H-3 and the β-epoxide (Fig. 9). A natural clerodane with the same constitution and relative stereochemistry as **8** had been previously reported from *Ageratina saltillensis* (Fang et al., 1988). However, our NMR data of **8** did not match with those reported previously. A similar discrepancy was found by Piers *et al* (Piers et al., 1995) who synthesized the (+)-enantiomer of **8** ($[\alpha]^{25}_D$ +11, MeOH). Hence, on the basis of the levorotatory optical rotation of **8** ($[\alpha]^{25}_D$ -5, MeOH), we assume the stereostructure of **8** to be new, and we assign its absolute configuration as 3*S*,4*R*,5*S*,8*R*,9*S*,10*R*. It is worthy of note that **7** and **8**, isolated from seeds and leaves, respectively, have mirror-image stereochemistry.

Compound **9** showed the same mass and the same planar structure as compound **10** and was a diastereoisomer of the latter [HRESIMS *m/z* 343.2258 (calcd for $C_{20}H_{32}NaO_3$, 343.2244)]. Diagnostic NOEs allowed us to identify the cofacial orientation of the three methyl groups H_3-17 (δ_H 0.81), H_3-19 (δ_H 1.02) and H_3-20 (δ_H 0.74), as well as the antifacial orientation of H-10 (δ_H 1.37), arbitrarily assigned as β (Fig. 10). The *trans* junction of the decaline system arising from these assignments was further supported by the ^{13}C shift of H_3-19 (δ_C 21.3) that appeared upfield as compared to the shift of a *cis*-clerodane (H_3-19 of **8** δ_C 35.9) (Manabe and Nishino, 1986; Pacheco et al., 2009). Compound **9** showed the same relative stereochemistry assigned to 16,18-dihydroxykolavenic acid lactone, as confirmed by the excellent agreement of their NMR data (Cao et al., 2011).

Diterpenes of different skeletal types have shown promising antimicrobial activities (Bisio et al., 2015; Garcá-Sánchez et al., 2014). Compound **11** showed good activity against *Escherichia coli* ATCC 8739 (MIC 15.6 µg/ml), *Staphylococcus aureus* ATCC 25923 (MIC 15.6 µg/ml) and *Enterococcus faecalis* ATCC 29212 (MIC 31.3 µg/ml) while the other diterpenoids showed MIC values mostly ≥62.5 µg/ml. Isolated compounds with antimicrobial activities of 64–100 µg/ml are considered as having some clinical relevance (Gibbons, 2004). Hence the good activity found for compound **11** shows some promise. The crude leaf extract was also found to be the most active against *Staphylococcus aureus* (125 µg/ml).

Given that structurally related diterpenes had shown positive $GABA_A$ receptor modulatory

properties (Schramm et al., 2013), compounds **1-11** were tested for enhancement of GABA-induced chloride currents in a *Xenopus* oocytes model, but were found to possess only negligible activity.

3. Conclusions

Labdane and clerodane diterpenoids represent a large group of secondary metabolites that have shown interesting biological activities. Structurally, they have four or five contiguous stereocenters on a decaline system. According to biosynthetic arguments (Peters, 2010), natural labdane diterpenes only bear *trans* stereochemistry at the bridging carbons of the decaline moiety although both *syn*- and *ent*-enantiomers have been reported. On the other hand, clerodane-type diterpenes can exhibit *trans* and *cis* ring fusion (Tokoroyama, 2000). For both compound classes, the stereochemistry at C-8 and C-9 can be either *cis* or *trans*, thereby allowing many diasteroisomeric combinations. Severely overlapping NMR signals, and the lack of strong chromophores render the stereochemical assignment of these compounds a challenging task, as documented by numerous discrepancies reported in the literature. Within this work, we have employed different approaches to assign relative and/or absolute configuration to a small series of diterpenes that may be helpful for future unambiguous identification of structurally related compounds.

Microscale derivatization along with selective 1D experiments have been employed to overcome the problem of severe overlapping of NMR signals that is characteristic for these molecules. The matching of spectroscopic data with energy-minimized structures confirmed the reliability of assignments of the relative configurations. For eight out of eleven compounds their absolute configuration could be assigned by X-ray crystallography, Mosher's method, and chemical correlations. Finally, we showed that introduction of a strong chromophore like the *p*-bromobenzoyl group may facilitate the assignment of the absolute configuration by ECD for compounds lacking suitable chromophores.

4. Experimetal

4.1 General Experimental Procedures

Solvents used for extraction and preparative separation were obtained from Merck Chemical Co., (South Africa) and were analytical reagent (AR) grade. HPLC-grade methanol (MeOH), acetonitrile (MeCN) (Scharlau Chemie S.A.), and water (obtained by an EASY-pure II from Barnstead water

purification system, Dubuque) were used for HPLC separations. Dimethylsulfoxide (DMSO) (Scharlau) was used for dissolving the samples. Chloroform-*d* (100 atom% D) (Armar Chemicals), chloroform-*d* (99.8 atom% D) (Sigma-Aldrich) and methanol-d_4 (99.8 atom% D) (Sigma-Aldrich) were used for NMR. Optical rotations were measured with a Perkin Elmer polarimeter (model 341) equipped with a sodium lamp (589 nm) and a 10 cm microcell. UV spectra were recorded in *n*-hexane on a Hewlett Packard 8453 Photometer (UV). CD spectra were measured in MeOH on a Chirascan CD spectrometer and were analyzed with Pro-Data V2.4 software.

HPLC-PDA-MS analyses were performed with an Agilent 1100 system consisting of a degasser, quaternary pump, column oven, a PDA detector connected to a Gilson 215 injector, and to an Esquire 3000 plus ion trap mass spectrometer (Bruker Daltonics). Data acquisition and processing were performed using HyStar 3.0 software (Bruker Daltonics). Materials for column chromatography were silica (200-300 mesh, Merck), Sephadex LH-20 (40-70 μm; Amersham Pharmacia Biotech AB, Uppsala, Sweden), and YMC-Gel ODS-A (50 μm; YMC, Milford, MA, USA). HSGF254 silica gel TLC plates (Merck) were used for analytical TLC. A Spectrum model (Dynamic Extractions, Slough, UK) multilayer coil-planet J-type centrifuge was used for hydrodynamic high-speed countercurrent chromatography (HSCCC) according to the instrumental setup described in a previous report (Shikanga et al., 2011). The operaion conditions of HSCCC were the same as a previous report (Shikanga et al., 2011). Semi-preparative HPLC was performed with an Agilent 1100 series instrument equipped with a PDA detector. Data acquisition and processing were performed using HyStar 3.2 software (Bruker Daltonics). For HR-ESIMS a micrOTOF ESI-MS system (Bruker Daltonics) was used. Mass calibration was performed with a solution of formic acid 0.1% in 2-propanol-water (1:1) containing 5 mM NaOH. Mass spectra were recorded in the range of *m/z* 150 - 1500 in positive ion mode with the aid of micrOTOF control software 1.1 (Bruker Daltonics). NMR spectra were recorded on a Bruker 600 AVANCE II^{TM} operating at 600 (^{1}H) and 150 MHz (^{13}C), or on a Bruker AVANCE III^{TM} 500 MHz spectrometer equipped with a 1 mm TXI microprobe (^{1}H and 2D NMR) or a 5 mm BBO probe (^{13}C NMR) (Bruker BioSpin) operating at 500 (^{1}H) and 125 MHz (^{13}C). 2D NMR experiments were performed using standard Bruker programs. All measurements were carried out at 291.15 K. Chemical shifts are reported as δ values (ppm) with the residual solvent signal (for 500 MHz NMR with microprobe) or TMS (for 600 MHz NMR) as internal reference, *J* in Hz. Standard pulse sequences from Topspin

2.1 software package were used.

4.2 Plant Material

The seeds, husks and leaves of *C. mopane* were collected in the Messina Magisterial District (Limpopo Province), South Africa, in March 2012 (PC & L Zietsman 5241). A voucher specimen (NMB 26692) was deposited in the herbarium of the National Museum, Bloemfontein, South Africa (NMB).

4.3 Extraction

The air-dried seeds (277 g), husks (369 g) and leaves (709 g) of *C. mopane* were separately powdered and extracted with DCM (3 x 1.5 l, 3 x 3.0 l and 3 x 3.0 l, respectively; each 24 h) at room temperature. The solvents were evaporated under vacuum at 40 ℃ to yield 76.0 g of the seeds extract, 15.4 g of the husks extract and 37.1 g of the leaves extract.

4.4 Isolation of compounds 1-3, 5, 7, 10 and 11.

The DCM extract of the seeds (63 g) was separated by open column chromatography (85 × 5 cm) on silica gel (230-400 mesh) with a step-gradient [DCM-MeOH: 40-1 (4.1 l), 20-1 (0.84 l), 10-1 (0.88 l), 5-1 (0.6 l), 2.5-1 (0.7 l), 1-1 (0.4 l) and 0-1 (1 l)] at a flow rate of 10 ml/min. Fractions were combined based on TLC analysis [Fr. A (14.3 g), Fr. B (17.0 g), Fr. C (5.2 g), Fr. D (0.9 g), Fr. E (1.4 g), Fr. F (1.0 g), Fr. G (0.6 g)].

A portion of fraction B (500 mg) was purified by HSCCC [*n*-heptane-EtOAc-MeOH-H_2O (19:1:19: 1); lower phase as mobile phase; flow rate: 3 ml/min. The sample was dissolved in a mixture of the upper (2.0 ml) and the lower phases (2.0 ml) for injection] to give **5** (160 mg).

Fraction C (5.2 g) was separated by open column chromatography (33 x 2.3 cm) on silica gel (230-400 mesh) with an isocratic solvent system [*n*-hexane-EtOAc 3-7 (1 l), and washed with EtOAc-MeOH 1-1 (2 l)] . A flow rate of 5 ml/min was used, and subfractions C_1-C_3 were obtained.

Subfraction C_2 (3.0 g) was separated by HSCCC [*n*-heptane-EtOAc-MeOH-H_2O (3:1:3:1); lower phase as mobile phase; flow rate: 3 ml/min. The sample was dissolved in a mixture of the upper (5.0

ml) and the lower phases (5.0 ml) for injection] to give $C_{2.1}$-$C_{2.9}$. Purification of **11** (6.0 mg, t_R 22.0 min) from subfraction $C_{2.7}$ (24 mg) was by semiprep HPLC [SunFire™ C18 column (5 μm, 10 × 150 mm, Waters)] using a gradient [H_2O (A), MeCN (B); 55% → 68% B (0-5 min), 68% B (5-10 min), 68% → 87% B (10-15 min), 87% B (15-20 min), 87% → 91% B (20-21 min), 91% B (21-23 min), 91% → 100% B (23-24 min), 100% B (24-26 min); flow rate 4 ml/min]. Sample conc. was 80 mg/ml in DMSO, and injection volume was 50 μl.

Subfraction C_3 (904 mg) was separated by HSCCC [*n*-heptane-EtOAc-MeOH-H_2O (2:1:2:1); upper phase as mobile phase; flow rate: 3 ml/min. The sample was dissolved in a mixture of the upper (2.0 ml) and the lower phases (2.0 ml) for injection] to give $C_{3.1}$-$C_{3.10}$. Compound **1** (5.0 mg) was crystallized from an EtOAc solution of $C_{3.5}$ (24.7 mg). Subfraction $C_{3.2}$ (153 mg) was separated by HSCCC [*n*-heptane-EtOAc-MeOH-H_2O (3:1:3:1); lower phase as mobile phase; flow rate: 3 ml/min; sample was dissolved in a mixture of the upper (2.0 ml) and the lower phases (2.0 ml) for injection] to give $C_{3.2.1}$-$C_{3.2.3}$. Compound **3** (15.0 mg) was precipitated from a solution of $C_{3.2.2}$ (20.0 mg) in the upper phase of *n*-heptane-EtOAc-MeOH-H_2O (3:1: 3:1).

Fraction D (820 mg) was separated by HSCCC [*n*-heptane-EtOAc-MeOH-H_2O (5:2:5:2); lower phase as mobile phase; flow rate: 3 ml/min; sample was dissolved in a mixture of the upper (5.0 ml) and the lower phases (5.0 ml) for injection] to give D_1-D_9. Compound **7** (150 mg) was crystallized out of a MeOH solution of D_6 (155 mg). Compound **7** (150 mg) was obtained by precipitation in a MeOH solution of D_6 (155 mg). Recrystallization from methanol-d_4 afforded white crystals suitable for X-ray analysis.

Fraction E (1.3 g) was separated by HSCCC [*n*-heptane-EtOAc-MeOH-H_2O (5:2:5:2); upper phase as mobile phase; flow rate: 3 ml/min; sample was dissolved in a mixture of the upper (5.0 ml) and the lower phases (5.0 ml) for injection] to give E_1-E_8. Subfraction E_4 (831 mg) was separated by HSCCC [*n*-heptane-EtOAc-MeOH-H_2O (6:5:6:5); lower phase as mobile phase; flow rate: 3 ml/min; sample was dissolved in a mixture of the upper (2.0 ml) and the lower phases (2.0 ml) for injection] to give $E_{4.1}$-$E_{4.6}$. Compound **10** (172 mg) was crystallized from a MeOH solution of $E_{4.3}$ (180 mg).

Fraction G (588 mg) was separated by HSCCC [*n*-heptane-EtOAc-MeOH-H_2O (6:5:6:5); lower

phase as mobile phase; flow rate: 3 ml/min; sample was dissolved in a mixture of the upper (2.0 ml) and the lower phases (2.0 ml) for injection] to give G_1-G_8. The subfraction G_7 (200 mg) was separated by HSCCC [*n*-heptane-EtOAc-MeOH-H_2O (2:1:2:1); lower phase as mobile phase; flow rate: 3 ml/min; sample was dissolved in a mixture of the upper (2.0 ml) and the lower phases (2.0 ml) for injection] to give $G_{7.1}$-$E_{7.10}$. Compound **2** (51.0 mg) was precipitated from a MeOH solution of $G_{7.8}$ (55 mg).

4.5 Isolation of compounds 4, 6 and 9

The DCM extract of leaves (36.0 g) was separated by open column chromatography (51 × 4 cm) on silica gel (230-400 mesh) with an isocratic solvent system [DCM-MeOH 40-1 (4.8 l), and washed with EtOAc (2 l)] at a flow rate of 10 ml/min. Fractions were combined based on TLC analysis [Fr. A (5.8 g), Fr. B (8.3 g), Fr. C (5.3 g), Fr. D (2.2 g), Fr. E (1.8 g), Fr. F (3.3 g), Fr. G (2.8 g), Fr. H (0.4 g) and Fr. I (3.1 g)].

Fraction E (1.8 g) was separated by open column chromatography (15 × 2.5 cm) on silica gel (230-400 mesh) with an isocratic solvent system [*n*-hexane-EtOAc 7-3 (3 l), and washed with EtOAc (1 l)] at a flow rate of 5 ml/min to give E_1-E_5. The E_4 (220 mg) was further cleaned on Sephadex LH-20 (column i.d. 36 x 3 cm, MeOH-$CHCl_3$ 1:1) and silica gel (230-400 mesh, column i.d. 15 x 2.5 cm, *n*-hexane-EtOAc 6-4) to give **6** (100 mg).

Fraction G (2.8 g) was separated on a Sephadex LH-20 column (36 x 3 cm) with MeOH at a flow rate of 3 ml/min to give G_1-G_3. Subfraction G_2 (1.9 g) was separated on a Sephadex LH-20 column (36 x 3 cm) with MeOH-$CHCl_3$ 1-1 at a flow rate of 3 ml/min to give $G_{2.1}$-$G_{2.2}$. The $G_{2.2}$ (1.75 g) was separated by open column chromatography (71 x 2.3 cm) on silica gel (230-400 mesh) with an isocratic solvent system [$CHCl_3$-EtOAc-AcOH 9-1-0.1] at a flow rate of 3 ml/min to give $G_{2.2.1}$-$G_{2.2.12}$. Purification of the $G_{2.2.11}$ (1.75 g) by a Sephadex LH-20 column (20 x 2.5 cm) with EtOAc at a flow rate of 3 ml/min gave **4** (65 mg).

Subfraction $G_{2.2.5}$ (70 mg) was separated by open column chromatography (8 x 2.5 cm) on ODS with a step-gradient [H_2O-MeOH: 6-4 (0.1 l), 1-1 (0.6 l), 4-6 (0.8 l), 3-7 (1.1 l)] at a flow rate of 3 ml/min to give $G_{2.2.5.1}$-$G_{2.2.5.7}$. Purification of the $G_{2.2.5.6}$ (20 mg) by semiprep HPLC [SunFire™

C18 column (5 μm, 10 × 150 mm, Waters)] with a gradient [H_2O (A), MeOH (B); 5% → 70% B (0-18 min), 70% B (18-20 min), 70% → 100% B (20-23 min) and 100% B (23-25 min); flow rate 4 ml/min; sample conc. 66 mg/ml in DMSO; injection volume 50-100 μl] gave **9** (8.0 mg, t_R 20.5 min).

4.6 Isolation of compound 8

The DCM extract of hulls (15.0 g) was separated by open column chromatography (55 × 3.5 cm) on silica gel (230-400 mesh) with an isocratic solvent system [DCM-MeOH 40-1 (4.5 l), and washed with EtOAc (2 l)] at a flow rate of 10 ml/min. Fractions were combined based on TLC analysis [Fr. A (1.9 g), Fr. B (4.3 g), Fr. C (2.0 g), Fr. D (2.5 g), Fr. E (0.5 g), Fr. F (0.9 g), Fr. G (0.9 g), Fr. H (0.5 g) and Fr. I (0.7 g)]. Fraction B (4.3 g) was separated by open column chromatography (57.5 × 3.5 cm) on silica gel (230-400 mesh) with an isocratic solvent system [*n*-hexane-EtOAc 8:2 (7.7 l)] at a flow rate of 3 ml/min to give B_1-B_{14}. The B_{12} (680 mg) was further cleaned on Sephadex LH-20 (EtOAc) and then silica gel (230-400 mesh, column i.d. 15 x 2.5 cm, *n*-hexane-EtOAc 6-4) to give **8** (160 mg).

*Compound **1***: colorless, fine crystal; $[\alpha]^{25}_D$ +21.5 (*c* 0. 12, MeOH); UV λ_{max} (*n*-hexane) nm (log ε): 203 (2.65), 222 (*sh*); (2.1HRESIMS m/z 343.2257 $[M + Na]^+$ (calcd for $C_{20}H_{32}NaO_3$, 343.2244); for ^1H and ^{13}C NMR data, see Table 1;

*Compound **2***: white powder; $[\alpha]^{25}_D$ -21.1 (*c* 0. 11, MeOH); UV λ_{max} (*n*-hexane) nm (log ε): 206 (2.88); HRESIMS m/z 361.2359 $[M + Na]^+$ (calcd for $C_{20}H_{34}NaO_4$, 361.2349); for ^1H and ^{13}C NMR data, see Table 1;

*Compound **3***: white crystals; $[\alpha]^{25}_D$ - 50.0 (*c* 0. 10, MeOH); UV λ_{max} (*n*-hexane) nm (log ε): 203 (2.85), 222 (*sh*); HRESIMS m/z 403.2473 $[M + Na]^+$ (calcd for $C_{22}H_{36}NaO_5$, 403.2455); for ^1H and ^{13}C NMR data, see Table 1;

*Compound **6***: colorless gum; $[\alpha]^{25}_D$+ 38.2 (c 0.6, MeOH); UV λ_{max} (*n*-hexane) nm (log ε): 213 (2.95); HRESIMS m/z 341.2102 $[M + Na]^+$ (calcd for $C_{20}H_{30}NaO_3$, 341.2087); for ^1H and ^{13}C NMR data, see Table 1;

*Compound **7***: white crystals; $[\alpha]^{25}_D$ +56.5 (*c* 0.15, MeOH); UV λ_{max} (*n*-hexane) nm (log ε): 221 (3.12); HRESIMS m/z 343.2260 $[M + Na]^+$ (calcd for $C_{20}H_{32}NaO_3$, 343.2244); for ^1H and ^{13}C NMR data, see Tables 1 and 2.

*Compound **8***: colorless gum; $[\alpha]^{25}_{D}$ -5.0 (*c* 0. 26, MeOH); UV λ_{max} (*n*-hexane) nm (log ε): 206 (3.25); HRESIMS m/z 341.2101[M + Na]$^+$ (calcd for $C_{20}H_{30}NaO_3$, 341.2087); for ^{1}H and ^{13}C NMR data, see Table 2.

*Compound **9***: colorless gum; $[\alpha]^{25}_{D}$ +45.4 (*c* 0.61, MeOH); UV λ_{max} (*n*-hexane) nm (log ε): 206 (2.38); HRESIMS m/z 343.2258 [M + Na]$^+$ (calcd for $C_{20}H_{32}NaO_3$, 343.2244); for ^{1}H and ^{13}C NMR data, see Tables 1 and 2;

4.7 Computational methods

Conformational analysis of compounds **2**, **2a**, **6, 6a**, **8** and **9** was performed with Schrödinger MacroModel 9.8 (Schrödinger, LLC, New York) employing the OPLS2005 (optimized potential for liquid simulations) force field in H_2O. Conformers within a 2 Kcal/mol energy window from the global minimum were selected for geometrical optimization and energy calculation applying DFT with the Becke's nonlocal three parameter exchange and correlation functional, and the Lee-Yang-Parr correlation functional level (B3LYP) using the B3LYP/6-31 G** or B3LYP/6-31 G* (for **2a**) basis set in the gas phase with the Gaussian 09 program package (Frisch et al., 2009). Vibrational evaluation was done at the same level to confirm minima. For 3-*p*-bromo-benzoate derivatives **2a** and **6a** the excitation energy (denoted by wavelength in nm), rotator strength dipole velocity (R_{vel}), and dipole length (R_{len}) were calculated in MeOH by TD-DFT/B3LYP/6-31 G**, using the SCRF method, with the CPCM model. ECD curves were obtained on the basis of rotator strengths with a half-band of 0.16 eV and UV shift using SpecDis v1.61 (T. Bruhn, 2014). ECD spectra were calculated from the spectra of individual conformers according to their contribution calculated by Boltzmann-weighting.

4.8 Synthesis of derivatives of 2 and 6

4.8.1 Synthesis of 15-methylester of compound 2

To a solution of **2** (1.3 mg; 3.8 μmol) in *n*-hexane (0.2 ml) and anhydrous MeOH (20 μl) $TMSCHN_2$ (20 μl; 10% in hexane, 0.6 mol/l) was added under argon atmosphere. The pale yellow solution was allowed to stand in a sealed HPLC vial, at room temperature, for 1 hour. Then, the reaction was quenched by adding acetic acid (10 μl) and dried under N_2 flow (99% yield).

4.8.2 General procedure for the synthesis of p-bromobenzoyl derivatives 2a and 6a

To a stirred solution of methyl ester of **2** (1.5 mg; 4.2 μmol) and **6** (1.0 mg; 3.1 μmol) in dichloromethane (0.5 ml), *p*-bromobenzoyl chloride (2.5 eq), Et_3N (2.5 eq) and 4-(dimethylamino)pyridine (0.5 eq) were added. The mixtures were stirred in sealed HPLC vials, at room temperature, for 12 hours. Then, the reactions were quenched by adding HCl 1N (0.5 ml). Next, the organic phases were washed with sodium hydrogen carbonate (0.5 ml) and brine (0.5 ml). After drying over sodium sulfate and filtration, the solvents were removed under N_2. The *p*-bromobenzoyl derivatives **2a** and **6a** were then purified by semipreparative HPLC [H_2O (A), MeOH (B); 20% → 100% B (0-20 min), (20-25 min) and 100% B; flow rate 4 ml/min; detection at 254 nm] (75-80% yield).

4.8.3 General procedure for the synthesis of Mosher esters of 2 and 6

To a solution of the methyl ester of **2** (1.5 mg; 4.2 μmol) and **6** (1.0 mg; 3.1 μmol) in anhydrous dichloromethane (0.2 ml), (*R*)-(-) and (*S*)-(+)-MTPA-chloride (2.0 eq), anhydrous pyridine (10 eq) and 4-(dimethylamino)pyridine (0.5 eq) were added. The mixtures were allowed to stand in a sealed HPLC vials, at room temperature, for 16 hours (or 80 h for compound **2**). The reactions were then quenched by adding HCl 1N (0.5 ml). Next, the organic phases were washed with sodium hydrogen carbonate (0.5 ml) and brine (0.5 ml). After drying over sodium sulfate and filtration, the solvents were removed under N_2. The Mosher esters of **2** and **6** were then purified by semipreparative HPLC [H_2O (A), MeOH (B); 40% → 100% B (0-20 min), (20-25 min) and 100% B; flow rate 4 ml/min; detection at 254 nm] (60-70% yield).

4.8.4 X-ray diffraction analysis

The crystallographic data of **1**, **7** and **10** have been compiled in Table S1. The crystals were measured on a Bruker Kappa Apex2 diffractometer at 123K using graphite-monochromated Cu K_α-radiation with $\lambda = 1.5418$ Å. The Apex2 software (Bruker Analytical X-ray Systems) was used for data collection and integration. The structures were solved by the charge flipping method using the program Superflip (Palatinus and Chapuis, 2007). Least-squares refinement against F was carried out on all non-hydrogen atoms using the program CRYSTALS (Betteridge et al., 2003). Plots were produced using MERCURY (Macrae et al., 2008). Crystallographic data for the structures in this paper have been deposited with the Cambridge Crystallographic Data Center, the deposition numbers are 1049108-1049110. The data can be obtained free of charge at

http://www.ccdc.cam.ac.uk/. The crystal structure of **3** could not be elucidated. Numerous attempts were made to grow crystals and to measure X-ray diffraction data. It is likely that they were badly twinned, but in all cases the attempts to solve the structure were not successful.

4.9 Antimicrobial activity

4.9.1 Micro-organisms

Extracts and compounds were evaluated for their anti-bacterial activity against four reference bacterial pathogens (*Escherichia coli* ATCC 8739, *Klebsiella pneumoniae* ATCC 13883, *Staphylococcus aureus* ATCC 25923 and *Enterococcus faecalis* ATCC 29212) (Table 3).

4.9.2 Antimicrobial activity test

The *Colophospermum mopane* crude extracts (starting concentration of 32 mg/ml) and isolated compounds (starting concentration of 5 mg/ml) were reconstituted in acetone and quantitatively evaluated for antimicrobial activity using the minimum inhibitory concentration (MIC) assay (CLSI, 2012). Briefly, each well of a 96 well micro-titre plate was filled with 100 µl of sterilized distilled water and extracts and compounds (100 µl) introduced into the wells of the first row. Serial doubling dilutions were performed. Cultures were added (100 µl) into all wells yielding an inoculum size of approximately 1×10^6 colony forming units (CFU)/ml. Plates, sealed with a sterile adhesive sealer, were then incubated at 37 °C for 24 h. After incubation, 40 µl of the colour indicator, *p*-iodonitrotetrazolium violet (0.4 mg/ml; Sigma-Aldrich) was added to each well, which turned purple-pink in the presence of microbial growth. The end point MIC value was considered for the lowest concentration demonstrating no bacterial growth. The positive control (to confirm antimicrobial susceptibility) was ciprofloxacin (0.01 mg/ml). A negative control was included containing media and acetone (to determine the effect of solvent on microbial growth). Lastly, a culture control was included to confirm viability of micro-organisms.

Acknowledgments

ECD spectra were measured at the Biophysics Facility, Biozentrum, University of Basel. Kun Du acknowledges the South African National Research Foundation (NRF) for financial support. We are grateful to Prof. Steffen Hering and Dr. Sophia Khom for the $GABA_A$ modulatory test. Thanks are due to Dr Samad Nejad Ebrahimi for helpful discussions.

Appendix A. Supplementary data

^{1}H and ^{13}C shifts of known compounds **4**, **5**, **10** and **11**. 1D and 2D NMR spectra of the new compounds **1-3**, **6-9**. Crystallgraphic informations relative to **1, 7** and **10**.

Table 1. ^{1}H and ^{13}C NMR spectroscopic data for compounds **1**, **2**, **3**, **6** ($CDCl_3$, 600 MHz for ^{1}H, and 150 MHz for ^{13}C NMR, δ in ppm).

	1		2		3		6	
Position	**δ_H (*J* in Hz)**	**δ_C, type**	**δ_H (*J* in Hz)**	**δ_C, type**	**δ_H (*J* in Hz)**	**δ_C, type**	**δ_H (*J* in Hz)**	**δ_C, type**
1	1.41-1.37, m	32.6, CH_2	1.94, m[a]	26.2, CH_2	1.66, m[a]	27.1, CH_2	1.65, m	24.5, CH_2
			1.08, m[a]		1.20, ddd (12.2, 4.0, 2.7)		1.14, td (13.3, 3.6)	
2	1.61, m	18.2, CH_2	1.94m	24.2, CH_2	1.91, tdd (15.2, 4.3, 2.7)	22.2, CH_2	1.78, m[a]	30.3, CH_2
	1.47, m		1.63, m		1.66, m[a]		1.49, m[a]	
3	1.37, m	41.5, CH_2	3.43, dd (2.5, 1.0)	76.4, CH	4.62, t (2.67)	77.6, CH	3.19, dd (11.5, 4.2)	76.6, CH
	1.15, ddd (13.5, 13.5, 4.0)		-	-	-	-	-	
4	-	33.4, C	-	37.6, C	-	36.8, C	-	41.8, C
5	1.45, m	47.5, CH	1.88, m[a]	40.9, CH	1.77, m[a]	43.1, CH	-	144.7, C
6	1.49-1.45, m	17.3, CH_2	1.33 -1.45, m	16.7, CH_2	1.44, m[a]	16.5, CH_2	5.52, br d (5.5)	118.4, CH
7	1.85, m	29.2, CH_2	1.99, m[a]	29.4, CH_2	1.98, m[a]	29.2, CH_2	1.88, br dt (17.6, 5.5)	31.4, CH_2
	1.48, m		1.36, m[a]		1.47, m[a]		1.77, m[a]	
8	1.87, m	35.7, CH	1.88, m[a]	39.3, CH	1.98, m[a]	38.5, CH	1.49, m[a]	33.2, CH
9	-	78.4, C	-	94.0, C	-	96.2, C	-	36.9, C
10		42.6, C	-	41.6, C	-	41.5, C	2.05, br d (13.3)	39.0, C
11	1.97, ddd (13.8, 12.0, 5.0)	29.6, CH_2	1.99, m[a]	28.7, CH_2	2.00, m[a]	28.3, CH_2	1.62, dd (12.4, 5.3)	33.9, CH_2

	1.70, ddd (13.8, 12.7, 4.5)		1.88, m[a]		2.00, m[a]		1.49, m[a]	
12	2.58, dddd (16.5, 12.0, 4.5, 1.5)	22.6, CH_2	1.92, m	38.8, CH_2	2.00, m	38.0, CH_2	2.24-2.36, m	22.3, CH_2
	2.35, dddd (16.5, 12.7, 5.0, 1.5)		1.81, m		1.79, m			
13	-	171.6, C	-	80.7, C	-	80.8, CH	-	171.3, C
14	5.84, quint (1.5)	115.0, CH	2.67, d (13.3)	46.8, CH_2	2.70, d (15.4)	46.6, CH_2	5.81, br m	114.9, CH
	-		2.43, d (13.3)		2.48, d (15.4)		-	-
15	-	174.2, C	-	173.2, C	-	171.6, C	-	174.2, C
16	4.77, d (1.5)	73.2, CH_2	1.39, s	27.8, CH_3	1.41, s	27.5, CH_3	4.73, d (1.3)	73.2, CH_2
17	1.06, d (7.7)	17.9, CH_3	1.03, d (7.8)	18.1, CH_3	1.08, d (7.7)	18.1, CH_3	0.79, d (6.8)	15.0, CH_3
18 (α)	0.91, s	33.8, CH_3	0.96, s	28.4, CH_3	0.87, s	28.0, CH_3	0.91, s	21.3, CH_3
19	0.86, s	21.8, CH_3	0.82, s	21.9, CH_3	0.90, s	21.5, CH_3	1.10, s	24.4, CH_3
20	1.03, s	17.1, CH_3	0.95, s	18.2, CH_3	1.00, s	18.3, CH_3	0.64, s	16.3, CH_3
21	-	-	-	-	-	171.2, C	-	-
22	-	-	-	-	2.10, s	21.2, CH_3	-	-

[a] overlapping signals

Table 2. ^{1}H and ^{13}C NMR spectroscopic data for compounds **7**, **8** and **9** (CD_3OD for **7**, $CDCl_3$ for **8** and **9**; 600 MHz for ^{1}H, and 150 MHz for ^{13}C NMR, δ in ppm).

	7		8		9	
Position	**δ_H (mult, *J* in Hz)**	**δ_C, type**	**δ_H (mult, *J* in Hz)**	**δ_C, type**	**δ_H (mult,*J* in Hz)**	**δ_C, type**
1	1.60, m	16.9, CH_2	1.60, m[a]	17.9, CH_2	1.60, m	18.2, CH_2
			1.43, m		1.51, m[a]	
2	2.10, m	23.1, CH_2	2.00, m	23.7, CH_2	2.21, m	26.6, CH_2
	1.79, ddd		1.83, ddd		2.08, m	
	(15.7, 7.0, 3.3)		(15.7, 7.2, 3.5)			
3	2.95, d (3.3)	62.2, CH	2.94, d (3.5)	61.9, CH	5.60, t (3.6)	122.0, CH
4	-	62.3, C	-	62.1, C	-	147.8, C
5	-	35.0, C	-	35.5, C	-	37.7, C
6	2.06, m[a]	35.4, CH_2	2.00, m[a]	35.0, CH_2	1.75, dt (12.6, 2.6)	36.2, CH_2
	1.37, m[a]		1.32, m[a]		1.33, m	
7	1.46, m[a]	28.3, CH_2	1.49, m	28.3, CH_2	1.42-1.47, m[a]	27.2, CH_2
	1.40, m[a]		1.36, m[a]		1.42-1.47, m[a]	
8	1.49, m[a]	37.3, CH	1.46, m[a]	37.4, CH	1.48, m[a]	36.3, CH
9	-	38.8, C	-	39.0, C	-	38.7, C
10	1.13, t (4.2)	43.8, CH	1.08, t (4.5)	43.8, CH	1.37, m[a]	46.3, CH
11	1.57, m[a]	36.7, CH_2	1.65, dd (10.1, 6.8)	36.2, CH_2	1.55, m	36.3, CH_2
	1.52, m[a]				1.43, m[a]	
12	1.98-2.08, m	33.9, CH_2	2.33-2.22, m	22.3, CH_2	2.02, td (13.0, 4.8)	34.9, CH_2
					1.94, td (13.0, 4.8)	
13	-	160.9, C	-	171.1, C	-	163.9, C
14	5.65, brs	115.3, CH	5.84, quint(1.6)	115.1, CH	5.67, s	114.8, CH
15	-	168.9, C	-	174.1, C	-	171.6, C

16	2.14, d (1.1)	17.7, CH_3	4.75, d (1.6)	73.1, CH_2	2.16, d (1.0)	19.4, CH_3
17	0.87, d (6.7)	14.8, CH_3	0.84, d (6.8)	16.0, CH_3	0.81, d (6.0)	15.9, CH_3
18	1.33, s	19.6, CH_3	1.33, s	20.7, CH_3	4.08, m	62.9, CH_2
19	1.10, s	27.6 CH_3	1.11, s	28.3, CH_3	1.02, s	21.3, CH_3
20	0.90, s	18.7, CH_3	0.91, s	19.8, CH_3	0.74, s	18.2, CH_3

[b]overlapping signals

Table 3. Antibacterial activities of *Colophospermum mopane* crude extract and compounds **1-11**. MIC values are given as µg/ml.

	K. pneumoniae **ATCC 13883**	***E. coli*** **ATCC 8739**	***E. feacalis*** **ATCC 29212**	***S. aureus*** **ATCC 25923**
1	62.5	250	125	125
2	62.5	125	62.5	125
3	62.5	125	62.5	125
4	62.5	125	125	93.7
5	46.9	125	125	62.5
6	62.5	125	62.5	93.7
7	62.5	>250	62.5	62.5
8	62.5	125	62.5	62.5
9	93.8	125	125	62.5
10	625	125	62.5	62.5
11	93.8	15.6	31.3	15.6
Seeds DCM extract.	2600	2000	4000	1000
Leaves DCM extract	3000	1500	2000	125
Husks DCM extract.	2000	2000	2000	500
Ciprofloxacin	0.078	0.156	0.156	0.156
Negative control	>8	>8	>8	8
Culture control	>8	>8	>8	>8

References

Betteridge, P. W., Carruthers, J. R., Cooper, R. I., Prout, K., Watkin, D. J., 2003. CRYSTALS version 12: software for guided crystal structure analysis. J. Appl. Crystallogr. 36, 1487.

Bisio, A., Schito, A. M., Ebrahimi, S. N., Hamburger, M., Mele, G., Piatti, G., Romussi, G., Dal Piaz, F., De Tommasi, N., 2015. Antibacterial compounds from Salvia adenophora Fernald (Lamiaceae). Phytochemistry 110, 120-132.

Borquez, J., Mancilla, A., Pedreros, S., Loyola, L. A., Morales, G., Wittke, O., Brito, I., 1995. Isolation and structure of crotonic acid, a clerodane diterpenoid from Croton chilensis. Bol. Soc. Chil. Quim. 40, 157-162.

Bruker Analytical X-ray Systems, I., 2006. Apex2, Version 2 User Manual, M86-E01078, Madison, WI.

Cao, S., Hou, Y., Brodie, P., Miller, J. S., Randrianaivo, R., Rakotobe, E., Rasamison, V. E., Kingston, D. G. I., 2011. Antiproliferative compounds of Cyphostemma greveana from a Madagascar dry forest. Chem. Biodiversity 8, 643-650.

Cavin, A. L., Hay, A. E., Marston, A., Stoeckli-Evans, H., Scopelliti, R., Diallo, D., Hostettmann, K., 2006. Bioactive diterpenes from the fruits of Detarium microcarpum. J Nat Prod 69, 768-773.

CLSI, 2012. Clinical and laboratory standards institute, methods for dilution antimicrobial susceptibility tests for bacteria that grow aerobically, approved standard M100-S22, national committee for clinical laboratory standards, Fort Wayne, Ind, USA, 22nd Edition.

Du, K., Marston, A., van Vuuren, S. F., van Zyl, R. L., Coleman, C., Zietsman, P. C., Bonnet, S. L., Ferreira, D., van der Westhuizen, J. H., 2014. Flavonolacyl glucosides from the aril of Schotia brachypetala Sond. and their antioxidant, antibacterial and antimalarial activities. Phytochemistry Lett. 10, cxxiii-cxxviii.

Englund, B. M., Griffeth, L., Clausen, T. P., 2009. A 9,13-epoxylabdane from Colophospermum mopane. Phytochemistry Lett. 2, 144-147.

Fang, N., Yu, S., Mabry, T. J., Abboud, K. A., Simonsen, S. H., 1988. Terpenoids from Ageratina saltillensis. Phytochemistry 27, 3187-3196.

Ferreira, D., Marais, J. P. J., Slade, D., 2003. Phytochemistry of the mopane, Colophospermum mopane. Phytochemistry 64, 31-51.

Frisch, M. J., Trucks, G. W., Schlegel, H. B., Scuseria, G. E., Robb, M. A., Cheeseman, J. R., Scalmani, G., Barone, V., Mennucci, B., Petersson, G. A., Nakatsuji, H., Caricato, M., Li, X., Hratchian, H. P., Izmaylov, A. F., Bloino, J., Zheng, G., Sonnenberg, J. L., Hada, M., Ehara, M., Toyota, K., Fukuda,

R., Hasegawa, J., Ishida, M., Nakajima, T., Honda, Y., Kitao, O., Nakai, H., Vreven, T., Montgomery Jr., J. A., Peralta, J. E., Ogliaro, F., Bearpark, M. J., Heyd, J., Brothers, E. N., Kudin, K. N., Staroverov, V. N., Kobayashi, R., Normand, J., Raghavachari, K., Rendell, A. P., Burant, J. C., Iyengar, S. S., Tomasi, J., Cossi, M., Rega, N., Millam, N. J., Klene, M., Knox, J. E., Cross, J. B., Bakken, V., Adamo, C., Jaramillo, J., Gomperts, R., Stratmann, R. E., Yazyev, O., Austin, A. J., Cammi, R., Pomelli, C., Ochterski, J. W., Martin, R. L., Morokuma, K., Zakrzewski, V. G., Voth, G. A., Salvador, P., Dannenberg, J. J., Dapprich, S., Daniels, A. D., Farkas, Ö., Foresman, J. B., Ortiz, J. V., Cioslowski, J., Fox, D. J., Gaussian 09, 2009.

Garcá-Sánchez, E., Ramírez-López, C. B., Talavera-Alemán, A., León-Hernández, A., Martínez-Muñoz, R. E., Martínez-Pacheco, M. M., Gómez-Hurtado, M. A., Cerda-Garcá-Rojas, C. M., Joseph-Nathan, P., del Río, R. E., 2014. Absolute configuration of (13R)- and (13S)-labdane diterpenes coexisting in Ageratina jocotepecana. J Nat Prod 77, 1005-1012.

Gibbons, S., 2004. Anti-staphylococcal plant natural products. Nat prod rep 21, 263-277.

Hata, Y., Ebrahimi, S. N., De Mieri, M., Zimmermann, S., Mokoka, T., Naidoo, D., Fouche, G., Maharaj, V., Kaiser, M., Brun, R., Potterat, O., Hamburger, M., 2014. Antitrypanosomal isoflavan quinones from Abrus precatorius. Fitoterapia 93, 81-87.

Hata, Y., Raith, M., Ebrahimi, S. N., Zimmermann, S., Mokoka, T., Naidoo, D., Fouche, G., Maharaj, V., Kaiser, M., Brun, R., Hamburger, M., 2013. Antiprotozoal isoflavan quinones from Abrus precatorius ssp. africanus. Planta Med 79, 492-498.

Hoye, T. R., Jeffrey, C. S., Shao, F., 2007. Mosher ester analysis for the determination of absolute configuration of stereogenic (chiral) carbinol carbons. Nat. Protocols 2, 2451-2458.

Jakupovic, J., Baruah, R. N., Zdero, C., Eid, F., Pathak, V. P., Chau-Thi, T. V., Bohlmann, F., King, R. M., Robinson, H., 1986. Further diterpenes from plants of the Compositae, subtribe Solidagininae. Phytochemistry 25, 1873-1881.

Lee, C., Lee, J. W., Jin, Q., Lee, H. J., Lee, S.-J., Lee, D., Lee, M. K., Lee, C. K., Hong, J. T., Lee, M. K., Hwang, B. Y., 2013. Anti-inflammatory constituents from the fruits of Vitex rotundifolia. Bioorg. Med. Chem. Lett. 23, 6010-6014.

Lewis, G., Schrire, B., Mackinder, B., Lock, M., 2005. Legumes of the world. In: Gardens, R. B. (Ed.). E-Publishing Inc., Kew, Richmond, Surrey, UK.

Lopes, L. M. X., Bolzani, V. D., Trevisan, L. M. V., 1987. Clerodane diterpenes from aristolochia species. Phytochemistry 26, 2781-2784.

Macrae, C. F., Bruno, I. J., Chisholm, J. A., Edgington, P. R., McCabe, P., Pidcock, E., Rodriguez-Monge, L., Taylor, R., van de Streek, J., Wood, P. A., 2008. Mercury CSD 2.0 - new features for the visualization and investigation of crystal structures. J. Appl. Crystallogr. 41, 466-470.

Manabe, S., Nishino, C., 1986. Stereochemistry of cis-clerodane diterpenes. Tetrahedron 42, 3461-3470.

McCrindle, R., Nakamura, E., 1974. Constituents of *Solidago* species part IV. The constitution of a chemically distincted variety of *Solidago serotina*. Can. J. Chem. 52, 2029-2036.

McCrindle, R., Nakamura, E., Anderson, A. B., 1976. Constituents of solidago species. Part VII. Constitution and stereochemistry of the cis-clerodanes from Solidago arguta Ait. and of related diterpenoids. J. Chem. Soc., Perkin Trans. 1, l590-597.

Mebe, P. P., 2001. Diterpenes from the bark and seeds of Colophospermum mopane. Phytochemistry 57, 537-541.

Pacheco, A. G., Machado de Oliveira, P., Pilo-Veloso, D., Flávio de Carvalho Alcântara, A., 2009. ^{13}C-NMR data of diterpenes isolated from aristolochia species. Molecules 14, 1245-1262.

Palatinus, L., Chapuis, G., 2007. SUPERFLIP - a computer program for the solution of crystal structures by charge flipping in arbitrary dimensions. J. Appl. Crystallogr. 40, 786-790.

Palgrave, K. C., 1983. Trees of Southern Africa. C. Struik, Cape town.

Peters, R. J., 2010. Two rings in them all: the labdane-related diterpenoids. Nat prod rep 27, 1521-1530.

Piers, E., Breau, M. L., Han, Y., Plourde, G. L., Yeh, W.-L., 1995. Total synthesis of cis-clerodane diterpenoids: (-)-agelasine A and (+)-(3R,4S,5R,8S,9R,10S)-3,4-epoxyclerod-13-en-15,16-olide. J. Chem. Soc., Perkin Trans. 1, 963-966.

Reiter, E., Treadwell, E., Cederstrom, E., Reichardt, P. B., Clausen, T. P., 2003. Diterpenes from Colophospermum mopane: "missing links" in the biogenesis of 9,13-epoxylabdanes. J Nat Prod 66, 30-33.

Schramm, A., Ebrahimi, S. N., Raith, M., Zaugg, J., Rueda, D. C., Hering, S., Hamburger, M., 2013. Phytochemical profiling of Curcuma kwangsiensis rhizome extract, and identification of labdane diterpenoids as positive GABAA receptor modulators. Phytochemistry 96, 318-329.

Shikanga, E. A., Viljoen, A., Combrinck, S., Marston, A., 2011. Isolation of Sceletium alkaloids by high-speed countercurrent chromatography. Phytochemistry Lett. 4, 190-193.

T. Bruhn, A. S., Y. Hemberger, G. Bringmann, 2014. SpecDis version 1.61. University of Wuerzburg, Germany,.

Tokoroyama, T., 2000. Synthesis of clerodane diterpenoids and related compounds - stereoselective

construction of the decalin skeleton with multiple contiguous stereogenic centers. Synthesis 2000, 611-633.

Venter, F., Venter, J. A., 2002. Making the most indigenous trees. Briza, Pretoria, p. P 100.

Watt, J. M., Breyer-Brandwijl, M. G., 1962. The medicinal poisonous plants of Southern and Eastern Africa. Livingstone, London.

Legends for Figures

Fig. 1 Diterpenoids from *Colophospermum mopane*.

Fig. 2 Ellipsoid plot of compound **10**. There are four molecules present in the asymmetric unit which are not related by symmetry. For clarity reasons only one out of the four is shown here. All four molecules have the same stereochemistry, but show slightly different conformations in the peripherical substituents.

Fig. 3 Ellipsoid plot of compound **1**.

Fig. 4. Lowest energy conformer of *p*-bromo benzoyl 15-methylester **2a** after DFT minimization in gas phase at the B3LYP/6-31G* level. Key NOESY correlations (blue arrows) for compounds **2a** and **3** are shown.

Fig. 5 Configurational assignment for alcohols **2** and **6** by modified Mosher's method. ^{1}H NMR $\Delta\delta$ (δ_S- δ_R) shifts for the 3-O-*S*-and 3-O-*R*-MTPA esters of compounds **2** and **6** are reported in Hertz.

Fig. 6 Experimental ECD spectra of compounds **2a** and **6a**, and calculated spectra for the 3*R*,8*S*,9*R*,10*S* stereoisomer of **2a** in MeOH.

Fig. 7 Lowest energy conformer of compound **6** after DFT minimization in gas phase at the B3LYP/6-31G** level. Key NOESY correlations (blue arrows) are shown on the corresponding 2D structure.

Fig. 8 Ellipsoid plot of structure of **7**. There are two molecules present in the asymmetric unit which are not related by symmetry. Both molecules have the same stereochemistry, but show slightly different

conformations in the peripherical substituents. For clarity reasons only one out of the two is shown here.

Fig. 9 Lowest energy conformer of compound **8** after DFT minimization in gas phase at the B3LYP/6-31G** level. Key NOESY correlations (blue arrows) are shown on the 2D structure.

Fig. 10 Lowest energy conformer of compound **9** after DFT minimization in gas phase at the B3LYP/6-31G** level. Key NOESY correlations (blue arrows) are shown on the 2D structure.

Fig.1

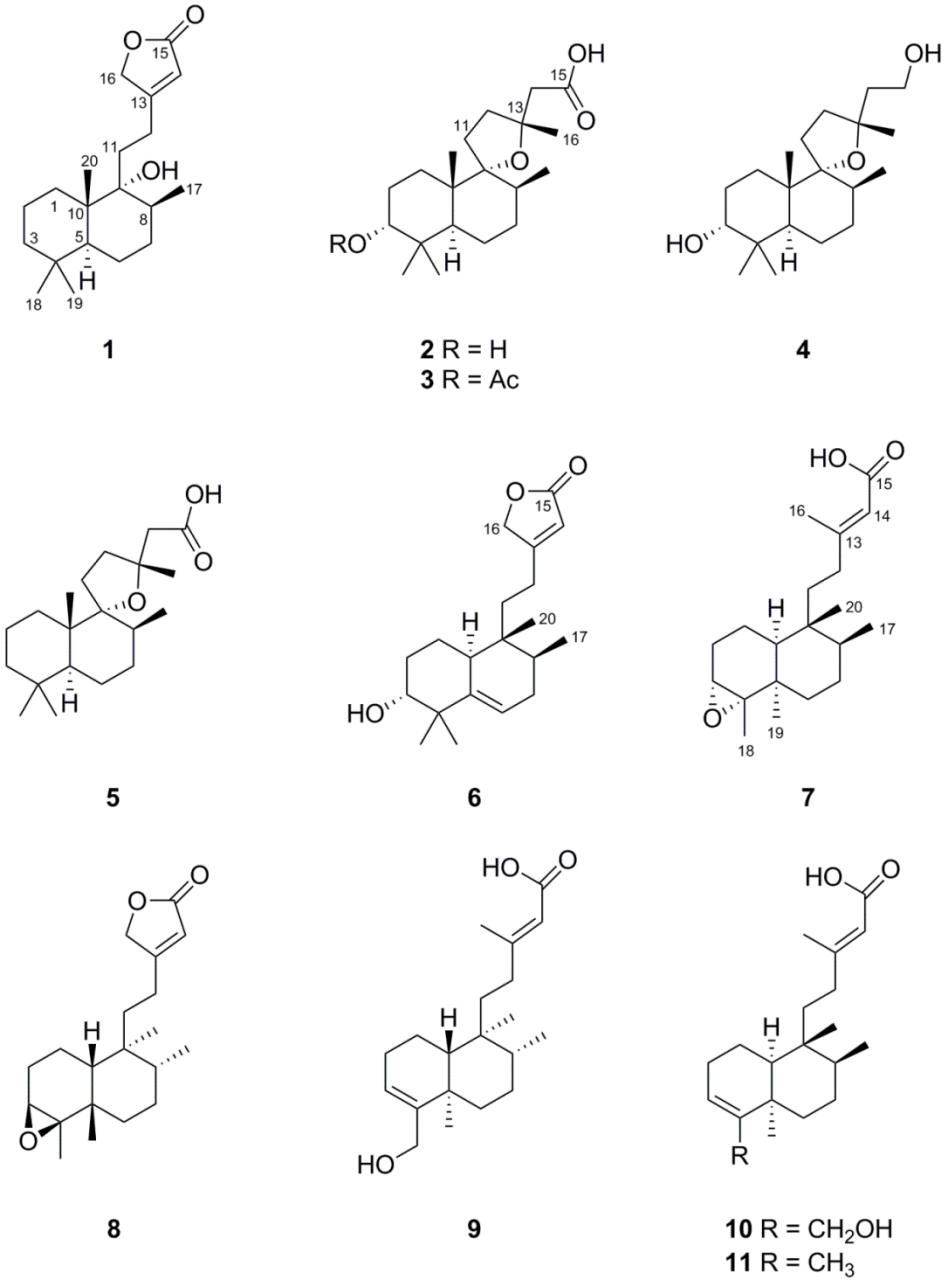

Fig.2

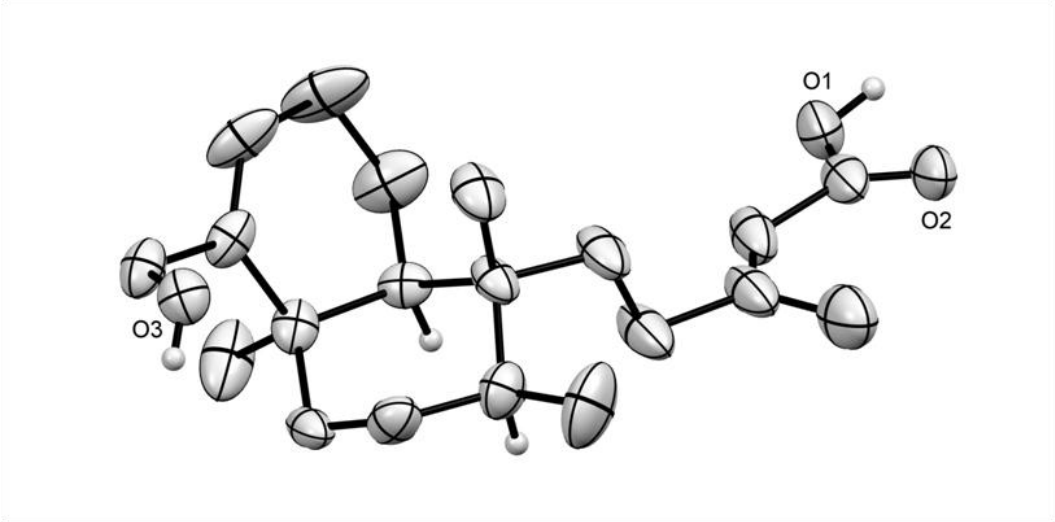

Fig.3

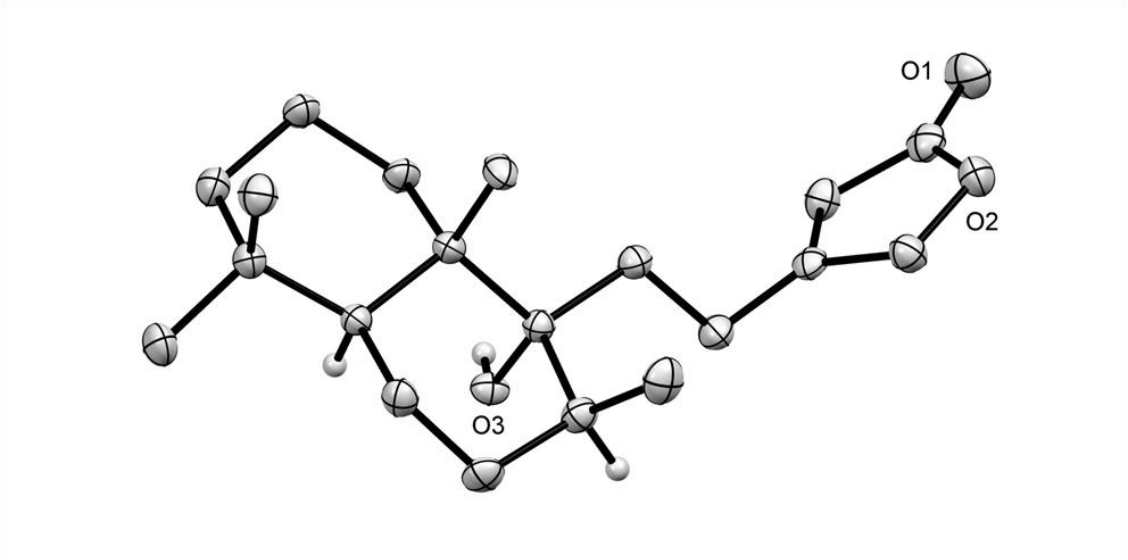

Fig.4

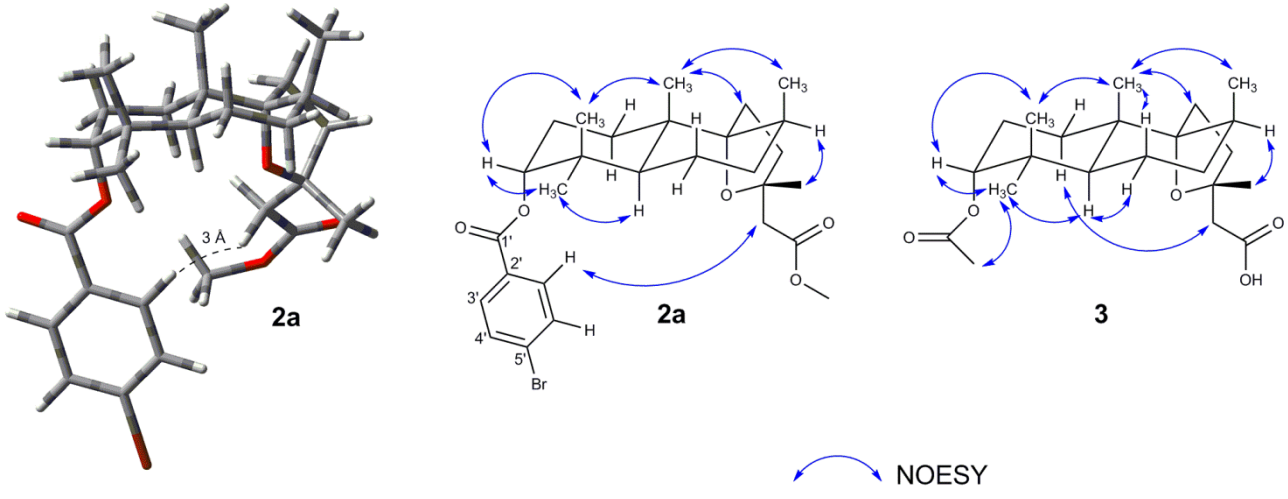

Fig.5

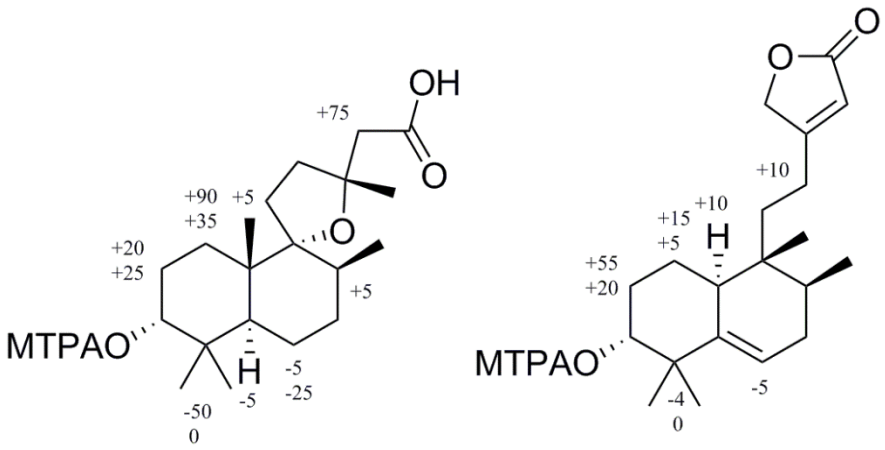
OH
O
+75
+90
+5
+35
+20
+25
+5
MTPAO
H
-5
-25
-50
0
-5
O
O
+10
+15
+10
+5
H
+55
+20
MTPAO
-4
0
-5

2 **6**

Fig.6

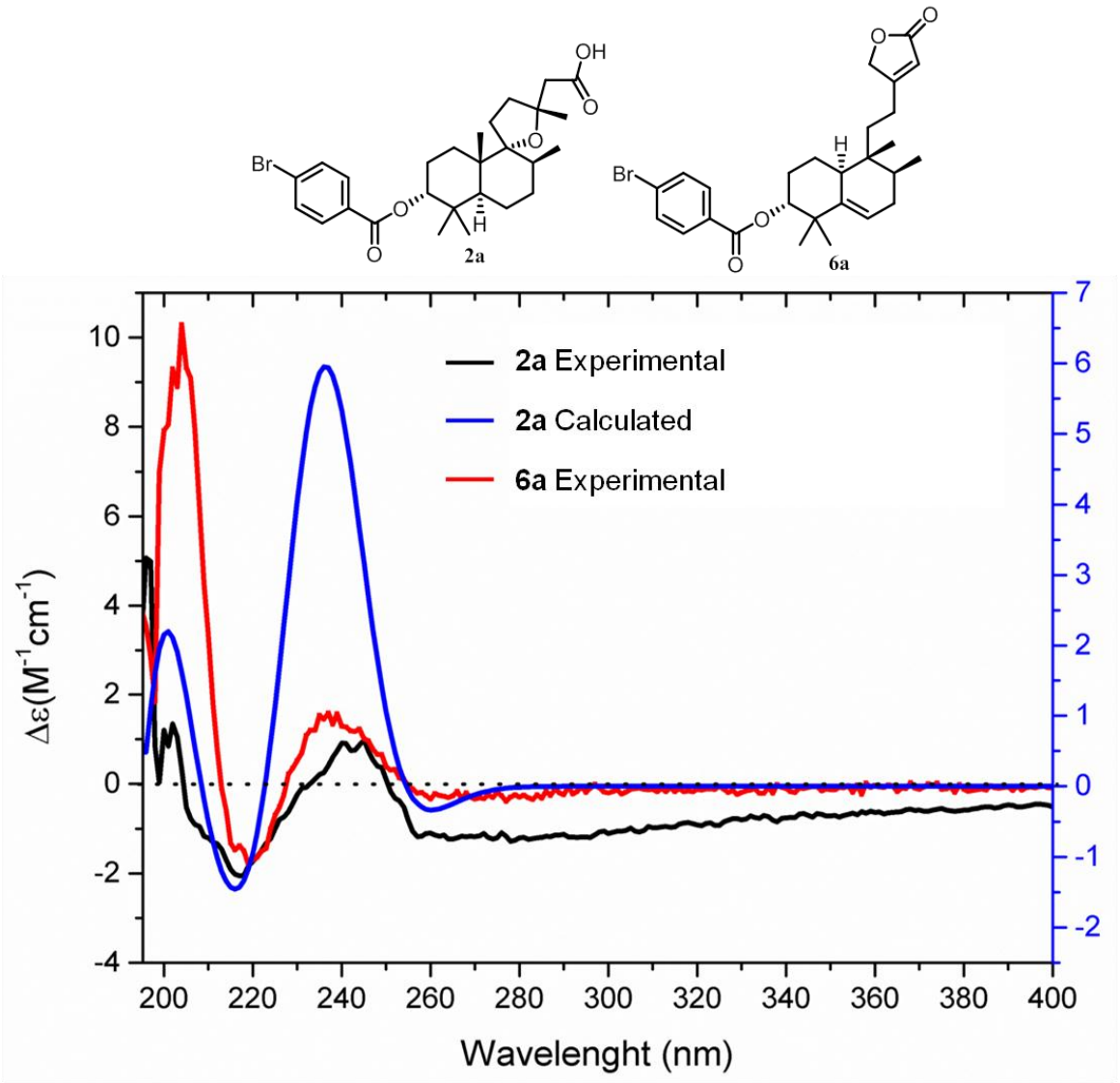
Br
OH
O
O
O
H
2a
Br
O
O
O
H
6a
2a Experimental
2a Calculated
6a Experimental
Δε(M-1cm-1)
Wavelenght (nm)
10
8
6
4
2
0
-2
-4
7
6
5
4
3
2
1
0
-1
-2
200
220
240
260
280
300
320
340
360
380
400

Fig.7

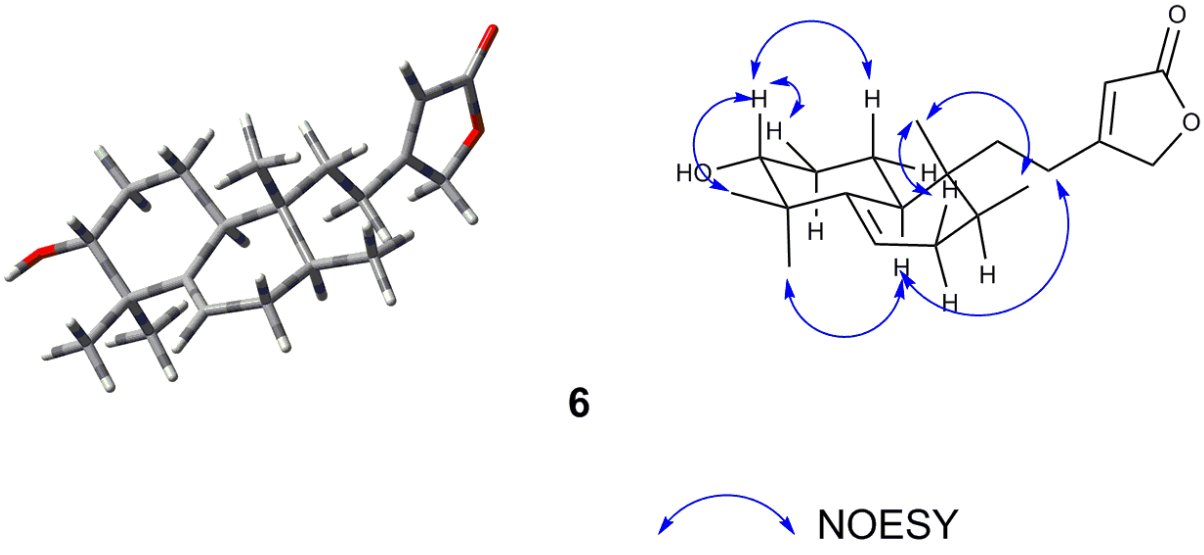

Fig.8

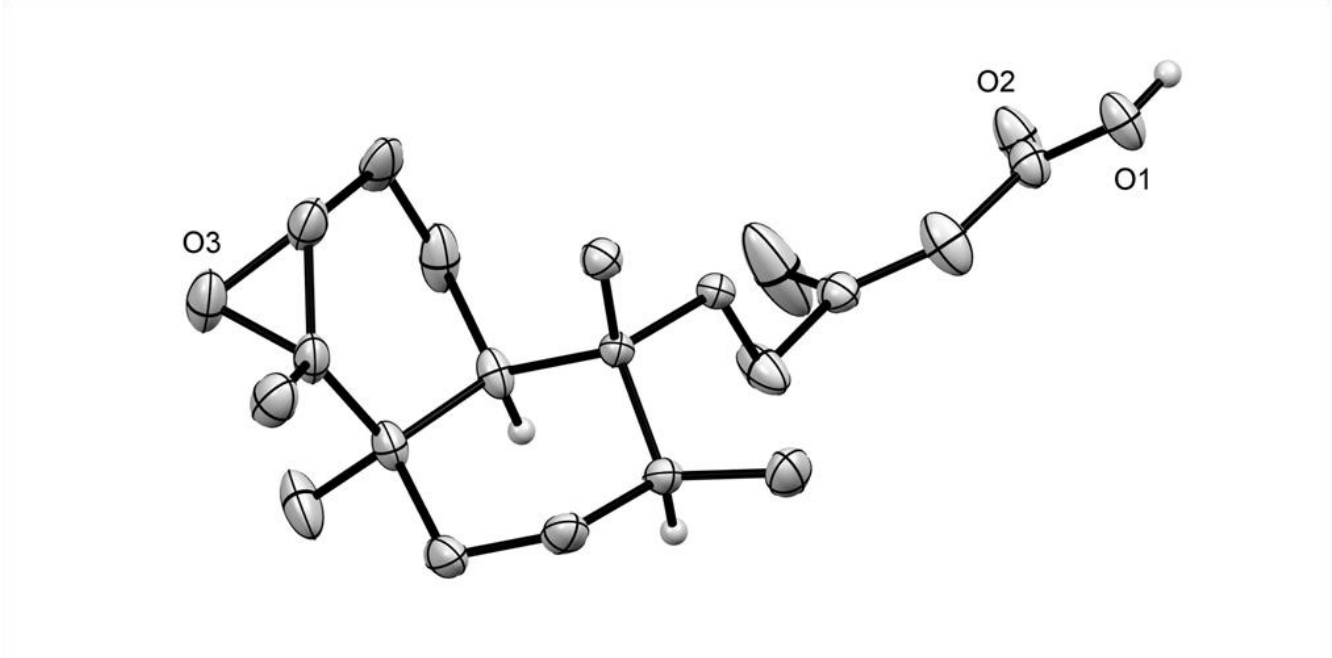

Fig.9

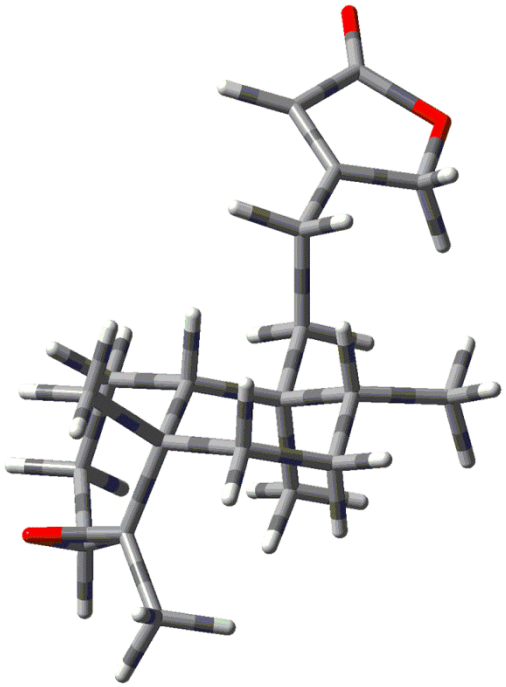

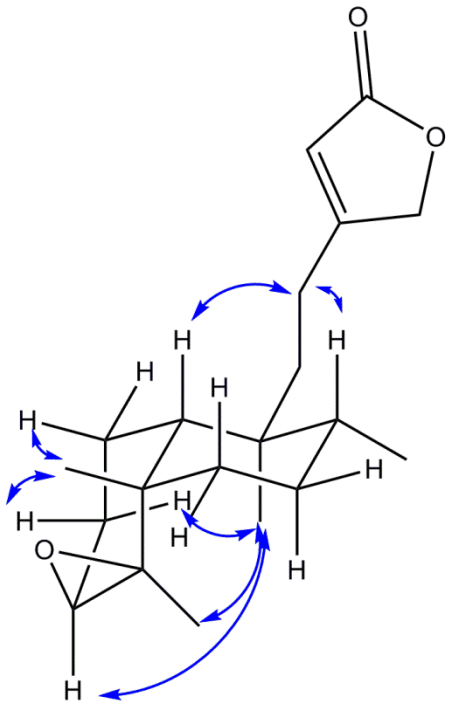

8

NOESY

Fig.10

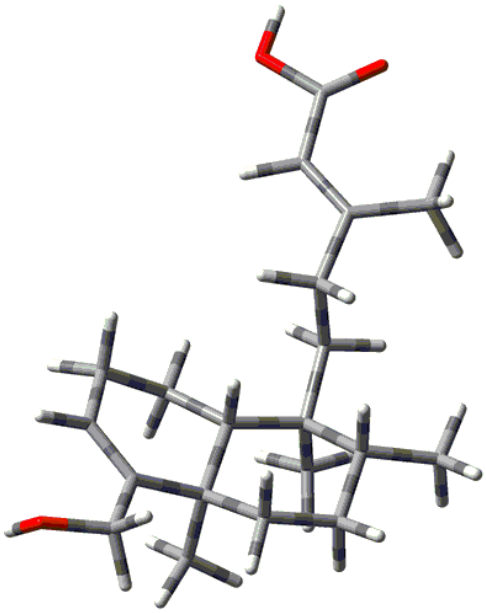

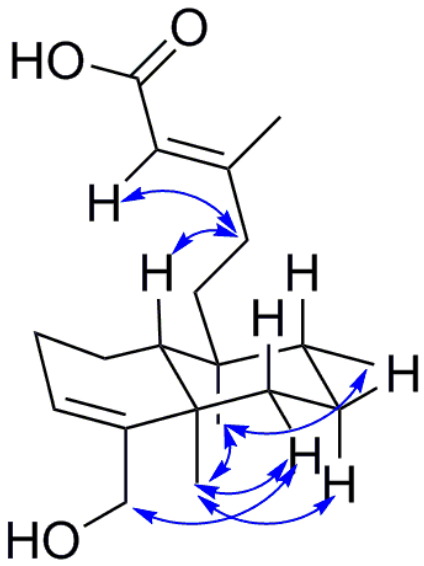

9

NOESY

Labdane and clerodane diterpenoids from *Colophospermum mopane*

(Supporting Information)

Kun Du [a,1], Maria De Mieri [b,1], Markus Neuburger [c], Pieter C. Zietsman [d,e], Andrew Marston [a,#], Sandy F. van Vuuren [f], Matthias Hamburger [b,*], and Jan H. van der Westhuizen [g,*]

[a]Department of Chemistry, University of the Free State, Nelson Mandela Avenue, Bloemfontein 9301, South Africa

[b]Division of Pharmaceutical Biology, University of Basel, Klingelbergstrasse 50, 4056 Basel, Switzerland

[c]Division of Inorganic Chemistry, Department of Chemistry, University of Basel, Basel, Switzerland

[d]National Museum, P. O. Box 266, Bloemfontein 9300, South Africa

[e]Centre for Environmental Management, University of the Free State, P.O. Box 339, Bloemfontein, 9301, South Africa

[f]Department of Pharmacy and Pharmacology, Faculty of Health Sciences, University of the Witwatersrand, Parktown, South Africa

[g]Directorate Research Development, University of the Free State, Nelson Mandela Avenue, Bloemfontein 9301, South Africa

[*]Corresponding authors at:

Prof. Jan H. van der Westhuizen, Department of Chemistry, University of the Free State, Bloemfontain 9301, South Africa.

Prof. Matthias Hamburger, Division of Pharmaceutical Biology, University of Basel, Klingelbergstrasse 50, CH-4056 Basel, Switzerland.

[1]These authors contributed equally to this work

[#] Deceased

E-mail addresses: vdwestjh.@ufs.ac.za, Phone: +27 828935113

matthias.hamburger@unibas.ch, Phone: +41 61 267 14 25 Fax: +41 61 267 14 74

Content

Figure S25: Superimposed conformers of compound **5**

Figure S26: ^{1}H NMR spectrum of compound **6** (500MHz, $CDCl_3$)

Figure S27: ^{13}C NMR spectrum of compound **6** (125 MHz, $CDCl_3$)

Figure S28: ^{1}H-^{1}H COSY spectrum of compound **6** (600 MHz, $CDCl_3$)

Figure S29: Overlay of HSQC and HMBC spectra of compound **6** (600 MHz, $CDCl_3$)

Figure S30: 2D ^{1}H-^{1}H NOESY spectrum of compound **6** (600 MHz, $CDCl_3$)

Figure S31: 1D Selective NOESY spectra of compound **6** (500 MHz, $CDCl_3$)

Figure S32: ^{1}H NMR spectrum of 3-*p*-bromobenzoate derivative of **6** (500 MHz, $CDCl_3$)

Figure S33: Overlay of ^{1}H-NMR spectra of (*R*)-MTPA and (*S*)-MTPA esters of compound **2** (500 MHz, $CDCl_3$)

Figure S34: ^{1}H NMR spectrum of compound **7** (600MHz, methanol-d_4)

Figure S35: ^{13}C NMR spectrum of compound **7** (150 MHz, methanol-d_4)

Figure S36: ^{1}H-^{1}H COSY spectrum of compound **7** (600 MHz, methanol-d_4)

Figure S37: Overlay of HSQC and HMBC spectra of compound **7** (600 MHz, methanol-d_4)

Figure S38: 2D ^{1}H-^{1}H NOESY spectrum of compound **7** (600 MHz, methanol-d_4)

Figure S39: ^{1}H NMR spectrum of compound **8** (600MHz, $CDCl_3$)

Figure S40: ^{13}C NMR spectrum of compound **8** (150 MHz, $CDCl_3$)

Figure S41: ^{1}H-^{1}H COSY spectrum of compound **8** (600 MHz, $CDCl_3$)

Figure S42: Overlay of HSQC and HMBC spectra of compound **8** (600 MHz, $CDCl_3$)

Figure S43: 2D ^{1}H-^{1}H NOESY spectrum of compound **8** (600 MHz, $CDCl_3$)

Figure S44: ^{1}H NMR spectrum of compound **9** (500 MHz, $CDCl_3$)

Figure S45: ^{13}C NMR spectrum of compound **9** (125 MHz, $CDCl_3$)

Figure S46: ^{1}H-^{1}H COSY spectrum of compound **9** (500 MHz, $CDCl_3$)

Figure S47: Overlay of HSQC and HMBC spectra of compound **9** (500 MHz, $CDCl_3$)

Figure S48: 2D ^{1}H-^{1}H NOESY spectrum of compound **9** (500 MHz, $CDCl_3$)

*Compound **4***: colorless powder; $[\alpha]^{25}_{D}$ - 37.7 (*c* 0. 07, MeOH); HRESIMS m/z 347.2562 $[M + Na]^+$ (calcd for $C_{20}H_{36}NaO_3$, 347.2557); for ^1H and ^{13}C NMR data, see Tables S1;
*Compound **5***: colorless powder; $[\alpha]^{25}_{D}$ - 54.7 (*c* 0. 61, $CHCl_3$); HRESIMS m/z 345.2400 $[M + Na]^+$ (calcd for $C_{20}H_{34}NaO_3$, 345.2423); for ^1H and ^{13}C NMR data, see Tables S1;
*Compound **10***: colorless crystals; $[\alpha]^{25}_{D}$ -29.7 (*c* 0.18, MeOH); HRESIMS m/z 343.2244 $[M + Na]^+$ (calcd for $C_{20}H_{32}NaO_3$, 343.2274); for ^1H and ^{13}C NMR data, see Table S2;
*Compound **11***: colorless gum; $[\alpha]^{25}_{D}$ -19.1 (*c* 0.41, MeOH); HRESIMS m/z 327.2316 $[M + Na]^+$ (calcd for $C_{20}H_{32}NaO_2$, 327.2295); for ^1H and ^{13}C NMR data, see Table S2;

Table S1 Crystallographic data for compounds **1**, **7** and **10**.

Structure	1	7	10
Formula	$C_{20}H_{32}O_3$	$C_{20}H_{32}O_3$	$C_{20}H_{32}O_3$
Formula weight	320.47	320.47	320.47
Z, density (Mg m^{-3})	4, 1.200	8, 1.171	16, 1.124
F(000)	704	1408	2816
Crystal size (mm)	0.05*0.13*0.19	0.06*0.11*0.21	0.05*0.11*0.24
Abs. coeff. (mm^{-1})	0.616	0.601	0.577
Min/max transmiss.	0.92/0.97	0.94/0.96	0.94/0.97
Temperature (K)	123	123	123
Radiation	Cu K_α	Cu K_α	Cu K_α
Wavelength	1.54178 Å	1.54178 Å	1.54178 Å
Crystal system	orthorhombic	monoclinic	orthorhombic
Space group	P 2_1 2_1 2_1	C 2	P 2_1 2_1 2_1
a (Å)	7.6689(5)	33.5582(15)	14.0499(7)
b (Å)	10.2286(6)	7.4109(3)	17.2599(9)
c (Å)	22.6080(14)	14.7554(7)	31.2403(16)
α (°)	90	90	90
β (°)	90	97.8284(18)	90
γ (°)	90	90	90
Volume ($Å^3$)	1773.42(19)	3635.4(3)	7575.8(7)
Θ (°)	68.127	70.075	68.940
Collected refl.	19188	22323	79503
Independent refl.	3226	6632	13943
Merging r	0.024	0.027	0.052
Observed refl.	3214, I>2.0σ(I)	6529, I>2.0σ(I)	13079, I>2.0σ(I)
Refined parameters	209	416	830
R (observed data)	0.0304	0.0347	0.0424
rW (all data)	0.0292	0.0333	0.0413
Gof	0.9540	0.9679	0.9664
Flack parameter	-0.04(6)	0.04(6)	0.02(5)

Table S2. ^{1}H and ^{13}C NMR spectroscopic data for compounds **4**, **5** ($CDCl_3$, 600 MHz for ^{1}H, and 150 MHz for ^{13}C NMR; δ in ppm).

	4		5	
Position	**δ_H (*J* in Hz)**	**δ_C, type**	**δ_H[b] (*J* in Hz)**	**δ_C, type**
1	1.96, m[a]	26.3, CH_2	1.33, m[a]	33.3, CH_2
	1.02, m[a]			
2	1.94, m[a]	24.4, CH_2	1.59, m	18.0, CH_2
	1.62, m[a]		1.44, m[a]	
3	3.31 t (3.0)	76.0, CH	1.33, m[a]	41.7, CH_2
			1.13, td (13.5, 4.0)	
4	-	37.6, C	-	33.4, C
5	1.67, dd (12.5, 2.5)	41.3, CH	1.34, m[a]	48.8, C
6	1.43, ddd (14.0, 12.5, 3.4)	16.6, CH_2	1.41, m[a]	17.0, CH_2
	1.32, m		1.47, m[a]	
7	2.00, m[a]	29.6, CH_2	1.96, m[a]	29.4, CH_2
	1.39, m[a]		1.42, m[a]	
8	1.87, m	40.2, CH	1.93, m[a]	38.9, CH
9	-	93.9, C	-	95.7, C
10	-	41.9, C	-	41.9, C
11	2.00, m[a]	29.1, CH_2	2.00, m	28.5, CH_2
	1.83, m[a]		1.92, m[a]	
12	1.84, m[a]	39.8, CH_2	1.93, m[a]	37.9, CH_2
	1.84, ddd (16.1, 12.5, 8.5)		1.84, m	
13	-	83.7, C	-	80.7, C
14	2.06, ddd (15.0, 10.0, 4.6)	42.3, CH_2	2.65, d (15.4)	46.4, CH
	1.61, m[a]		2.49, d (15.4)	
15	4.00, td (10.8, 3.2)	60.0, CH_2	-	173.0, C
	3.75, d (10.8)		-	
16	1.28, s	26.3, CH_3	1.37, s	27.5, CH_3
17	1.03, d (7.7)	18.0, CH_3	1.04, d (7.9)	18.1, CH_3
18(α)	0.94, s	29.1 CH_3	0.86, s	33.4, CH_3
19	0.82, s	22.0, CH_3	0.79, s	21.6, CH_3
20	0.95, s	18.1, CH_3	0.94, s	18.3, CH_3

[a] overlapped signals; [b]measured at 500 MHz.

Table S3. ^{1}H and ^{13}C NMR spectroscopic data for compounds **10** and **11** ($CDCl_3$, 600 MHz for ^{1}H, and 150 MHz for ^{13}C for compounds **9**; 500 MHz for ^{1}H, and 125 MHz for ^{13}C for compound **10**, δ in ppm).

	10		**11**	
Position	**δ_H (*J* in Hz)**	**δ_C, type**	**δ_H (*J* in Hz)**	**δ_C[a], type**
1	2.03, m[a]	17.4, CH_2	2.02, m	17.8, CH_2
	1.81, dd (14.8, 8.7)		1.79, ddd (13.5, 9.5, 1.6)	
2	2.19, m[a]	23.7, CH_2	2.13,m[a]	24.0, CH_2
	2.09, m[a]		2.04,m[a]	
3	5.63, t (4.0)	124.8, CH	5.28, brs	123.2, CH
4	-	142.9, C	-	140.2, C
5	-	36.2, C	-	37.3, C
6	2.09, m[a]	36.7, CH_2	2.03, m[a]	37.8, CH_2
	1.13, m[a]		1.08, td (13.5, 4.3)	
7	1.30, m[a]	28.9, CH_2	1.26-1.22, m	28.8, CH_2
	1.24, qd (13.0, 2.0)	28.9	1.26-1.22, m	
8	1.44, m	37.4, CH	1.43, m	37.6, CH
9	-	40.2, C	-	40.5, C
10	1.33, m	45.2, C	1.34, dd (6.0, 1.6)	44.9, C
11	1.61, m	36.0, CH_2	1.65, m	36.4, CH_2
	1.37, m		1.40, m	
12	2.00-2.02, m	34.7, CH_2	2.04, m[a]	34.9, CH_2
	2.00-2.02, m		2.04, m[a]	
13	-	164.4, C	-	163.0, C
14	5.71, brs	114.9, CH	5.70, brs	115.1, CH
15	-	172.0, C	-	171.3, C
16	2.20, s	19.5, CH_3	2.18, s	19.4, CH_3
17	0.78, d (6.9)	15.9, CH_3	0.78, d (6.7)	16.0, CH_3
18	4.23, d (13.7)	64.6, CH_2	1.68, q (1.9)	19.7, CH_3
	4.12, d (13.7)		-	-
19	1.14, s	35.9, CH_3	1.05, brs	33.1, CH_3
20	0.79, s	17.3, CH_3	0.83, s	17.3, CH_3

[a]extracted from ^{1}H-^{13}C 2D inverse detected experiments.

Table S4. ^{1}H and ^{13}C NMR spectroscopic data for *p*-bromobenzoyl derivative 15- methyl ester **2a** ($CDCl_3$, 500 MHz for ^{1}H, and 125 MHz for ^{13}C NMR; δ in ppm).

Position	**δ_H (*J* in Hz)**	**δ_C[a], type**
1	1.83, m[a]	27.2, CH_2
	1.01, m	
2	1.89, m[a]	22.3, CH_2
	1.66, dq (14.0, 3.4)	
3	4.78 dd (3.4, 3.0)	79.3, CH
4	-	37.3, C
5	2.10, dd (12.0, 2.9)	42.2, CH
6	1.38, m	16.6, CH_2
	1.33, m	
7	2.04, m[a]	29.5, CH_2
	1.33, m[a]	
8	1.87, m	39.3, CH
9	-	92.0, C
10	-	41.6, C
11	1.90, m[a]	29.0, CH_2
	1.81, m[a]	
12	1.90, m[a]	36.9, CH_2
	1.81, m[a]	
13	-	80.7, C
14	2.47, ABq (14.0)	46.6, CH_2
15	-	171.5, C
16	1.28, s	27.7, CH_3
17	0.98, d (7.7)	18.2, CH_3
18(α)	0.83, s	28.0 CH_3
19	0.87, s	21.6, CH_3
20	0.92, s	18.1, CH_3
1'	-	165.0, C
2'	-	130.3, C
3'	7.92, d (8.6)	127.6, CH
4'	7.92, d (8.6)	129.9, CH
2'	-	130.3, C
15-$COCH_3$	3.52, s	51.3, CH_3

[a]extracted from ^{1}H-^{13}C 2D inverse detected experiments.

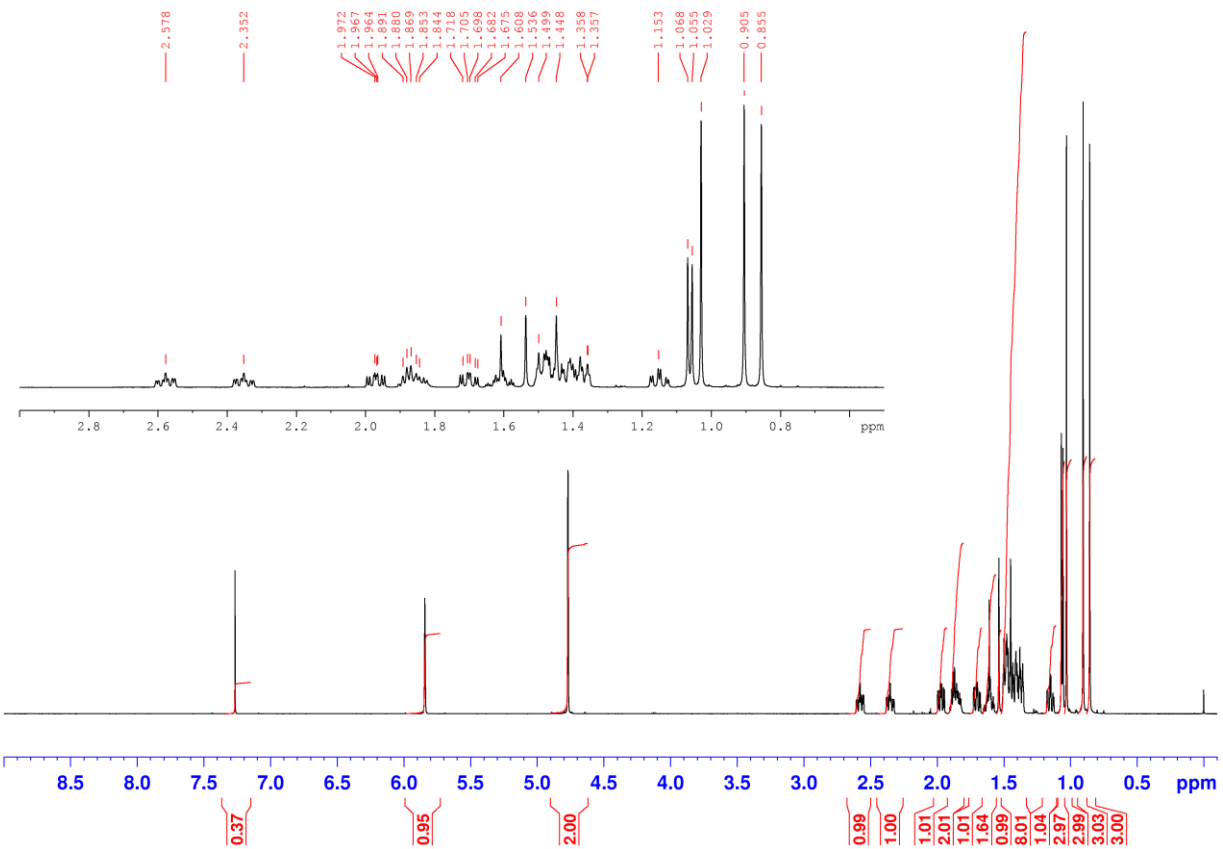

Fig. 1S. ^{1}H NMR spectrum of compound **1** in $CDCl_3$.

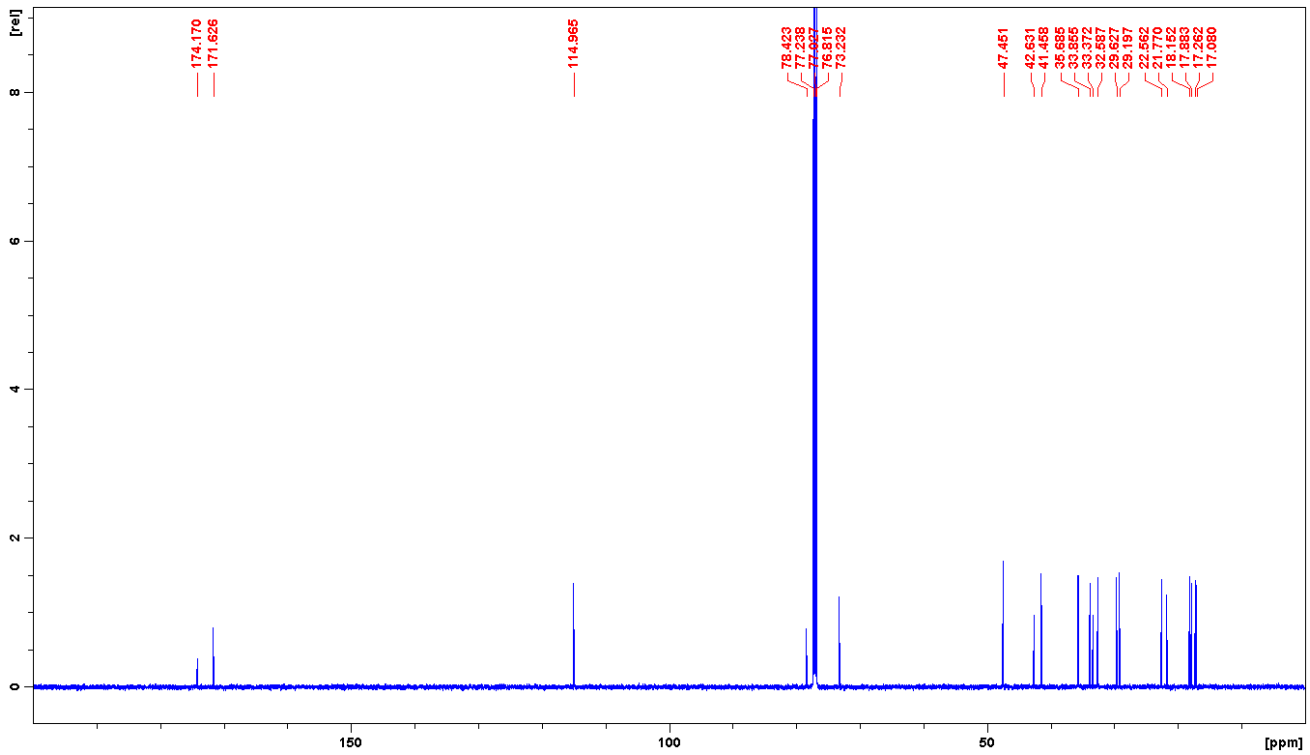

Fig. 2S. ^{13}C NMR spectrum of compound **1** in $CDCl_3$.

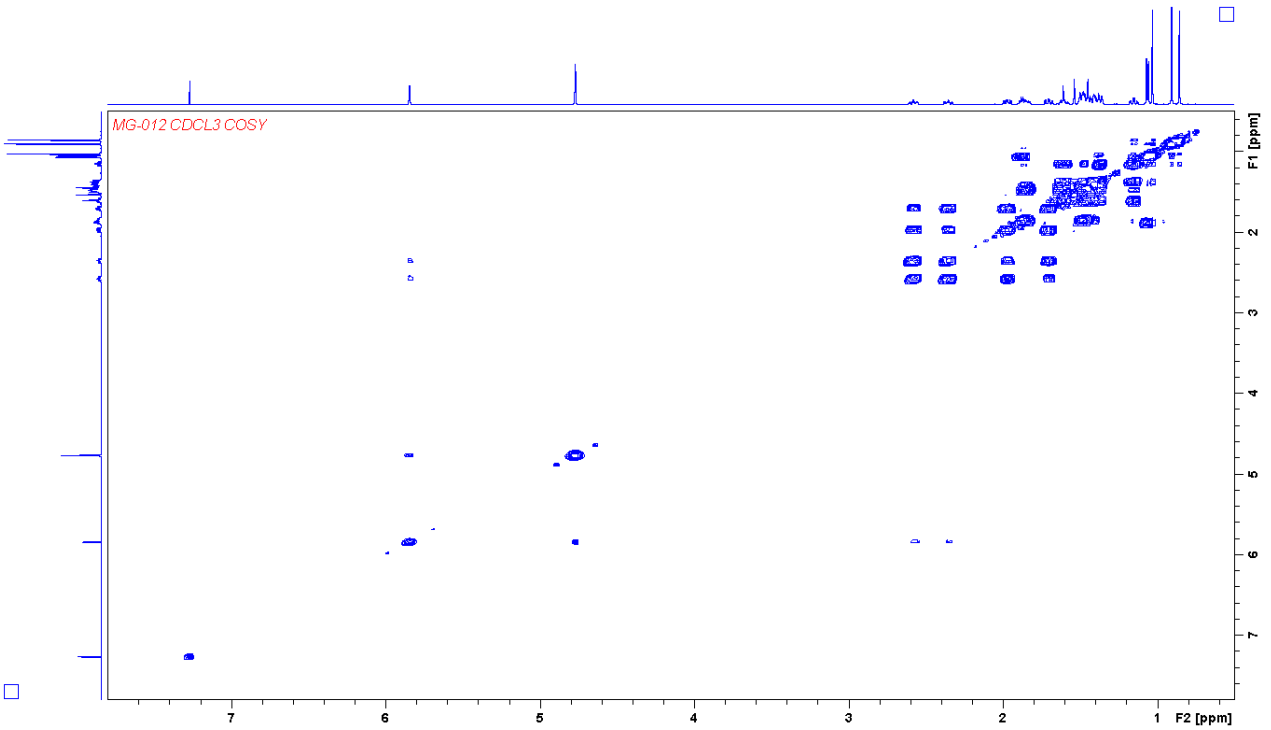

Fig. 3S. ^{1}H-^{1}H-COSY spectrum of compound **1** in $CDCl_3$.

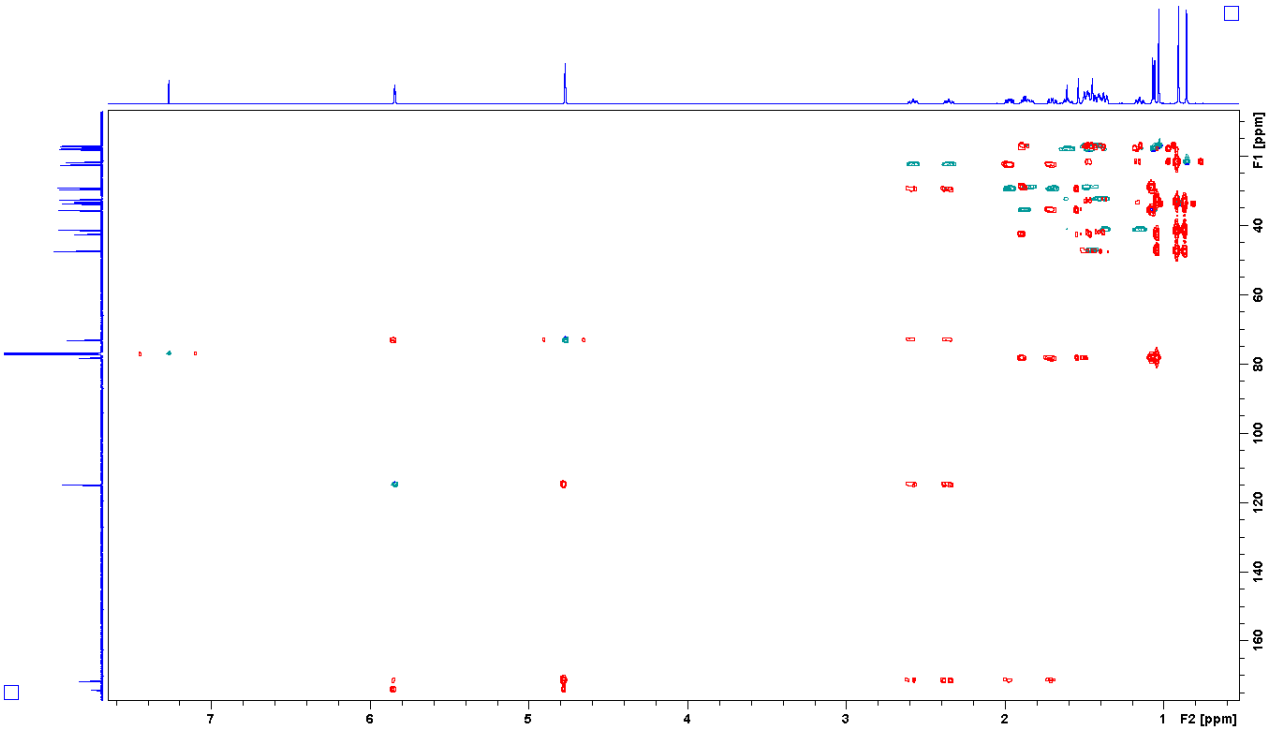

Fig. 4S. HSQC (green) and HMBC(red) overlaid spectra of compound **1** in $CDCl_3$.

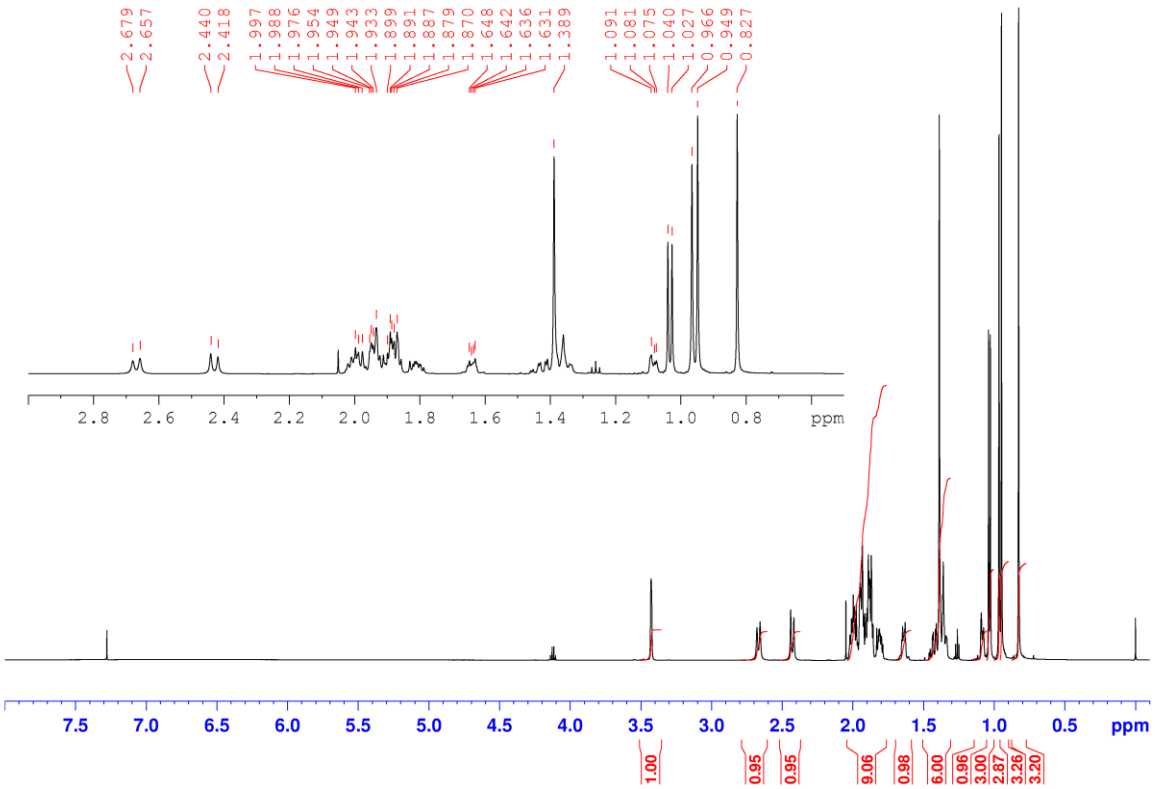

Figure S5: ^{1}H NMR spectrum of compound **2** (600 MHz, $CDCl_3$).

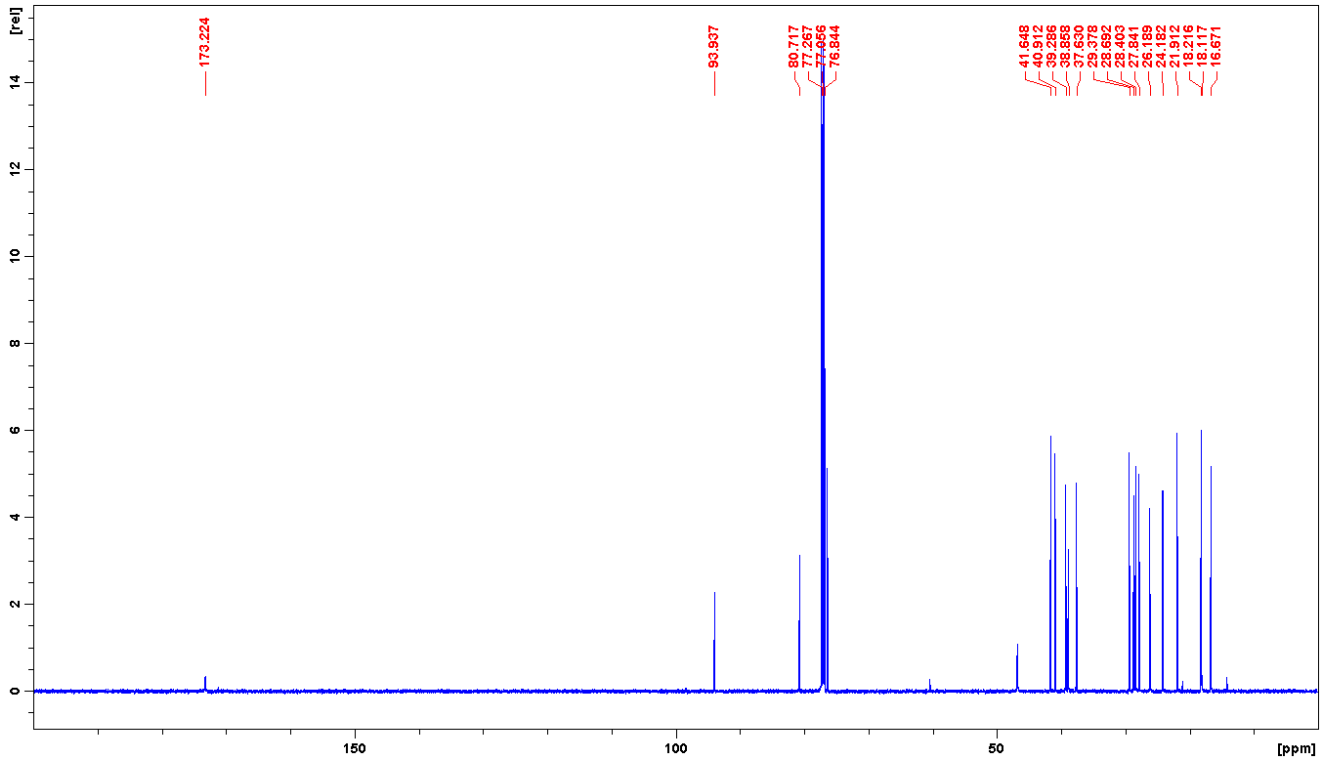

Figure S6:^{13}C NMR spectrum of compound **2** (150 MHz, $CDCl_3$).

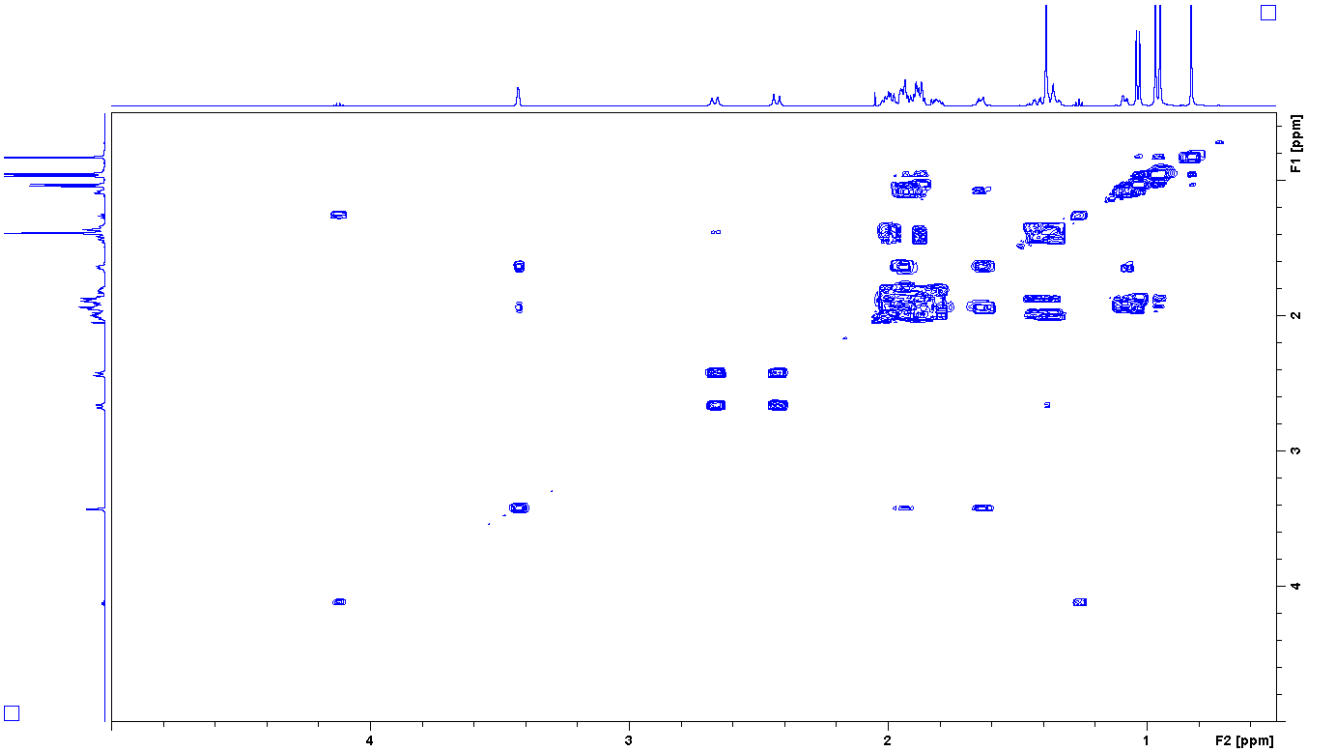

Figure S7: ^{1}H-^{1}H COSY spectrum of compound **2** (600 MHz, $CDCl_3$).

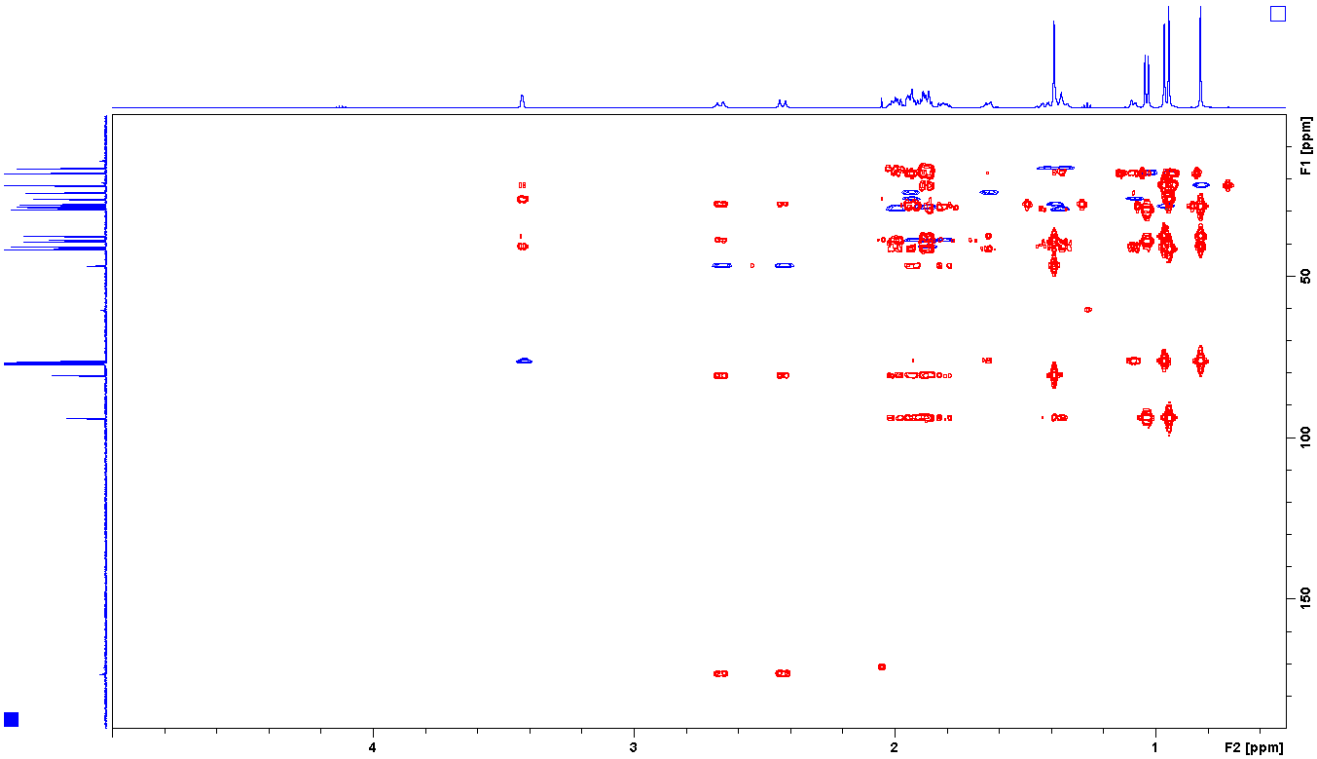

Figure S8: Overlay of HSQC (blue) and HMBC (red) spectra of compound **2** (600 MHz, $CDCl_3$).

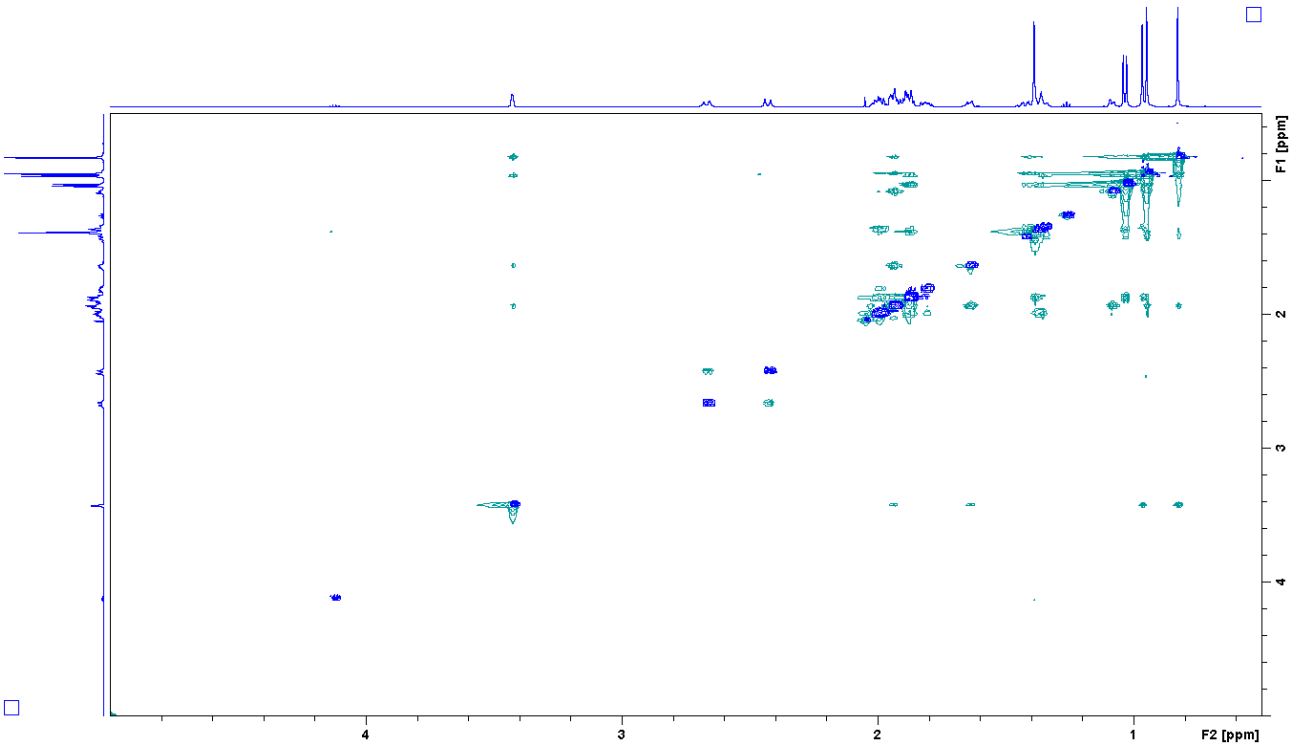

Figure S9: 2D ^{1}H-^{1}H NOESY spectrum of compound **2** (600 MHz, $CDCl_3$).

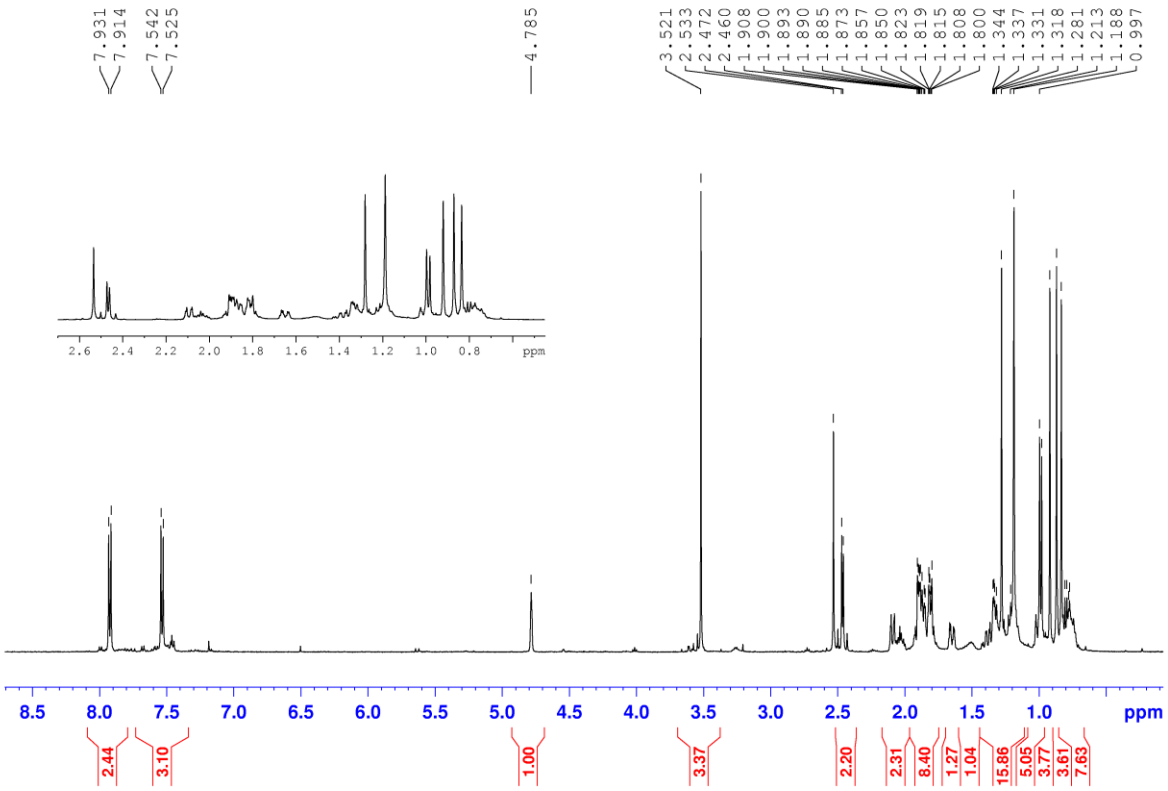

Figure S10: ^{1}H NMR spectrum of 3-*p*-bromobenzoate 15-methyl ester of **2** (500 MHz, $CDCl_3$).

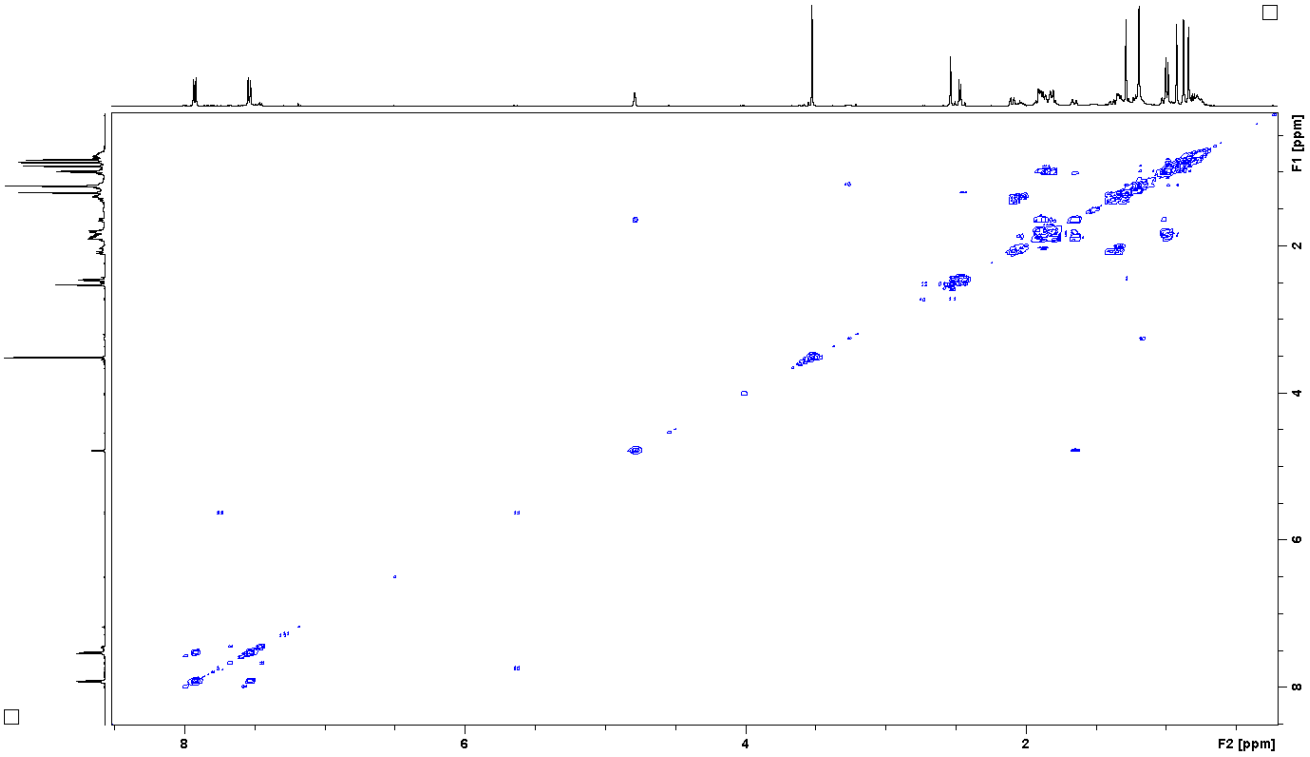

Figure S11: ^{1}H-^{1}H COSY spectrum of 3-*p*-bromobenzoate 15-methyl ester of **2** (500 MHz, $CDCl_3$).

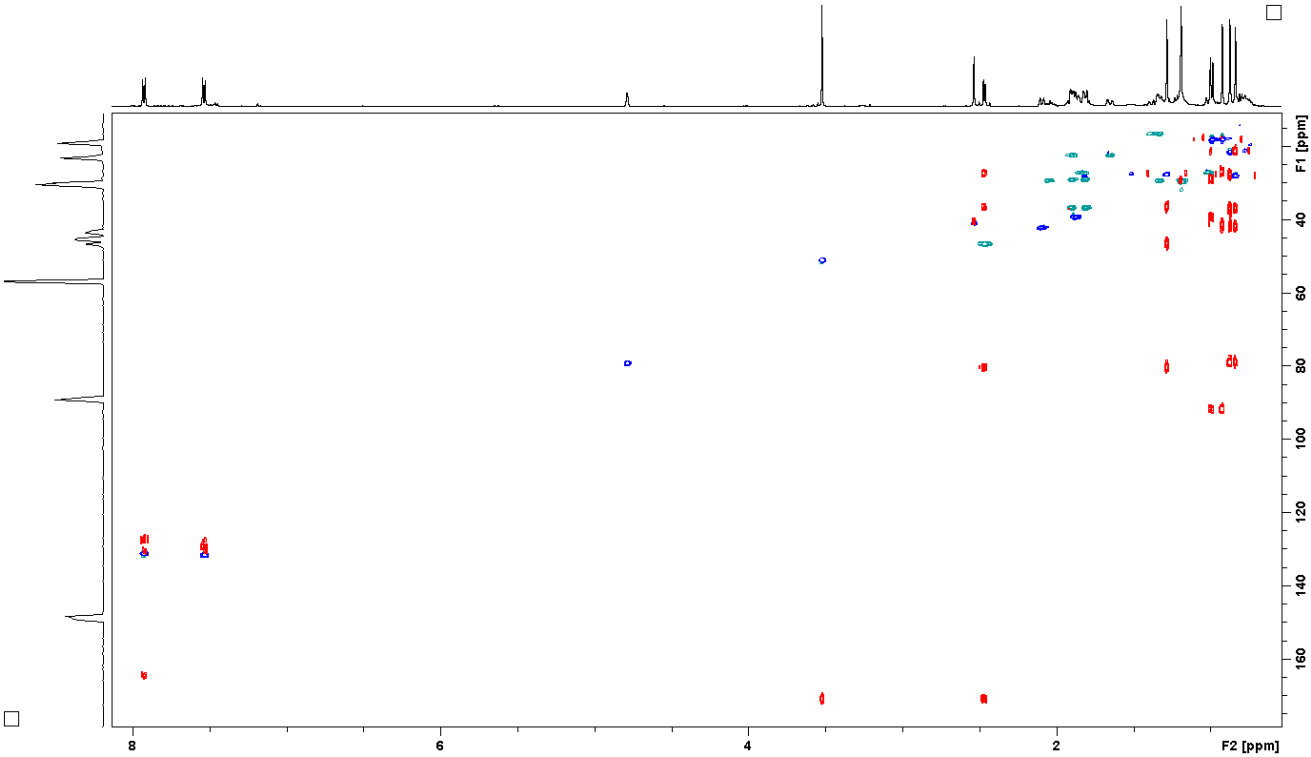

Figure S12: Overlay of HSQC and HMBC spectra of 3-*p*-bromobenzoate 15-methyl ester of **2** (500 MHz, $CDCl_3$).

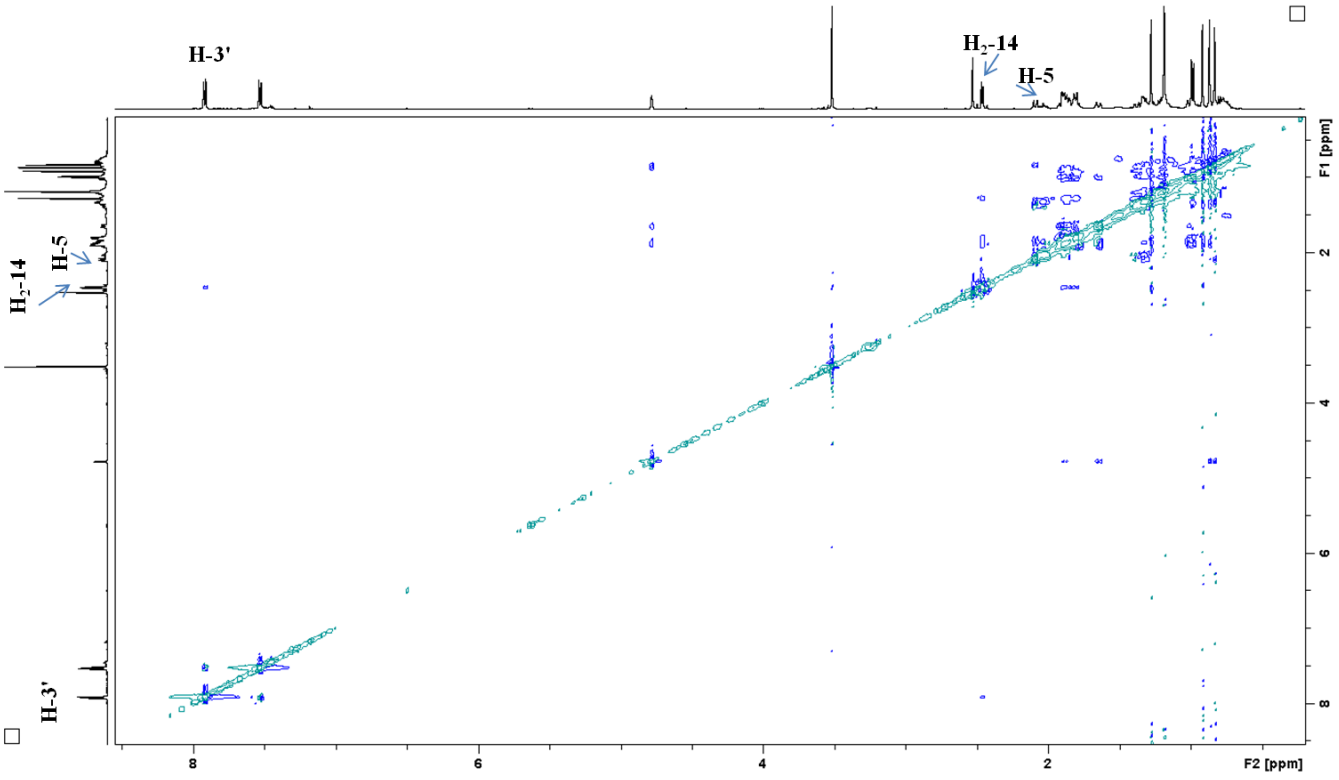

Figure S13: 2D ^{1}H-^{1}H ROESY spectrum of 3-*p*-bromobenzoate 15-methyl ester of **2** (500 MHz, $CDCl_3$).

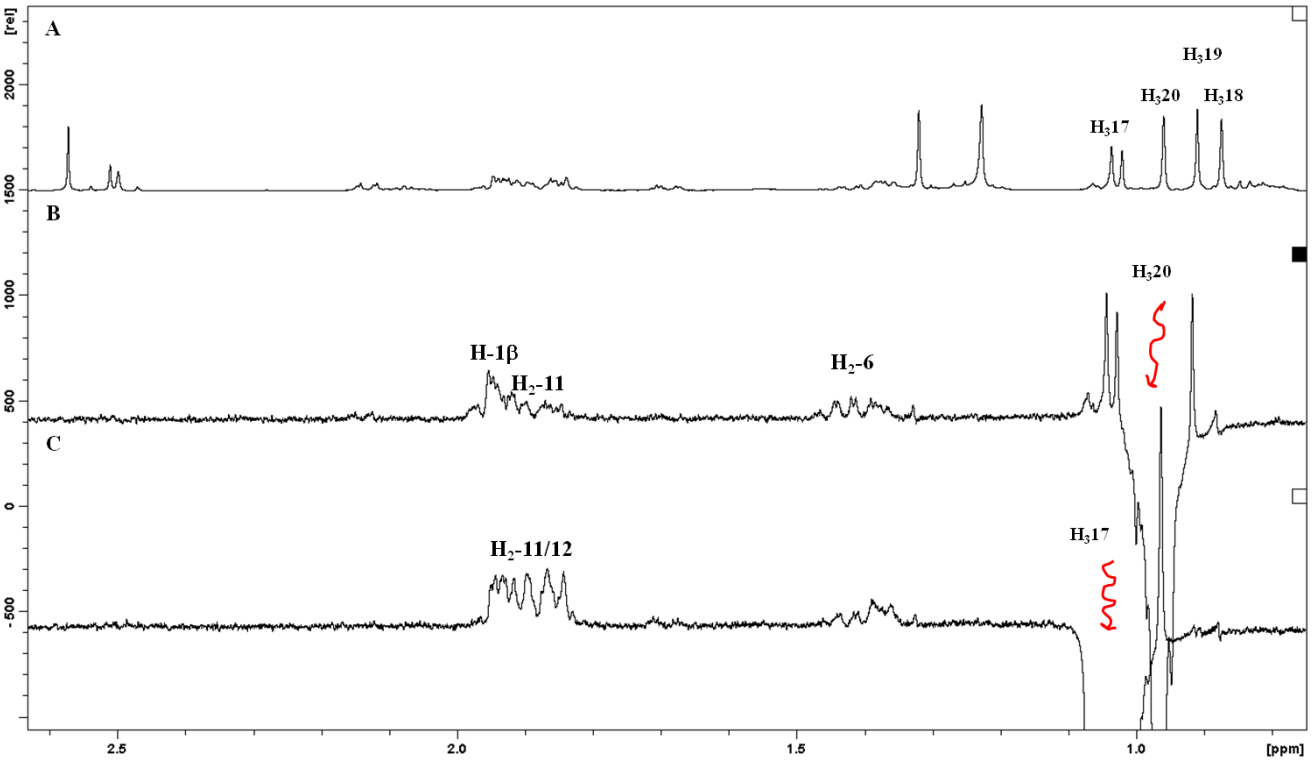

Figure S14: 1D Selective NOESY spectra of 3-*p*-bromobenzoate 15-methyl ester of **2** (D8 = 0.4 sec; 500 MHz, $CDCl_3$).

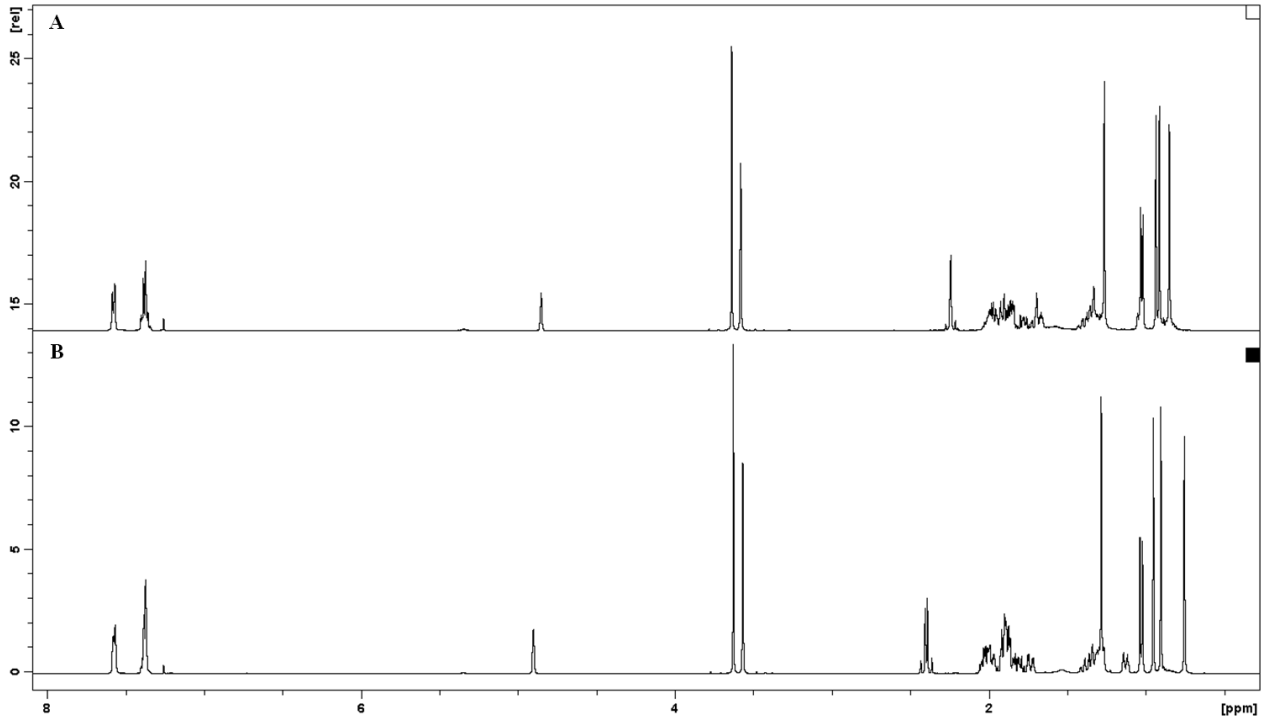

Figure S15: Overlay of ^{1}H NMR spectra of 3-O-(*R*)-MTPA (**A**) and 3-O-(*S*)-MTPA (**B**) esters of compound **2** (500MHz, $CDCl_3$).

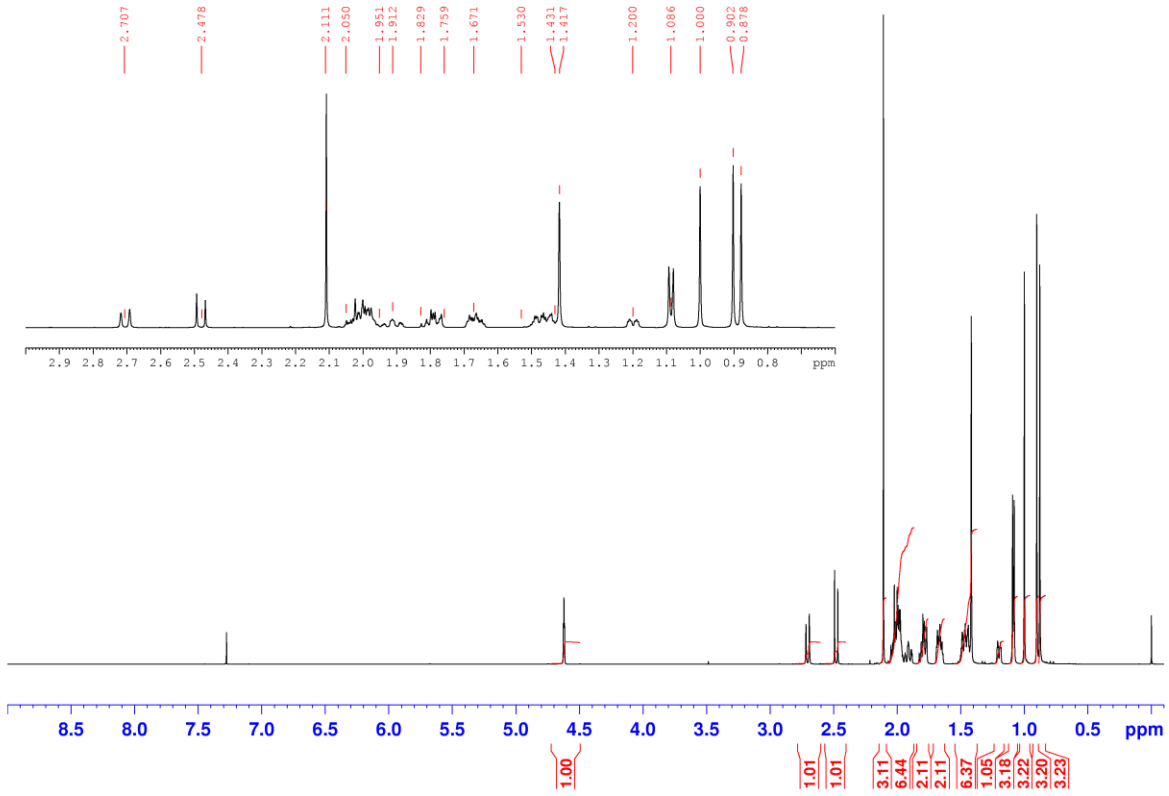

Figure S16: ^{1}H NMR spectrum of compound **3** (600 MHz, $CDCl_3$).

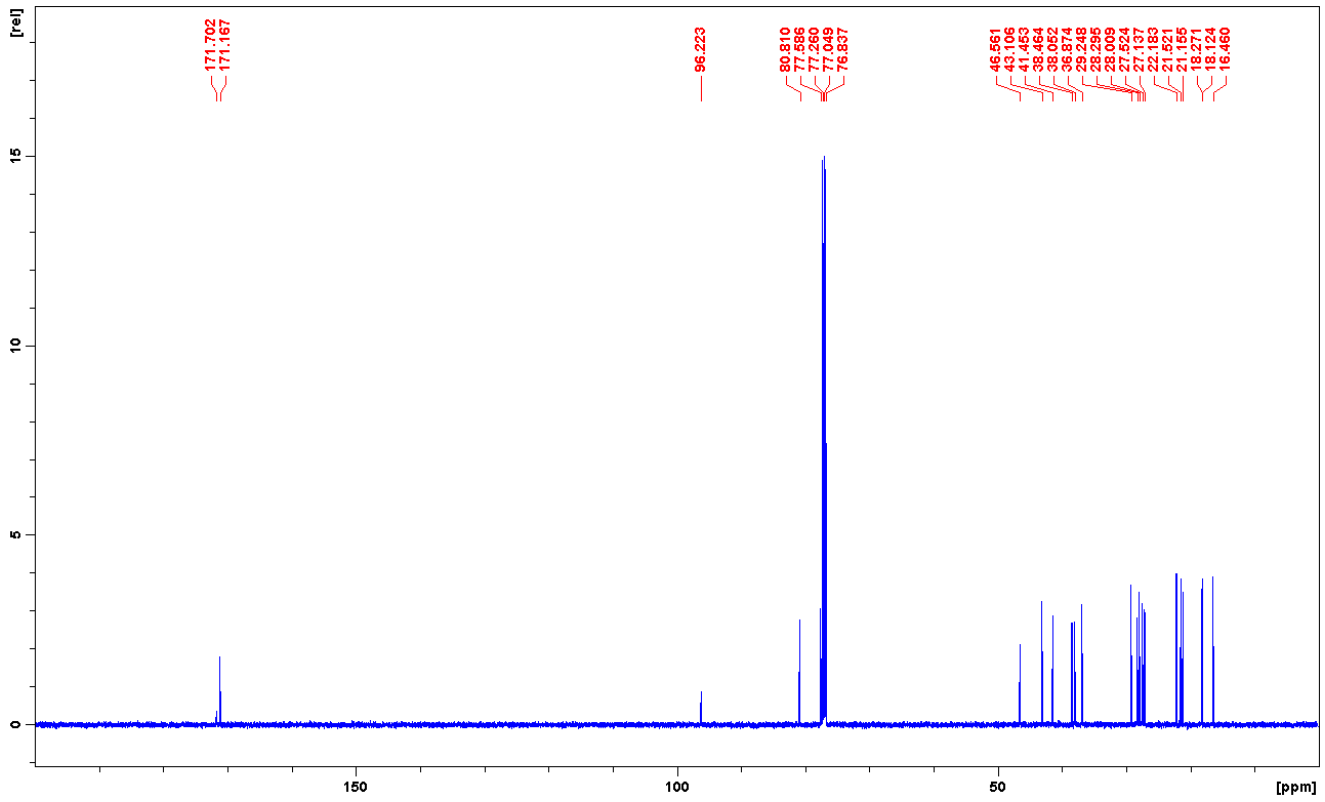

Figure S17: ^{13}C NMR spectrum of compound **3** (125 MHz, $CDCl_3$).

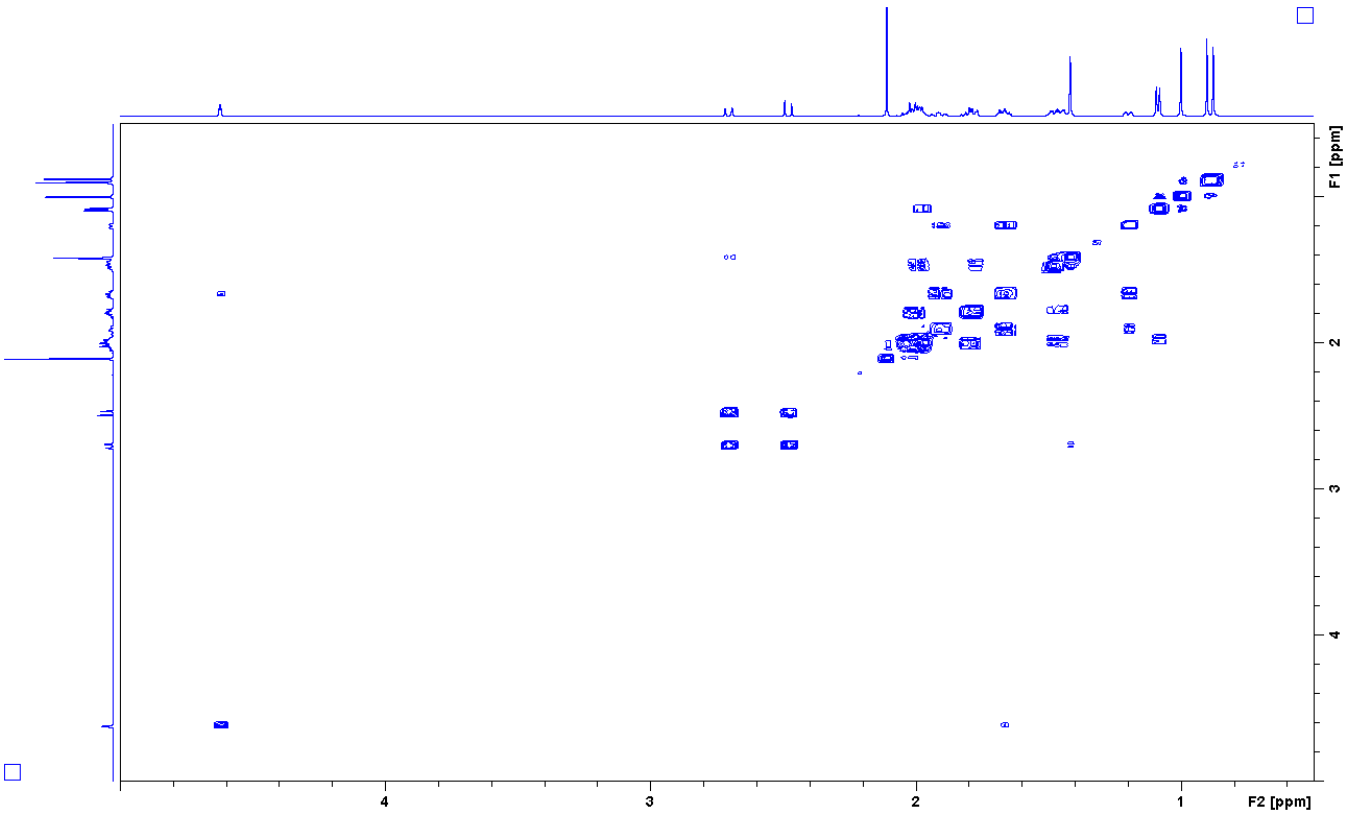

Figure S18: ^{1}H-^{1}H COSY spectrum of compound **3** (600 MHz, $CDCl_3$).

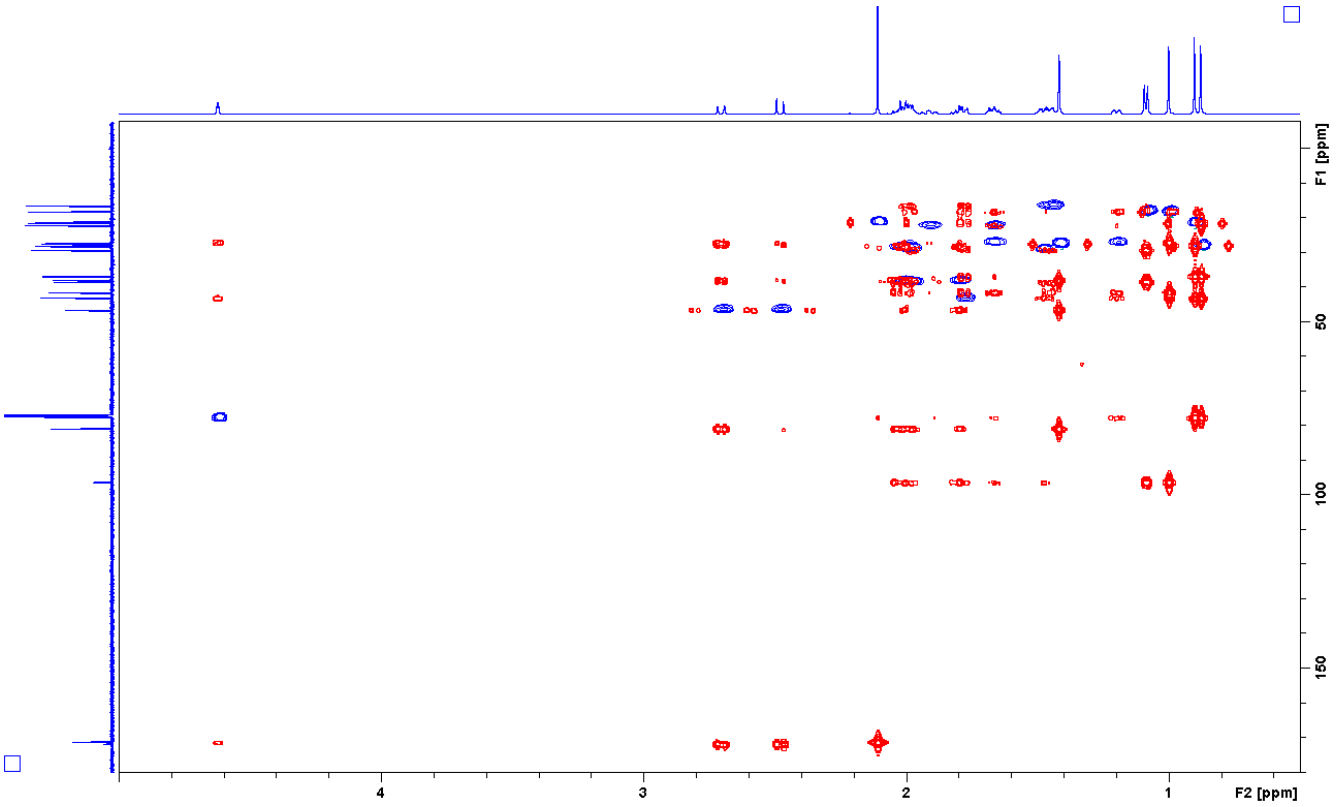

Figure S19: Overlay of HSQC (blue) and HMBC (red) spectra of compound **3** (600 MHz, $CDCl_3$).

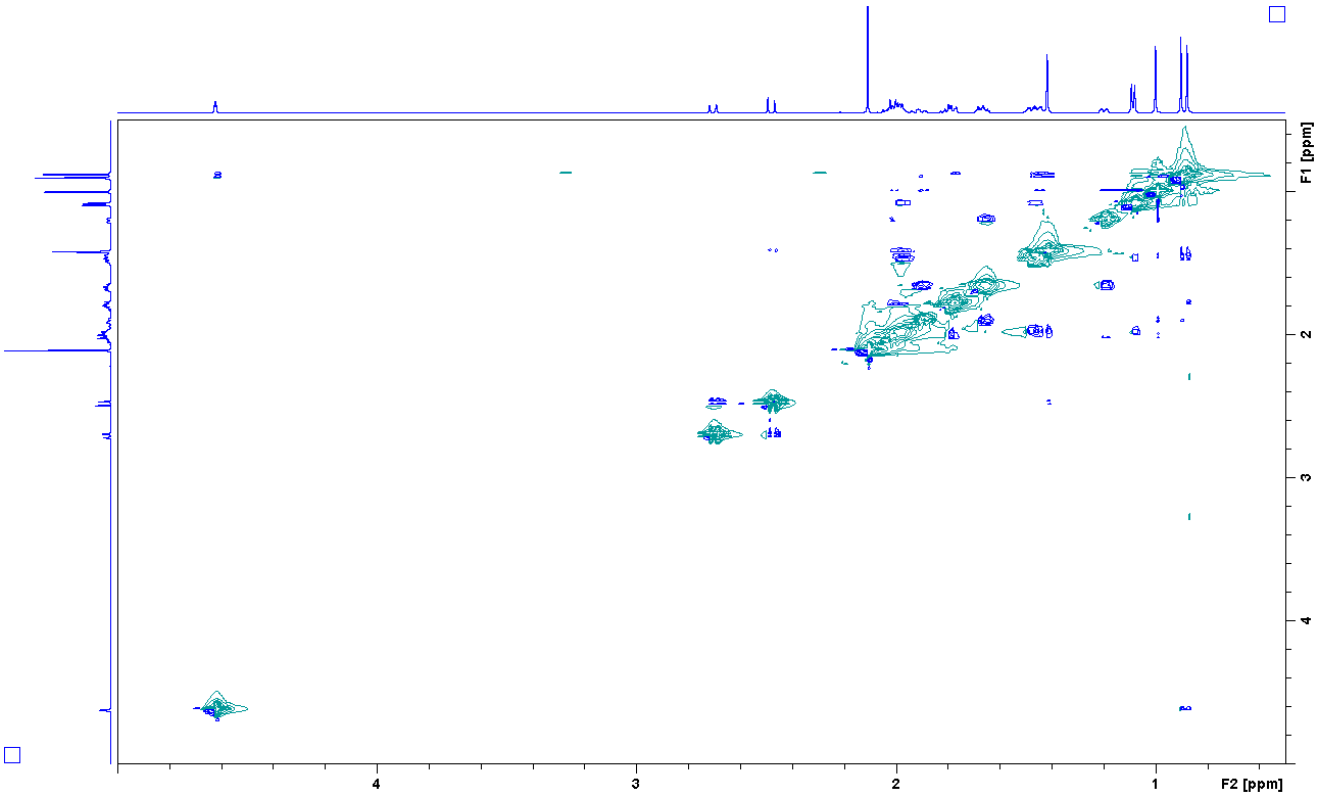

Figure S20: 2D ^{1}H-^{1}H NOESY spectrum of compound **3** (600 MHz, $CDCl_3$).

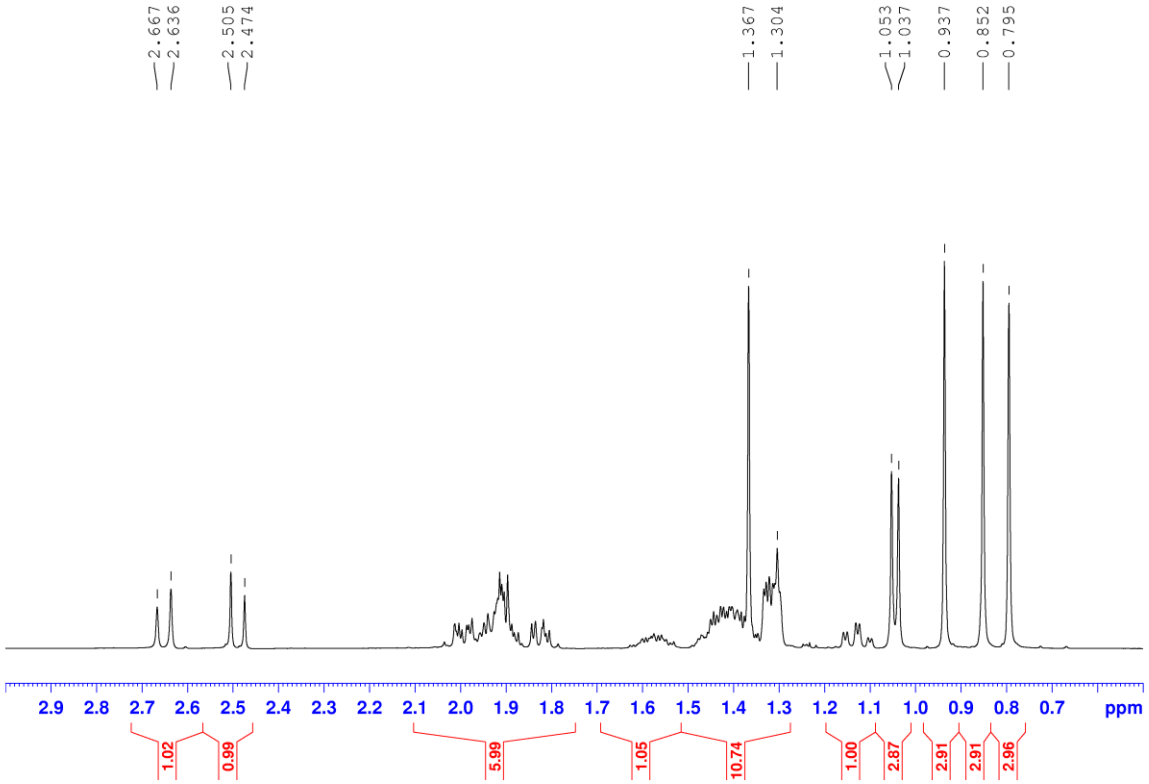

Figure S21: ^{1}H NMR spectrum of compound **5** (500 MHz, $CDCl_3$).

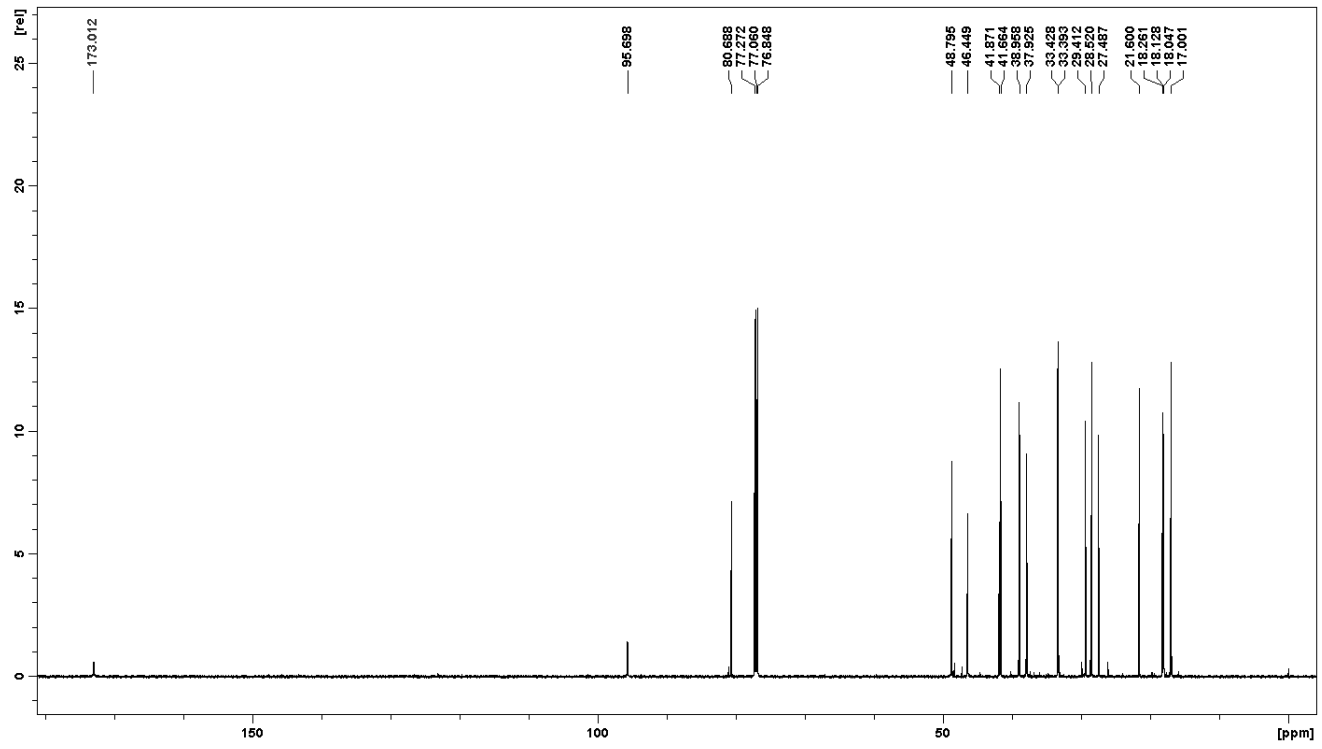

Figure S22: ^{13}C spectrum of compound **5** (150 MHz, $CDCl_3$).

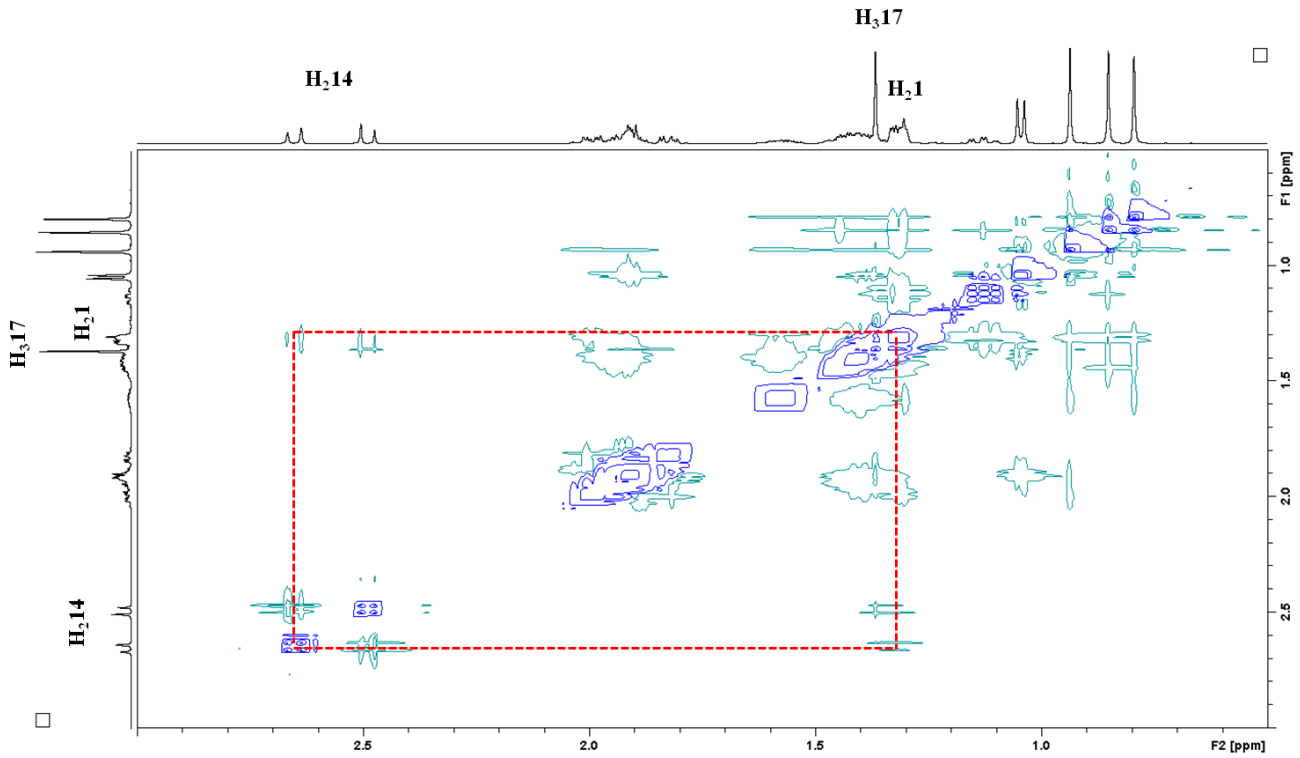

Figure S23: 2D ^{1}H-^{1}H NOESY spectrum of compound **5** (500 MHz, $CDCl_3$). The red square underlines the key H_2-14/H_2-1 that allowed to assign the *rel*-13-(*R*) stereochemistry.

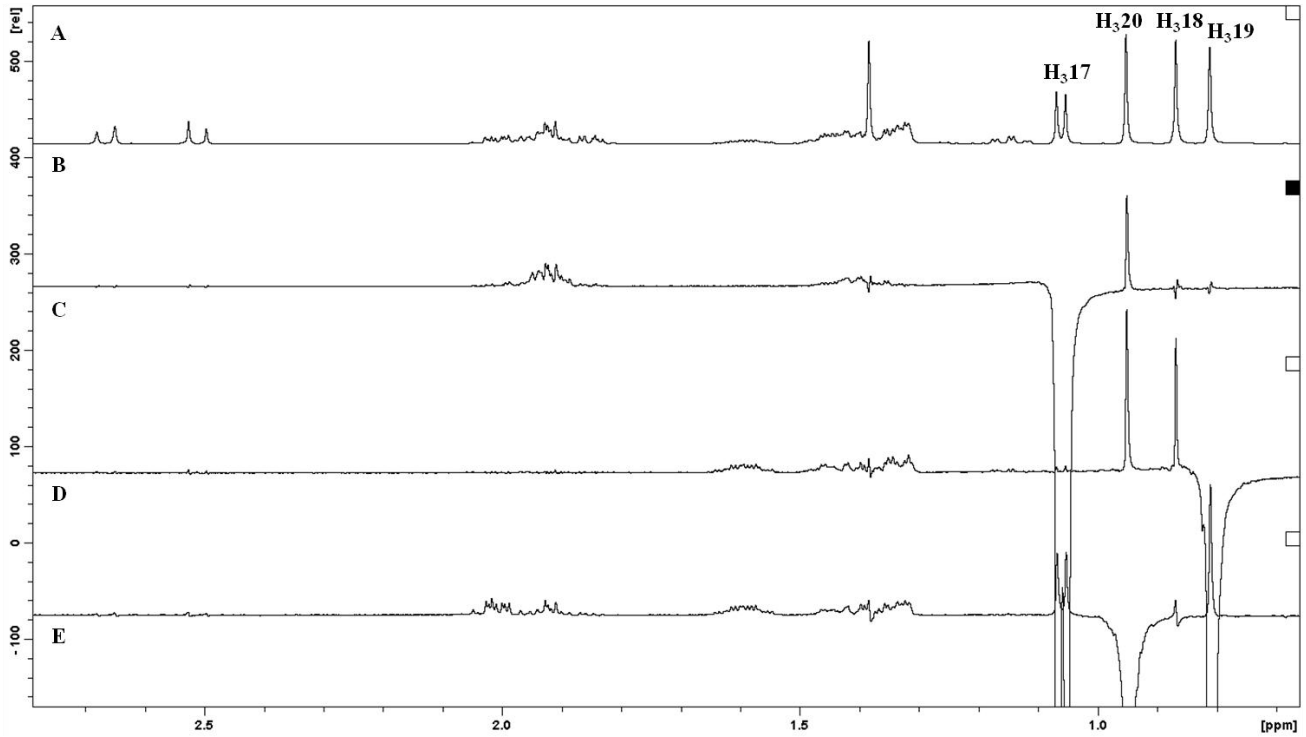

Figure S24: 1D Selective NOESY spectra of compound **5** (500 MHz, $CDCl_3$; D8=0.7 sec) (**A**) Full ^{1}H NMR spectrum (**B**-**E**) Selective irradiations of H_3-17/19/20 that confirm their cophacial orientation.

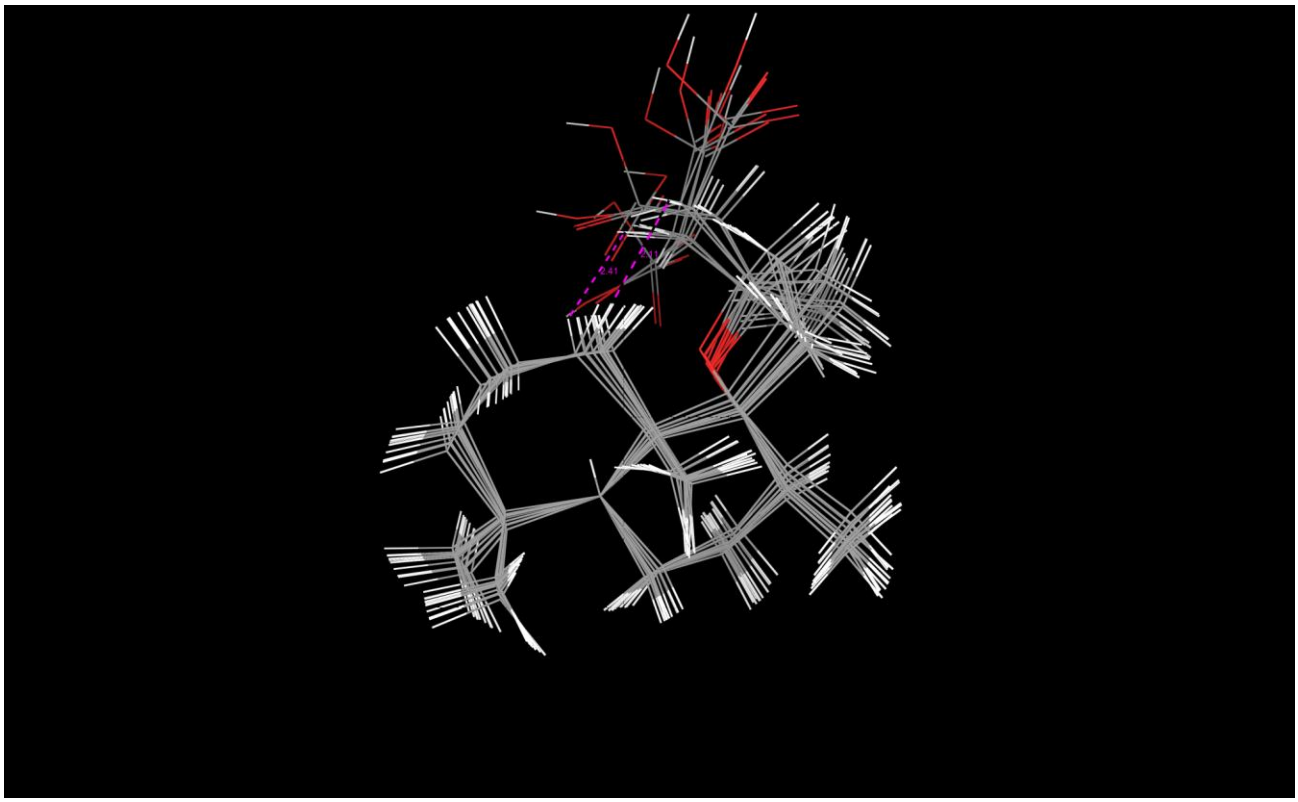

Figure S25: Superimposed conformers of compound **5** within 2Kcal from the global minimum. The key distance H_2-1/H_2-14 is underlined in Å.

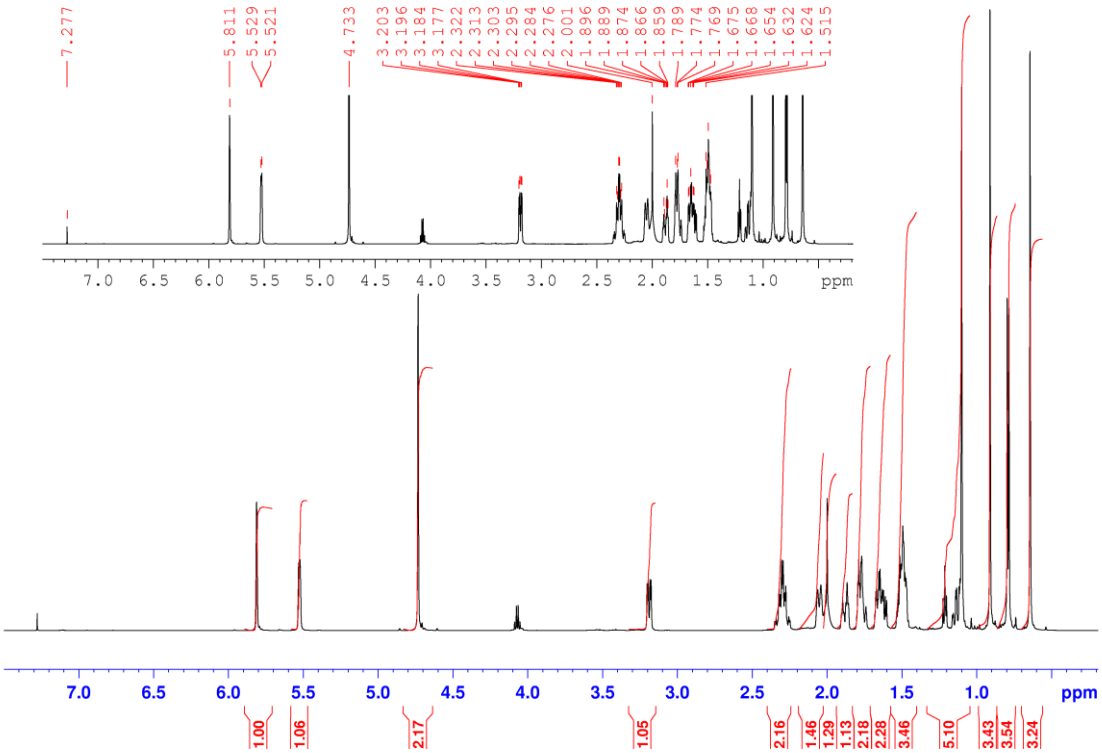

Figure S26: ^{1}H NMR spectrum of compound **6** (600 MHz, $CDCl_3$).

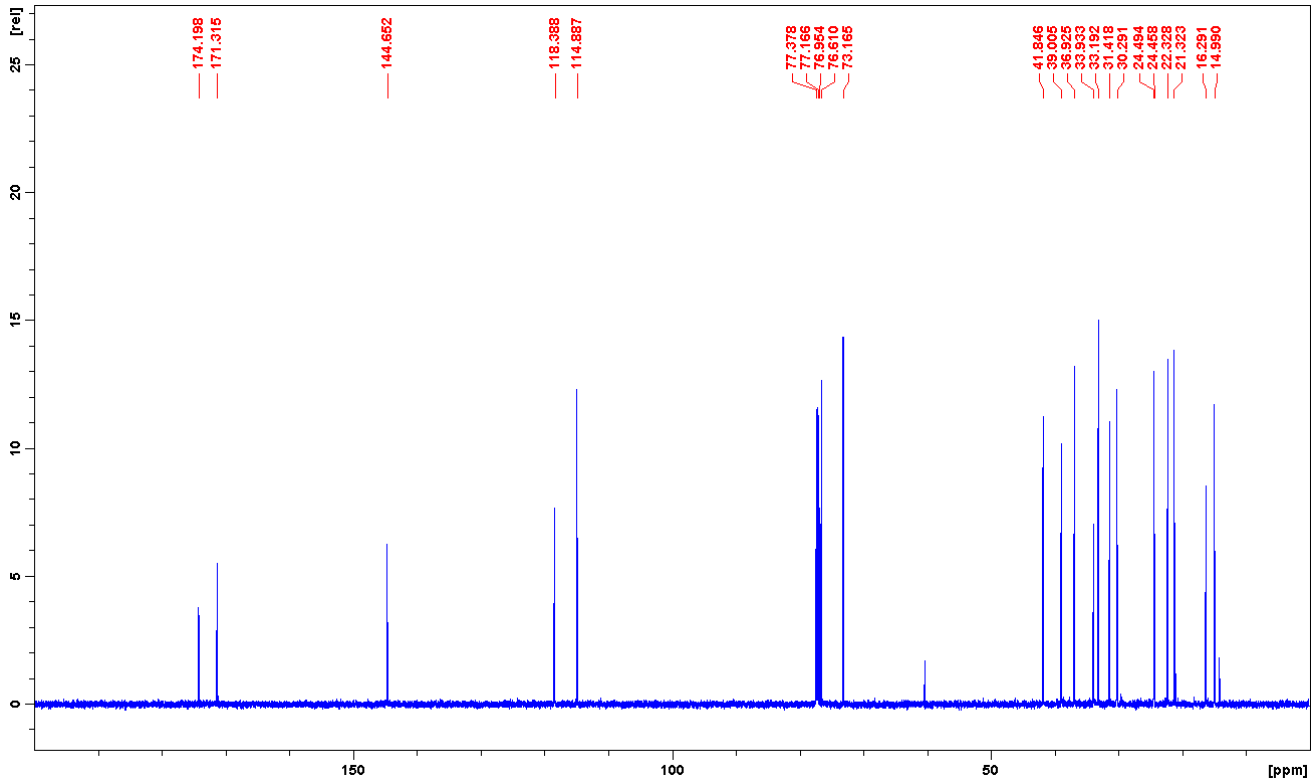

Figure S27: ^{13}C NMR spectrum of compound **6** (150 MHz, $CDCl_3$).

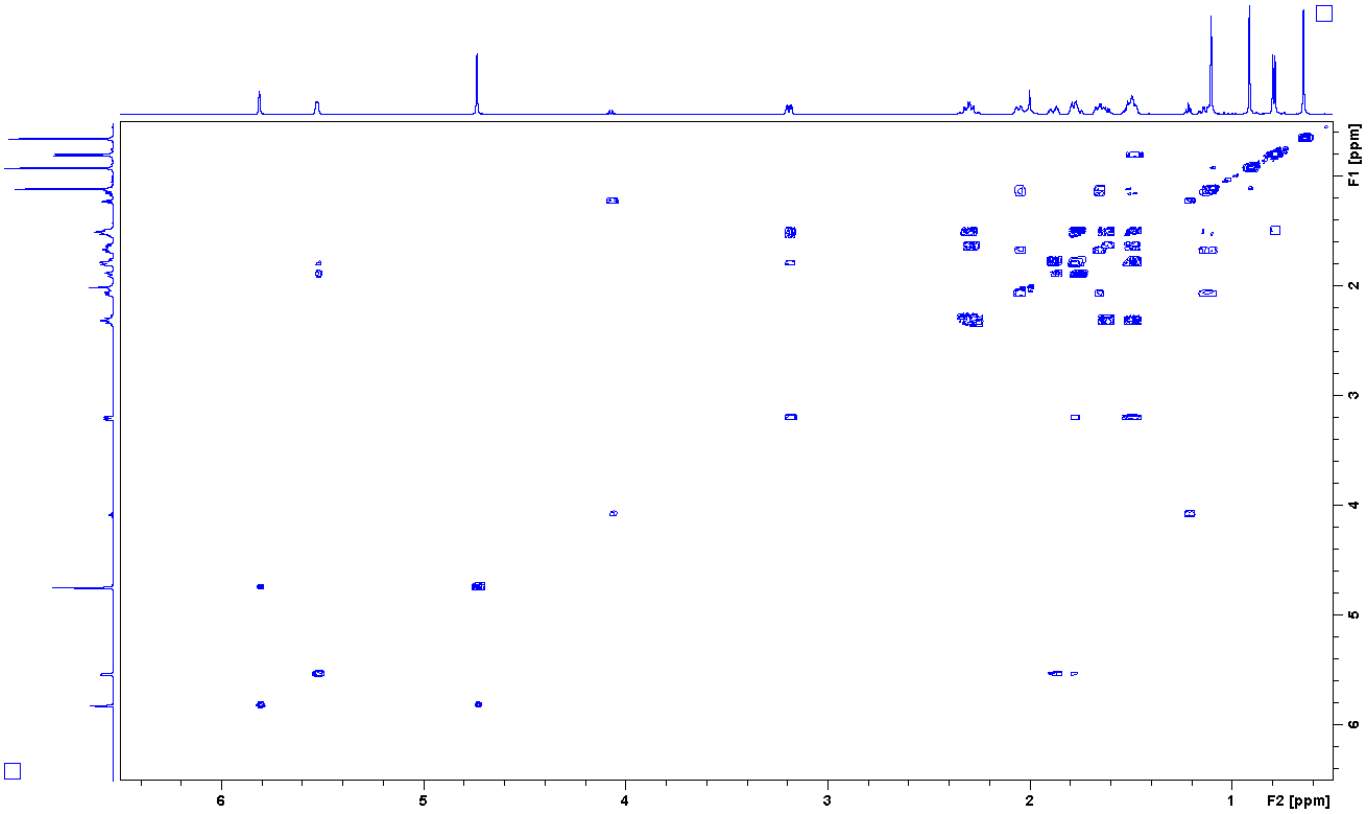

Figure S28: ^{1}H-^{1}H COSY spectrum of compound **6** (600 MHz, $CDCl_3$).

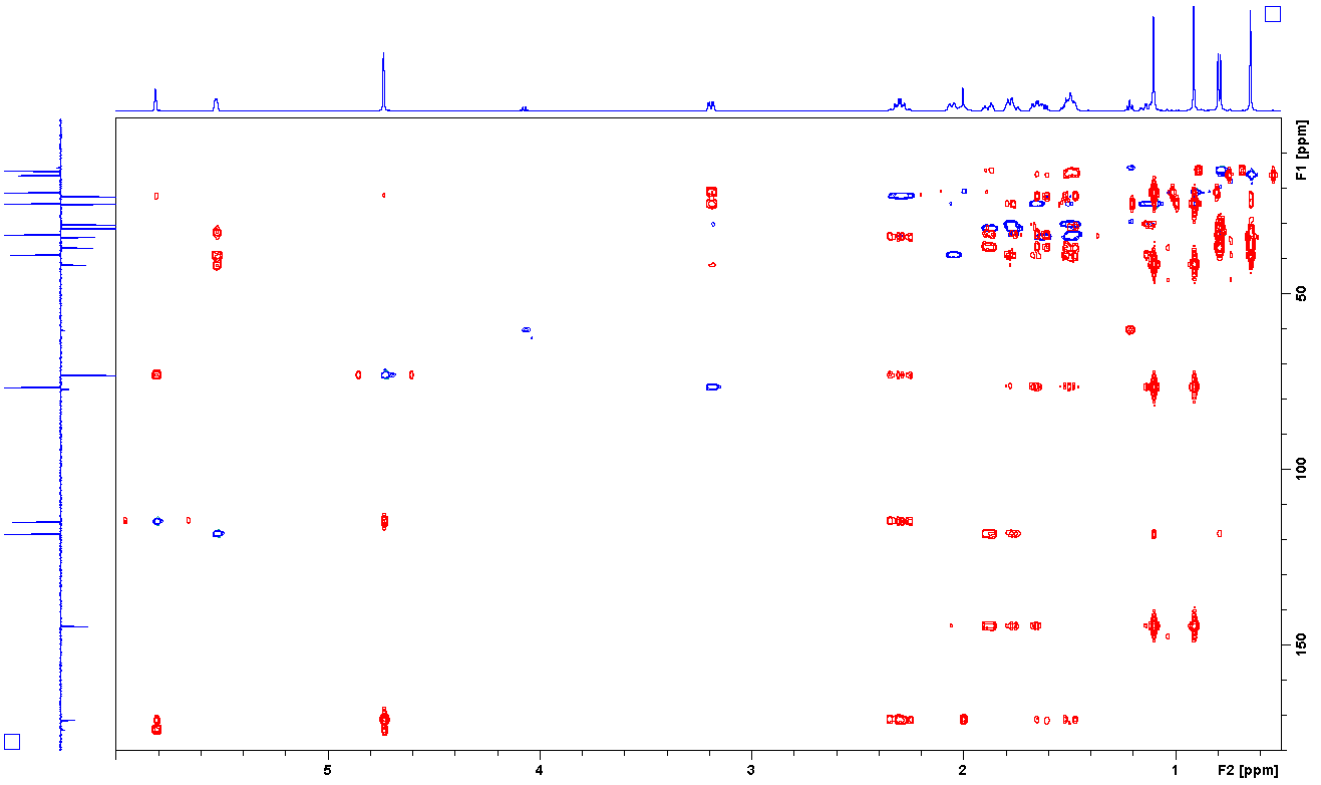

Figure S29: HSQC (blue) and HMBC (red) overlaid spectra of compound **6** (600 MHz, $CDCl_3$).

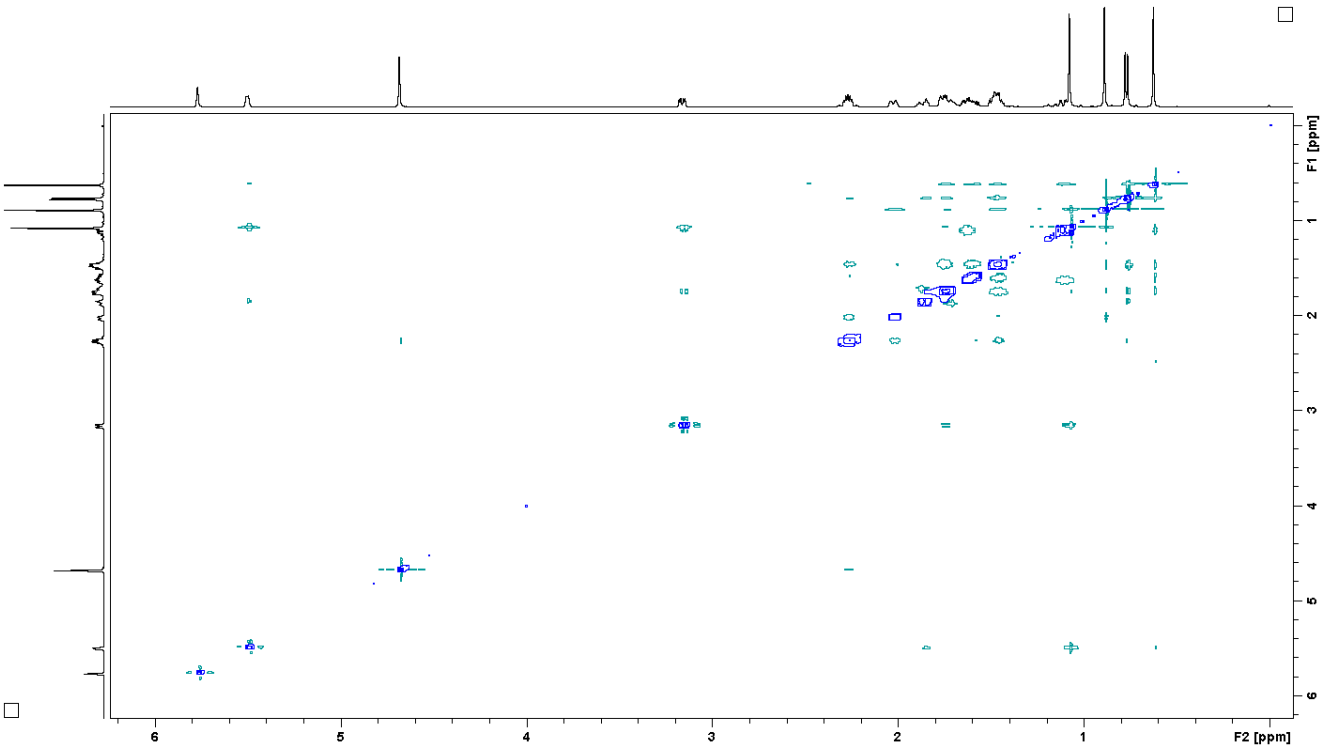

Figure S30: 2D ^{1}H-^{1}H NOESY spectrum of compound **6** (600 MHz, $CDCl_3$).

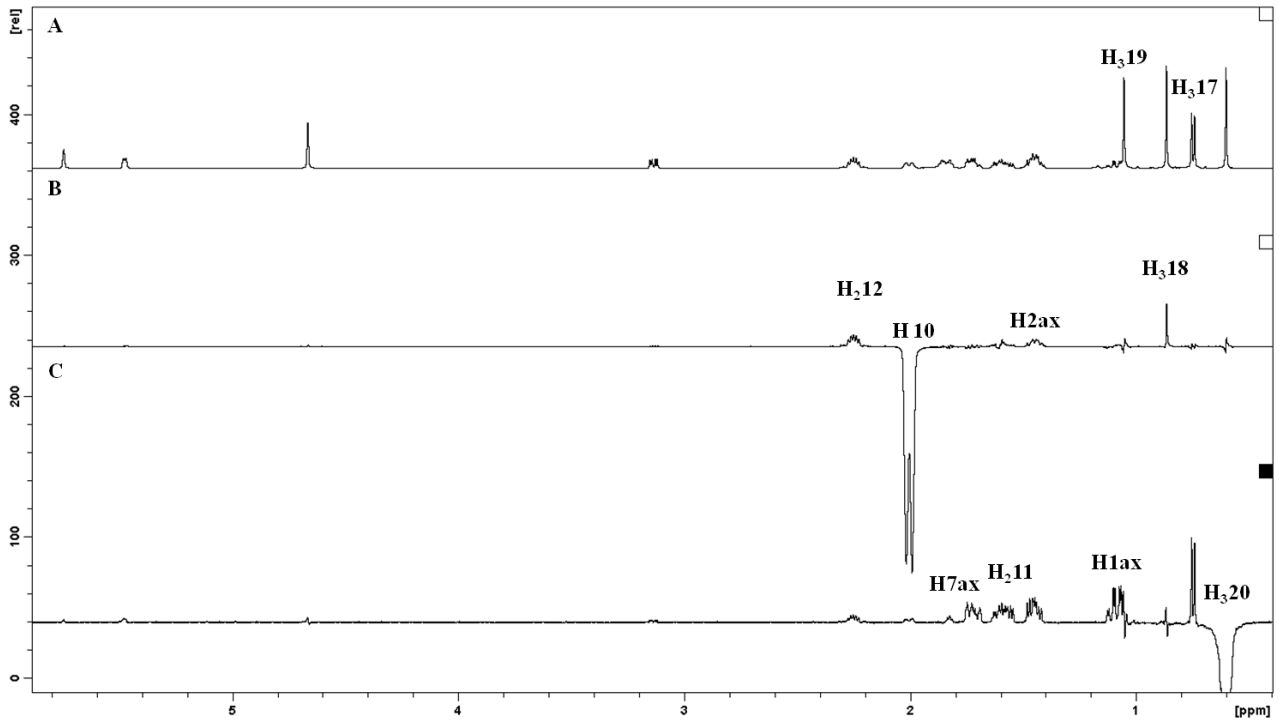

Figure S31: 1D Selective NOESY spectra of compound **6** (500 MHz, $CDCl_3$) (**A**) Full ^{1}H NMR spectrum; (**B**) Selective irradiation of H-10 (D8 = 0.7 sec); (**C**) selective irradiation of $H_3$20 (D8 = 0.7 sec).

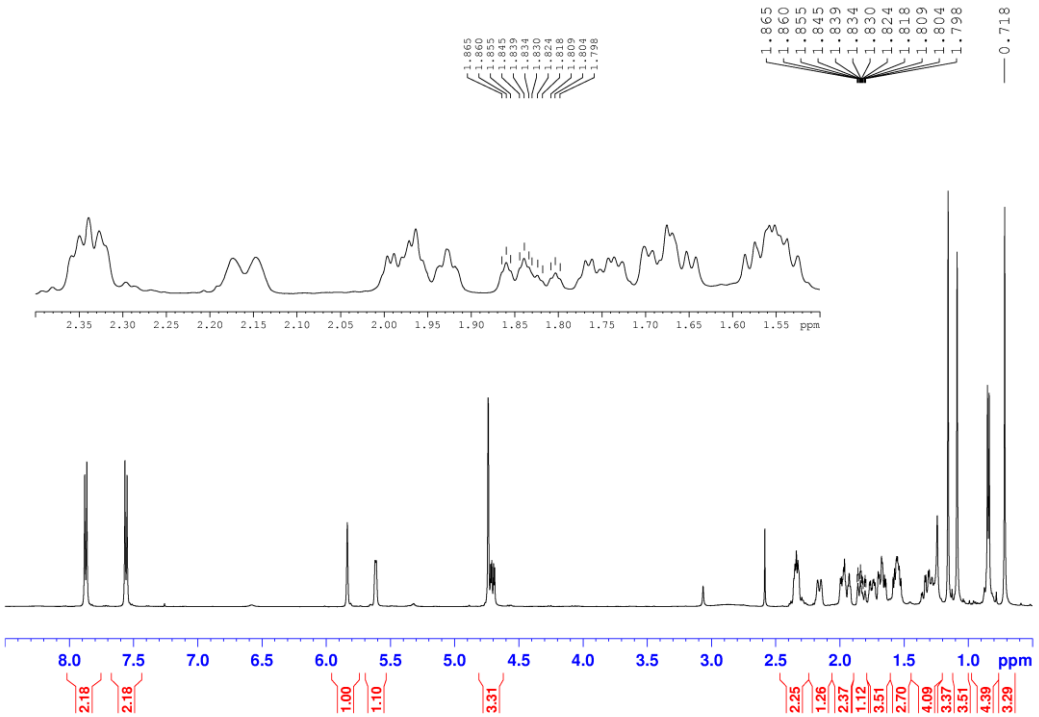

Figure S32: ^{1}H NMR spectrum of 3-*p*-bromobenzoate derivative of compound **6** (500 MHz, $CDCl_3$).

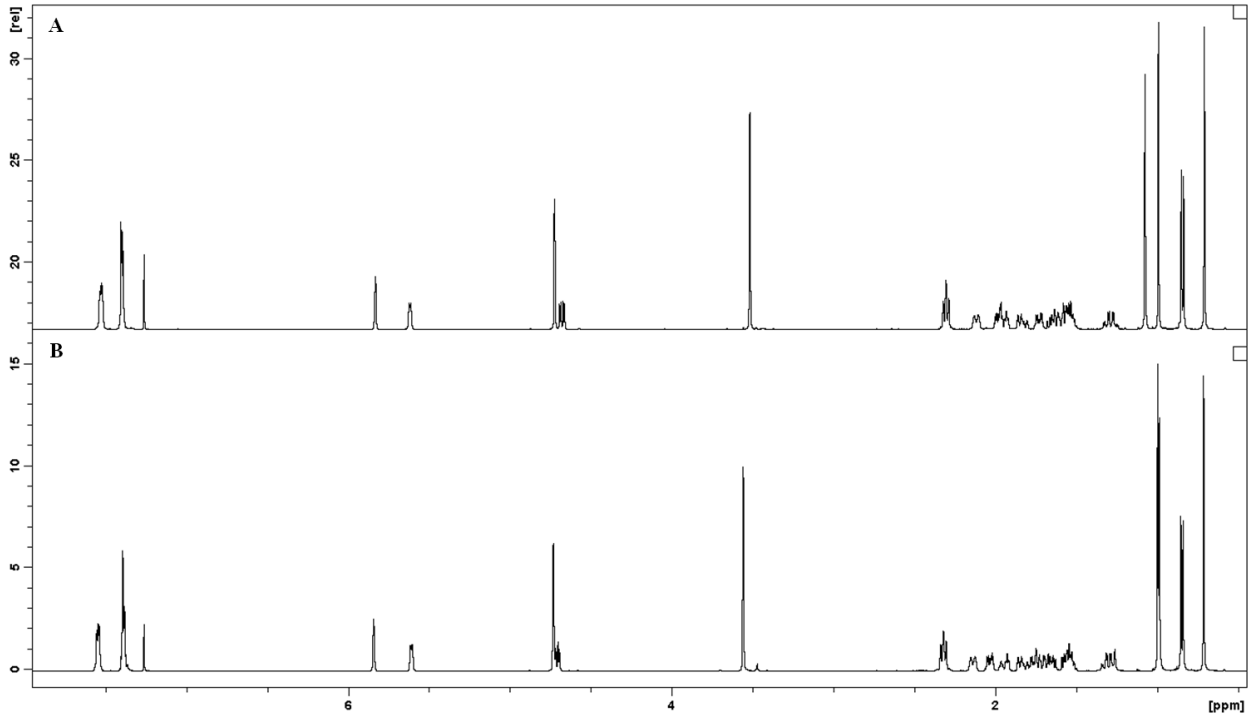

Figure S33: Overlay of ^{1}H-NMR spectra of (*R*)-MTPA (**A**) and (*S*)-MTPA (**B**) esters of compound **2** (500MHz, $CDCl_3$).

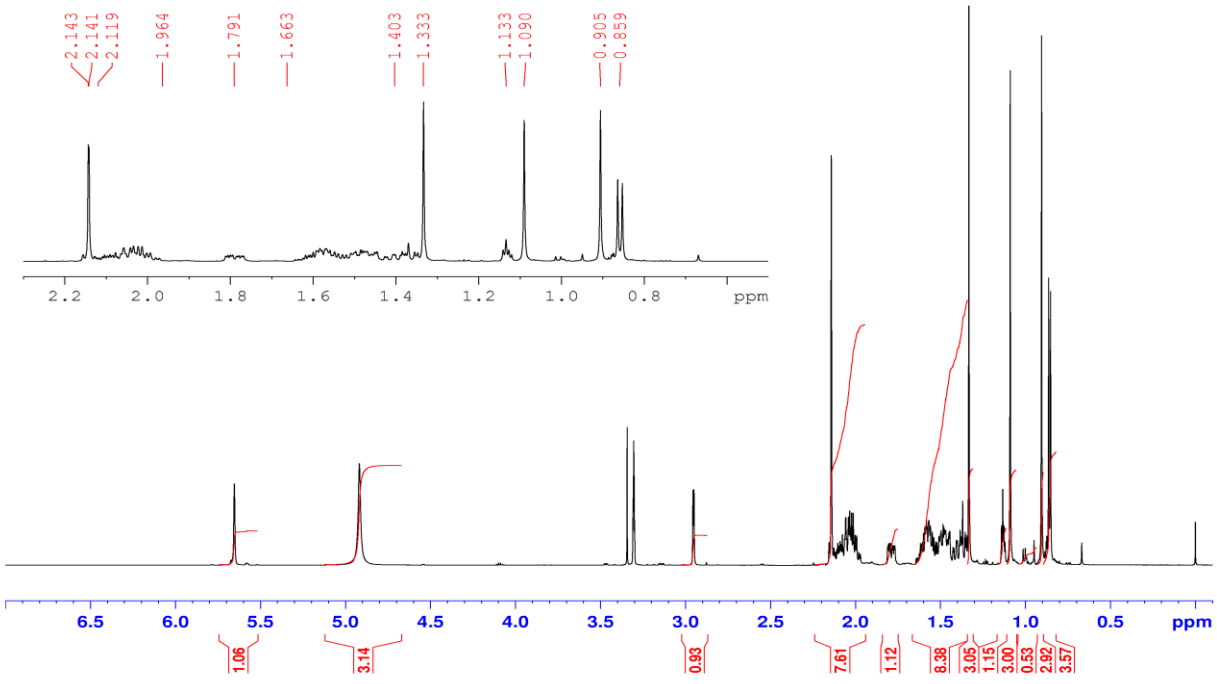

Figure S34: ^{1}H NMR spectrum of compound **7** (600 MHz, methanol-d_4).

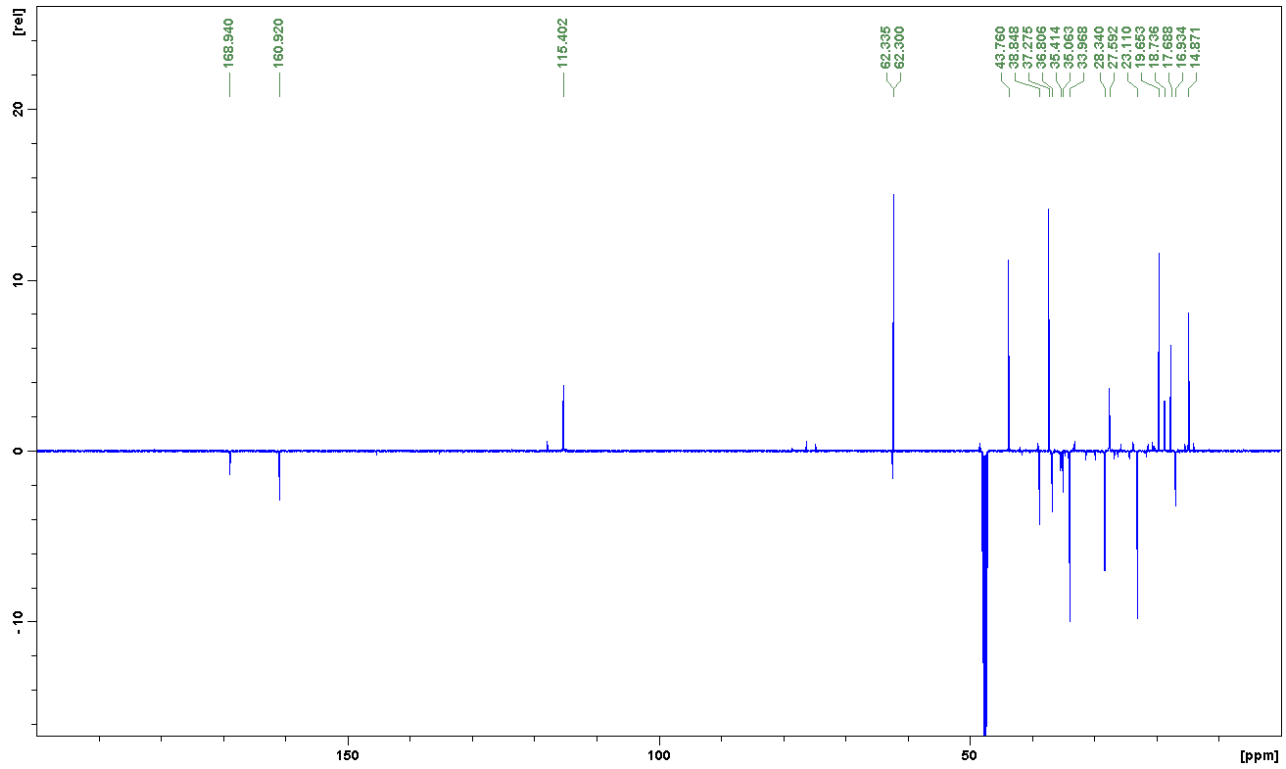

Figure S35: ^{13}C NMR spectrum of compound **7** (150 MHz, methanol-d_4).

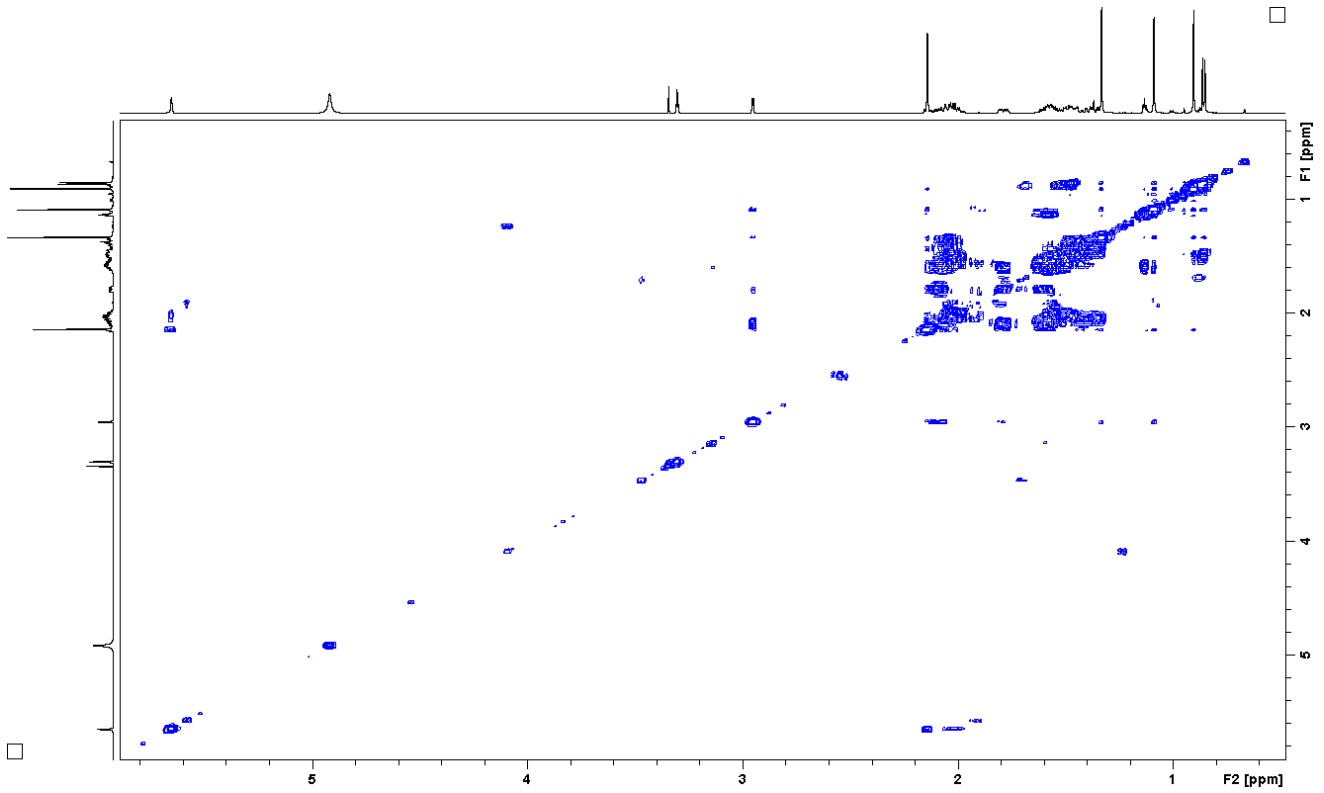

Figure S36: ^{1}H-^{1}H COSY spectrum of compound **7** (600 MHz, methanol-d_4).

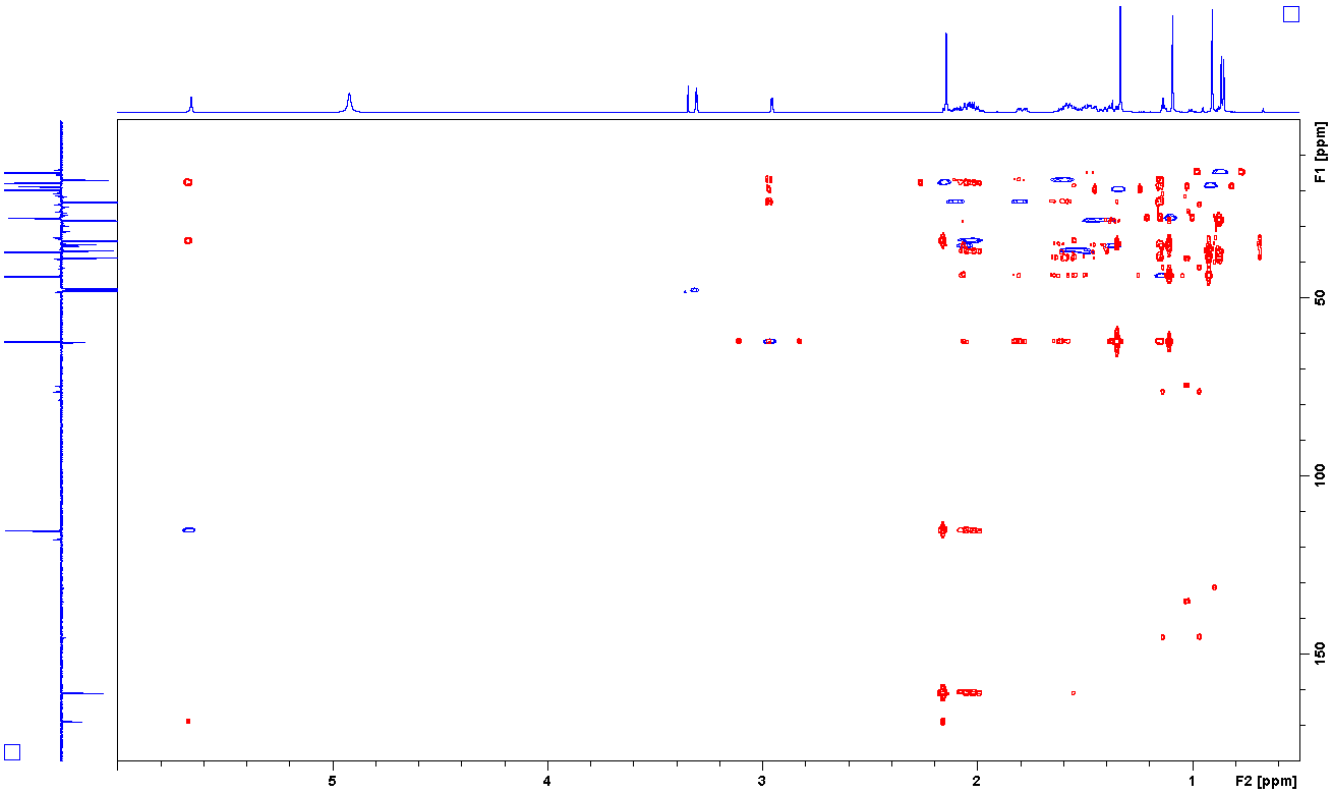

Figure S37: Overlay of HSQC (blue) and HMBC (red) spectra of compound **7** (600 MHz, methanol-d_4).

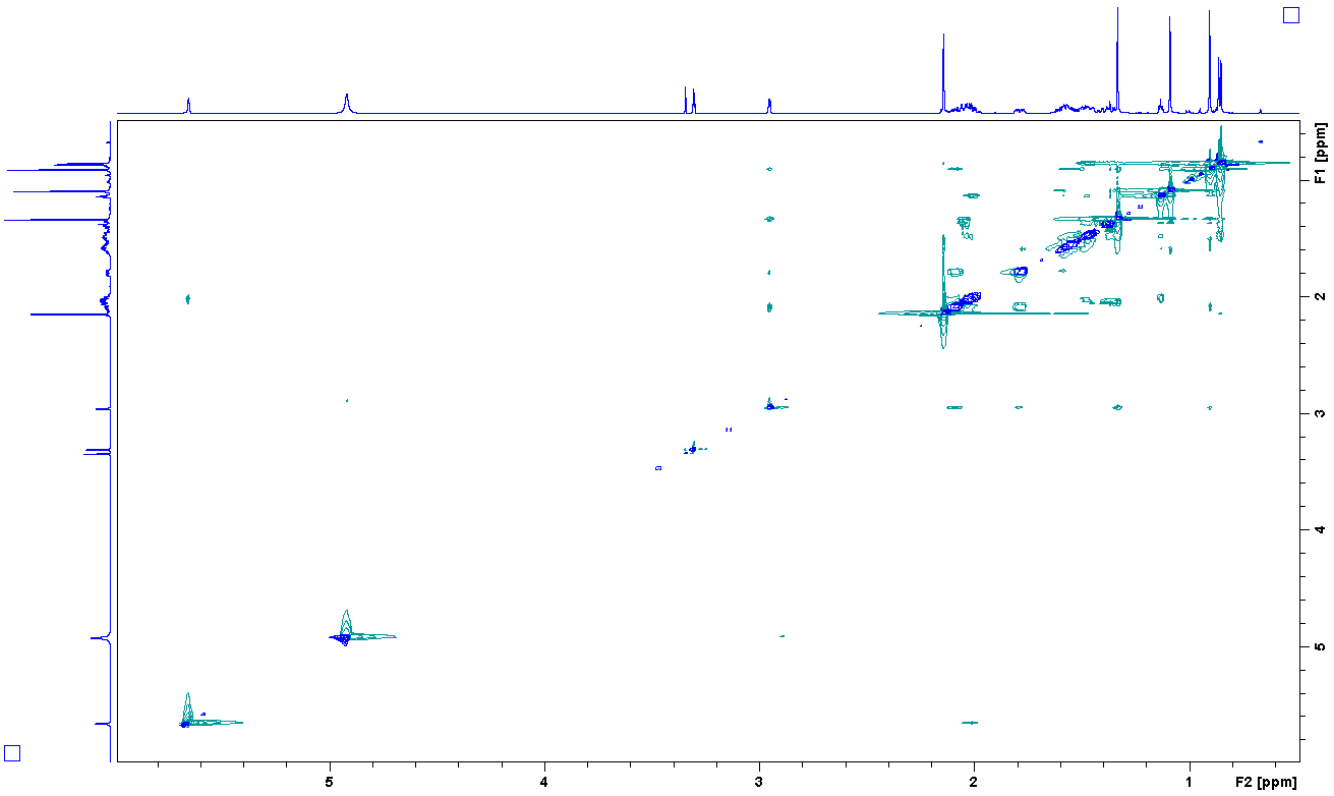

Figure S38: 2D ^{1}H-^{1}H NOESY spectrum of compound **7** (600 MHz, methanol-d_4).

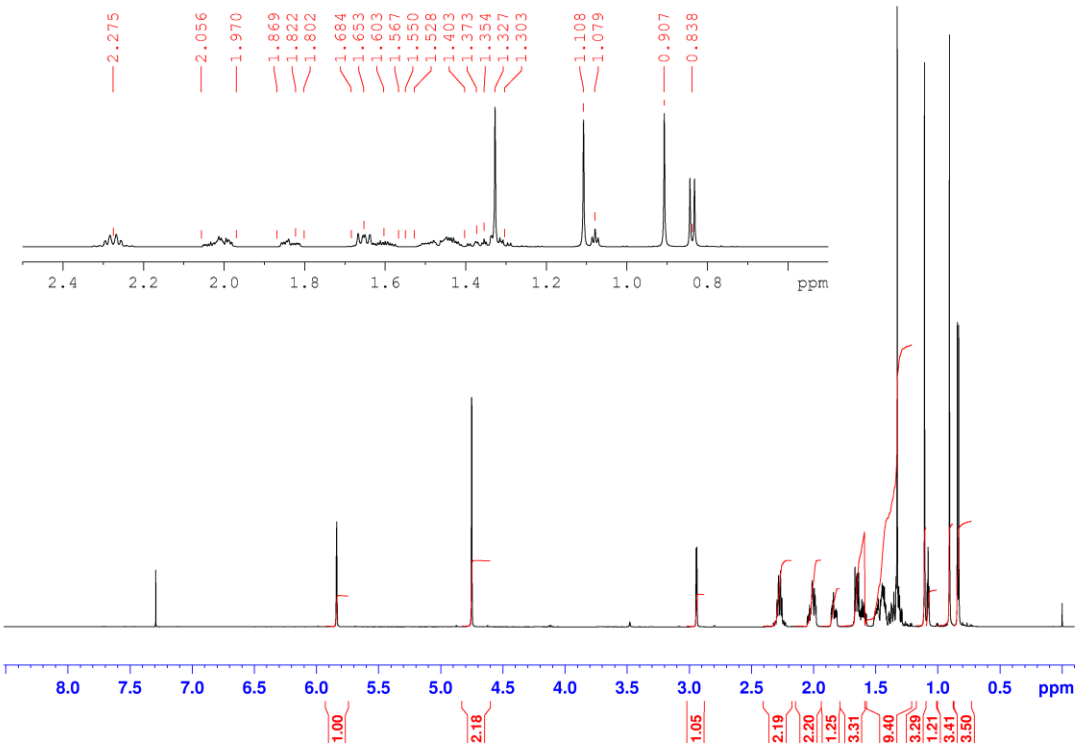

Figure S39: ^{1}H NMR spectrum of compound **8** (600 MHz, $CDCl_3$).

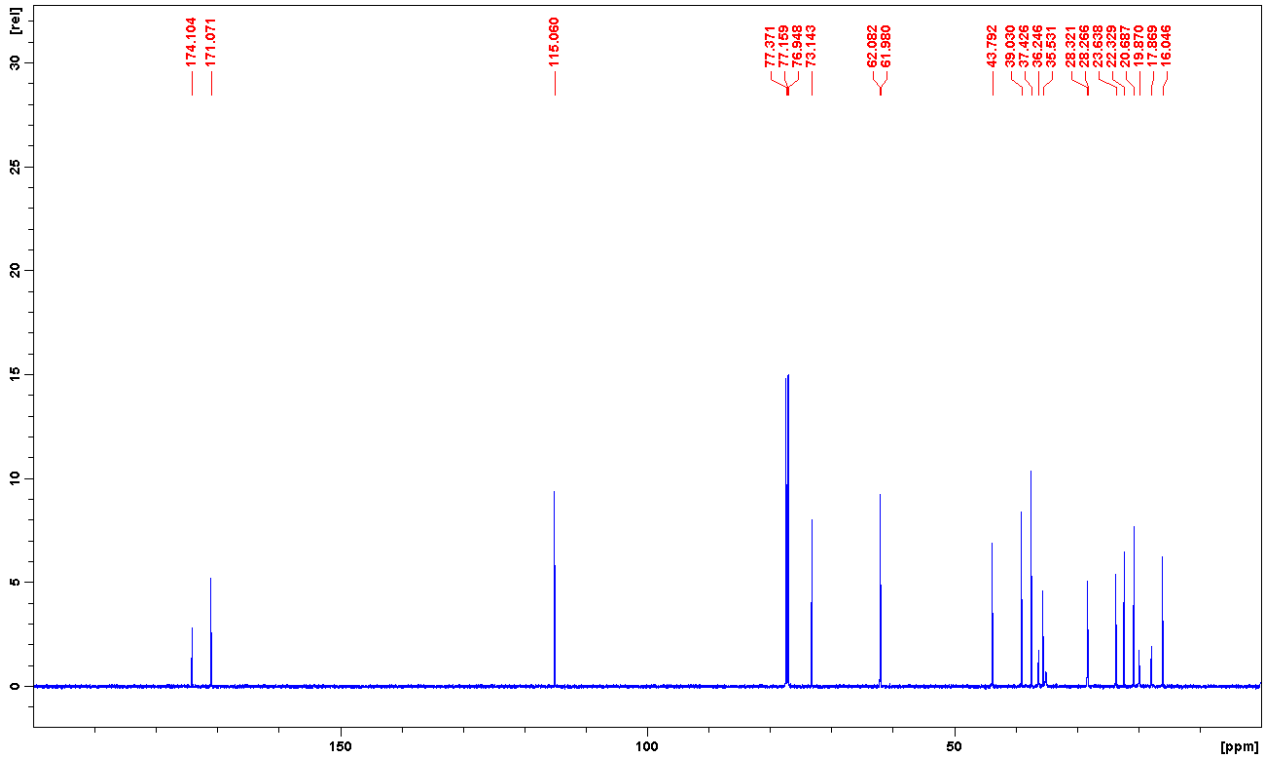

Figure S40: ^{13}C NMR spectrum of compound **8** (150 MHz, $CDCl_3$).

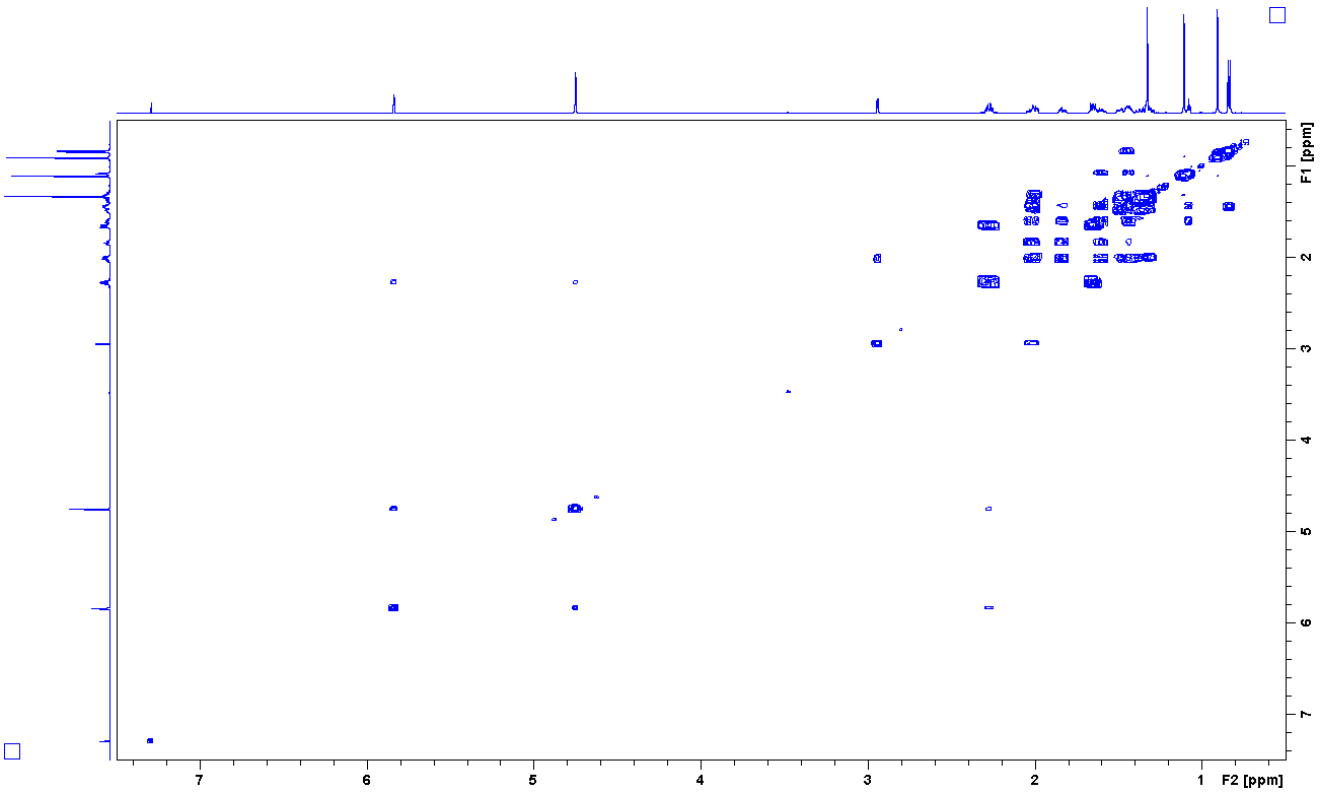

Figure S41: ^{1}H-^{1}H COSY spectrum of compound **8** (600 MHz, $CDCl_3$).

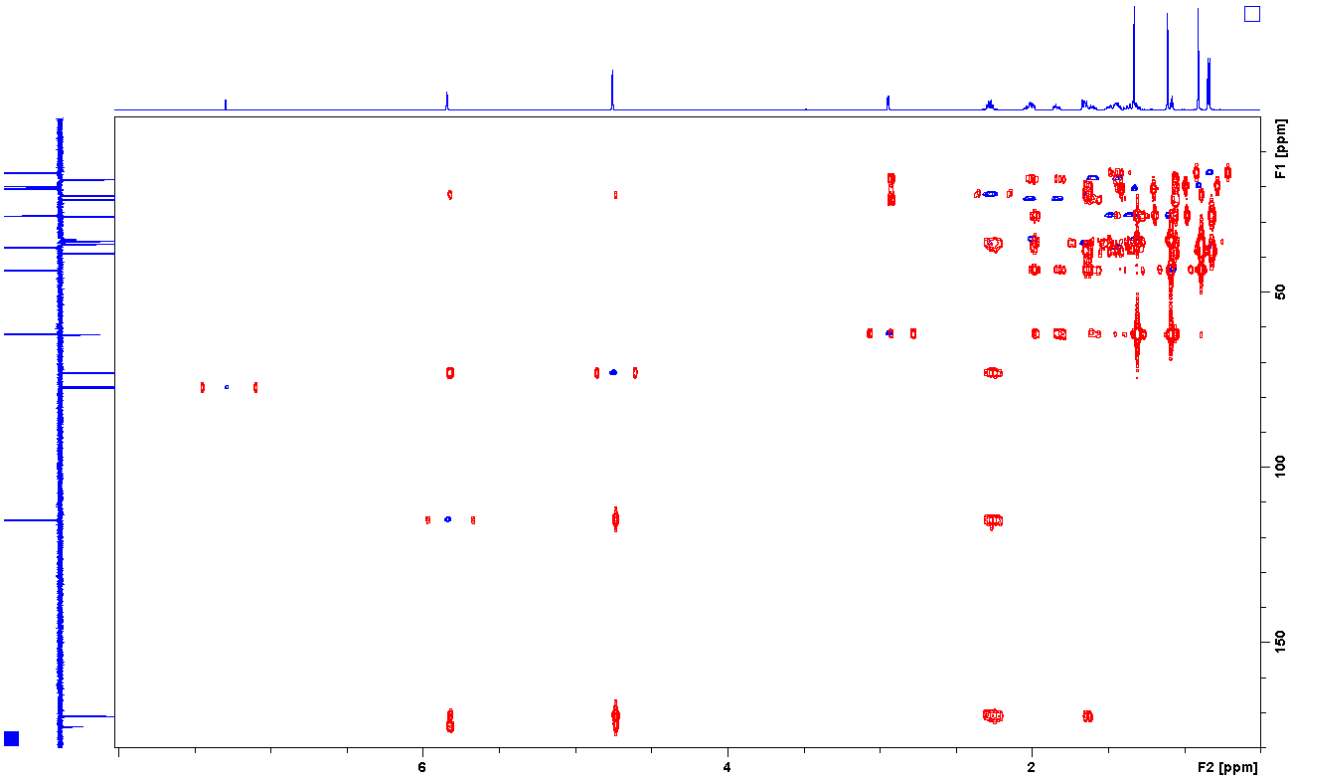

Figure S42: Overlay of HSQC (blue) and HMBC (red) spectra of compound **8** (600 MHz, $CDCl_3$).

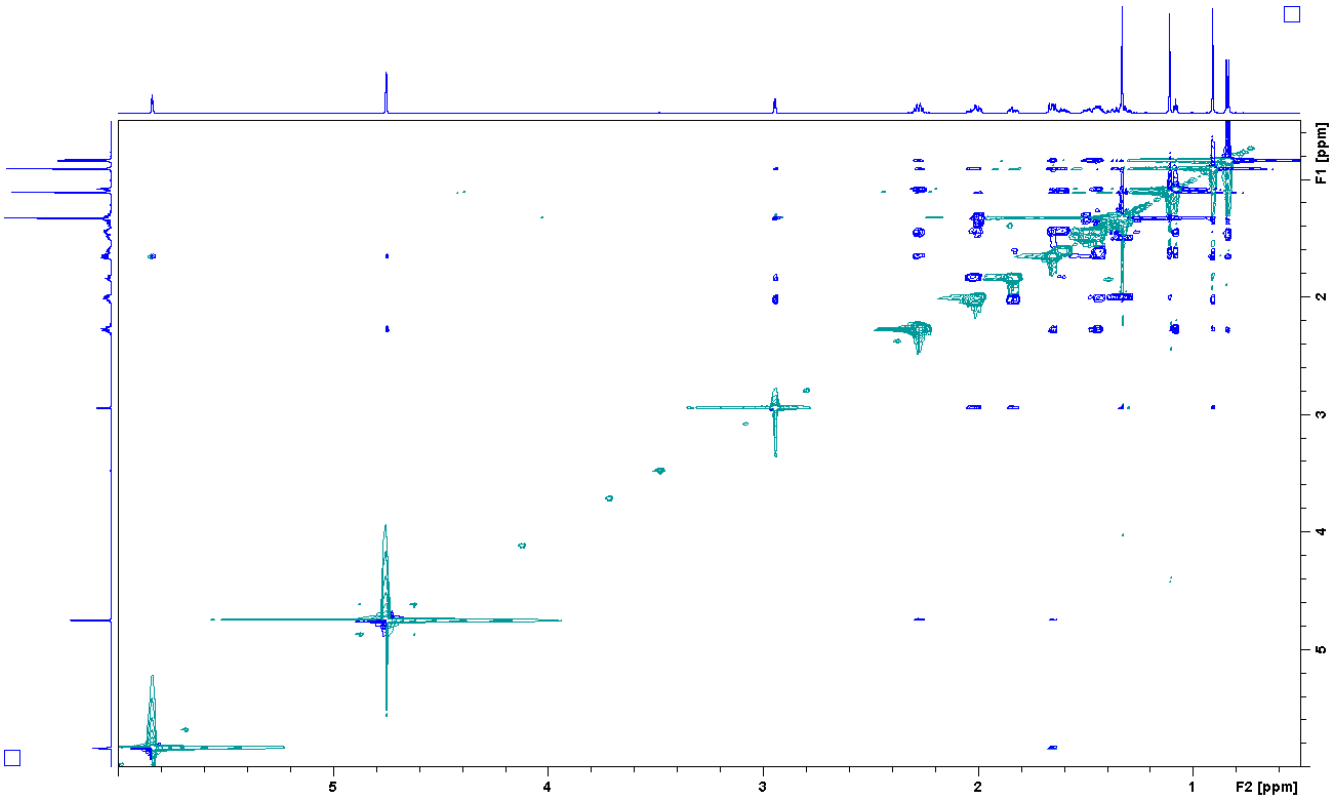

Figure S43: 2D ^{1}H-^{1}H NOESY spectrum of compound **8** (600 MHz, $CDCl_3$).

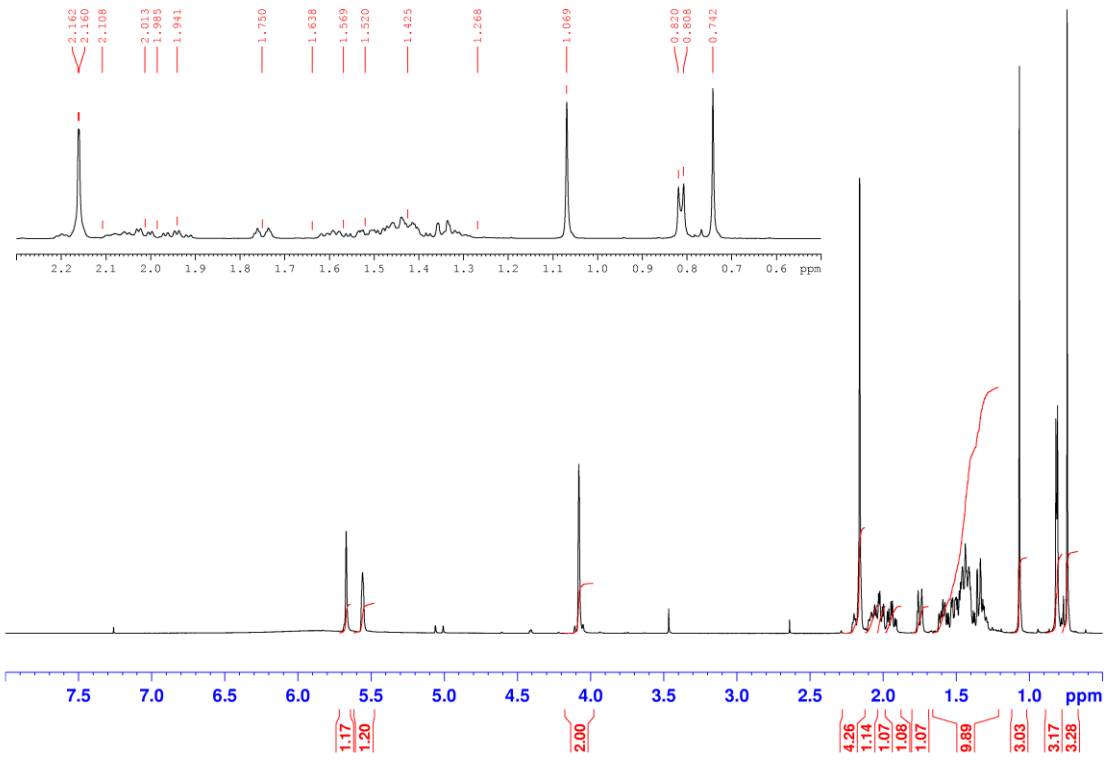

Figure S44: ^{1}H NMR spectrum of compound **9** (500 MHz, $CDCl_3$).

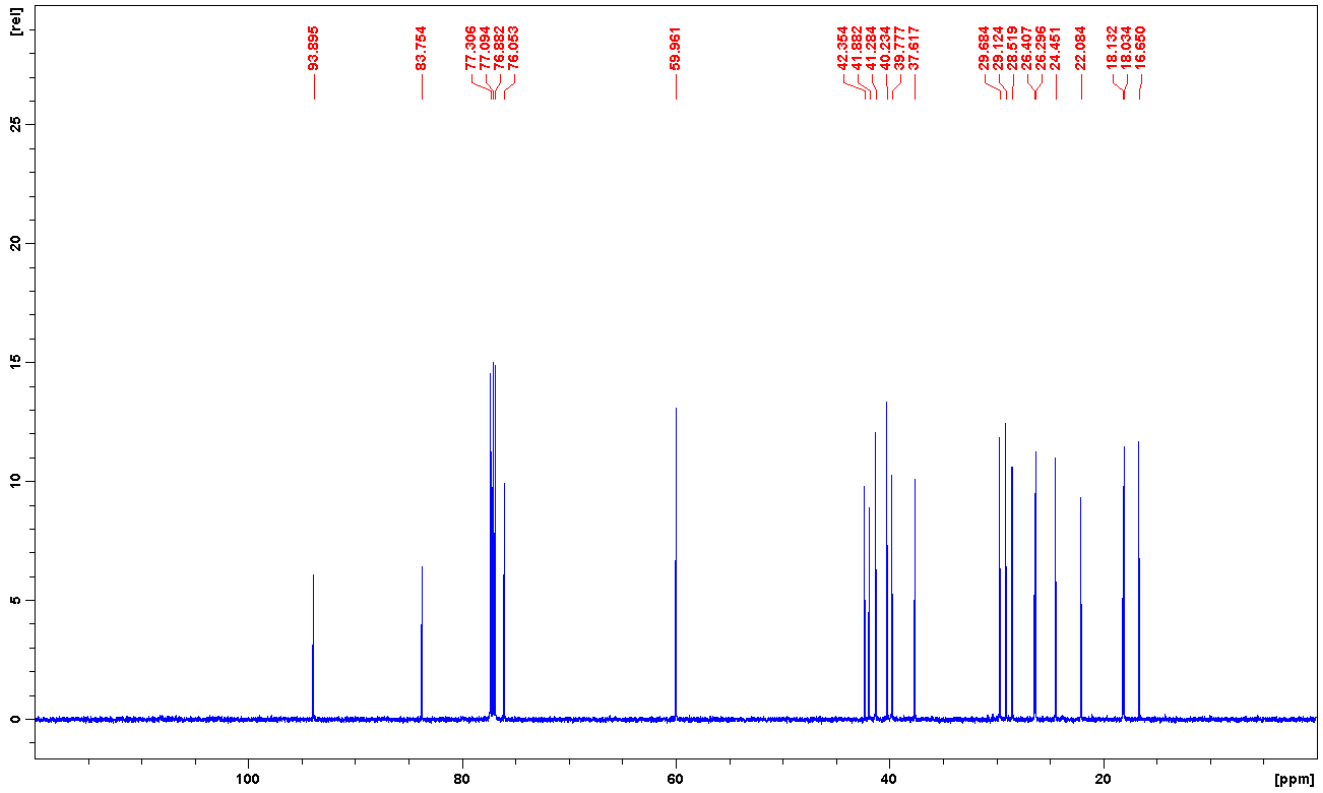

Figure S45: ^{13}C NMR spectrum of compound **9** (125 MHz, $CDCl_3$).

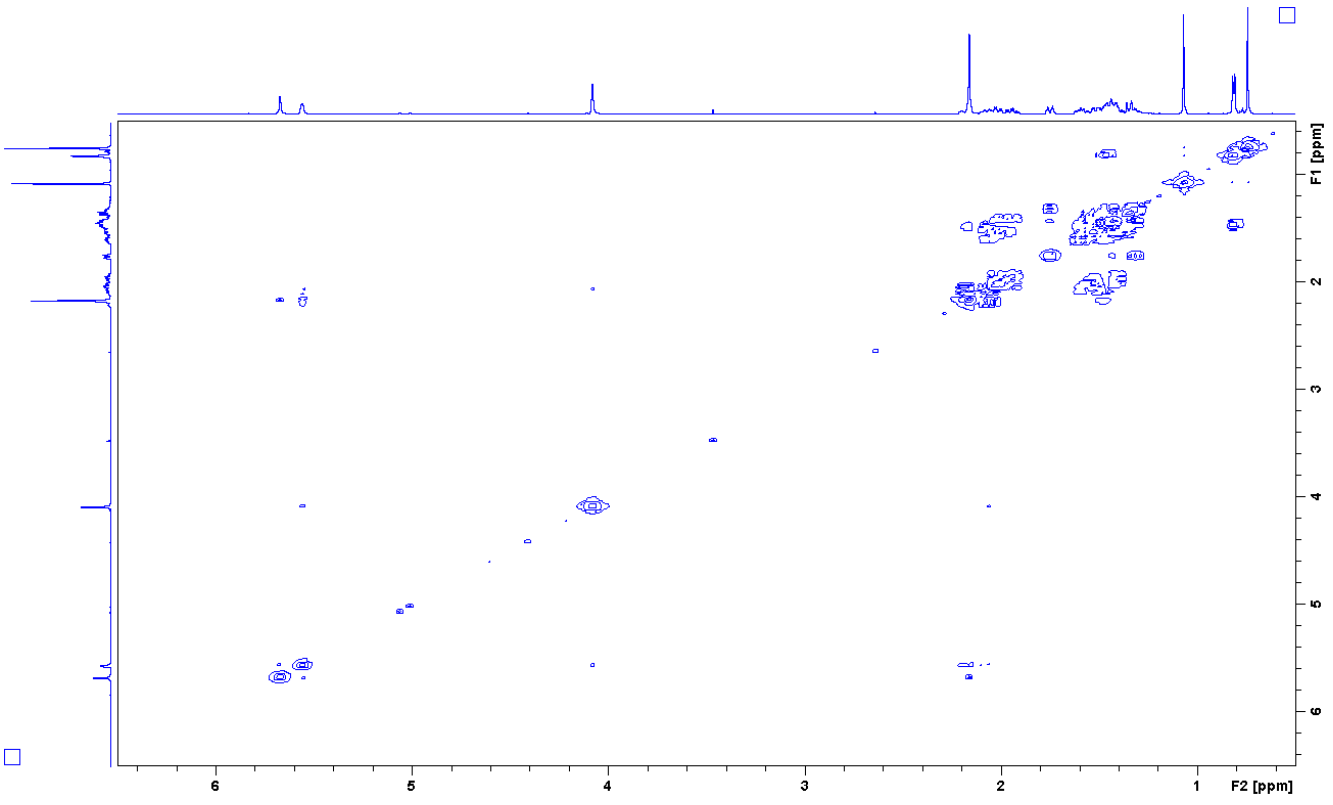

Figure S46: ^{1}H-^{1}H COSY spectrum of compound **9** (500 MHz, $CDCl_3$).

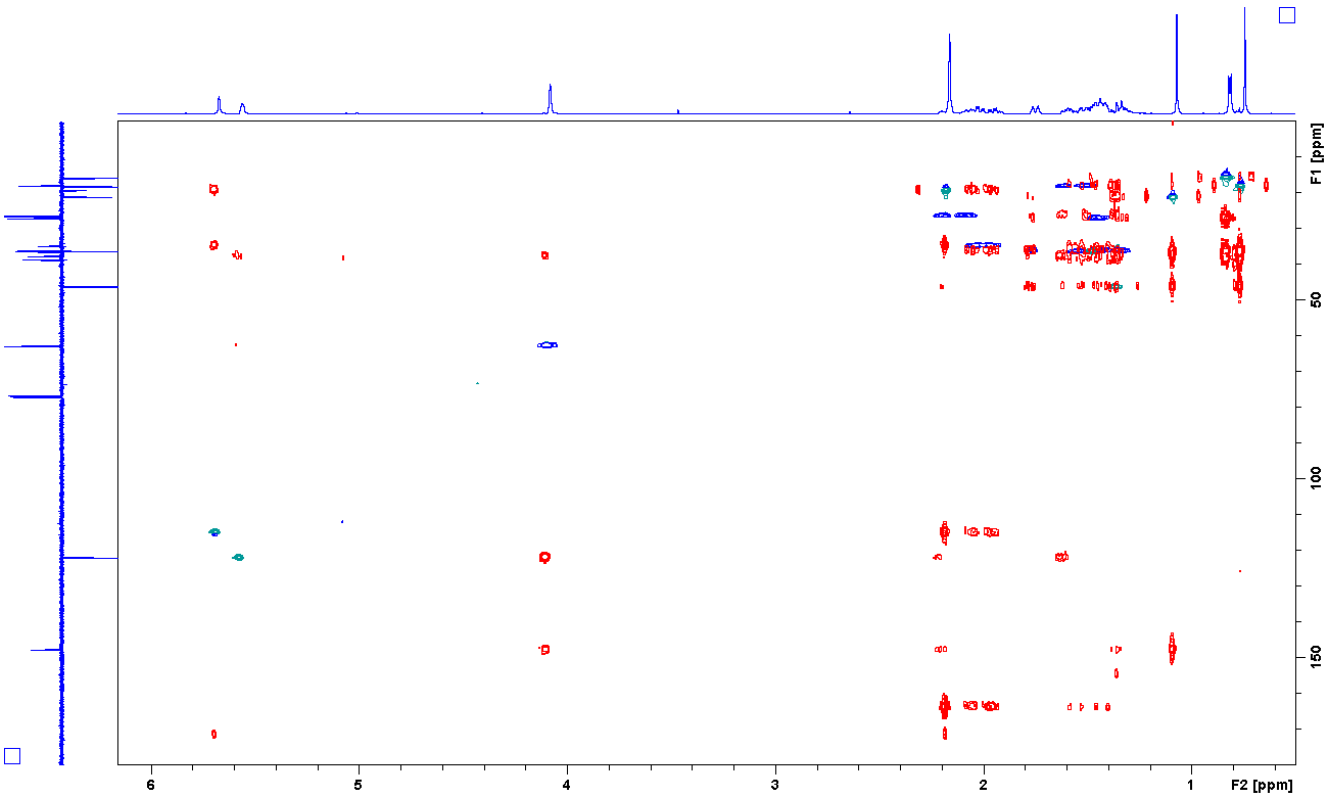

Figure S47: Overlay of HSQC (blue) and HMBC (red) spectra of compound **9** (500 MHz, $CDCl_3$).

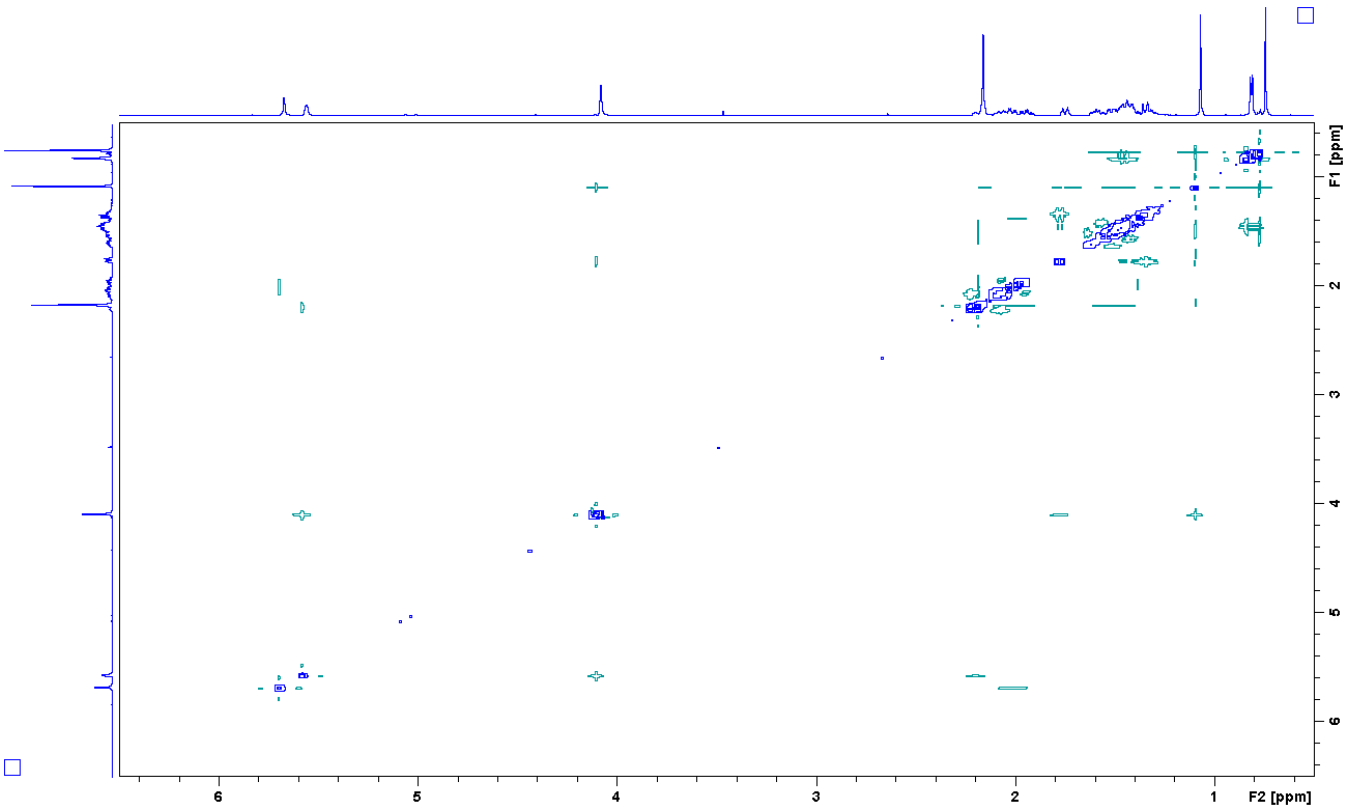

Figure S48: 2D ^{1}H-^{1}H NOESY spectrum of compound **9** (500 MHz, $CDCl_3$).

3. CONCLUSION

Our group screened 700 extracts from different parts of 142 medicinal plants from South Africa for hERG channel inhibition. Only a few species showed activities, suggesting that most South African medicinal plants are associated with a low risk for hERG toxicity. However, *Galenia africana* and *Gnidia polycephala* showed activities [50.3 ± 5.4% (n = 3) and 58.8 ± 13.4% (n = 3) respectively at a concentration of 100 μg/mL] and need further assessment and probably control of their use. Screening of medicinal plants for hERG channel inhibition is important to facilitate regulation, standardization and modernization of herbal medicine.

We used HPLC-based activity profiling for the dereplication and tracking the bioactivity in the above mentioned active extracts. The efficient identification of hERG channel inhibitors in *Galenia africana* and *Gnidia polycephala* has demonstrated the benefits of this approach. Only a few milligrams of extracts were required to generate the chromatogram-activity correlation data. Extract was separated into highly resolved peaks with the latest HPLC and column technologies. UV and MS data were used for early dereplication and tentative identification of bioactive compounds. Highly-sensitive microprobe NMR allows the identification of compounds available in quantities of less than one milligram. With the integration of more and more diverse sensitive off-line bioassays, this platform has the key position in modern drug discovery of natural products.

A total of twenty phenolic compounds, including six new ones were isolated and identified from *Galenia africana*. Among the nine compounds isolated from the active time window, five compounds were obtained in sufficient amounts for testing in the oocyte assay at a concentration of 100 μM. All screened compounds displayed weak and comparable hERG blocker activity. Considering that 7,8-methylenedioxyflavone and 7,8-dimethoxyflavone were the by far most abundant compounds in the active time window and corresponded to the two dominant peaks in the UV chromatogram of the extract, we hypothesized that the pronounced activity of the extract was imputable to their high concentration. The content of 7,8-methylenedioxyflavone and 7,8-dimethoxyflavone in the DCM extract was determined by HPLC and found to be 43.02 ± 0.01 mg/g extract (4.3%) and 94.31 ± 0.02 mg/g extract (9.4%), respectively. Additional concentration-response experiments were performed with 7,8-methylenedioxyflavone and

7,8-dimethoxyflavone at 300 μM, and confirmed a concentration-dependent hERG inhibitory activity for both compounds. This study further demonstrated the potential effect of flavonoids on cardiac electrophysiology. The structurally related flavonoids in *Galenia africana* showed low-affinity block *in vitro*, thus suggesting a low risk for hERG mediated cardiotoxicity. However, the concentration-dependent inhibition of 7,8-methylenedioxyflavone and 7,8-dimethoxyflavone emphasizes the need for more extensive safety assessment of traditional herbal remedies.

A total of sixteen compounds, including two new Daphnane-type diterpenoid orthoesters (DDOs), two new guaiane sesquiterpenoids, and polycephalones A and B with unprecedented carbon skeletons were isolated and characterized from *Gnidia polycephala*. The absolute configuration of polycephalone A was established with X-ray crystallography and computational methods. Five DDOs were identified in the active time window. However, only three of the five were isolated in sufficient quantity for the relative insensitive hERG bioassay. Of the three DDOs screened, one is new and two are known. Their hERG activity was significant [55.4 ± 7.0% (n = 4); 42.5 ± 16.0% (n = 3) and 51.3 ± 9.4% (n = 4) respectively at 100 μM]. No previous hERG activity has been reported for DDO's and these results thus identified a new scaffold for hERG channel inhibitors. DDOs have novel structures and remarkable bioactivities that have attracted much attention. The hERG channel inhibitory activities reported in this study may inhibit their progress in drug discovery programs.

The DCM extracts of seeds, leaves and hulls of *Colophospermum mopane* (Fabaceae) had shown positive antimicrobial activities. HSCCC was employed to preparatively isolate new compounds from the DCM extracts. CCC avoided the tailing normally associated with silica-based chromatography that had inhibited isolation of pure compounds with carboxylic acid moieties which are common in *Colophospermum mopane.* We thus isolated three new and two known labdane diterpenoids, one new isolabdane, and three new and two known clerodane diterpenoids. This demonstrated the unique separation mechanism and preparative potential of HSCCC. The absolute configuration of eight out of eleven compounds could be assigned by X-ray crystallography, modified Mosher's method, and chemical correlations. Finally, we showed that introduction of a strong chromophore such as the *p*-bromobenzoyl group may facilitate the assignment of the absolute configuration by ECD for compounds lacking suitable chromophores.

The compounds isolated were evaluated for their antimicrobial activities. A clerodane diterpenoid isolated from the seeds is the most active with MIC value as low as 51.3 µM, 51.3 µM and 102.9 µM against *Escherichia coli*, *Staphylococcus aureus* and *Enterococcus faecalis*, respectively. This suggests that it is one of the compounds that are responsible to the activity of the seed extract. However, the compounds isolated from leaves and husks are weakly active or inactive, suggesting that the active compounds in lower concentrations from these plant parts have not been isolated. Activity guided fractionation and HPLC-based activity profiling should solve this.

This thesis underscores the efficiency of CCC to obtain larger quantities of material from plant extracts and the efficiency of the HPLC-based activity profiling to track bioactivity and characterize bioactive compounds in plant extracts.

About 40% (19 out of 47) isolated compounds from the three plants investigated in this thesis are new structures. Among them, polycephalones A and B from *G. polycephala* represent a new carbon skeleton.

Only a small portion of the plants in Southern Africa have been investigated. Hence, with its great biodiversity, South Africa is a hotspot in natural product research globally. This indicates the great potential for discovery of novel compounds from South African plants.

4. OUTLOOK

In the HPLC-based activity profiling for hERG channel inhibitors in *Galenia africana*, the strongest inhibition was observed in microfractions 7-9 that showed current inhibition values of 24.1 ± 2.5%, 25.1 ± 3.4% and 22.3 ± 1.8% at 100 μg/mL, respectively. This is significantly weaker than that of the crude extract (50.3 ± 5.4% at 100 μg/mL). The question of synergy may be investigated. For example, the two major compounds 7,8-methylenedioxyflavone and 7,8-dimethoxyflavonein the active microfractions 8 and 9 respectively with a concentration-dependent hERG inhibitory activity (33.2 ± 12.4% and 30.0 ± 7.4% at 300 μM, respectively) are interesting for the synergic studies. In addition, only five of the nine flavonoids identified in the active time window were isolated in sufficient quantities to the test in the hERG bioassay. The weak and similar activity of the pure compounds (Figure 1) compared to the extract may also be explained by these compounds being more active than the tested compounds. It may be argued that the hERG toxicity of *G. africana* has been established and no further work is required to identify the molecules responsible. However, this work underscores the role of flavonoids in hERG toxicity and it may be worthwhile to identify the hERG activity of the unscreened flavonoids in the active time window and the influence of structure on hERG activity (structure-activity relationship). Sufficient quantities of these compounds for hERG screening can be obtained from other natural sources where they may occur in larger quantities, via synthesis or by repeating the methods described in this thesis starting with larger quantities of raw material. Further work should also be considered on medicinal plants botanically related to *Galenia africana* for hERG activity.

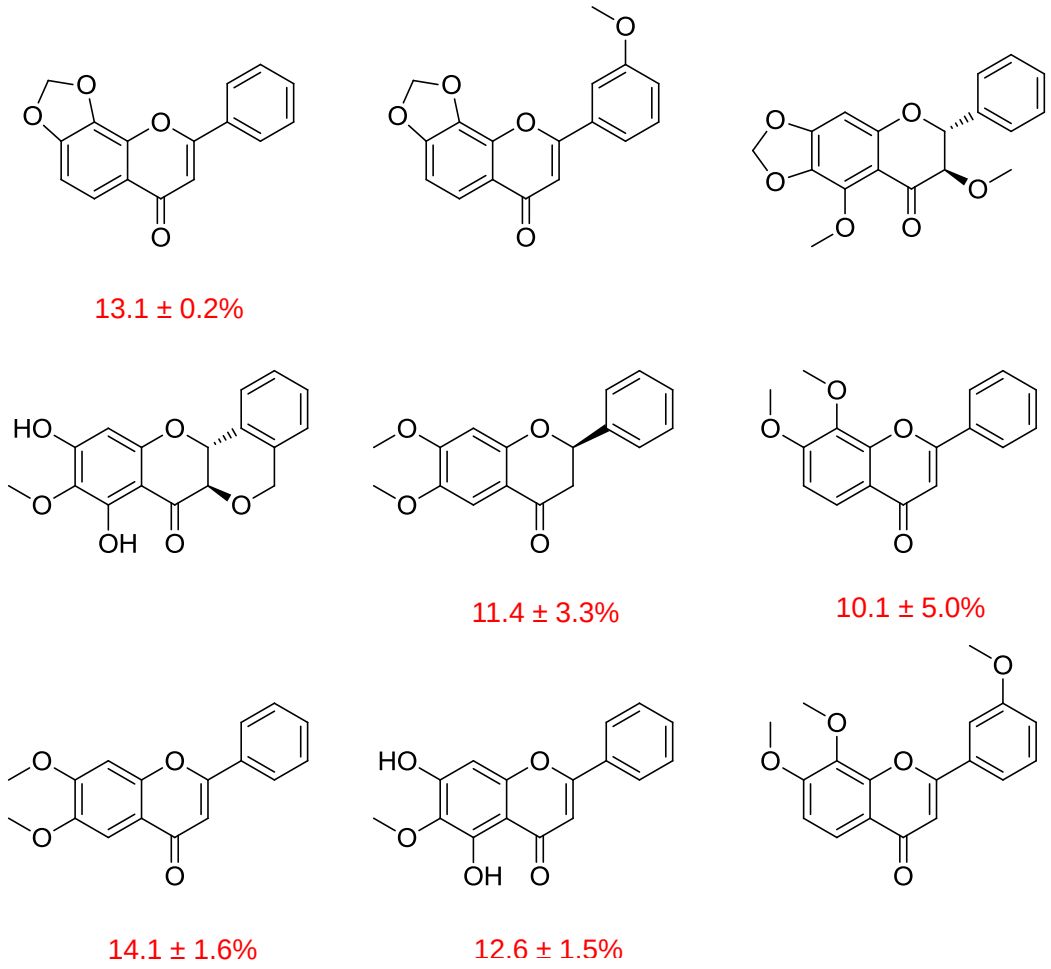

Figure 1. Compounds identified in the active time window of the HPLC-based activity profiling of *G. africana* and the weak and similar hERG inhibition activity of the five compounds tested at 100 μM.

This thesis reported the first hERG inhibition by daphnane-type diterpenoid orthoesters (DDOs). Five (DDOs) from *Gnidia polycephala* were identified in the active time window. Only three of the five DDOs were isolated in a sufficient quantity for the hERG screen and all three showed potent hERG channel inhibition at 100 μM (Figure 2). DDOs are found only in the plant families of Thymelaeaceae and Euphorbiaceae. Thus, screening the hERG channel inhibition of medicinal species in these two families may identify DDOs with diverse structural features that correlate with hERG channel inhibition. Medicinal plants that contain other daphnane-type diterpenoids should also be screened, not only to explore their toxicity, but also to establish whether the *ortho* ester moiety is important for hERG inhibition.

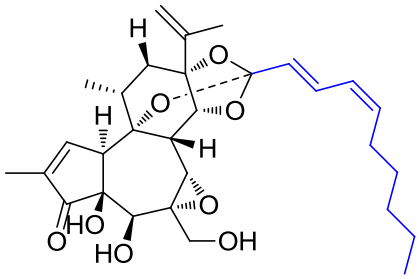

Excoecariatoxin A

55.4± 7.0%

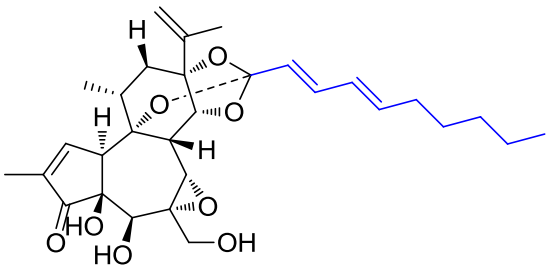

Excoecariatoxin

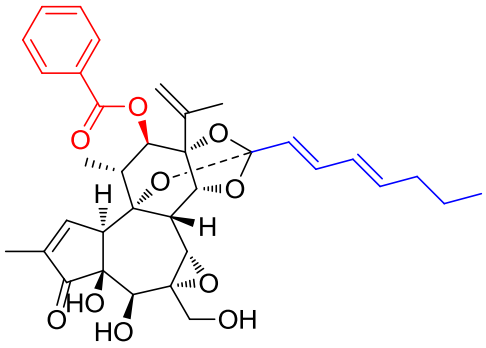

Yuanhuacine A

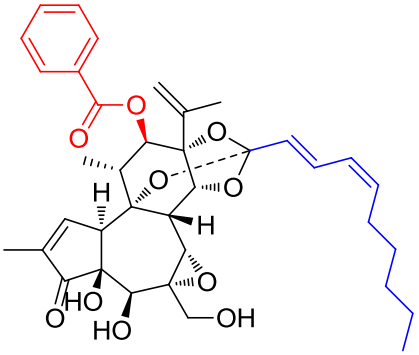

Yuanhuacine B

42.5 ± 16.0%

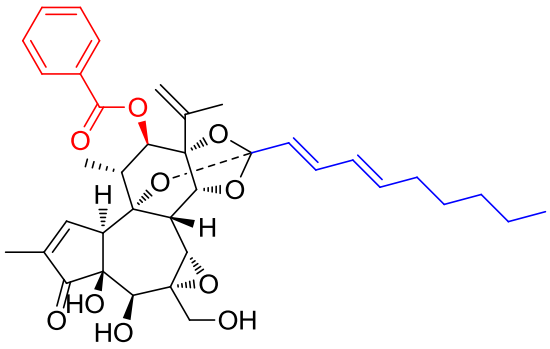

Yuanhuacine

51.3 ± 9.4%

Figure 2. Compounds identified in the active time window of the HPLC-based activity profiling of *G. polycephala*, and the potent hERG inhibition activity of the three compounds tested at 100 μM.

The isolation of two totally new compounds (polycephalone A and B) with novel scaffolds isolated from *Gnidia polycephala* suggests the inclusion of these compounds in a variety of bioassays to establish possible novel bioactivity.

Our investigation of *Colophospermum mopane* did not follow an activity guided approach. Only the major compounds in the extracts were isolated and tested for antimicrobial activity. The husk and leave extracts of *Colophospermum mopane* showed more promising antimicrobial activity than the seeds. However, all of the compounds isolated from husks and leaves were weakly active or inactive. The only antimicrobial molecule was isolated from the seed with significant activities of 51.3 µM, 51.3 µM and 102.9 µM (MIC) against *Escherichia coli*, *Staphylococcus aureus* and *Enterococcus faecalis*, respectively. This may indicate a limitation in the approach followed and suggested that all active compounds have not been identified. Further investigation with HPLC-based activity profiling, similar to the approach followed with *Galenia africana* and *Gnidia polycephala* is required.

This thesis demonstrated the advantages of HPLC-based activity profiling as an efficient approach to track bioactivity and identify bioactive molecules in a complex natural extracts. Common use of this approach in the future is suggested.